SYNTHESIS AND ASSEMBLY OF HIGH ASPECT RATIO NANOSTRUCTURES OF SILVER AND GOLD

JADAB SHARMA

PHYSICAL AND MATERIALS CHEMISTRY DIVISION

NATIONAL CHEMICAL LABORATORY

PUNE – 411 008

INDIA

May - 2006

SYNTHESIS AND ASSEMBLY OF HIGH ASPECT RATIO NANOSTRUCTURES OF SILVER AND GOLD

A THESIS

SUBMITTED TO THE

UNIVERSITY OF PUNE

FOR THE DEGREE OF

DOCTOR OF PHILOSOPHY

IN

CHEMISTRY

BY

JADAB SHARMA

PHYSICAL AND MATERIALS CHEMISTRY DIVISION

NATIONAL CHEMICAL LABORATORY

PUNE – 411 008

INDIA

May 2006

Dedicated To My Parents...

DECLARATION

I hereby declare that the thesis entitled "**SYNTHESIS AND ASSEMBLY OF HIGH ASPECT RATIO NANOSTRUCTURES OF SILVER AND GOLD**" submitted for the degree of Doctor of Philosophy in Chemistry to the University of Pune has been carried out by me at Physical and Materials Chemistry Division, National Chemical Laboratory, Pune, 411008, India, under the supervision of Dr. K. Vijayamohanan. The work is original and has not been submitted in part or full by me for any degree or diploma to this or any other University.

Date: 17th May 2006   **JADAB SHARMA**

Physical and Materials Chemistry Division

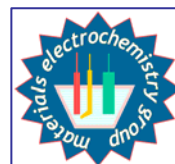National Chemical Laboratory

Pune – 411 008

Dr. K. Vijayamohanan

Scientist

Physical and Materials
Chemistry Division
National Chemical Laboratory
Pune – 411008
INDIA

Tel: +91-020-25902588
     +91-020-25902635
Res: +91-020-25893307
Fax: +91-020-25902636
Email:vk.pillai@ncl.res.in

CERTIFICATE

This is to certify that the work incorporated in the thesis "**SYNTHESIS AND ASSEMBLY OF HIGH ASPECT RATIO NANOSTRUCTURES OF SILVER AND GOLD**" submitted by **JADAB SHARMA** was carried out by him under my supervision at Physical and Materials Chemistry Division, National Chemical Laboratory, Pune, 411008, India. All the materials from other sources have been duly acknowledged in the thesis.

Date   : 17th May 2006

Place   : Pune

Dr. K. Vijayamohanan

(Research Guide)

Acknowledgements

List of Abbreviations

Abbreviation	Expansion
0-D	Zero-Dimensional
1-D	One-Dimensional
2-D	Two-Dimensional
3-D	Three-Dimensional
3-ABA	3-Aminobenzoic Acid
4-ATP	4-Aminothiophenol
ADDL	Amyloid β-Derived Diffusible Ligands
AFM	Atomic Force Microscope
BBR/Y	Bismarck Brown R/Y
B.E.	Binding Energy
Bcc	Body Centered Cubic
CAR	Carbene Anion Radical
CCR	Carbene Cation Radical
CD	Chrysoidine
CMC	Critical Micelle Concentration
CNT	Carbon Nanotube
CPC	Controlled Potential Coulometry
CTAB	Cetyltrimethyl ammonium bromide
CV	Cyclic Voltammetry
DBTJ	Double Barrier Tunnel Junction
DCM	Dichloromethane
DDA	Discrete Dipole Approximation
DDT	Dodecanethiol
DPN	Dip Pen Nanolithography
DPV	Differential Pulse Voltammetry
DMF	N,N-dimethylformamide
DMSO	Dimethylsulfoxide
DSC	Differential Scanning Calorimetry

EBL	Electron Beam Lithography
EDAX	Energy Dispersive Analysis of X-ray
EDT	1,2-Ethanediol
EELS	Electron Energy Loss Spectroscopy
EG	Ethylene Glycol
ET	Electron Transfer
Fcc	Faced Centered Cubic
FDTD	Finite Difference Time Domain
FET	Field-Effect Transistors
FB	Fat Brown
FTIR	Fourier Transform Infrared
FWHM	Full Width at Half Maximum
Hcp	Hexagonal Closed Pack
HOMO	Highest Occupied Molecular Orbital
HOPG	Highly Oriented Pyrolytic Graphite
HREELS	High-Resolution Electron Energy Loss Spectroscopy
HRTEM	High-Resolution Transmission Electron Microscopy
LB	Langmuir Blodgett
LFM	Lateral Force Microscope
LON	Local Oxidation Nanolithography
LRRT	Long Range Resonant Energy Transfer
LSPR	Localized Plasmon Resonance
LUMO	Lowest Unoccupied Molecular Orbital
MB	Mordant Brown
MBE	Molecular Beam Epitaxy
MEMS/NEMS	Micro/Nano-Electromechanical Systems
MFM	Magnetic Force Microscope
MIT	Metal-to-Insulator Transition
MLWA	Modified Long Wavelength Approximation
MOSFET	Metal Oxide Semiconductor Field-Effect Transistor
MPCs	Monolayer Protected Nanoclusters

MR	Magnetic Resonance
MRFM	Magnetic Resonance Force Microscope
MRI	Magnetic Resonance Imaging
MTP	Multiple Twinned Particles
NcAFM	Non-contact Atomic Force Microscopy
NHE	Normal Hydrogen Electrode
NPs	Nanoparticles
NSOM	Near-field Scanning Optical Microscope
NWs	Nanowires
OCP	Open Circuit Potential
PC-NRs	Phosphatidylcholine Passivated Nanorods
PRPs	Plasmon Resonant Particles
PTC	Positive Temperature Coefficient
PVP	Poly(N-vinyl pyrrolidone)
QDL	Quantized Double Layer Charging
Q-dots	Quantum Dots
RDE	Radiative Decay Engineering
RSS	Critical Resolved Shear Stress
SAED	Selected Area Electron Diffraction
SAM	Self-assembled Monolayer
SAXS	Small Angle X-ray Scattering
SCE	Saturated Calomel Electrode
SECM	Scanning Electrochemical Microscopy
SEM	Scanning Electron Microscope/copy
SERS	Surface Enhanced Raman Spectroscopy/Scattering
SET	Single-Electron Transistors
SIMS	Secondary Ion Mass Spectroscopy
SNAP	Superlattice Nanowire Pattern Transfer Process
SPB	Surface Plasmon Resonance Band
SPM	Scanning Probe Microscope
SPR	Surface Plasmon Resonance
SPS	Surface Plasmon Spectroscopy
SPPERS	surface-plasmon-polariton-enhanced Raman

	spectroscopy
STM	Scanning Tunnelling Microscope/copy
STS	Scanning Tunnelling Spectroscopy
TDA	Tridecylamine
TEA	Triethylamine
TEM	Transmission Electron Microscope/copy
TG	Thermogravimetry
UPD	Under Potential Deposition
XPS	X-ray Photoelectron Spectroscopy
XRD	X-ray Diffraction

Table of Contents

Chapter 1

Chapter 2 *74-111*

A Comparative Study on Nanoparticles and Nanowires of Silver

Chapter 3

Shape Selective Preparation of Gold Nanoparticles: Role of Polyfunctional Organic Molecules as Capping and Reducing Agents

Chapter 4

Bimetallic Assembly: Formation of Interlinked Gold and Silver Nanoparticles

Chapter 5

Hybrid Nanostructure Assembly: Controlled Organization of Gold Nanoparticles on Silver Nanowires

Chapter 6

Conclusions and Future Prospects

List of Publications

Erratum

Chapter 1

High Aspect Ratio Metallic Nanostructures: A Critical Survey

This chapter describes a critical survey of various methods for the shape and size selective synthesis of anisotropic nanostructures of gold, silver and similar metals. A brief account of all recent developments on different synthetic procedures for metallic nanowires and their remarkable size dependant electronic structure and properties is given. The growth mechanism is also discussed for such structures illustrating the importance of several key variables like ligand to metal ion ratio, ligand chain length, nature of surfactants, solvent, temperature and the presence of foreign ions with special emphasis on silver.

The Figure shows various types of representative high aspect ratio nanostructures (not to the scale) rods (a), star-shaped (b), and truncated triangular plate (e) of gold and cubes (c), wires (d), and truncated triangular plates (f) of silver.
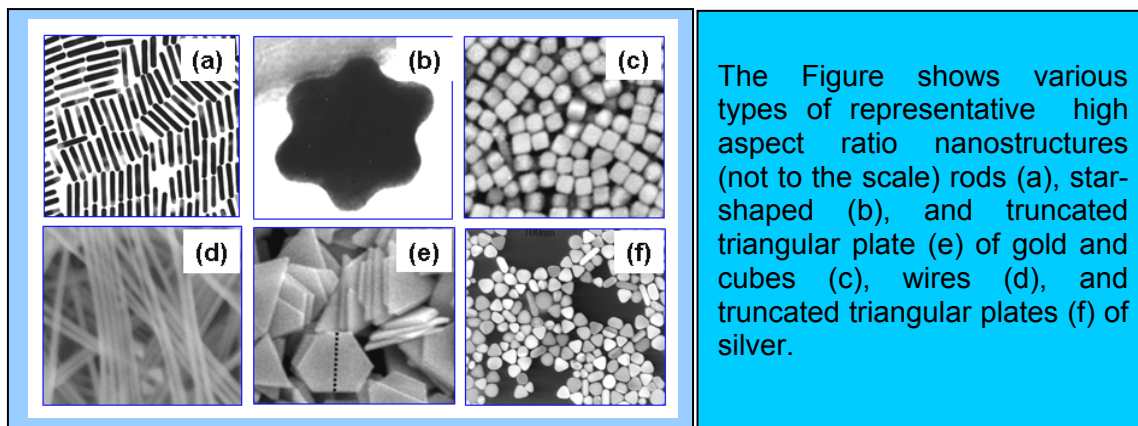
Several interesting (e.g. optical, electrical, mechanical and thermal) shape and size dependent properties of such nanostructures have been discussed elaborately. For example, gold nanorods show surface plasmon absorption peaks at 520 and 600 – 900 nm corresponding to the transverse and longitudinal oscillations respectively, while silver nanorods give peaks at 350, 380, and 410 nm. Optical properties of nanoprisms of gold and silver are more interesting as they show several absorptions at 800, 1300 nm and 350, 431, 465, 552 nm depending on their critical dimensions. Similarly, mechanical properties also show interesting variation as illustrated by the average value of the Young's modulus of silver nanowires (30 nm diameter) to be 102 ± 23 GPa which is significantly higher than that of bulk silver (83 GPa). Many applications of these high aspect ratio nanostructures also have been discussed with the help of specific recent examples. The chapter ends describing the overall organizations of the thesis, primary objectives of these investigations and an abstract of the present study.

1.1 Introduction

"There is plenty of room at the bottom" – the famous statement made by Prof. Richard Feynman in 1959, has initiated a new branch of science which is presently known as 'Nanoscience' and 'Nanotechnology', where everything depends on our ability to manipulate and design materials atom by atom and molecule by molecule at the nanoscale.[1] These nanoscale materials possess novel size and shape dependent properties useful for diverse applications in various fields of science and engineering. Accordingly, recent technological development makes it possible to generate structures or devices less than 100 nanometers in size with noteworthy functional advantages over conventional devices leading to the threshold of a revolution having the potential to change the entire scenario of present technology. Indeed, promises are so high that it can even cope up with the millennium goal of achieving affordable amenities to all human beings from equally distributed technological developments touching all major aspects of life.[2] It is expected that the nanotechnology will have an impact from sophisticated weapons in the battle field to the day-to-day house hold materials and interestingly few of such changes already have been realized in the field of catalysis, microelectronics and composite materials.[2b-d] Further miniaturization in the field of electronics will lead to the faster, smarter devices for information storage operating at low power consumption.[3] A list of recent review articles on nanoscience and nanotechnology has been compiled by El-Sayed and co-workers, signifying the importance, future expectations, and different levels of growth in this field.[4]

The origin of unusual optical properties of nanostructured materials, however, could be dated back to 17th century when the brilliant color of some of these nanoparticles was used advantageously to make stained glass windows of cathedrals. Faraday explained the origin of their color as due to the presence of metallic gold nanoparticles especially in colloidal form. In 1908, Mie theoretically explained the origin of color of these nanoparticles by applying Maxwell's equations.[5] However, research on nanomaterials has got the momentum only during the last few decades. The term 'Nanotechnology' was christened by Norio Taniguchi of Tokyo Science University in 1974.[6] According to him "Nanotechnology mainly consists of the processing of separation, consolidation, and deformation of materials by one atom or one molecule". Further, real pace for the

....

Physical and Materials Chemistry Division, National Chemical Laboratory   2

research on these materials took place when Eric Drexler popularized and supported nanotechnology during 1980's although many others later horrified general public by a hypothetical explanation of ending of the world due to the formation of self-replicated robots (grey goo) as the outcome of nanotechnology.[7]

Research on nanomaterials is driven by two motivating factors: (i) they exhibit interesting properties at nanometer size scale different from that of bulk materials and (ii) application of these properties for devices (especially linked with health – bio-inspired nanotechnology) for the prosperity of mankind. As the size of materials enters nanometer level, electronic motion is restricted to a smaller space comparable to that of the mean free path of electrons leading to the stronger confinement of electronic motion (spatial confinement). These materials do not follow the classical theory of electronic motion at this size regime and a new set of laws govern their electronic motion which exhibits quantum effect. The quantization of electronic motion in metallic nanoparticles restricts them into certain discrete energy levels making the valence and conduction band no longer inseparable. This energy gap between valence band and conduction band (Kubo gap) becomes comparable to or larger than thermal energy ($k_B T$) at certain size regime and hence metallic nanomaterials become semiconductors. Further reduction of size causes higher confinement and reaches a stage when the material becomes an insulator. At this size regime materials behave differently towards various perturbations and exhibit properties not achievable from its individual counterparts or from the bulk.[8a]

Apart from the size dependence of various properties of nanomaterials, they also exhibit interesting shape dependence due to the execution of electronic motion in different dimensions.[8-12] For example, electron tunneling phenomena observed for 0-D nanostructures is the key concept used for building artificial atoms and devices like single electron transistors.[9] Similarly, electrons can oscillate in two distinct ways in 1-D nanostructures under an electromagnetic field, namely in longitudinal and transverse modes. The way electrons execute its motion alters their various properties and thus, nanorods and nanotubes give two surface plasmon absorption peaks due to the two different types of electronic motion.[10, 11]

1.2 Definition and Classification of Nanostructured Materials

According to Hunt, "Nanomaterials are an enabling component of the popularly labeled area of 'nanotechnology', but are generally not well understood by the materials community at large".[13] Although a variety of prosaic definitions of nanotechnology is available, almost all lack definitional precision despite providing a deeper insight into the subject. One of such definitions described in Scientific American states: "The field is a vast grab bag of stuff that has to do with creating tiny things that sometimes just happen to be useful. It borrows liberally from condensed-matter physics, engineering, molecular biology and large swaths of chemistry".[14] However, a more comprehensive definition is given by the US National Nanotechnology Initiative (NNI)[15] as: (i) research and technology development at the atomic, molecular, or macromolecular levels, approximately 1-100 nanometers in length, (ii) creation and use of structures, devices, and systems that have novel properties and functions because of their small and/or intermediate size, and (iii) ability to control or manipulate on the atomic scale. Another definition given by 'The Royal Society' and 'The Royal Academy of Engineering' states: 'nanotechnology as the design, characterization, production, and application of structures, devices, and systems by controlling shape and size at the nanometer scale'.[16] Thus, improvement of properties of materials by controlling their nanoscale structures is the heart of nanotechnology or can be better called as incremental nanotechnology. Similarly, another term radical nanotechnology means the development of nanoscale machines that would exist at the convergence of nanotechnology, biotechnology, information technology, and cognitive technology. Another most commonly used word to describe nanotechnology is evolutionary nanotechnology. Evolutionary nanotechnology takes advantage of the changes that can occur in materials at the nanoscale related to both, increase in chemical reactivity and quantum effects. The best known examples are nanoscale sensors that exploit the large surface area of nanotubes and semiconductor nanostructures such as quantum dots and quantum wells or nanowires.[17] Silica-based nanomaterials, molecular imprinted polymers, silver nanowires, and silicon platforms are envisioned for collection, concentration, and detection of chemical and biological weapons and other related compounds in security and defense applications. The biggest steps are being made in evolutionary nanotechnology, with more and more products expected to appear in the coming

....

Physical and Materials Chemistry Division, National Chemical Laboratory   4

days.[16,18] However, each new technology has its potential drawbacks and may be a threat to the society, unless the implications of such development are not understood properly.[19] Similarly, as nanotechnology has created brighter future, simultaneously it generates a general apprehension that nanotechnology will pose severe risks. Therefore, opponents of nanotechnology sometimes gain momentum, demanding a complete halt on such research at least in few places (anti-nanotechnology).[20]

Metallic nanoparticles can be classified as bi-metallic or tri-metallic depending on the number of constituent metallic parts. Most of the cases, they form alloys, and commonly known as alloy nanoparticles. Similarly, core-shell nanoparticles constitute another class of nanomaterials which are cross-linked nanosized particles with a chemical composition that is different on the surface compared to the core region.[21] Non-metallic nanoparticles (nanotubes) are another class consisting of non metals and organic molecules with interesting electrical behavior which can be tuned to be insulating or metallic based on size and composition.[22] The most familiar example of non-metallic nanoparticle is Fullerenes which constitute a different class of nanomaterials.[23] Carbon nanotubes constitute another celebrated class of nanomaterials that can be metallic or semiconducting depending on their diameter and chirality.[24]

Another way of classifying nanomaterials is based on their dimensionality. If we consider the three dimensional space vectors for a specific nanomaterial and length scales are in the critical regime of 1-100 nm, they can be known as 0-dimensional particles or quantum dots, typical examples being spherical (1-10 nm diameter) nanoparticles of Au, Ag, CdS, CdSe etc. Similarly, if two spatial vectors are restricted in that critical length scale allowing nanomaterial to grow only in the third direction, then the resultant nanomaterial is known as 1D nanostructure (quantum wires), specific examples being nanorods, nanowires, etc. Single walled carbon nanotubes can be considered as an important example of such material. In 2D nanostructures, only one dimension is restricted to that critical length scale and these nanomaterials (quantum sheets) are allowed to grow along the other two spatial directions.

A more interesting method of classifying nanomaterials is based on their shape. Thus, nanomaterials are known as quantum dots or nanoparticles (monolayer protected nanoclusters, MPCs or simply NPs), nanowires, nanorods, nanoribbons, nanobelts, nanobipods, nanotetrapods, nanocubes, nanoboxes, nanotriangles, etc. Nanoparticles

that consist of homogeneous material, especially those that are almost spherical or cubical in shape are called quantum dots. Nanostructures that are shaped like long sticks or dowels, with a diameter in the nanoscale and a length very much longer are known as nanorods or nanowires. If a normal nanorod is coated with a different metal layer, then it is known as core-sell nanorod or coaxial nanocables.[25a, b] Similarly, if the inside of a nanorod is hollow, then it is known as nanotubes or nanorods with hollow interiors.[25c] Nanoparticles of triangular or prismatic shape are called nanoprisms or nanotriangles.[25d] All such nanomaterials having aspect ratio (R, division of length by diameter or more precisely, division of length along the major axis by the length along the minor axis), R >1 come under a broad term high aspect ratio nanostructures. Accordingly, an enormous number of differently shaped nanomaterials of metals, non metals, and semiconductors have been categorized as high aspect ratio nanomaterials and reviewed recently.[25e] **The present review, however, discusses only the metallic high aspect ratio nanostructures, especially nanomaterials of gold and silver since our studies are mainly focused on these two metals.**

1.3 Significance of High Aspect Ratio Nanomaterials

High aspect ratio nanostructures are of particular interest since their shape anisotropy offers additional degrees of freedom for manipulation of their properties as compared to that of spherical particles.[26] One of their fascinating properties is optical properties, which strongly depends on both the particle size and shape. This is because optical measurements are one of the easiest ways to monitor electron transfer or other surface processes. Subsequently, many feasibility studies of molecules on anisotropic metal surfaces have been carried out with techniques such as surface enhanced Raman spectroscopy (SERS) and various such geometries have been proposed for molecular recognition. Apart from SERS studies, these high aspect ratio nanostructures are also important for the high density circuitry.[27] Similarly, they exhibit thermal properties important for biomedical community for the treatment of cancer cells as they generate local heating under near-IR irradiation due to specific absorptions at particular wavelength, generally not harmful towards the normal living cells. For example, irradiation of living tissues by NIR light (700-1,000 nm, usually from a laser) does not affect or damage the intervening cells or tissues, while nanorods and nanoshells absorb

it and cause local heating, which can be used for the destruction of tumor cells.[28] Another fact of general interest is that they provide experimental confirmation of theoretical predictions, which describes the unique properties of high aspect ratio nanomaterials based on few theoretical approaches such as the discrete dipole approximation (DDA), finite difference time domain methods (FDTD), and the modified long wavelength approximation (MLWA).[10, 29] In essence, apart from their aesthetic appeal, synthesis of high aspect ratio nanostructures is compelling for many fundamental and technological reasons leading to the understanding of intrinsic shape-dependent properties of metal and semiconductor nanocrystals and their application opportunities.

1.4 Theoretical Background on High Aspect Ratio Nanomaterials

High aspect ratio nanomaterials have drawn special interest as several theoretical calculations can simultaneously provide explanations for the optical spectra, made predictions, and set guidelines for synthesis. It has been predicted that Ag nanowires with circular and polygonal cross-sectional symmetry would exhibit different resonances, and that a dielectric coating would lead to a red-shift of the SPR band.[30] For example, Kottmann et al. have investigated numerically the surface plasmon spectrum of metallic nanowires with a non-regular cross section, in the 20-50 nm range by solving the Maxwell's equation.[30a, b] In this model, a complete description of the material properties of metal is encompassed in the dispersion relation, which gives the complex permittivity, $\varepsilon(\omega)$, as a function of the frequency (wavelength). Near the metal plasma frequency (ω_p) of the metal, the dispersion relation is governed by the interaction between light and the conduction electron gas or expressed with their quantum counterparts by the photon-plasmon interaction. For certain metals such as silver and gold, ω_p is in the visible frequency range and plasmon resonances can be excited at specific permittivity values, which strongly depend on the particle size and shape. For example, in a small sphere one single resonance can be excited, when $\varepsilon = -2$ whereas a cylinder is in resonance when $\varepsilon = -1$. More than one resonance can be excited in a non regular structure, irrespective of its size. For instance, a small ellipse exhibits two resonances, while a triangular nanoparticle has several resonances (more than five distinct resonances) for each illumination direction.[30b] The spectral range covered by these different resonances

....

Physical and Materials Chemistry Division, National Chemical Laboratory   7

becomes very large, giving to the particle distinct colors. When the particles are in resonance, dramatic field enhancement has been observed at the vicinity of non-regular particles, where the field amplitude can reach several hundred times than that of the illumination field. This corresponds to the surface-enhanced Raman scattering enhancement locally in excess of 10^{12}. This is indeed the basis for the single molecule detection by SERS technique.[31] The strong localization of near field at specific positions around the metallic particle, as well as its rapid decay when one moves further away from the particle surface, can also explain the experimentally determined "hot spots" observed in SERS experiments.[32]
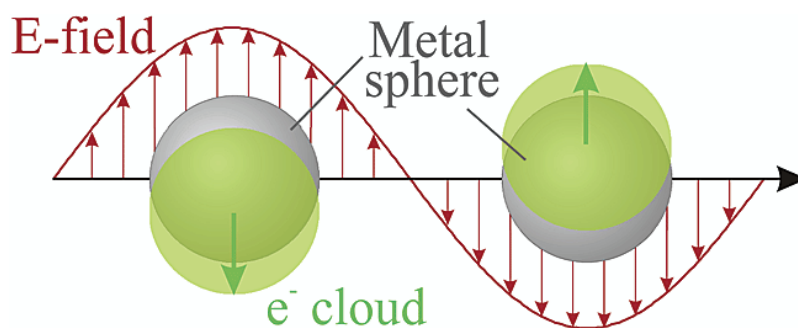
Figure 1.1: Displacement of the conduction electron charge cloud relative to the nuclei of a sphere. [Adopted from 10].

When a small spherical metallic particle is irradiated by light, the oscillating electric field causes the conduction electrons to oscillate coherently, known as dipole surface plasmon resonance (Figure 1.1). The restoring forces due to the Coulombic attraction of electrons with nuclei oppose the displacement of electrons with incoming electric field ultimately leading to the oscillations, frequency of which is strongly influenced by: (1) density of electrons, (2) the effective electron mass, and (3) the shape and size of the charge distribution. Higher modes of plasmon excitation can also occur, such as quadrupole mode where half of the electrons moves parallel to the electric field and the other half moves anti-parallel.[10]

Several approaches have been made for the explanation of light scattering from nanoparticles of arbitrary shape, where extinction is considered as the sum of scattering and absorption. [5, 10, 33, 34] The refinement of the Mie's equation leads to the better understanding of the optical properties of high aspect ratio metal nanoparticles.[35] One of such theoretical approaches is DDA, which has been the most successful one in

explaining such properties of nanoparticles with arbitrary shapes. [29f-j] For instance, a metal nanorod exhibits two plasmon bands corresponding to the longitudinal and transverse oscillations of plasmon electrons. The transverse band is relatively fixed, while longitudinal mode of oscillations generally varies with the aspect ratio (R), as

$$\lambda_{max} = 33.34\varepsilon_m R - 46.31\varepsilon_m + 472.31 = (33.34R - 46.31)\varepsilon_m + 472.31 \quad \text{(1.1)}$$

where, λ_{max} is the maximum of the longitudinal plasmon band and ε_m is the medium dielectric constant.

Similarly, Gray and co-workers have studied the propagation of light in metallic nanowire arrays based on FDTD calculations.[30c] They showed that reasonable estimation of scattering and absorption cross sections for metallic nanoscale objects can be obtained by such calculations. The intensity of light developing and propagating between the parallel double chains of nanowires can be significantly enhanced by varying the distance between the parallel chains, cylinder radii, relative placements, and wavelength and propagation direction of incident light. Similarly, several other attempts have been made to understand plasmon resonances of isolated nanowires with non-regular shapes, dielectrically coated metallic nanowires, and arrays of metal nanoprisms.[8a, 30b, d]

These theoretical studies have stimulated much of the subsequent experimental work on the growth and synthesis of gold and metal nanoparticles of different shapes. For example, atomistic simulations to study the effect of free surfaces on the yield of gold nanowires showed that the magnitudes of the tensile and compressive yield stress of <100> nanowires increase and decrease, respectively, with a decrease of the wire width.[36] The critical resolved shear stress (RSS) by external forces depends on wire width, orientation and loading condition (tension vs. compression). Free surfaces play two important roles in the generation of nanowires: (i) free surfaces act as preferential nucleation sites for defects, (ii) surface stresses exist on the free surfaces of nanowires. The implication is that if the material growth parameters can be controlled, materials with tunable properties can be synthesized. In particular, several similar theoretical calculations form the basis for modern applications of such nanomaterials in near-field optical microscopy, non-radiative optical transfer, and for building new active optical components.[37]

1.5 Synthesis

1.5.1 Nanorods and Nanowires: Several advanced methods enable present day researchers to synthesize well defined high aspect ratio nanostructures with surprisingly subtle precision.[27] Few of such techniques are photolithography, nanoimprinting, microcontact printing, and other soft lithography methods.[38] These techniques are advantageously utilized for the patterned generation of metallic and semiconductor arrays of nanowires. However, they also constitute a part of techniques for the general preparation of nanowires. Accordingly, a clear demarcation amongst these procedures for generation of different types of nanowires does not exist; instead these procedures are more general and can be applied for few metallic as well as semiconducting nanowires. Therefore, a brief description of such synthetic procedures is presented below irrespective of metallic or semiconductor nanowires or other structures, which will be helpful to draw a comparison between these advanced techniques to that of solution based techniques.

One of the convenient ways of patterning or aligning materials is photolithography.[39] To overcome the drawbacks associated with photolithography, Electron Beam Lithography (EBL) has been developed.[40a] EBL uses a focused beam of electrons to form the circuit patterns needed for material deposition on (or removal from) the substrate, in contrast with optical lithography which uses light for the same purpose. Electron lithography offers higher patterning resolution than optical lithography because of the shorter wavelength possessed by the 10-50 keV electrons that it employs. The resolution of optical lithography is limited by diffraction, but this is not a problem for electron lithography.[40] Another important technique used by the semiconductor industry is molecular beam epitaxy (MBE) as demonstrated by fabricating aligned metal nanowires through a one-step deposition process.[27] This so called "superlattice nanowire pattern transfer process" (SNAP) does not rely on photolithography or EBL providing advantages of fabricating thinner metal wires with narrow spacings. Similarly, scanning tunneling microscopy provides a convenient way of patterning by selective etching and has been applied for the generation of Ag nanowire arrays on Cu (100) substrates.[41] Another technique called local oxidation nanolithography (LON) is developed by advancing STM methods and uses tip induced

....

Physical and Materials Chemistry Division, National Chemical Laboratory   10

local oxidation on surfaces as tool to perform an astonishing variety of pattern generation. For example, a clever combination of self-assembly monolayers (SAM) and LON can be useful for the fabrication of conjugated molecular tracks, gold patterns, and nanowires onto SAM templates. In this way gold wires and electrodes were fabricated by immersing a pre-modified amino terminated SAM surface in a solution containing gold nanoclusters (Au_{55}).[42] Schmid *et al.* have demonstrated recently the quasi 1D nanostructures of Au_{55} clusters by electron beam lithographic technique and measured their electrical properties at room temperatures (RT).[43] Another technique especially used for the nanoscale patterning is dip-pen nanolithography (DPN), initially reported by Jashke and Butt and later re-discovered and further developed by Mirkin and co-workers.[44, 45]

Despite the development of all these advanced techniques, the solution based (commonly known as soft solution synthesis) preparation of such novel materials is a preferred choice to other methods because of easily available and inexpensive materials, versatility, and simplicity in synthetic procedures. The field is remarkably developed since the introduction of Brust's method for synthesizing thiol protected spherical gold nanoclusters.[46] The current trend is to utilize knowledge of solution chemistry to generate non-spherical nanoparticles where not only the size, but also other topological aspects can be controlled through a judicious choice of experimental conditions and additives. Unlike other techniques as discussed earlier, solution chemistry is highly specific for different materials.

1.5.1.1 Gold

Diverse procedures for gold nanorods and nanowires have been developed under different experimental conditions using various surfactants, solvents, and reducing agents with moderate success. All these methods can be classified as (i) template methods, (ii) electrochemical methods, and (iii) seeded growth methods.

(i) Template Method: This method involves the use of templates such as alumina or polymeric membranes with highly ordered nanochannel-array where gold is deposited electrochemically into the pores.[47] The membrane is initially sputtered with Ag or Cu at the rear side to provide electrical contact and electrodeposition occurs at the front side

followed by the electrochemical growth of nanorods within the pores. In the successive steps, the membrane can be selectively dissolved in the presence of stabilizers such as poly (N-vinyl pyrrolidone) (PVP) to get the nanorods and finally nanorods are dispersed in solvents using appropriate methods such as sonication. Pioneering work carried out by Martin, Moskovits, and Searson on different Au nanorods and nanowires illustrates the details of this methodology.[48] This method has been extended to synthesize gold nanorods with controlled diameter by tuning the pore diameter and selectively leaching out the membrane by chemical methods.[49] Similarly, desired length of the nanorods can also be achieved by controlled deposition of gold.[50] Further, the method is extended using membranes other than alumina to synthesize nanorods and nanowires of several other metals.[51] Template technique is also useful for the preparation of free-standing nanowire arrays, which can be used as electrodes to study their electrochemical properties.[52] Subsequent development of similar techniques lead to the synthesis of nanowires with hollow interiors or nanotubes, coaxial nanotubes etc. of gold and various other materials.[25c, 53] More recently, high aspect ratio nanowires and nanotubes of Prussian blue, TiO_2, single crystalline bismuth, $PbTiO_3$, Nickel etc. have been reported by adopting similar or slightly modified template methods.[54] Similarly, the photochemical template uses reduction of gold salts by UV-irradiation using cationic micelles.[55] Interestingly, capillaries of carbon nanotubes can also be used as template for the growth of metal nanowires; accordingly, nanowires of Au, Ag, Pd, and Pt have been synthesized by this intercalation method.[56, 57] Although several such advances have been made, the template method suffers from the very low yield.

(ii) Electrochemical Method: A general method for the synthesis of various nanowires using electrochemical techniques has been explicitly illustrated by Wang and co-workers for synthesizing gold nanowires.[58] The method involves electrolysis using Au as sacrificial anode (3 × 1 × 0.05 cm) and another metal plate (3 × 1 × 0.05 cm) like Pt as cathode at 3 mA current passing for 30 min under constant sonication at ~ 310 K in presence of cationic surfactants, like hexadecyltrimethylammonium bromide (C_nTAB, n = 16), tetradodecylammonium bromide ($TC_{12}AB$) or tetraoctylammonium bromide (C_8TAB), as supporting electrolytes. The presence of these shape-inducing surfactants is very important for the growth and stabilization of gold nanorods. A controlled current

electrolysis leads to the dissolution of gold ions from the anode into the solution, which successively gets reduced at the cathode. The addition of appropriate amount of acetone and cyclohexane are also important for the loosening of micellar framework and
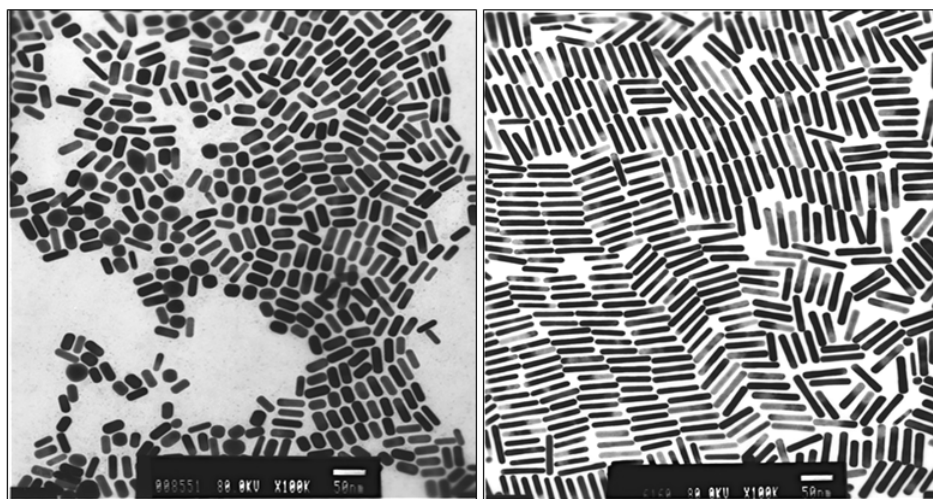
Figure 1.2: TEM images of Au nanorods with two different mean aspect ratios: 2.7 (left) and 6.1 (right). Scale bars represent 50 nm. [Adopted from 58b].

enhancing elongation of rod-shaped micelles respectively. Interestingly, a silver plate immersed in the electrolytic solution can control the growth of gold nanorods. The rate of generation of Ag^+ ions from the silver plate by trans-metallic electrochemical reaction governs the aspect ratio, though a complete growth mechanism is still not known. This method was initially applied for the synthesis of different metal nanoparticles, such as transition metal nanoclusters.[59, 60] The electrochemical method provides a simple technique to synthesize high yield of nanowires or nanorods with controlled aspect ratio (Figure 1.2).

(iii) Seed Mediated Growth: Seeded growth technique is purely chemical and highly specific for nanorod or nanowire synthesis. Accordingly, different recipes have been developed to synthesize gold nanorods by different groups. However, Henglein and co-workers had initially used this method for the synthesis of spherical nanoparticles.[61] Natan and co-workers first pointed out that a substantial amount of gold nanorods can be synthesized by surface catalyzed reduction of Au^{3+} by hydroxylamine in presence of

seeds.[62] Murphy and co-workers investigated systematically the role of seed concentration on the particle size using ascorbic acid as reducing agent and monitored the kinetics of particle growth improving the earlier work of Frens.[63, 64] All these experiments involve reduction of aqueous gold salt by sodium borohydride, ascorbic acid or hydroxylamine in presence of surfactants. The growth of nanoparticles depends on several factors such as external surfactants, rate of reduction, nature of reducing agents and size of seed particles. In one of their experiments, Murphy and co-workers had found that presence of cationic surfactant $C_{16}TAB$ in controlled amount leads to the formation of gold nanorods. Subsequent development had enabled them to improve the yield from a mere 4 % to 90 % at controlled pH with aspect ratios 4.6, 13, 18.[65, 66] Mulvaney and co-workers pinpointed the actual parameters that control the growth of nanorods.[67] They found that binding of Au^{III} and Au^{I} ions into the cationic micelles present in the solution is the key phenomenon influenced by the local electrical double layer formation. The flux of solution-phase ions and micelles to the gold seed particle surface in the presence of this field increases with the local curvature and leads to the preferential growth at the tips. $AuCl_4^-$ can be reduced to Au^0 via two distinct pathways. Following reduction of $AuCl_4^-$ to $AuCl_2^-$ via reaction,

$$AuCl_4^- + 2e^- \leftrightarrow AuCl_2^- + 2Cl^- \qquad (1.2)$$
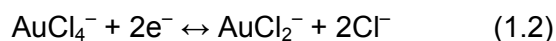
$AuCl_2^-$ may spontaneously disproportionate on the Au colloid surface (equation 1.3),

$$3AuCl_2^- \leftrightarrow AuCl_4^- + 2Au^0 + 2Cl^- \; ; \text{Equilibrium constant, } K_{eq} = 15.5 \times 10^7 \qquad (1.3)$$

or it may be discharged directly through the electron transfer at the surface of the electron rich seeds (equation 1.4).

$$AuCl_2^- + e^- \leftrightarrow 2Au^0 + 2Cl^- \qquad (1.4)$$
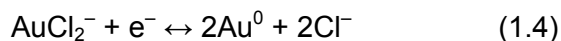
In presence of CTAB, disproportionation reaction (1.3) does not occur, because electron transfer occurs only at the electron rich surface of gold seed particles. As a result, reduction of Au^I in presence of CTAB takes place by:

$$AuCl_2^- –CTAB_{mic} + Au_m \leftrightarrow Au_{m+1} –CTAB_{mic} + CTAB_{mic} + 2Cl^- \qquad (1.5)$$

The zeta potential of CTAB micelles and CTAB-coated gold surfaces are both around +90 mV.[68] As the length of the surfactant tail, C_n, increases the yield and the aspect ratio of the nanorods also increase.[69] More recently, synthesis of gold nanorods with enhanced yields has been reported by the controlled addition of different amount of nitric acid.[70] Despite several such successes on gold nanorods synthesis, the growth

mechanism is still not well understood. A "zipping" mechanism is proposed based on different speculations and taking into account the van der Waals interactions between the tails within the surfactant bi-layer.[69, 71]

It has been demonstrated that growth of gold nanorods and thereby the aspect ratio can be altered by the addition of Ag^+ ion in a method which is essentially an extension of the earlier procedure as already has been discussed [section 1.5.1.1 (ii) in page 13]. Addition of a small amount of silver nitrate (5 x 10^{-6} M) induces and controls the rod-shaped morphology, while another additive cyclohexane substantially increases the aspect ratio of gold nanorods.[72, 73] Nevertheless, a fine tuning of the aspect ratio and yield of gold nanorods can be achieved by changing silver and gold ion concentration and using the appropriate choice of surfactants.[74]

(iii) Other Methods: There are few other methods that have been developed by modifications of earlier procedures either by minor variations of the chemical constituents or by changing reduction conditions of gold salt such as the use of photochemical methods. For example, gold nanorods have been synthesized by photochemical reduction method in presence of different amount of silver nitrate.[75] This approach confirms the assumption that one-dimensional gold nanostructures are formed through a combination of aggregation and specific crystal face stabilization due to the presence of silver ions.[76] A combination of chemical and photo-reduction accelerates the nanorod formation and Yamada and co-workers have found an increment of a factor around 60.[77] Similarly, gold nanorods are also synthesized on the surface of mica and glass by surface-bound seed techniques.[78] An interesting example of using block copolymers as capping/templating agent to synthesize gold nanowires and nanosheets (triangular nanoplates) has been demonstrated recently.[79]

Although different methods have been developed, the key factor which controls the 1D growth is the presence of appropriate growth directing surfactants. The most common surfactant is CTAB, which forms rod-shaped micelles in solution if a critical concentration is maintained [CMC of $C_{16}TAB$ is (4.8 ± 3) x 10^{-4} $molL^{-1}$].[68b] Generally, aspect ratio of the nanorods depends on the chain length of surfactants, as C_n of C_nTAB increases, the yield and aspect ratio of the nanorods also increase.[69] The growth of nanorods occurs via a slow reduction process; therefore, reducing agents also play a role in the

....

Physical and Materials Chemistry Division, National Chemical Laboratory   15

morphological evolution. Accordingly, reduction of gold salt by very slow reduction process, such as electrochemical reduction or ascorbic acid reduction is an important step. However, an increase in the ionic strength or increase in the solution temperature causes a decrease in the yield of rods.[80] The third growth controlling factor is the presence of silver ions as has been discussed earlier.[74]

Table 1.1: Different methods for the shape-selective synthesis of Au nanoparticles

Shape	Methods	Reducing agents and surfactants or growth directing agent	Aspect ratio (R) or size (nm) or yield	Ref.
Nanorods and Nanowires	(1) Template method	Electrochemical reduction, Alumina membrane in presence of PVP	Variable R, depends on deposition time	50
	(ii) Electrochemical method	Au as sacrificial anode (electrochemical reduction) in presence of CTAB and with or without Ag^+ ions	Adjustable R from 1 to 7	58b
	(iii) Seed mediated growth	(a) Ascorbic acid in presence seeds and CTAB as growth directing surfactant. (b) Aspect ratio can be controlled by adding Ag^+ ions.	R = 4.6, 13, 18	65, 72
Nanoprisms or Nanotriangles	Photo-induced conversion	Galvanic exchange reaction with silver nanoprisms	Depends on the size of silver nanoprisms and extent of reaction.	107, 108
	Biological synthesis	(a) Seaweed and (b) lemon grass extract	80 % yield	110, 111
	Chemical method	Citrate reduction in presence of PVP under refluxing conditions	Machinable quantity	121
Multipods	Chemical manipulation	(a) Judicious mixing of gold chloride, silver nanoplates, L-ascorbic acid, NaOH. (b) Controlled addition of $HAuCl_4$ to bis(p-sulfonatophenyl) phenylphosphine dehydrate dipotassium, hydrogen peroxide, sodium citrate.	-	133, 134
Star-shaped	Chemical manipulation	Judicious addition of $HAuCl_4$, PVP, L-ascorbic acid.	Thickness 25 nm, and variable sizes (83 ± 13, 93 ± 18, and 95 ± 21 nm)	137a

....

Physical and Materials Chemistry Division, National Chemical Laboratory   16

1.5.1.2 Silver

   Although most of the methods for the synthesis of silver nanowires are completely independent to that of methods for gold nanowires, few of them closely resemble. For example, synthesis of double and multiwalled silver nanotubes using template method has been demonstrated recently.[81] This method involves the photo reduction of $AgNO_3$ in a mixed solvent water and ethanol in presence of low-molecular-mass organogelators. Similarly, silver nanowires have been also synthesized in a special developer solution containing gelatin and $AgNO_3$ and by pulse sonoelectrochemical technique.[82] However, all these methods lack selectivity and suffer from low yield. The template methods using porous alumina membrane or self-assembled calix[4]hydroquinone, provide a unique way to control diameter by adjusting the pore size.[83] For example, Hong *et al*. have synthesized ultrathin single-crystalline silver nanowires using self-assembled calix[4]hydroquinone in an ambient solution phase.[84] These organic nanotubes of calix[4]hydroquinone form chessboard-like arrays of rectangular pores in aqueous phase, into which silver ions are introduced by soaking in $AgNO_3$ solution followed by reduction with ultraviolet irradiation. Similarly, nanowire synthesis from zeolite precursor by electron-beam induced growth method has been demonstrated.[85] Silver nanowires (40 nm diameter) have been also grown inside the pores of silica gel by introducing $AgNO_3$ followed by heat treatment.[86] However, synthesis by porous alumina membrane template offers greater flexibility with respect to diameter and length of nanowires. For example, Sauer *et al*. have synthesized highly ordered nanocrsytalline silver wires with diameter 30-70 nm by electrodeposition into the pores from silver sulfate salt in a solution of diammoniumhydrogencitrate at controlled pH of around 4.5.[87, 88] More recently, Rubinstein and co-workers applied alumina membrane template to synthesize silver nanotubes.[89] However, a more facile method involves the filling of membrane pores with colloidal silver nanoparticles followed by their spontaneous coalescence into nanotubes.[90] Similarly, capillarity of carbon nanotubes (CNTs) offers a unique template for the growth of metallic or semiconductor nanowires.[91] In this method, CNTs are filled with metal salt by capillary action followed by reduction of metal ions leading to the growth of nanowires inside the tube.[56, 92] The major disadvantage of the template method is the tedious reduction or deposition process and difficulty in removing the template, and in few cases higher diameter of the silver nanowires as compared to

nanowires synthesized by other methods. Interestingly, Kijima and co-workers have reported the synthesis of platinum, palladium, and silver nanotubes with inner diameters as small as up to 3-4 nm and outer diameters of 6-7 nm.[93]

Soft solution techniques provide more versatility with respect to ease of synthesis and controlling different factors and ability to manipulate synthetic conditions. However, this method also suffers from low yield and difficulty in separating nanowires from other shapes. For example, silver nanowires have been synthesized by reducing Ag_2O with 1,2-ethanedithiol (EDT) under microwave irradiation.[94] In one of such methods, silver nanowires have been synthesized by reduction of silver thiolate in polyol/toluene medium.[95] Silver nanowires can also be prepared by reducing $AgNO_3$ with L-ascorbic acid in the mixed surfactant solutions of CTAB and sodium dodecyl sulfate (SDS), where morphology of silver nanowires are found to be drastically influenced by concentration of ascorbic acid.[96] Similarly, reducing action of polypyrrole (PP) and DMF have been successfully utilized for the synthesis of Ag coaxial nanocables and nanowires assisted by PVP at room temperature.[97, 98] More recently, glucose and dextran reduction routes for the large scale synthesis of silver nanowires have been demonstrated.[99, 100]

The best known method for silver nanowires is polyol synthesis and was initially used for the synthesis of fine, highly pure, and monodispersed metallic particles (Ag, Au, Co, Ir, Ni, Pd, Pt, Ru etc.) of uniform shape. Liquid polyols such as diethylene glycol (DG) and ethylene glycol (EG) are used as both solvent medium and reducing agent.[101] Figlarz and co-workers initially demonstrated that silver particles with uniform size and shape can be prepared by adding $AgNO_3$ solution drop-wise to EG at 430-450 K in presence of PVP.[101f] Xia and co-workers extensively investigated the polyol synthesis of silver nanowires and established the critical role of nanoparticle seeds (Pt) in determining the morphological evolution.[102] EG serves as a good solvent for both $AgNO_3$ and PVP, because of its relatively high dielectric constant (37 at 293 K).[103] A typical polyol synthesis involves heating of anhydrous ethylene glycol (5 mL) at 433 K for 1 h and then simultaneous controlled addition of EG solutions containing appropriate amounts of $AgNO_3$ and PVP from two syringe pumps. The synthesis of nanowires can be accomplished in presence of little amount of $PtCl_2$ or its absence.[102a, b] PVP interacts more strongly with silver atoms on the {100} facets than those on the {111} facets, the differences is due to the variation in surface atom density, which controls the growth of

Ph. D. Thesis   *Chapter 1*   *University of Pune, May 2006*

----

nanowires.[53g]

1.5.2 Nanoprisms or Nanotriangles

1.5.2.1 Gold: The discovery and successive development of metallic triangular shaped nanoparticles, also known as nanoprisms, is relatively new compared to other shapes. Initially, Kirkland et al. have investigated the mechanistic aspect of trigonal lamellar particles of both gold and silver.[104] However, their method could produce trace quantities of gold nanoprisms only as byproducts. Later, Klasu et. al. reported the biological synthesis of silver-based crystals with sizes up to 200 nm in the *periplasmic* space of *Pseudomonas stutzeri AG259*, a bacterial strain that was originally isolated from a silver mine.[105] Similarly, gold nanoplates of different shapes had been synthesized using various capping polymers by UV-reduction method.[106] However, Mirkin and co-workers had carried out the systematic studies on metal nanoprisms by photoinduced conversion of silver nanospheres into nanoprisms for the first time.[25d] They extended this method to synthesize triangular nanoframes and nanoprisms made of gold by selective etching of silver nanoprisms with aqueous $HAuCl_4$ through galvanic exchange reaction (Figure 1.3).[107]

Xia and co-workers have reported a similar method for the synthesis of triangular gold nanorings by 'template-engaged' replacement reaction of silver nanoplate with aqueous $HAuCl_4$.[108] Interestingly, the synthesis of gold nanoprisms by biological approach has been demonstrated recently.[109, 110] Hexagonal, truncated triangular, and triangular nanoplates of gold have been obtained by the reduction of chloroaurate anions in water by seaweed extract, *Sargassum sp.* (brown seaweed). The yield of flat gold nanocrystals relative to the total number of nanoparticle formed under neutral pH (at room temperature) was around ~80-90%. Several factors, such as pH of the reaction mixture, reaction temperature, ageing time of the seaweed extract, initial reactant concentrations, and reaction time have been found to affect the nanoplate growth.

Several other methods, such as aspartate and salicylic acid reduction of gold chloride, microwave-assisted polyol reduction of $HAuCl_4$, photoreduction of $NaAuCl_4$ in presence of anionic phospholipids have also been developed.[111, 112] Kim et al. have demonstrated that under UV-reduction of chloroauric acid in presence of the block

....

Physical and Materials Chemistry Division, National Chemical Laboratory   19

copolymer poly(ethylene oxide)-poly(propylene oxide)-poly(ethylene oxide) (PEO_{20}-PPO_{70}-PEO_{20}) gives predominantly gold nanowires, while thermal reduction at 343 K gives only triangular nanosheets.[79] Similar investigations have been carried out for the synthesis of gold nanoplates with other polymers such as poly(vinyl alcohol), however with much lower yield.[113]
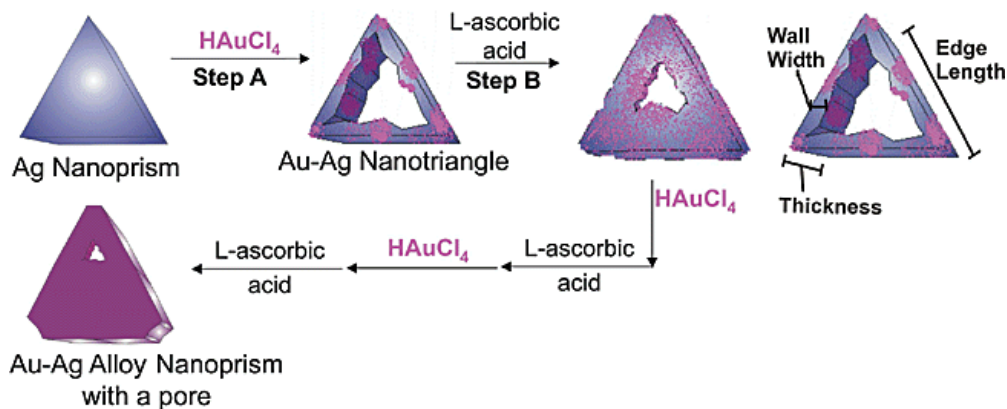
Scheme 1.3: Sacrificial template synthesis of nanoframes and nanoprisms of gold from silver nanoprisms. [Adopted from 107].

Gold nanoplates have also been synthesized by using ortho-phenylenediamine and linear polyethylene amine as shape directing and reducing agents.[114, 115] It has been suggested that concentration of reactants is an important factor for the high yield synthesis of nanoplates. However, a clear understanding of mechanistic details for the synthesis of gold nanoplates is not yet established. All such synthesis procedures lack coherence leading to many uncertainties about the factors actually controlling the shape-selective growth process. For example, addition of an appropriate amount of gold chloride (0.08 M) to a boiling ethylene glycol solution containing PVP (0.37 M) also leads to the formation of mixed tetrahedral, octahedral, decahedral, and icosahedral gold nanocrystals.[116] These face-centered-cubic (fcc) structures consist of mostly multiple twinned particles (MTPs).[117]

In general, metal nanoparticles tend to nucleate and grow into MTPs with their surfaces bounded by the lowest energy (111) facets, thereby making other morphologies with less stable facets more difficult to prepare.[118] The shape of an fcc nanocrystal is mainly determined by the ratio (R_r) of the growth rate along the [100] versus the [111]

----

direction. It has been observed that, tetrahedra and icosahedra bound by the most stable (111) will be formed when R_r is large ($\approx$ 1.73), while in other cases (R_r is less, $\approx$ 0.58) perfect cubes bounded by less stable (100) planes will form.[119] Generally, other morphologies with less stable facets are difficult to grow and can be kinetically achieved on addition of chemical capping reagents to generate directional
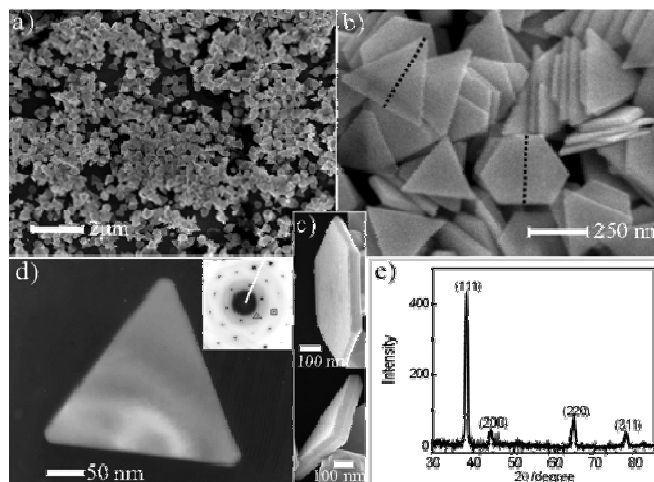
Figure 1.4: (a) Low and (b) high-magnification SEM images of gold nanoplates. (c) FE-SEM images of edges of individual hexagonal and triangular gold nanoplates. The inset shows a diffraction pattern of a triangular nanoplate. (e) XRD pattern of nanoplates. [Adopted from 121].

constraints.[120] This has been applied to synthesize machinable single crystalline triangular and hexagonal nanoplates by a judicious manipulation of surfactant (PVP) to metal ratio (0 to 8) and kinetic control of the reaction pathway (Figure 1.4).[121] Interestingly, a wise choice of reaction conditions to control the growth can also lead to various such structures as has been recently demonstrated by Murphy and co-workers.[122] The experimental methods involve the addition of an appropriate quantity of the Au seed solution to the aqueous growth solutions containing various quantities of cetyltrimethylammonium bromide ($C_{16}TAB$), $HAuCl_4$, ascorbic acid (AA), and in some cases a small quantity of $AgNO_3$.

1.5.2.2 Silver: The most widely studied nanoplates are of silver due to the ease of synthesis compared to other similar structures. For example, Mirkin and co-workers have developed the photoinduced conversion method for the preparation of silver nanoprisms (Figure 1.5).[25d] Typical synthesis procedure involves the initial preparation of

----

spherical silver nanoparticles by injection of $NaBH_4$ solution (50 mM) to an aqueous solution of $AgNO_3$ (0.1 mM) in the presence of trisodium citrate (0.3 mM). Bis(p-sulfonatophenyl) phenylphosphine dehydrate dipotassium salt solution (BSPP) (5 mM)

Figure 1.5: Schematic of photoinduced conversion of silver nanospheres to nanoprisms. [Adopted from 25d].

was subsequently added drop-wise to the solution as particle stabilizer. The silver nanoprisms were formed upon irradiation of the above system with a normal 40 W fluorescent light (350 to 700 nm). The method is also useful for the synthesis of relatively mono-dispersed nanoprisms with desired edge lengths in the 30 – 120 nm range by controlling the growth process using either dual-beam illumination or controlling wavelength.[123] Xia and co-workers have synthesized silver triangular plates by a method closely similar to that of photoinduced conversion technique using PVP as a surfactant.[124] This process also generates nanoplates whose edge lengths vary from ~30 to ~ 90 nm. Few other methods are ultrasound-assisted Ostwald ripening of spherical nanoparticles into nanoplates, synthesis in DMF, and polyethylene glycol.[125-127]

Several other soft solution based procedures have also been developed for the synthesis of silver nanoplates.[128] A combination of sodium borohydride and ascorbic acid reduction of silver nitrate in presence of sodium citrate and CTAB has been used for the synthesis of truncated triangular silver nanoplates.[129-131] Silver nanoplates of triangular and hexagonal shapes can be synthesized by reverse micellar process as well. For instance, Pileni and co-workers have used silver di(2-ethyl-hexyl) sulfosucinate [Ag(AOT)] and Na(AOT) in isooctane for the synthesis of nanoplates.[132]

Another interesting method is the thermal synthesis of nanoplates (Figure 1.6). Xia and co-workers have demonstrated that refluxing a solution containing Ag nanoparticles, which were prepared by $NaBH_4$ reduction of $AgNO_3$ in presence of PVP and sodium citrate, leads to the gradual formation of triangular nanoplates.[108, 133] Further

....

----

development of the thermal method has been done by Mirkin and co-workers and they could succeed synthesizing unimodal size distribution of nanoplates with good control over edge length.[134] Both photochemical and thermal methods give nearly monodispersed silver nanoprisms, however photochemical method needs longer time period for the completion of the conversion process.
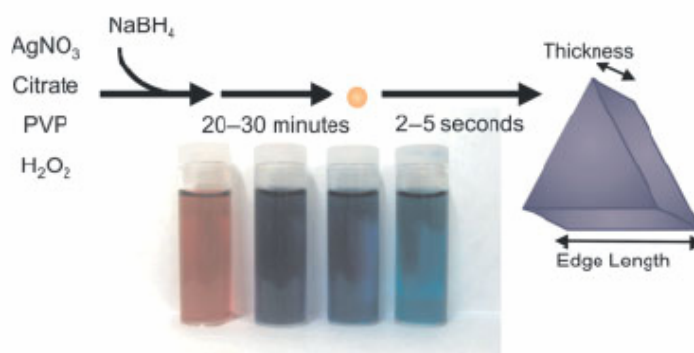
Figure 1.6: Schematic of thermal conversion of silver nanoparticles to silver nanoprisms. [Adopted from 134].

1.5.3 Other Shapes

There are various interesting structures with different properties that have been synthesized both for gold and silver. For example, Caroll and co-workers have synthesized monopod, bipod, tripod, and tetrapod gold nanocrystals by mixing aqueous CTAB, gold chloride, concentrated silver nanoplates, and L-ascorbic acid followed by rapid addition of NaOH solution (Figure 1.7).[135] Similarly, Schatz and co-workers have synthesized multipod structures by controlled addition of $HAuCl_4$ to a solution containing bis(p-sulfonatophenyl) phenylphosphine dehydrate dipotassium (BSPP), hydrogen peroxide, and sodium citrate under constant stirring.[136]

Several other architecturally controlled nanocrystals, such as star-shaped gold nanoplates, silver nanodisks, nanocubes, nanoscale hollow structures, and silver-gold bimetallic nanoshells bearing spikes have also been synthesized recently.[137] A typical procedure describes the addition of aqueous $HAuCl_4$ (0.1 mM) solution to a solution containing PVP (3 wt %) and then addition of freshly prepared aqueous L-ascorbic solution (2 equivalent) to the mixture at room temperature. On prolonged standing, the above reaction mixture generates star-shaped gold nanoplates (Figure 1.8). Minor

----

modifications of experimental conditions also have a dramatic effect on the morphology and give variety of structures. For example, gold nanocrystals with various structural architectures, such as star-shaped crystals, multi-pods, rods, rectangles, hexagons, cubes, triangles, icosahedra can be synthesized by minor variations of the experimental conditions.[116, 122] Similarly, silver nanodisks having diameter 36 ± 8 nm with thickness 9 ± 1.0 nm have been synthesized using carboxylate-functionalized polystyrene and CTAB.[138]
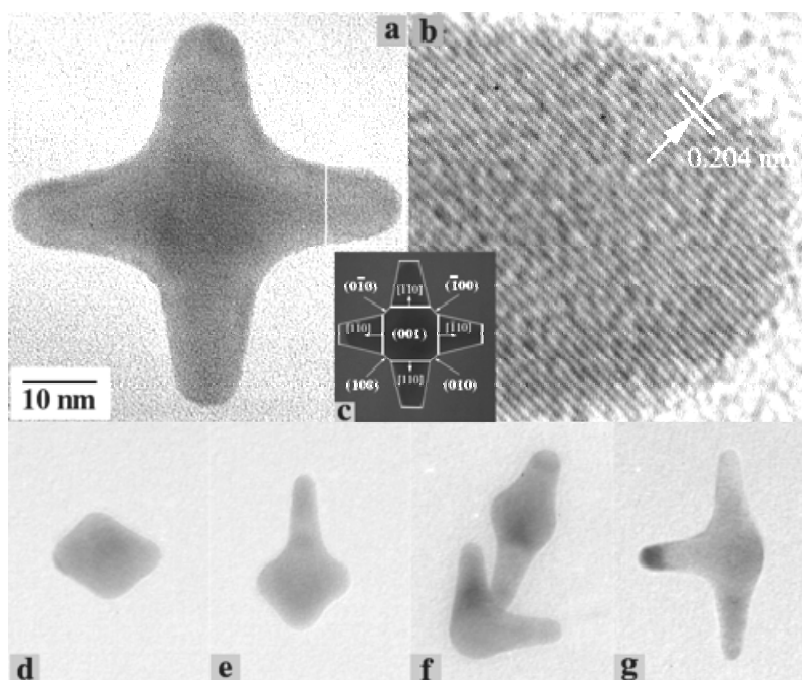
Figure 1.7: (a) TEM image of a tetrapod nanocrystal, and (b) high-resolution image of the end of one pod as marked by a white frame shown in panel a. (c) represents a schematic illustration of crystal planes and pod directions. The lower row of panels exhibits the particles developed at various stages: (d) embryo of diamond-like shape, (e) monopod, (f) L-type and I-type bipods, and (g) T-type tripod. [Adopted from 135].

Xia and co-workers have extensively investigated the polyol method and established that various architectures of silver and gold nanoparticles can be achieved by minor modifications of the experimental conditions.[102a, b] For example, when the concentration of $AgNO_3$ was increased by a factor of three and the molar ratio between the repeating unit of PVP and $AgNO_3$ was kept at 1.5; single-crystalline nanocubes of silver had been

obtained instead of nanowires.[139] These nanocubes had a mean edge length of 175 nm, with a standard deviation of 13 nm. These crystals were mainly bounded by [100] facets as had been confirmed by selected area electron diffraction (SAED) studies. Further, these nanocubes were used as sacrificial template to generate gold nanoboxes with a well-defined shape and hollow structure. The reaction takes place by the following trans-metallic reaction:

$$3Ag(s) + HAuCl_4 \text{ (ag)} \rightarrow Au(s) + 3AgCl(aq) + HCl(aq) \qquad (1.6)$$
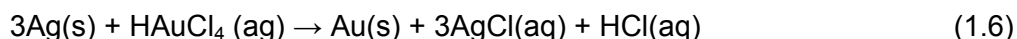
Table 1.2: Different methods for the shape-selective synthesis of Ag nanoparticles

Shape	Methods	Reducing agents and surfactants or growth directing agent	Aspect ratio (R) or size (nm) or yield	Ref.
Nanorods and Nanowires	Template method	Electrodeposition from silver sulfate on porous alumina membrane at pH 4.5	(a) 30-70 nm diameter and (b) controlled length and diameter	87, 88
		Filling of carbon nanotubes	Depends on extent of filling	92, 56
	Polyol method	Reduction of $AgNO_3$ by ethylene glycol in presence of PVP with (a) or without (b) Pt seeds.	Variable length and diameter	102a, b
Nanotubes	Template method	Porous alumina membrane as template		90
		Lyotopic mixed liquid crystals as template	Inner diameter 3-4 nm, outer diameter 6-7 nm	93
Nanoprisms or Nanotriangles	Photoche mical	Photo-induced conversion of spherical nanoparticles to nanoprisms	Edge length 30-120 nm	124a, 123b
	Chemical	Sodium borohydride reduction of silver salt in presence of sodium citrate and PVP	Edge length 30 – 90 nm	124
		Sodium borohydride and ascorbic reduction of silver nitrate in presence of sodium citrate and PVP	Truncated	129
	Thermal	Sodium borohydride reduction of silver nitrate in presence of sodium citrate and hydrogen peroxide	Good control over edge length	134
Nanocubes	Polyol method	Reduction of $AgNO_3$ by ethylene glycol	Edge length 175 nm	139

Tables 1.1 and 1.2 summarize the important synthesis procedures for different

....

Physical and Materials Chemistry Division, National Chemical Laboratory   25

shapes of gold and silver nanoparticles, respectively.
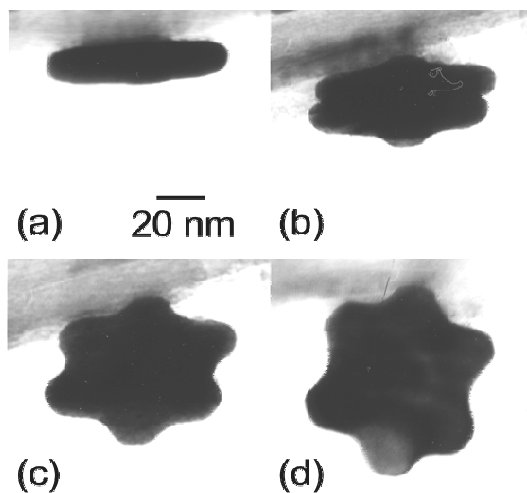
Figure 1.8: TEM image of a star-shaped nanoplate at different angles. [Adopted from 137a].

1.6 Mechanism of Anisotropic Growth

The standard explanation for such anisotropic particle growth in liquid media assumes that appropriate capping reagents kinetically control the growth rate of various facets of seed particle. For example according to Xia and co-workers, lowering the precursor concentration reduces the chemical potential for crystallization.[53g] Normally, the multiply twinned decahedra is the most thermodynamically stable structure, as it is bound entirely by the lower energy {111} facets (Figure 1.9).[117] Thus a manipulation of the precursor concentration enables one to decrease the chemical potential so as to synthesize MTPs (thermodynamically more stable) compared to kinetically stable single-crystals. Twin defects represent the highest energy site of MTPs, naturally undergoing energy minimization process by preferential crystallization of Ag atoms. This leads to the uniaxial elongation of the seed (decahedra) into pentagonal rod or wire, whose sides are bounded by {100} crystal facets. PVP present in the reaction mixture, preferentially binds the {100} sides rather than the {111} ends, allowing further deposition of Ag atoms at the ends. This process can further continue to grow longer silver nanowires.[140] Guyot-Sionnest and co-workers have elaborately investigated the growth of silver (I) assisted growth of gold nanorods and bipyramids.[141] Initial seeding process assisted by Ag^+ ions leads to the formation of single-crystalline particles, which finally grow into single

crystalline nanorods. Surfaces of these single crystalline particles are defects-free leading to the deposition of gold atoms over the seed surfaces with little or no stacking default. This is a unique property of silver(I) assisted growth of gold nanorods. This growth process is comparatively slower than the growth process without
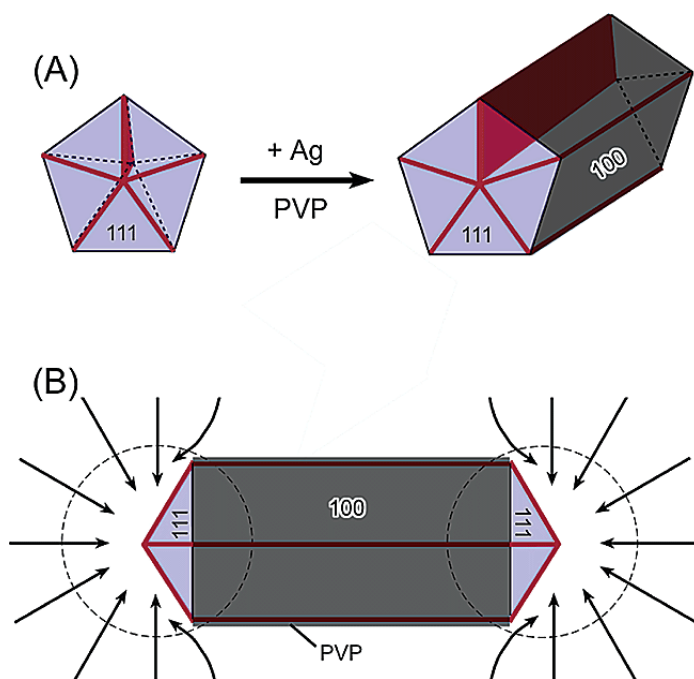
Figure 1.9: Schematic representation of the mechanism proposed to account for the growth of silver nanowires: (A) Evolution of a nanorod from a multiply twinned nanoparticle (MTP) of silver. The strong interaction between PVP and the {100} facets is indicated with a dark-gray color, and the weak interaction with the {111} facets is marked by a light-blue color. The red lines on the end surfaces represent the twin boundaries that can serve as active sites for the addition of silver atoms. (B) Schematic model illustrating the diffusion of silver atoms toward the two ends of a nanorod. [Adopted from 53g].

Ag(I). The slower growth rate in presence of Ag(I) allows Au atoms to be preferentially deposited at the most energy favorable fcc stacking series with no defects. However, they have also found that single-crystalline nanorod has its four side surfaces as {110} facets, which is energetically unfavorable [it is of higher energy facet compared to {100} and {111} facets] and rarely appear in gold nanocrystals.[73c] This can be explained by preferential underpotential deposition (UPD) of silver on certain surfaces. A metal submonolayer or monolayer can be deposited onto a different metal surface at a

----

potential significantly less negative than for bulk deposition, known as UPD.[142] The underpotential shift is proportional to the work function difference, which is in qualitative agreement with experimental results.[143] It is possible to have UPD of silver on gold favorable, since work function of silver is lower than that of gold by 0.5 eV. Interestingly, different surfaces have different work functions. For example, work function differences of various crystal planes of Au and Ag are 0.83, 0.85, and 0.57 eV for their (100), (110), and (111) crystal planes. Clearly, Au(110) plane is the preferred choice over other planes for the UPD of Ag$^+$ ions. These considerations lead to the expectation that the UPD shifts of silver on gold surfaces should be in the order (110) > (100) > (111). The reaction mixtures having ascorbic acid as reducing agent allows the formation of a

{111}   {100}   {110}
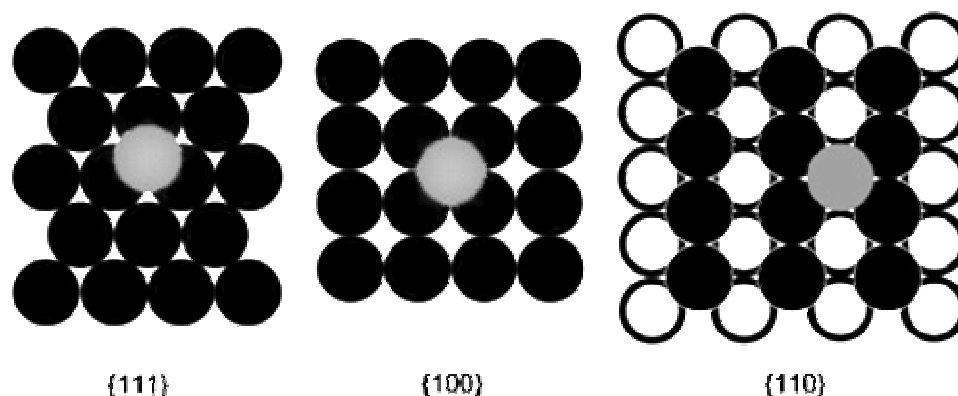
Figure 1.10: This schematic illustrates that an underpotential deposited silver atom (gray circles) has more nearest neighbors on a more open facet. For Au {111} facets, each silver atom has three nearest neighbors. For Au {100} facets, each silver atom has four nearest neighbors. For Au {110} facets, each silver atom has five nearest neighbors. The gold atoms of the first layer are represented by black closed circles. [Adopted from 141].

compact monolayer on the {110} facets of gold nanocrystals, since reduction potential of ascorbic acid is ca. 0.3 V higher than the bulk deposition of silver. Thus the silver monolayer over Au{110} acts as a strongly binding surfactant to protect the facet from further growth. Therefore, top of the nanorods (i.e., Au{100} facets) are only partially covered by silver, leading to the unusual one-dimensional growth along the [100] direction (Figure 1.10). The ratio of the growth rates between Au{100} and Au{110} is adjustable by varying the Ag(I) concentration.[141]

However, Murphy et al. have proposed a different mechanism for the growth of C$_n$TAB protected gold nanorods with a close resemblance to Xia's proposition relevant to

....

fcc metals.[12b, 53g] The mechanism suggests that C_nTAB can preferentially bind to certain crystal faces of the seed, or growing nanorod. C_nTAB can exist as rod-shaped micelles in solution if a critical concentration is maintained (critical micelle concentration, CMC), which was initially assumed as templates for the growth.[144] The tail contribution to the standard free energy of micellization for C_nTAB in aqueous solution has been estimated to be:

$$\Delta G^0 = 2.303(2 - z/j)RT(0.1128 - 0.3074n) \qquad (1.7)$$

where n is the number of carbon atoms in the surfactant tail; z is the charge on the micelle; j is the aggregation number of the micelle; R is the gas constant, and T is temperature. Based on this equation, they have calculated that free energy of bi-layer stabilization between C_nTAB surfactants is approximately 6 kJ/mol per two methylene groups, which is much higher than RT (~ 2.5 kJ/mol). This provides a vital clue to their "zipper" mechanism, since surfactants provide stabilization of growing nanorods through their tails (Figure 1.11). It has been observed that longer nanorods are formed with surfactants with a longer tail due to the higher stabilization.[69] They postulated that CTA^+ headgroup binds to the side faces with some preference. Such binding stabilizes the side faces, which have relatively large surface energy and stress (tension) compared to other faces. This allows Au atoms to deposit along the [110] common axis on {111} faces containing no CTA^+ headgroups and growing process can continue unless some external agents are used or the process gets exhausted.

More interestingly, Chen and co-workers have explained the growth of triangular or hexagonal nanoplate based on a mechanism emphasizing the selective adsorption of C_nTAB molecules on the different crystal planes of metals.[130] They assumed that if the basal plane is (111), the side or edge of the plate should be bound by (100) and/or (111) planes. If C_nTAB molecules exert stronger adsorption on (111) than that of the (100) plane and due to weak adsorption of CTAB on the other side plane, epitaxial growth can be controlled through the amount of seeds. However, Sigmund and co-workers have concluded that none of the above mechanisms can explain several other observations of anisotropic growth of metal nanoparticles, since neither the crystal-face poisoning model nor the physical constrain model can explain how the highly symmetric gold and silver fcc systems can form particles with lower symmetry.[145] All these models also fail to explain why the mixture of particle shapes that is produced or the fact that identical

....

Physical and Materials Chemistry Division, National Chemical Laboratory   29

shapes are produced in widely differing synthesis environments and techniques with or without organic capping agents. A mechanism based on strictly thermodynamic considerations can not explain such anomalies, while a new mechanism which is based on kinetics can explain in part several of such nanoparticle growth. This kinetic-based mechanism does not rely on the effect of a particular reaction environment on the crystal growth, so it can explain the appearance of anisotropic particles in many synthesis
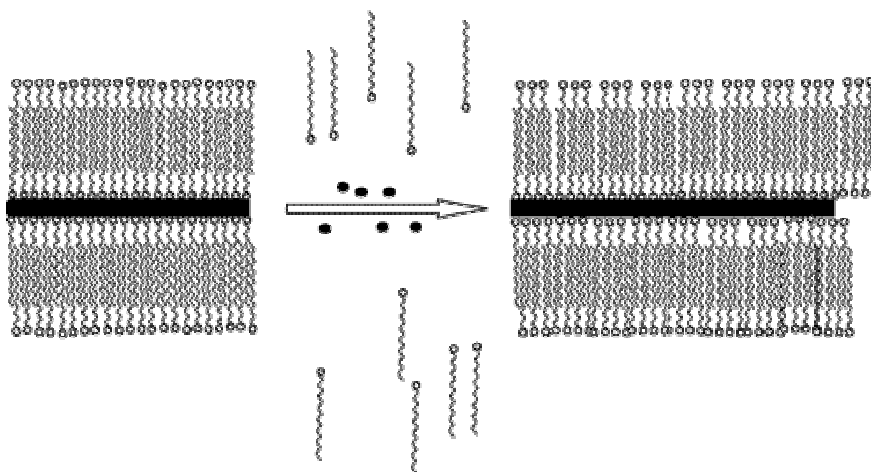
Figure 1.11: Cartoon illustrating "zipping" mechanism of gold nanorod formation. [Adopted from 69].

schemes and the variability of shape within a reaction scheme. The new mechanism was derived from the growth of silver halide particles in solution and relies on the presence of twin planes creating favorable sites for the addition of adatoms, leading to anisotropic growth. The mechanism for the growth of silver halide prisms is explained by the formation of twin planes on [111]-type faces. These twin planes readily form in silver halides, as well as in silver and gold, where the stacking fault energy is lower than most metals, decreasing the energy required to form a twin plane. These twined crystals form hexagonal-shaped nuclei because of the sixfold symmetry of fcc structure. At the six surfaces where the twin plane terminates, the stacking fault of the twin plane causes {111} faces to form in alternating concave and convex orientations, designated as "A-type" and "B-type" sides, respectively (Figure 1.12). The B-type side has limited stabilization energy and a new layer of adatoms can not form because they undergo dissolution back into solution making growth of the surface in this direction very slow. On

....

Physical and Materials Chemistry Division, National Chemical Laboratory   30

the other hand, A-type sides have higher stabilization energy due to the concave structure and therefore deposition of new layer is greatly accelerated. This makes the growth in one direction, because A sides are bounded on each side by slow-growing B sides in a crystal with a single twin plane, therefore, A sides quickly grow themselves out of existence, leading to the formation a triangular prism. This mechanism can be further extended to other similar anisotropic structures.
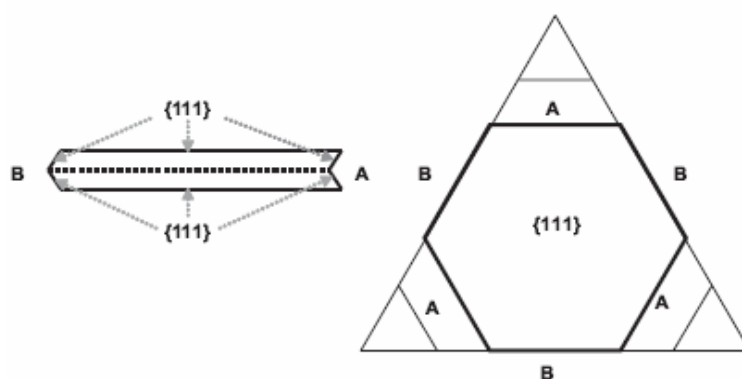
Figure 1.12: Silver halide model for a single twin plane. Alternating sides contain A-type and B-type faces. [Adopted from 145].

A relatively simple photoinduced crystal growth mechanism has been put forward by Mirkin and co-workers.[123a] The mechanism involves the bimodal growth process occurring through an edge-selective particle fusion, with four type 1 nanoprisms coming together in step-wise fashion to form a type 2 nanoprism as described in Figure 1.13.
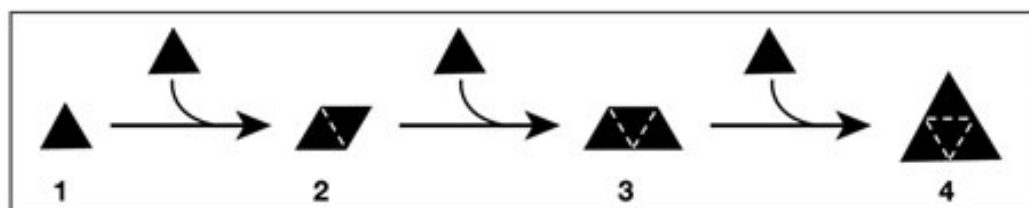
Figure 1.13: Schematic diagram of the light-induced fusion growth of Ag nanoprisms. [Adopted from 123a].

1.7 Characterization Techniques

To understand the properties of nanomaterials and correlate them with inherent structure, one needs to analyze several aspects of nanomaterials by a combination of

various characterization techniques. Following techniques are commonly employed to understand various properties of nanostructured materials in a more generalized way.

1.7.1 UV-visible Spectroscopy: It is well known that the intense color of colloidal noble metal particles is caused by the surface plasmon resonance. This surface plasmon resonance is a result of coherent motion of the conduction band electrons caused by their interaction with an electromagnetic field.[146] A dipolar oscillation is the result of such an interaction and when the frequency of the electromagnetic field becomes resonant with the coherent electron motion, a strong absorption in the spectrum is seen, which explains the origin of the observed color. Thus, UV-visible spectroscopy is one of the most common and fundamental technique to obtain useful information regarding size, shape and the degree of aggregation of nanoparticles.[11, 147] The frequency and width of the surface plasmon depend on the size and shape of the metal nanoparticle as well as on the dielectric constant of the metal itself and of the medium surrounding it.[146] For example, the UV-visible absorbance spectra of Au and Ag nanoparticles show a strong plasmon absorption band around 510-530 and 400-430 nm respectively depending upon the shape, size and capping layer, which decays exponentially into the visible region.[148] The surface plasmon absorbance peak is red shifted for Au NPs, while blue shifted for Ag NPs with increasing size along with concomitant increment in their peak full width at half maximum (FWHM).

The plasmon resonance is strongest and shifted into the visible part of the electromagnetic spectrum for the noble metals [copper, silver, and gold], while most other transition metals only show a broad and poorly resolved absorption band in the ultraviolet.[149] This difference can be attributed to the strong coupling between the plasmon transition and the interband excitation. The conduction band electrons of the noble metals can be well approximated by the Drude free electron model, which assumes that the conduction band electrons can be treated independently from the ionic background and can move "freely", whereas the ions only act as scattering centers.[150] Therefore, electrons in noble metals show higher polarizability, thereby shifting the plasmon resonance to lower frequencies and also giving rise to a sharp bandwidth. Experimentally size dependence is observed as the plasmon band is strongly dampened for small metal nanoparticles and even disappears completely for nanoparticles less

....

Physical and Materials Chemistry Division, National Chemical Laboratory   32

than about 2 nm. Very small nanoparticles in the size range below 2 nm are better treated as molecular clusters with discrete electronic states and the assumption of a delocalized free electron gas is no longer valid.

Similarly, high aspect ratio nanomaterials exhibit several shape dependent surface plasmon absorption peaks. The plasmon resonance for nanorods splits into two bands.[151] As the aspect ratio increases, the energy separation between the resonance frequencies of the two plasmon bands increases.[58a, 152] The high energy band corresponds to the oscillation of the electrons perpendicular to the major axis and is referred to as transverse plasmon absorption. The other absorption band, which is red-shifted to lower energies, is caused by the oscillation of the electrons along major rod axis and is known as the longitudinal surface plasmon absorption. The absorption band is sensitive to the aspect ratio and can be seen in the entire visible to the near-IR region by increasing the aspect ratio for gold nanorods. Similarly, triangular nanoparticles have several resonances (more than five distinct resonances) for each illumination direction.[30b] The spectral range covered by these different resonances becomes very large, giving rise to distinct colors.

1.7.2 Transmission Electron Microscopy (TEM): In transmission electron microscopy (TEM), a thin specimen is illuminated with electrons in which the electron intensity is uniform over the illuminated area.[153] As electrons travel through the specimen, they are either scattered by a variety of processes or they may remain unaffected. The net result is that a non-uniform distribution of electrons emerges from the exit surface of the specimen that contains all the structural information about the specimen. Electron microscope is constructed to display this non-uniform distribution of electrons in two different ways: (i) angular distribution of scattering can be viewed in the form of scattering patterns in the reciprocal space, usually called diffraction patterns, commonly referred to as SAED and (ii) spatial distribution of scattering can be observed as contrast in images of the specimen.

Transmission electron microscopy is indispensable for characterization of nanocrystal materials, particularly when particle shape is important.[119a, 154] The particle shapes are closely related to the crystallographic surfaces that enclose the particles.

The {111}, {100}, and possibly {110} surfaces of face-centered cubic structured metal particles, for example, are different not only in surface atom densities but also the electronic structure, bonding, and possibly chemical activities. TEM is likely to be very powerful as a versatile tool that provides not only atomic resolution lattice images but also chemical information at a spatial resolution of 1 nm or better, allowing direct identification of the chemistry of single nanocrystal. With a finely focused electron probe, the structural characteristics of a single nanoparticle can be fully characterized. For example, Wang has illustrated the usefulness of TEM to explain the crystal structure of nanorods and several other such structures.[119a] Accordingly, almost all Au nanorods are single crystalline and contain no twins or dislocations. When the liquid droplet, containing the suspended Au nanorods is dispersed onto a flat carbon substrate, the nanorods will be preferentially aligned and oriented along [110] perpendicular to the substrate (Figure 1.14). This is possible only if the nanorods have {110} facets. A dark field TEM image recorded using a {111} reflected beam when the rod is oriented nearly parallel to the [110] direction gives the thickness fringes owing to thickness variation across the specimen. The intervals between the fringes would have an equal distance if the nanorods are bound only by four {100} facets and axial growth direction is [001]. Several other structures such as nanoprisms, nanowires can be fully characterized by similar approach.
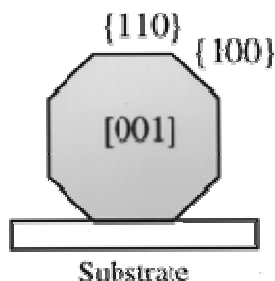
Figure 1.14: The cross-section of an Au nanorod on the substrate. [Adopted from 119a].

TEM is unique for characterizing the *in situ* structural evolution of nanocrystals resulting from annealing, electric field, or mechanical stress, such as imaging a single nanowire when a mechanical or electrical measurement is being carried out *in situ*. Further, high resolution TEM (HRTEM) studies are also useful to investigate the

....

Physical and Materials Chemistry Division, National Chemical Laboratory   34

faceting, crystallinity and ordering in nanocrystals.[155] Interestingly, various complex structures, like spherical to rod like transformation or vice versa and chain melting, can be studied *in-situ* in a TEM chamber, if suitable capping agents are selected.[119a] Thus TEM coupled with SAED can provide important information on the crystallographic directions in the structures, helpful to understand the growth kinetics.[156]

1.7.3 Scanning Electron Microscopy (SEM): Scanning electron microscope (SEM) is based on thermoionic emission of electrons (energy ranging from a few hundred eV to 50 keV) from a tungsten or lanthanum hexaboride (LaB_6) cathode or by field emission (FE).[157] These electrons are then projected towards an anode. Tungsten is used because it has the highest melting point and lowest vapour pressure of all metals. As the primary electrons strike the surface they are inelastically scattered by atoms in the sample.

The most common imaging mode monitors low energy (< 50 eV) secondary electrons. The electrons are detected by a scintillator-photomultiplier device and the resulting signal is rendered into a two-dimensional intensity distribution that can be viewed and saved as a digital image. Characteristic X-rays, which are also produced by the interaction of electrons with the sample, can also be detected in an SEM if it is equipped for energy dispersive X-ray spectroscopy (EDX) or wavelength dispersive X-ray spectroscopy (EDS). EDX or EDS is a method used to determine the energy spectrum of X-ray radiation using a semiconductor silicon drift or a silicon crystal doped with lithium (Si-Li) detector. Various drawbacks are: (1) elements below C in the periodic table cannot be detected, (2) the technique cannot be used for precise detection of elements below Na.

1.7.4 X-ray Diffraction (XRD): The atomic planes of a crystal cause an incident beam of X-rays (if wavelength is approximately the magnitude of the interatomic distance) to interfere with one another as they leave the crystal. If an incident X-ray beam encounters a crystal lattice, general scattering occurs. Although most scattering interferes with itself and is eliminated (destructive interference), diffraction occurs when scattering in a certain direction is in phase with scattered rays from other atomic planes. Under this condition the reflections combine to form new enhanced wave fronts that mutually reinforce each other (constructive interference). Crystals diffract X-rays in a unique

characteristic pattern, because each crystalline material has a characteristic atomic structure. For a given set of lattice planes with an inter-plane distance of d, the condition for a diffraction (peak) to occur can be simply written as the Bragg's law:

$$2d \sin\theta = n \lambda \qquad\qquad (1.8)$$

where, λ is the wavelength of the X-ray, θ the scattering angle, and n an integer. These energetic X-rays (100 eV-100 keV) can penetrate deep into the material and provide information about the structural arrangement of atoms and molecules.[158] Common targets used in X-ray tubes include Cu and Mo, which emit 8 keV and 14 keV X-rays with corresponding wavelengths of 1.54 Å and 0.8 Å, respectively.

The crystallinity and particle size of NPs are often experimentally determined by X-ray diffraction.[159] XRD has been recently used to characterize Ag or AuAg alloy NPs superlattices, where the effect of temperature and the length of the capping molecules are investigated with several other complementary techniques.[160] Further, particle or grain size can be calculated by using Scherrer equation:[158]

$$t = \frac{0.9\lambda}{B\cos\theta_B} \qquad\qquad (1.9)$$

where, B is the width, usually measured in radians, at an intensity equal to half the maximum intensity (FWHM) in terms of 2θ, and t is the thickness (particle size).

1.7.5 Scanning Probe Microscopy (SPM): The scanning probe microscopes (SPM) have enormous applications for characterizing nanoparticles due to their atomic level resolution capability.[161] Like high-resolution electron microscopy, these techniques also have facilities for direct imaging of structures. For example, The STM is a non-optical microscope which employs principles of quantum mechanics. An atomically sharp probe (the tip made of Pt-Ir, Pt-Rh alloys etc.) is moved over the surface of the material under study, and a voltage (~ 1 V) is applied between probe and the surface. Depending on the voltage electrons will tunnel or jump from the tip to the surface or vice-versa depending on the polarity, resulting in a weak electric current. This current is exponentially dependent on the distance ($\leq$ 10Å) between probe and the surface.[162] STM

....

Physical and Materials Chemistry Division, National Chemical Laboratory   36

experiments can be carried at either in (a) constant current or (b) constant height mode, whereas the samples for STM should have few desirable criteria such as (1) good electrical conductivity, (2) atomically flat surface and (3) limited surface mobility. Figure 1.15A shows block diagram of a typical STM.

Although limitations, like tip-induced artifacts and the possibility of monolayer damage, can complicate the interpretation, it has certain unique capabilities such as I-V measurements to provide local density of states (STS techniques) offering several powerful benefits. For example, apart from imaging, STS is a crucial tool to study the electrical properties of nanoparticle, which reveals the single electron charging features of smaller sized spherical particles (Coulomb blockade behaviour).[9b] However, the scanning probe microscopy data are to be interpreted carefully, because of the possibility of monolayer damage by tip.

Another similar technique is Atomic Force Microscope (AFM) used to measure the surface height profile as a function of distance, where a cantilever tip attached to a spring is dragged across the sample. AFM (Figure 1.15B) operates by measuring attractive or repulsive forces between a tip and the sample (Binnig et al., 1986). The force between the tip and the sample surface is very small, usually less than 10^{-9} N. The detection system does not measure force directly. In its repulsive "contact" mode, the instrument lightly touches a tip at the end of a leaf spring or "cantilever" to the sample.

As a raster-scan drags the tip over the sample, some sort of detection apparatus measures the vertical deflection of the cantilever, which indicates the local sample height. Thus, in contact mode the AFM measures hard-sphere repulsion forces between the tip and sample. In non-contact mode, the AFM derives topographic images from measurements of attractive forces; the tip does not touch the sample (Albrecht et al., 1991). Tapping mode is a key advance in AFM. Tapping mode imaging is implemented in ambient air by oscillating the cantilever assembly at or near the cantilever's resonant frequency using a piezoelectric crystal. The piezo motion causes the cantilever to oscillate with a high amplitude (typically greater than 20 nm) when the tip is not in contact with the surface. During scanning, the vertically oscillating tip alternately contacts the surface and lifts off, generally at a frequency of 50,000 to 500,000 cycles per second. Subsequent systems were based on the optical techniques. In the beam-

bounce method an optical beam is reflected from the mirrored surface on the back side of the cantilever onto a position-sensitive photodetector. A third optical system uses the cantilever as one of the mirrors in the cavity of a diode laser. Motion of the cantilever has a strong effect on the laser output, and this is exploited as a motion detector.
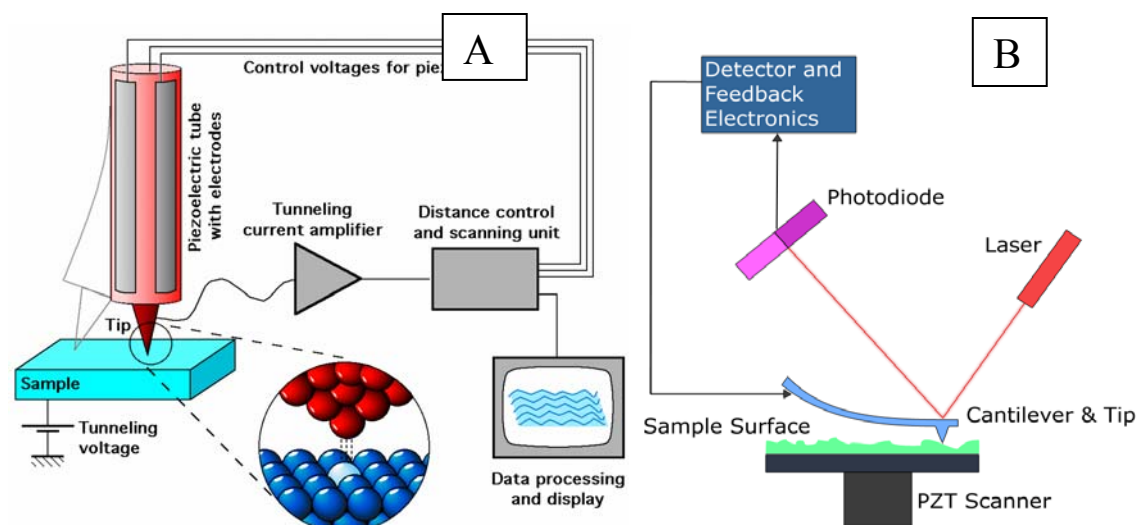
Figure 1.15: Block diagrams of scanning tunneling (A) and modern atomic force microscopes (B). [Adopted from 161(i)].

It is interesting to compare AFM and its precursor -- Scanning Tunneling Microscope. In some cases, the resolution of STM is better than AFM because of the exponential dependence of the tunneling current on distance. The force-distance dependence in AFM is much more complex when characteristics such as tip shape and contact force are considered. STM is generally applicable only to conducting samples while AFM is applied to both conductors and insulators and is a versatile tool. Furthermore, the AFM offers the advantage that the writing voltage and tip-to-substrate spacing can be controlled independently, whereas with STM the two parameters are integrally linked. AFMs can achieve a resolution of 10 pm, and unlike electron microscopes, can image samples in air and under liquids.

Several other force microscopes, including Magnetic Force Microscopes (MFM), Magnetic Resonance Force Microscopes (MRFM) Lateral Force Microscopes (LFM) and

Near-field Scanning Optical Microscopes (NSOM), are also widely used to investigate nanostructures.[161, 163] For example, in MFM a magnetic tip is used to probe the magnetic stray field above the sample surface to sense the deflection of the cantilever for imaging.[161] Accordingly, MRFM, LFM and NSOM are extended version of atomic force microscopy, having greater capabilities of imaging three-dimensional subsurface entities of a broad range of materials with chemical specificity and atomic resolution.[161, 163]

1.7.6 Conductivity Measurements: There are various methods for electrical (I-V) characterization, which are applicable to single crystalline as well as polycrystalline materials. Two basic methods are used for I-V characterization namely, 2-point probe and 4-point probe methods, respectively. Schematic representation of 4-point probe used in our study is shown in Figure 1.16. Resistivity, thus obtained also includes contact resistance, which is appreciable in case of semiconductors. Using 2-point probe, if the specimen cross-section is uniform, it can eliminate the effect of contact resistance. However, one needs to keep current low enough to prevent heating of the sample. Also,
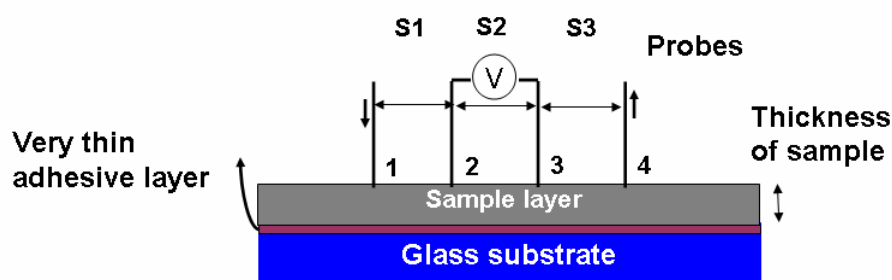
Figure 1.16: Schematic representation of 4-point probe method (home built).

the voltmeter must have high input impedances (above 10^{13} ohms) and measurements must be made far enough away from the contacts so that any minute carriers injected will have already recombined. The 4-point probe is preferable over a 2-point probe because the contact and the spreading resistance associated with the 2-point probe cannot be measured. This means that the true sheet resistance cannot be accurately separated from the measured resistance. The 4-point probe consists of two current carrying probes (1 and 4), and two voltage-measuring probes (2 and 3). Since very little contact and spreading resistance are associated with the voltage probes, one can obtain

----

a fairly accurate calculation of the sheet resistance, which is then used to calculate the resistivity. The resistivity (p) of a semi-infinite sample layer with equal probe spacing (s) is given by:

$$p = 2 * \pi * s * V/I \text{ , where } s = s_1 = s_2 = s_3 \qquad (1.9)$$

Since films of samples on various substrates are not semi-infinite in extent and may contain defects, a combination of correction factors must be multiplied by the right hand side of this equation.[164]

1.7.7 Electroanalytical Techniques: Several electroanalytical techniques, like voltammetry, impedance and chronoamperometry, are routinely used to study the electrochemical properties of nanoparticles and their assemblies.[165] Some of the most widely used techniques for NPs are cyclic and differential pulse voltammetry (CV and DPV respectively), where the current responses is monitored either applying a potential ramp (CV) or a differential of tiny potential pulse (DPV) and is plotted against the applied potentials. Since DPV allows discrimination between the faradaic and charging currents, it is more advantageous for measuring faradic current as compared to that of CV. Further, both the CV and DPV have been utilized to assess their single electron charging features in solution, which is often comparable with STM based measurements. However, adequate precautions have to be taken with the cleanliness of the electrode surface and with monolayer stability under electric field in order to get correct information.

1.7.8 Thermogravimetric and Differential Scanning Calorimetric (TG/DSC) Measurements: Valuable information regarding the thermal stability as well as the stoichiometry of NPs is obtained from TG analysis, whereas DSC is particularly useful to understand the change of orientations of monolayer upon heating. For example, TG results of alkanethiol protected Au NPs reveal stability up to 180-250 °C despite a slight increase with increasing the chain length.[166] The melting of alkanethiol monolayer of NPs is effectively characterized by DSC. For example, phases of Au NPs studied in the temperature range of –100 °C to 100 ^{o}C show that for smaller chains ($\leq$ C_8-thiolate NPs) no phase transition is observed, while for C_{12} and C_{16}-thiolate NPs a broad endotherm is seen, where the phase transition temperature increases with increasing chain lengths.[167]

1.7.9 Fourier Transform Infrared Spectroscopy (FTIR):   The capping monolayer surrounding NPs and its nature, i.e., orientation, packing and density are generally characterized by FTIR spectroscopy. Detailed information about the packing and the functional groups can, in principle, be obtained with polarized light, since the absorption in the vicinity of a molecular vibration frequency is dictated by the relative orientation of the electric field and the dipole transition moment.

FTIR studies have shown that alkanethiol chains are typically in all-trans, zig-zag configuration in two dimensional (2D) SAMs, while apart from all-trans configuration, significant (5.25%) gauche configurations at both inner and terminal chain ends are also present for solid-state nanoparticle films.[168]

1.7.10 X-Ray Photoelectron Spectroscopy: Significant qualitative and quantitative information about the chemical state of elements present in nanoparticles can be obtained from XPS analysis. X-ray photoelectron spectroscopy (XPS) is based on the well-known photoelectric effect (a single photon in/electron out process) first explained by Einstein in 1905.[169] Photoelectron spectroscopy uses monochromatic sources of radiation (i.e. photons of fixed energy given by the relation, E = $h\nu$).[170] In XPS the photon is absorbed by an atom in a molecule or solid, leading to ionization and the emission of a core (inner shell) electron. The kinetic energy distribution of the emitted photoelectrons (i.e. the number of emitted photoelectrons as a function of their kinetic energy) can be measured using any appropriate electron energy analyzer and a photoelectron spectrum can thus be recorded.

Employing photons with fixed energy $h\nu$, and if kinetic energy KE and work function ϕ of the sample are measured, it is possible to measure binding energy of electron in a solid. Binding energies being characteristic of atoms, different elements present in the sample under investigation can be easily identified. However, beam-induced damage and carbon contamination from XPS chamber are few limitations of XPS, thus necessitates the need for complementary information from other independent techniques.[171]

1.7.11 Other Characterization Techniques: Apart from these techniques, several other special characterization techniques, such as He, electron and neutron diffraction, surface plasmon spectroscopy (SPS), Raman spectroscopy, magnetoelectrochemistry,

secondary ion mass spectroscopy (SIMS), electron energy loss spectroscopy (EELS), and scanning electrochemical microscopy (SECM), have been applied for investigations of nanoparticles.[172] For example, EELS analysis on the centre regions of the silver nanorods demonstrates that the Ag-$M_{4.5}$ peaks shift to lower energy in comparison with results from the Ag crystal.[154]

1.8 Properties

Nanostructured materials exhibit size and shape dependent properties. However, gold and silver nanoparticles are mainly known for their distinct and variable optical properties. Accordingly, following section describes few of such properties, especially optical properties of high aspect ratio nanomaterials have been explained elaborately.

1.8.1 Optical Properties

1.8.1.1 Metal Nanorods and Nanowires: In general, spherical silver and gold nanoparticles have single plasmon absorption bands (SPBs) at ca. 400 and ca. 520 nm, respectively.[173] However, the SPB is absent for Au NPs with core diameter less than 2 nm, as well for bulk gold. For Au NPs of mean diameter of 9, 15, 22, 48, and 99 nm, the SPB maximum has been observed at 517, 520, 521, 533, and 575 nm, respectively, in aqueous medium. Other factors which strongly influence the SPB are particle shape, dielectric constant of the medium, temperature, and core or surface charge.[173a] We will discuss, however, only the optical properties of anisotropic nanostructures of gold and silver. For example, gold and silver nanorods have two principle plasmon absorption peaks; one at shorter wavelength corresponding to absorption and scattering of light along the short axis of the nanorod (transverse plasmon band), and the other band at longer wavelength corresponding to the long axis of nanorod (longitudinal plasmon band).[11] The transverse plasmon band is not that much sensitive towards the aspect ratio (fix absorption band at ca. 520 nm), while the longitudinal plasmon absorption bands are tunable with nanorod aspect ratio from the visible to the near-IR (Figure 1.17).[25a] Consequently, the color of solutions containing nanorods (e.g. Gold) sharply depends on aspect ratio (Figure 1.8).[80] A linear relationship between longitudinal surface plasmon peak position and aspect ratio is observed for gold nanorods.[67] In sharp

....

Physical and Materials Chemistry Division, National Chemical Laboratory   42
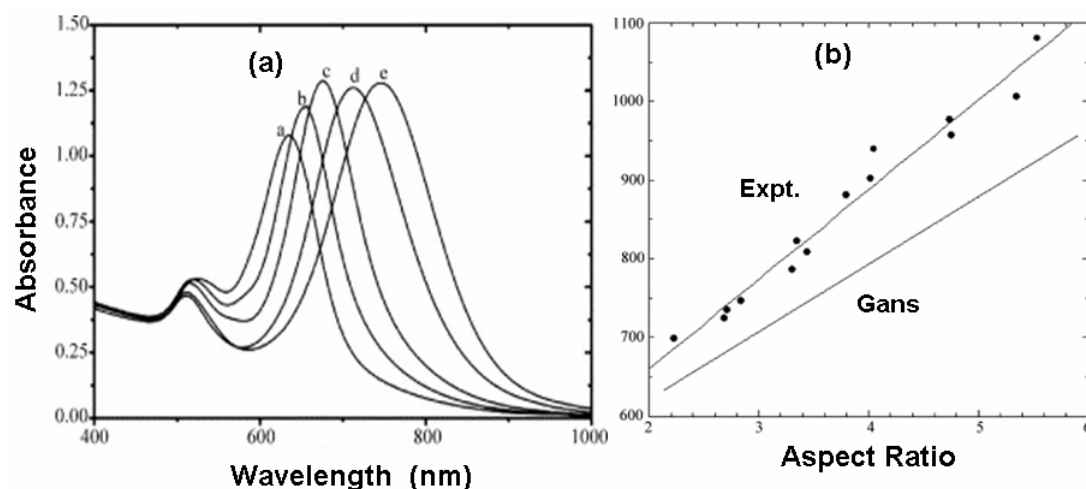
Figure 1.17: (a) UV-visible spectra of Au nanorods. (b) Experimental and theoretical plot of the surface plasmon longitudinal band position vs. aspect ratio for pure gold rods in water. [Adopted from 67, 74b].

contrast, SPB of silver nanowires does not vary prominently as compared to that of gold nanorods; however, it is sensitive to different morphologies.[174] Interestingly, as the aspect ratio exceeds 5, the plasmon absorption corresponding to longitudinal oscillations
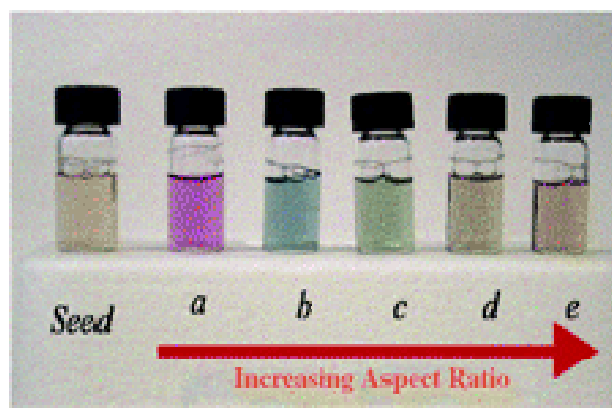
Figure 1.18: Photographs of aqueous solutions of gold nanorods of various aspect ratios. [Adopted from 12b].

is not observed for silver nanorods.[101a, 175] However, the SPR band splits into two peaks at 410 and 530-570 nm corresponding to the transverse and longitudinal plasmon resonance, respectively for low aspect ratio nanorods.[53g] It has been demonstrated that on increasing the aspect ration beyond 5, the longitudinal plasmon peak at 570 nm

disappears and the transverse peak marginally blue shifts (410 → 380 nm) to higher energy with an increase in intensity. The peak at 380 nm is usually considered as the optical signature of high aspect ratio silver nanowires. The appearance of bulk silver absorption at 350 nm has also been reported for silver nanowires with aspect ratio exceeding 5.[176]

1.8.1.2 Metal Nanoprisms or Triangular Nanoplates: The purified sample of gold nanoprisms in solution with average edge length 144 ± 30 nm and thickness 7.8 ± 0.5 nm exhibits an in-plane quadrupole band at 800 nm and an in-plane dipole absorption band at 1300 nm respectively. However, it has been observed that both these absorptions are strongly dependent on the edge length and thickness of the nanoplate.[177] Several absorption peaks corresponding to different excitations have been observed for truncated and sharp edged nanoprisms. For example, silver prisms with thickness 24 nm, edge length 68 nm, and overall degree of truncation 0.35 exhibit two absorption peaks at 552 and 465 nm corresponding to in-plane dipole and in-plane quadrupole resonances, respectively. Similarly, out-of-plane dipole and quadrupole absorptions have been observed at 431 and 351 nm respectively.[129] Whereas, for sharp edged prisms only three absorptions maxima are observed corresponding to in-plane dipole (670 nm), in-plane quadrupole (470 nm), and out-of-plane quadrupole (340 nm) absorptions.[121a] All such optical characteristics has been supported by the theoretical calculations based on discrete dipole approximation.[10]

1.8.1.3 Nanocubes, Nanoshells and Star-shaped Metal Nanoplates: Xia and co-workers have investigated the optical properties of silver nanocubes.[124, 139] Silver nanocubes with average edge length 80 nm show surface plasmon bands at 350, 400, and 470 nm respectively. On increasing the edge length to 175 nm, these three SPR peaks were found to be red-shifted to 370, 438, and 560 nm. Interesting optical properties for 9 nm thick silver nanodisks (diameter 36 nm) have been observed.[138a] A solution of such nanodisks exhibits several absorption peaks corresponding to out-of-plane quadrupole (340 nm) and in-plane quadrupole (430 nm) and dipole (574 nm) respectively. These SPR peaks are in close agreement with theoretical values calculated

....

Physical and Materials Chemistry Division, National Chemical Laboratory   44

by DDA approximation (Figure 1.19). However, appearance of an additional peak at 470 nm has not been clearly understood, though, assumed to be due to the aggregation. More interestingly, SPR property can be fine tuned by controlling the morphology and local dielectric environment as has been demonstrated for gold nanoshells synthesized
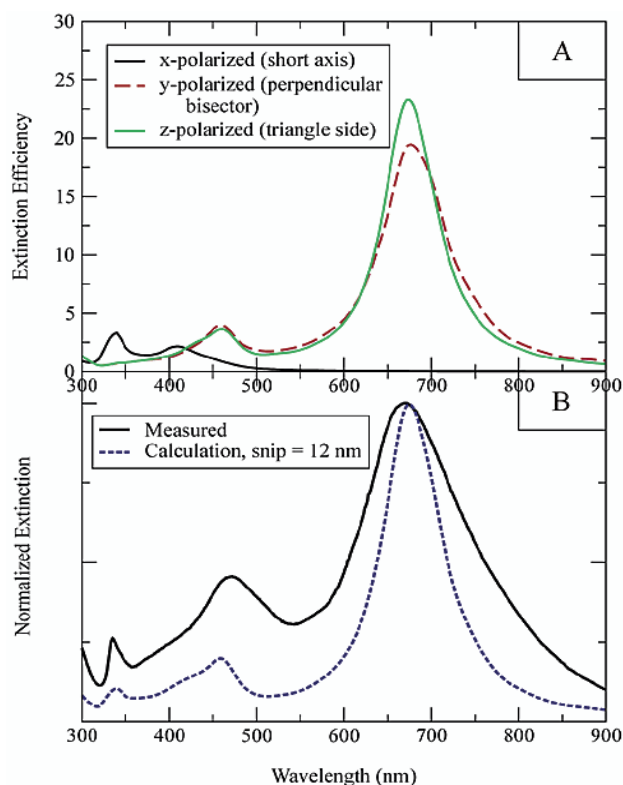
Figure 1.19: Experimental and theoretical UV-visible spectra of trigonal Ag prisms with side length = 100 nm, snip = 10 nm, and thickness = 16 nm. [Adopted from 10].

by template-engaged replacement reaction.[137b, e] These nanoshells exhibit interesting SPR absorptions at 720 nm, which is greatly red-shifted from the SPR peak of spherical nanoparticles. This peak is sensitive to the thickness of the nanoshells, indicating contribution of dielectric medium on scattering of electrons from the walls. Upon increasing the thickness of the shell-wall by deposition of additional gold, this peak was blue-shifted to 560 nm with a concomitant color change from dark blue through purple to pink.[124] A summary of the optical properties of different high aspect ratio nanoparticles of gold and silver is given in Table 1.3.

Table 1.3: Optical properties of gold and silver nanoparticles of different shapes

Gold			Silver		
Shape, size (nm) or aspect ratio (R)	**SPR band (nm)**		**Shape, size (nm) or aspect ratio (R)**	**SPR band (nm)**	
Spherical[147b] (R =1, < 20), (Size: 9, 22, 48, 99)	520 (517, 521, 533, 575)		**Spherical**[173b] R = 1	370 – 430 (usually depends on size, dielectric environment)	
Nanorod[58a] R = 1.8 3 5.2	transverse 520 520 520	longitudinal 600 710 873	**Nanowires**[53g] R < 5 R > 5	transverse 410	Longitudinal 530 - 570
Nanoprisms[177] Edge length 144 ± 30 Thickness 7.8 ± 0.5	in-plane 800 (quadrupole) 1300 (dipole)	out-of-plane	**Nanoprisms**[25d] Edge length 100 nm (sd. 15 %)	in-plane 470 (quadrupole) 670 (dipole)	out-of-plane 335-340 (quadrupole)
			Nanoprisms[129] (truncated) Thickness 24 nm Edge length 68 nm Degree of truncation 0.35	465 (quadrupole) 552 (dipole)	351 (quadrupole) 431 (dipole)
Star-shaped nanoplate[137f] 100 nm	Several polarization dependent scatterings from different tips (extended up to NIR-region) Strong absorptions at 647, 700, and 783		**Circular Nanodisk**[138a] Thickness 9.0 ± 1.0 Diameter 36 ± 8 nm	in-plane 574 (dipole) 470 (origin of this peak is not known)	out-of-plane 340 (quadrupole) 430 (dipole)
Nanoshell[124] Core diameter 25	Follows the equation: $\lambda_{max} = 503 + 363/t$ (t = wall thickness, in nm) 720 (t = 1.65) 685 (t = 2)		**Nanocubes**[124] Edge length 80 nm Edge length 175	350, 400, 470 370, 438, 560 (red-shifted with thickness)	

1.8.2 Mechanical Properties

Nanoscale materials exhibit mechanical properties different from their bulk counterpart. For example, the apparent elastic modulus of the smaller diameter metallic nanowire is significantly higher than that of the larger one.[178a] Similarly, micrometer-sized whiskers and nanowires have ultrahigh strength compared with that of their bulk counterparts, which are important for the applications in nanocomposites and probe microscopy.[178b, c] This effect is apparently attributed to a reduction in the number of defects per unit length compared with larger structures. Segall et al. have theoretically investigated the elasticity of nanowires which are defined in terms of physical
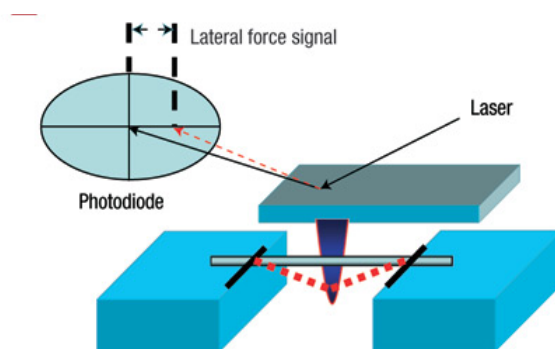
Figure 1.20: Schematic of bending test with an AFM tip for nanowire mechanical measurements. [Adopted from 180].

observables and depend only on the local environment.[179] Interestingly, average Young's modulus of 40-250 nm diameter Au nanowires has been found to be 70 ± 11 GPa.[180] The Young's modulus is essentially independent of diameter, whereas the yield strength is largest for the smallest diameter wires, with strength up to 100 times that of bulk materials. These structures also exhibit super elastic behavior followed by unexpected brittle failure without significant plastic deformation.[181] Thermal annealing resulted in a gradual transition to weaker, more ductile materials associated with the elimination of the twinned boundary. The average value of the Young's modulus of 22 to 35 nm diameter silver nanowires is 102 ± 23 GPa and is higher than that of bulk silver (83 GPa). In a different report, the elastic modulus of silver nanowires is 140 GPa, which has been determined by mechanical measurements (Figure 1.20).[99] However, the hardness and elastic modulus measured by nano-indentation technique are found to be 0.87 ± 4 and 88 ± 5 GPa, respectively.[182]
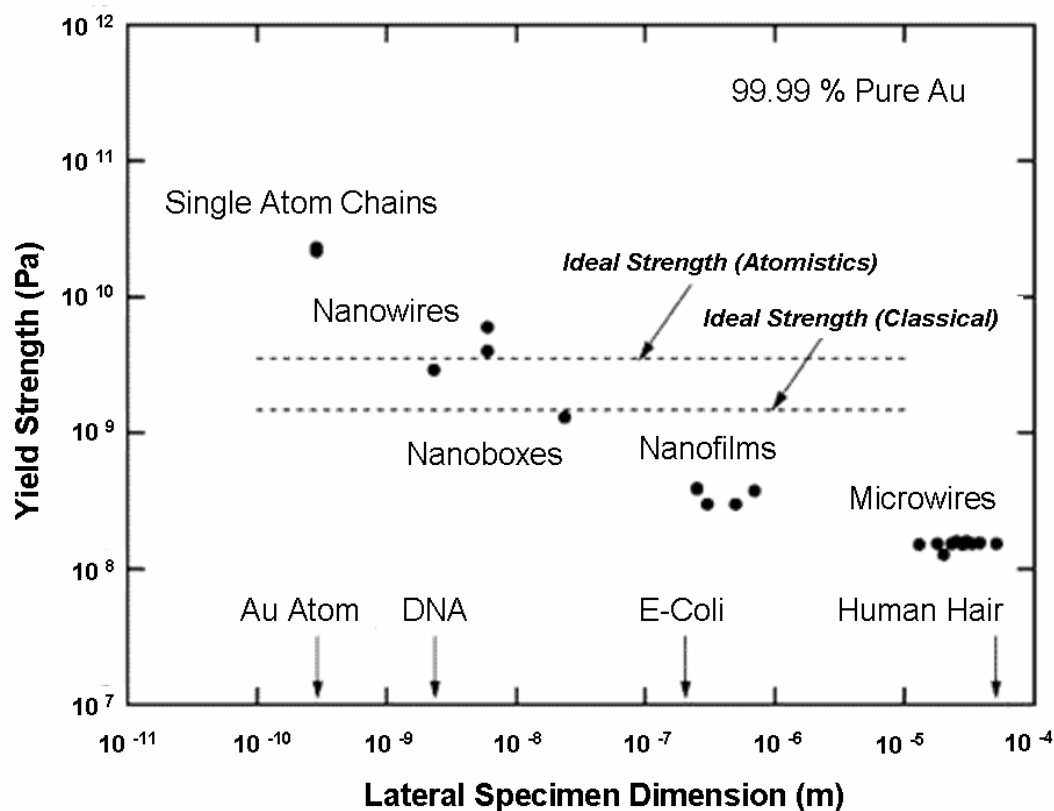
Figure 1.21: Ideal predictions and experimental measurements regarding the yield strength of pure Au as a function of lateral specimen dimension. [Adopted from 186].

Rubio-Bollinger et al. have provided a correlation between experimental measurements and *ab initio* theoretical calculations on freely suspended chain of single gold atoms.[183] They found that the bond strength of the nanowire is about twice that of a bulk metallic bond (Figure 1.21). NW mechanical behavior may be ductile or brittle, depending on the orientation. They have also estimated the NW atomic arrangement and conductance behavior based on crystallographic model. Thus, yield strength of nanowires has been investigated both by atomistic simulations and experimental techniques.[183-186] It has been demonstrated that at nanometer scales (diameter > 1 nm), the mechanism for strengthening involves the scarcity and low mobility of dislocations coupled with constraint from tensile stresses. As the wires approach the atomic scale (diameter < 1 nm), an increase in strength occurs concurrent with a surface-stress-induced change in the stable structure of the nanowires and the absence of dislocation-mediated yield. Interestingly, Marszalek et al. have reported the capture of plastic

deformation of a gold nanowire by AFM technique.[187] They found that nanowires elongate under force in quantized steps of up to three integer multiples of 1.76 Å and they shorten spontaneously in steps of 1.52 Å. The plausible explanation is that the sliding of crystal planes within the gold nanowires creating stacking faults that change the local structure from fcc to hcp (hexagonal-close packed). However, Rodrigues et al. have demonstrated that just before rupture, gold nanowires are crystalline and display only three possible atomic configurations where either [100], [110], or [111] directions lie approximately parallel to the elongation direction.[185]

1.8.3 Electrical Properties

Metal nanowires those are shorter that the mean free path of conduction electron exhibit ballistic transport properties.[188] It has been recently shown that conductance of wires of single gold atoms, up to seven atoms in length, is close to one quantum unit of conductance $G_0 = 2e^2/h$ (where e is the charge on an electron and h Planck's constant), because electron transport proceeds through one single quantum conductance channel.[184] Interestingly, metal nanowires exhibit clear quantized peaks up to five quanta of conductance at room temperature.[188d] However, resistance of nanowires is known to be changed due to the chemisorption of adsorbates such as thiols and amines. The conduction of these nanowires is quantized in units of $G_0 = 2e^2/h$, and chemisorption of different molecules reduces the number of channels of conductance, G_0 in the nanowire. However, such extraordinary sensitivity is restricted to nanowires that are less than 50 nm in length and less that 1 nm in diameter. A resistance change, $\Delta R/R_0$, of 100 % has been observed for such nanowires on chemisorption of adsorbates.[188b]

A 50 nm diameter silver nanowire exhibits linear I-V characteristic obeying Ohm's law, which gives a resistivity value, $\rho = 1.63 \times 10^{-6}$ Ωm at 4.2 K.[102d] However, Xia et al. has investigated the transport properties at room temperature on a 40 nm diameter silver nanowire exhibiting electrical continuity with a conductivity of ~ 0.8×10^5 Scm^{-1}, which is comparable to bulk conductivity 6.2×10^5 Scm^{-1}.[102a, b]

1.8.4 Thermal properties

High aspect ratio nanomaterials also exhibit interesting thermal properties. It has been demonstrated that laser heating of the electron gas of gold nanorods with an

average aspect ratio 3.8 leads to the bleaching of both transverse and longitudinal mode of the SP oscillations at 520 nm and 750 nm.[189] El-Sayed and co-workers have established that gold nanorods transform into spherical nanoparticles under intense femtosecond pulse laser irradiation with a typical melting time of 30 ps.[189b] These experiments suggest that phonon dependent relaxation processes in gold nanoparticles are independent of the shape, size, type of the surfaces, or the mode of the SP, oscillations excited. However, metal nanoparticles exhibit size dependent melting properties, melting temperature decreases with decreasing mean grain size.[190a] The melting point is depressed even up to 700 ^{0}C for silver nanoparticles compared to the bulk value for silver (960 ^{0}C).[190b, c]

1.8.5 Other Properties

High aspect ratio nanoparticles also exhibit several other important properties, such as surface enhanced scattering, fluorescence quenching or enhancing depending on the proximity to the surface.[191] Due to the strong electromagnetic field generated at the surface of metal nanoparticles, chromophores within ~ 5 nm of the surface of the metal nanoparticles have their fluorescence quenched, while chromophores at distances of ~10 nm or greater have their fluorescence enhanced up to 100-fold.[191b] Among all metals, silver has the most pronounced plasmon modes and long plasmon phase life times. Therefore, locally excited plasmon modes can propagate through silver nanowire and can be used to carry information from one end tip to other end tip, if the excitation region is restricted to a one of the tip ends.[102d] Interestingly, a composite of Ag NWs arranged into parallel pairs exhibits effective magnetic permeability and dielectric permittivity both negative in the visible and near-infrared spectral ranges.[192]

Anisotropic metal nanoparticles also exhibit interesting catalytic properties. For example, it has been recently demonstrated that high aspect ratio nanoparticles with more corners and edge atoms have higher catalytic reactivity than similar nanoparticles with fewer corner and edge atoms.[193]

1.9 Applications

1.9.1 SERS: Anisotropic metal nanoparticles show significant electric field enhancement

....

Physical and Materials Chemistry Division, National Chemical Laboratory   50

at the surface due to the photo-excitation of the conduction electrons. This property can be used advantageously as effective substrates for surface-enhanced Raman scattering.[32] This technique is promising for the single molecule detection when appropriate nanoparticles are used for the substrate. In particular, the local field enhancement factor increases many times, when nanoparticles with lower symmetry and/or bi-metallic concentric structures are used.[30a, b, 194] It has been demonstrated that triangular particles with dimensions smaller than 50 nm produce strong field enhancement near their vertices, reaching several hundred times the amplitude of the illumination wave. These strong fields, which are extremely localized, are the reason for the observation of hot spots and blinking phenomenon observed experimentally in Raman scattering.[32] For example, aligned silver nanowires that are ~ 50 nm in diameter and 2-3 µm in length have been assembled over an area of 20 cm^2, which serve as excellent substrates for SERS with large electromagnetic field enhancement factors (2 x 10^5 for thiol and 2,4-dinitrotoluene, and 2 x 10^9 for Rhodamine 6G).[195]

1.9.2 Plasmonics: Nanoscale materials are important components of plasmonics.[196] Plasmonics is envisioned as the next big thing in nanoscience having potential impact on electronics to medical diagnosis.[196b] Modern techniques, such as AFM, enable fabrication of nanoscale devices using such nanostructured materials as waveguides. They can be used effectively to develop multicolor labels on the basis of nanoparticle shape.[25d]

1.9.3 Nanosensor: Silver nanowires are known to be highly sensitive towards amines. Based on this property, silver nanowires with diameters ranging from 150 to 950 nm and lengths of 100 µm have been used for the sensing of ammonia vapor.[197a] Such nanowires show a resistance increase, $\Delta R/R_0$ of up to 1,000 %, fast (< 5 s), and reversible. Similarly, Pd nanowires can be used for fast hydrogen gas sensing with a response time of 20 ms to 5 s depending on the hydrogen concentration.[197b]

1.9.4 Detection of Bio-molecules: One of the important applications is the specific bio-molecule detection.[198] Various plasmon-resonant particles (PRPs, e.g. nanowires, nanoprisms with 40 -100 nm size) have been demonstrated as optical reporters in typical

....

Physical and Materials Chemistry Division, National Chemical Laboratory   51

biological assays recently.[199] PRPs are ultrabright, nanosized optical scatterers, which scatter light elastically and can be prepared with a scattering peak at any color in the visible spectrum. PRPs are readily observed individually with a microscope configured for dark-field microscopy, with white-light illumination of typical power. They can be used as target-specific labels for different bio-logical assays replacing or complementing established labels, such as those based on radioactivity, fluorescence, chemiluminescence, or enzymatic-colorimetric detection that are used routinely in biochemistry, cell biology, and medical diagnostic applications. PRP labels are nonbleaching and bright enough to be rapidly identified and counted. Therefore, an ultrasensitive assay format based on single-target molecule detection is now practical.

1.9.5 Disease Diagnosis: Haes et al. have developed localized plasmon resonance (LSPR) nanosensor based on the optical properties of Ag nanotriangles.[200] They studied the interaction between amyloid β-derived diffusible ligands (ADDL) and the anti-ADDL antibody molecules possibly responsible for the development of Alzheimer's disease and calculated the surface confined binding constant of 3.0×10^7 M^{-1} for the interaction of ADDLs and anti-ADDLs. It is important to note that the development of an accurate diagnostic test for Alzheimer's disease is crucial and will help millions of people to obtain timely and appropriate treatment for their symptoms. Interestingly, Lieber and co-workers have developed a highly sensitive, label free field-effect device for the electrical detection of cancer markers using silicon-nanowire.[201] Their device is highly selective and could detect femtomolar concentrations of prostate specific antigens (protein markers).

1.9.6 Cancer Treatment: Nanotechnology has opened the door to a new generation of diagnostics, imaging agents, and drugs for detecting and treating cancer at its early stages.[2b] Certain nanomaterials absorb light in the NIR-region. Metal nanoshells, nanoprisms are the examples whose SPR spectrum spreads up to visible region to NIR region. According to theoretical calculations, these materials possess absorption cross sections on the order of 1.3×10^{-14} m^2 implying that these materials are 1 million-fold more likely to encounter an absorption event and convert that light energy into thermal energy than that of the conventional dyes (Indocyanine green, posses absorption cross-section 1.66×10^{-20} m^2). This property of metal nanoshells has been applied for the

....

Physical and Materials Chemistry Division, National Chemical Laboratory   52

destruction of tumor cells by Hirsch et al.[28a] Light in the spectral region 700-1000 nm has been shown to penetrate tissue at depths beyond 1 cm with no observable damage to the intervening tissue, but it can generate heat if a nanoshell or a nanoprism is inserted inside the tissue.[28b] This noninvasive delivery of heat to a tissue volume by selectively photo-induced heat generation can be used for the destruction of cancer and tumor cells. For example, when cultured cells in the presence of phosphatidylcholine passivated (PC-NRs) gold nanorods were irradiated with a focused pulsed near-IR laser, photoreaction of the PC-NRs cause damage within a very small area around the PC-NRs and achieved selective cell death.[202]

1.9.7 Catalysis: High aspect ratio nanomaterials have important applications in catalysis due to their shape dependent catalytic activity. In particular, they exhibit different catalytic activity on their various crystallographic facets. For example, El-Sayed and co-workers have shown that during the early stages of the electron transfer reaction, where no shape changes occur, the catalytic activity is dependent on the shape of the nanocatalyst used.[191] Interestingly, shape changes occur during the course of the reaction, which also alters the corresponding activation energies. One interesting example of high aspect ration nanomaterials is of Pd nanotubes, which catalyze Suzuki coupling reaction.[25c, 203] Bulk gold is considered a noble and inert metal, however, small clusters of gold are found to be catalytically active as their chemical and electronic properties change with shape and size.[204]

1.9.8 Molecular Electronics: Nanowires are an important component of electronic devices and can be used as field effect transistors (FET), high speed integrated nanowire circuits.[205] Husain et al. have fabricated a Pt nanowire resonator of 43 nm diameter, 1.3 μm in length with a resonating frequency of 105.3 MHz at 4 K.[206]

High aspect ratio nanomaterials have several other useful applications, like probe materials for AFM, as optical imaging materials from gold nanocages.[207]

1.10 Conclusions and Perspectives

Thus some of the most recent developments of high aspect ratio nanomaterials have been presented in this chapter with particular emphasis on their preparation,

characterization, properties, and various applications. Future promises of these materials are bright, as already several attempts have been made to utilize these materials in cancer treatment, diagnosis, sensors, and in SERS successfully. However, there are several barriers to cross before coming to any conclusion about many nanomaterials and one of the daunting tasks is to address the environmental concern and societal impact of these materials as very little is known about how they behave inside living organisms. Moreover, processing and synthesis of 100 % pure materials with desired shape and size is still a dream of many researchers and after synthesis one has to face major challenges on how to control purity, thermal stability, time dependent reorganization/degradation, and finally scale-up issues.

1.11 Motivation, Scope and Organization of the Thesis

The genesis of the present thesis is inspired by several interesting issues unfolded during the foregoing critical review related to both fundamental and applied aspects of high aspect ratio nanostructures. This includes the development of new methods for the synthesis of high aspect ratio nanostructures and their assemblies. If such nanostructures are made to organize in a controlled fashion, resultant hybrid materials with many unusual properties can open up several application possibilities. Consequently it is imperative to study different properties such as electrochemical, electrical, optical, catalytic etc. for the pursuit of various applications.

1.11.1 Objectives of the Present Study

It is clear from the above discussions that several methods have been developed for the synthesis of high aspect ratio nanostructures encouraged by several interesting new properties. Despite such investigations, many issues related to the selective synthesis of high aspect ratio structures of gold and silver in high yields (better than 90%) have not been systematically investigated by controlling various experimental parameters like the effect of solvent properties, stirring rate, variation of the nature of capping agent and its ratio with respect to the metal ion, etc. A generalized method for the non-templated synthesis of these nanostructures for common metals is still lacking. More interestingly, although numerous studies have been carried out for optical, mechanical, and other properties, there is a big lacuna of understanding the electrochemical properties of such

....

Physical and Materials Chemistry Division, National Chemical Laboratory　　　　　　　54

high aspect ratio nano materials. The present study is an attempt to provide some of these information and the major objectives are:

(i)   To understand the role of 4-aminothiophenol, a bifunctional capping agent on the synthesis of high aspect ratio silver nanostructures,

(ii)   To understanding how mixture of two solvents affect the growth of silver nanowires and gold nanoparticles, especially when the dielectric constant varies systematically with solvent mole fraction,

(iii)   To understand and compare the fundamental difference in electrochemical properties of nanowires and nanoparticles of similar size,

(iv)   To investigate the role of poly-functional organic molecules in synthesis of high aspect ratio nanoparticles of gold and silver and to correlate their properties with size and shape,

(v)   To organize gold nanoparticle on silver nanowire for the investigation of new properties arising from the hybrid structures, and

(vi)   To study the possible applications, such as catalytic activity of silver nanoparticles.

1.11.2 Organization of Chapters

The present thesis addresses mostly the important aspect of synthesis, assembly, characterization, and applications of high aspect ratio nanoparticles in a form of **six chapters**. The **first chapter** represents a critical review of synthesis, characterization, properties and important applications of various high aspect ratio nanomaterials, mostly consisting of silver and gold. The importance of such nanomaterials and their theoretical significances has been discussed briefly. Apart from elaborate discussion on different methods of synthesis, a part of the chapter has been devoted explicitly for the discussion on different properties, mainly of optical properties. The impact of these materials on nanotechnology for diverse applications such as catalysis, optical, electronic and magnetic device construction, medical diagnostics and therapeutics, environmental and pollution control has been briefly discussed. The chapter concludes by specific objectives for the present study, future prospects and finally mentioning some of the existing limitations of these materials.

....

Physical and Materials Chemistry Division, National Chemical Laboratory   55

The **second chapter** describes a study on silver nanowire synthesized using 4-aminothiophenol as a new capping and reducing agent. These nanowires possess a diameter of about 60-80 nm and length of several micrometers revealing many interesting properties. Electrochemical behavior of well defined NWs has been compared with that of spherical silver nanoparticles (Ag NPs) of similar sizes and capping agents. Interestingly, Ag NWs have been found to show quasi-reversible electron transfer process at smaller rate constant as compared to the electron transfer features of Ag NPs. Finally, electrocatalytic activity of Ag NPs during the Wolff rearrangement of α-diazoketone has been demonstrated to reveal a remarkable application of these nanoclusters for electro-organic synthesis following a unique E($\uparrow$), C, E($\downarrow$) mechanism.

In the **third chapter**, the role of polyfunctional organic molecules on the shape controlled synthesis of nanoparticles has been investigated. In particular, three interesting organic molecules, viz. 4-aminothiophenol, Bismarck Brown R, and Bismarck brown Y have been employed to investigate their role in achieving shape control during the synthesis. Although spherical aggregates (70-80 nm) of gold nanoparticles (3 nm) are formed by 4-aminothiophenol as the capping agent, the use of more intricate multifunctional dye molecules like Bismarck brown R and Y, interestingly, gives gold nanoplates in good yield. These gold plates are of 500 nm to micrometer size with a thickness of around 80-108 nm. All these nanostructures are electrochemically active and their electron transfer properties have been studied by cyclic voltammetry along with their optical properties.

The **fourth chapter** describes bi-metallic assembly of silver and gold nanoparticles using 4-aminothiophenol as a cross linking unit. More precisely, interlinking of gold and silver nanoparticles has been demonstrated at controlled pH in contrast to the more commonly reported alloy formation. A judicious control of pH at 7.8 enables synthesis of gold nanoparticles surface functionalized with amino group, which is then used for the interlinking of *in situ* generated silver nanoparticles. Such interlinked assemblies show surface plasmon absorption in the range 540-580 nm presumably due to the intercrystal surface plasmon coupling. Interestingly, silver nanoparticles synthesized from silver benzoate gives a highly ordered assembly as compared to that from silver nitrate.

Benzoic acid generated in the reaction gets attached to silver nanoparticle surface providing the necessary stability for the as synthesized assemblies.

The theme of the **fifth chapter** is one-dimensional organization of gold nanoparticles on silver nanowire surfaces. More specifically, directional integration of tridecylamine protected gold (Au-TDA) nanoclusters (4-6 nm) on silver nanowires (Ag NWs, 60 nm) and their properties have been investigated using a variety of techniques including powder X-ray diffraction, Scanning and Transmission Electron Microscopy, X-ray Photoelectron Spectroscopy and four-probe electrical conductivity measurements to demonstrate significant changes in optical, and electrical properties. A new surface plasmon absorption peak is observed at 570 nm, while electrical measurement shows a transition from metallic to semiconductor behavior at 150 K.

Chapter six is the concluding part of the thesis outlining major conclusions drawn from the present study with respect to synthesis, assembly, and properties of various nanomaterials of gold and silver. One of the major observations is the electrocatalytic activity of silver nanoparticles. Similarly, electron transfer properties of silver nanowires are different to that of their spherical counterparts. The importance of poly-functional organic molecules in shape controlled synthesis of metal nanoparticles has also been demonstrated, particularly in the synthesis of silver nanowires and gold nanotriangles. Interestingly, linear organization of gold nanoparticles on silver nanoparticles gives a way to the manipulation of electrical and optical properties as these properties are different from their individual counterparts. Finally, the future prospects of these materials is outlined for next 10-15 years within a broad perspective of both fundamental and technological interest in diverse fields such as chemistry, physics, biology, engineering for these high aspect ratio materials.

1.12 References

1. http://www.zyvex.com/nanotech/feynman.html.

2. (a) www.un.org/millenniumgoals. (b) '*Nanotechnology Takes Aim at cancer*' Science (News) **2005**, *310*, 1132. (c) Roncone, K. *JOM* **2004**, 31. (d) Rittner, M. N. *JOM* **2004**, 22.

3. Kohler, M.; Fritzsche, W. Nanotechnology, *An Introduction to Nanostructuring Techniques*, Wiley-VCH Verlag GmbH and Co. KgaA, **2004**.

4. Eustis, S.; El-Sayed, M. A. *Chem. Soc. Rev.* **2006**, *35*, 209.

5. Mie, G. *Ann. Phys.* **1908**, *25*, 377.

6. Taniguchi, N. *On the Basic Concept of 'Nano-Technology*; Proc. Intl. Conf. Prod. Eng. Tokyo, Part II, Japan Society of Precision Engineering, **1974**.

7. (a) Drexler, E. *Engines of Creation: The Coming Era of Nanotechnology;* Anchor Press/ Doubleday: New York, **1986**. (b) Drexler, K. E. *Nanosystems: molecular machinery, manufacturing and computation;* John Wiley & Sons: New York, **1992**.

8. (a) Schmid, G.; Baumle, M.; Greekens, M.; Heim, I.; Osemann, C.; Sawitwoski, T. *Chem. Soc. Rev.* **1999**, *28*, 179. (b) Huang, W.; Qian, W.; El-Sayed, M. A. *J. Phys. Chem. B* **2005**, *109*, 18881. (c) Burda, C.; Chen, X.; Narayanan, R.; El-Sayed, M. A. *Chem. Rev.* **2005**, *105*, 1025.

9. (a) Feldheim, D. L. *Nature* **2000**, *408*, 45. (b) Feldheim, D. L.; Keating, C. D. *Chem. Soc. Rev.* **1998**, *27*, 1. (c) Brousseau, (III), L. C.; Zhao, Q.; Shultz, D. A.; Feldheim, D. L. *J. Am. Chem. Soc.* **1998**, *120*, 7645. (d) Fan, F.-R. F.; Bard, A. J. *Science* **1997**, *277*, 1791. (e) Klein, D. L.; McEuen, P. L.; Katari, J. E.; Roth, R.; Alivisatos, A. P. *Appl. Phys. Lett.* **1996**, *68*, 2574. (f) Alperson, B.; Cohen, S.; Rubenstein, I.; Hodes, G. *Phys. Rev. B* **1995**, *52*, 17017. (g) Andres, R. P.; Bein, T.; Dorogi, M.; Feng, S.; Henderson, J. I.; Kubiak, C. P.; Mahoney, W.; Osifchin, R. G.; Reifenberger, R. *Science* **1996**, *272*, 1323.

10. Kelly, K. L.; Coronado, E.; Zhao, L. L.; Schatz, G. C. *J. Phys. Chem. B* **2003**, *107*, 668.

11. El-Sayed, M. A. *Acc. Chem. Res.* **2001**, *34*, 257.

12. (a) Hao, E.; Schatz, G. C.; Hupp, J. T. *J. Fluresc.* **2004**, *14*, 331. (b) Murphy, C. J.;

....

Physical and Materials Chemistry Division, National Chemical Laboratory   58

Sau, T. K.; Gole, A. M.; Orendorff, C. J.; Gao, J.; Gou, L.; Hunyadi, S. E.; Li, T. *J. Phys. Chem. B* **2005**, *109*, 13857.

13. Warren H. Hunt, Jr. *JOM* **2004**, 13.

14. (a) G. Stix, "Little Big Science," ScientificAmerican.com (September 16, **2001**). (b) www.sciam.com/article.cfm?chanID=sa002&articleID=00018E72-2E88-1C6F-84A9809EC588EF21&catID=7.

15. http://www.nano.gov.

16. "Nanoscience and Nanotechnologies: Opportunities and Uncertainties," The Royal Society and The Royal Academy of Engineering (July 29, **2004**), www.royalsoc.ac.uk/policy.

17. Cui, Y.; Wei, Q. Q.; Park, H. K.; Lieber, C. M. *Science* **2001**, *293*, 1289.

18. http://physicsweb.org/articles/world/17/8/7.

19. www.nanoandthepoor.org.

20. http://www.crnano.org/solutions.htm.

21. Schärtl, W. *Adv. Mater.* **2000**, *12*, 1899.

22. (a) Park, R. J.; Meldrum, F. C. *Adv. Mater.* **2002**, *14*, 1167. (b) Wu, Q-S.; Sun, D-M.; Liu, H-J.; Ding, Y-P. *Cryst. Growth Design* **2004**, *4*, 717. (c) Bong, D. T.; Clark, T. D.; Granja, J. R.; Ghadiri, M. R. *Angew. Chem. Int. Ed.* **2001**, *40*, 988. (d) Görbitz, C. H.; *Chem. Eur. J.* **2001**, *7*, 5153. (e) Harada, A.; Li. J.; Kamachi, M. *Nature* **1993**, *364*, 516.

23. (a) Curl, R. F.; Smalley, R. E. *Science* **1988**, *242*, 1017. (b) Liu, J.; Rinzler, A. G.; Dai, H.; Hafner, J. H.; Bradley, R. K.; Boul, P. J.; Lu, A.; Iverson, T.; Shelimov, K.; Huffman, C. B.; Rodriguez-Macias, F.; Shon, Y-S.; Lee, T. R.; Colbert, D. T.; Smalley, R. E. *Science* **1998**, *280*, 1253.

24. 'A special issue on carbon nanotubes' *Acc. Chem. Res.* **2002**, *35*, 997.

25. (a) Liu, M. Z.; Guyot-Sionnest, P. *J. Phys. Chem. B* **2004**, *108*, 5882. (b) Yin, Y.; Lu, Y.; Sun, Y.; Xia, Y. Nano Lett. **2002**, *2*, 427. (c) Sun, Y.; Mayers, B.; Xia, Y. *Adv. Mater.* **2003**, *15*, 641. (d) Jin, R.; Cao, Y.; Mirkin, C. A.; Kelly, K. L.; Schatz, G. C.; Zheng, J. G. *Science* **2001**, *294*, 1901. (e) Chen, C.; Wang, L.; Jiang, G.; Yu, H. *Rev. Adv. Mater. Sci.* **2006**, *11*, 1.

26. Chen, M.; Sun, L.; Bonevich, J. E.; Reich, D. H.; Chien, C. L.; Searson, P. C. *Appl. Phys. Lett.* **2003**, *82*, 3310.

27.   Melosh, N. A.; Boukai, A.; Diana, F.; Geradot, B.; Badolato, A.; Petroff, P. M.; Heath, J. R. *Science* **2003**, *300*, 112.

28.   (a) Hirsch, L. R.; Stafford, R. J.; Bankson, J. A.; Serchen, S. R.; Rivera, B.; Price, R. E.; Hazle, J. D.; Halas, N. J. *Proc. Natl. Acad. Sci. USA.* **2003**, *100*, 13549. (b) Shah, N.; Cerussi, A.; Eker, C.; Espinoza, J.; Butler, J.; Fishkin, J.; Hornung, R.; Tromberg, B. *Proc. Natl. Acad. Sci. USA* **2001**, *98*, 4420.

29.   (a) Draine, B. T.; Flateau, P. J. *User Guide for the Discrete Dipole Approximation* DDSCAT.6.0, http://arxiv.org/abs/astro-ph0309069. (b) Yang, W. H.; Schatz, G. C.; Van Duyne, R. P. *J. Chem. Phys.* **1995**, *103*, 869. (c) Jensen, T.; Kelly, K. L.; Lazarides, A.; Schatz, G. C. *J. Cluster Sci.* **1999**, *10*, 295. (d) Kelly, K. L.; Lazarides, A. A.; Schatz, G. C. *Comput. Sci. Eng.* **2001**, *3*, 67. (e) Bian, R. X.; Dunn, R. C.; Xie, X. S.; Leung, P. T. *Phys. Rev. Lett.* **1995**, *75*, 4772. (f) Dabbousi, B. O.; Rodriguez-Viejo, J.; Mikulec, F. V.; Heine, J. R.; Mattoussi, H.; Ober, R.; Jensen, K. F.; Bwaendi, M. G. *J. Phys. Chem. B* **1997**, *101*, 9463. (g) Yang, J.; Fendler, J. H. *J. Phys. Chem* **1995**, *99*, 5505. (h) Hao, E.; Schatz, G. C. *J. Chem. Phys.* **2004**, *120*, 357. (i) Coronado, E.; Schatz, G. C. *J. Chem. Phys.* **2003**, *119*, 3926. (j) Jensen, T.; Kelly, K. L.; Lazarides, A.; Schatz, G. C. *J. Clust. Sci.* **1999**, *10*, 295.

30.   (a) Kottmann, J. P.; Martin, O. J. F.; Smith, D. R.; Schultz, S. *Phys. Rev. B* **2001**, *64*, 235402. (b) Kottmann, J. P.; Martin, O. J. F.; Smith, D. R.; Schultz, S. *Chem. Phys. Lett.* **2001**, *341*, 1. (c) Gray, S. K.; Kupka, T. *Phys. Rev. B: Condens. Matter* **2003**, *68*, 45415. (d) Oliva, J. M.; Gray, S. K. *Chem. Phys. Lett.* **2003**, *379*, 325.

31.   Nie, S.; Emory, S. R. *Science* **1997**, *275*, 1102.

32.   Lee, S. J.; Morrill, A. R.; Moskovits, M. *J. Am. Chem. Soc.* **2006**, *128*, 2200.

33.   Felidj, N.; Aubard, J.; Levi, G. *J. Chem. Phys.* **1999**, *111*, 1195.

34.   Bohren, C. F.; Huffman, D. R. Absorption and scattering of light by small particles; Wiley Interscience: New York, **1983**.

35.   Link, S.; El-Sayed, M. A. *J. Phys. Chem. B* **1999**, *103*, 8410.

36.   Diao, J.; Gall, K.; Dunn, M. L.; Zimmerman, J. A. *Acta Materialia* **2006**, *54*, 643.

37.   (a) Krenn, J. R.; Dereux, A.; Weeber, J. C.; Bourillot, E.; Lacroute, Y.; Goudonnet, J. P.; Schider, G.; Gotschy, W.; Leitner, A.; Aussengg, F. R.; Girard, C. *Phys. Rev. Lett.* **1999**, *82*, 2590. (b) Weeber, J. –C.; Dereux, A.; Girard, C.; Krenn, J. R.; Goudonnet, J. P. *Phys. Rev. B* **1999**, *60*, 9061. (c) Tominaga, J.; Mihalcea, C.; Büchel, D.;

....

Physical and Materials Chemistry Division, National Chemical Laboratory   60

Ph. D. Thesis   *Chapter 1*   *University of Pune, May 2006*

Fukuda, H.; Nakano, T.; Atoda, N.; fuji, H.; Kikukawa, T. *Appl. Phys. Lett.* **2001**, *78*, 2417. (d) Kottamann, J. P.; Martin, O. J. f.; Smith, D. R.; Schultz, S. *J. Microsc.* **2001**, *202*, 60.

38. (a) Chou, S. Y.; Krauss, P. R.; Renstrom, P. J. *Science* **1996**, *272*, 85. (b) Sotomayer Torres, C. M. *Alternative Lithography: Unleashing the potential of Nanotechnology*, Kluwer Academic/Plenum Publishers, New York, 2003. (c) Geissler, M.; Xia, Y. *Adv. Mater.* **2004**, *16*, 1249. (d) Quate, C. F. *Surf. Sci.* **1997**, *386*, 259.

39. Gotschy, W.; Vonmetz, K.; Leitner, A.; Aussenegg, F. R. *Opt. Lett.* **1996**, *21*, 1099.

40. (a) Lugstein, A.; Bernardi, J.; Tomastik, C.; Bertagnilli, E. Appl. Phys. Lett. **2006**, *88*, 163114. (b) Vieu, C.; Carcenac, F.; Pépin, A.; Chen, Y.; Mejias, M.; Lebib, A.; Manin-Ferlazzo, L.; Couraud, L.; Launois, H. *App. Surf. Sci.* **2000**, *164*, 111.

41. (a) Silva, S. L.; Leibsle, F. M. *Surf. Sci. Lett.* **1999**, *440*, L835. (b) York, S. M.; Leibsle, F. M. *Appl. Phys. Lett.* **2001**, *78*, 2763.

42. Liu, S. T.; Maoz, R.; Sagiv, J. *Nano Lett.* **2004**, *4*, 845.

43. Schmid, G.; Liu, Y.-P.; Schumann, M. ; Raschke, T.; Radehaus, C. *Nano Lett.* **2001**, *1*, 405.

44. (a) Jashke, M.; Butt, H. J. *Langmuir* **1995**, *11*, 1061. (b) Piner, R.D.; Zhu, J.; Xu, F.; Hong, S.; Mirkin, C. A. *Science* **1999**, *283,* 661.

45. (a) Qin, L.; Park, S.; Huang, L.; Mirkin C. A. *Science* **2005**, *309*, 113. (b) Liu, X.; Fu, L.; Hong, S.; Dravid, V. P.; Mirkin, C. A. *Adv. Mater.* **2002**, *14,* 231.

46. Brust, M.; Walker, M.; Bethell, D.; Schiffrin, D. J.; Whyman, R. *J. Chem. Soc. Chem. Commun.* **1994**, 801.

47. (a) Masuda, H.; Yamada, H.; Satoh, M.; Asoh, H.; Nakao, M.; Tamamura, T. *Appl. Phys. Lett.* **1997**, *71*, 2770. (b) Yuan, J. H.; He, F. Y.; Sun, D. C.; Xia, X. H. **2004**, *16,* 1841. (c) Scho¨nenberger, C.; van der Zande, B. M. I.; Fokkink, L. G. J.; Henny, M.; Schmid, C.; Krüger, M.; Bachtold, A.; Huber, R.; Birk, H.; Stauder, U. *J. Phys. Chem. B* **1997**, *101*, 5497.

48. (a) Foss, C. A. Jr.; Hornyak, G. L.; Stockert, J. A.; Martin, C. R. *J. Phys. Chem.* **1992**, *96*, 7497. (b) Martin, C. R. *Science* **1994**, *266*, 1961. (c) Penner, R. M.; Martin, C. R. *Anal. Chem.* **1987**, *59*, 2625. (d) Martin, C. R. *Chem. Mater.* **1996**, *8*, 1739. (e) Foss, C. A. Jr.; Hornyak, G. L.; Stockert, J. A.; Martin, C. R. *Adv. Mater.* **1993**, *5,* 135. (f) Preston, C. K.; Moskovits, M. *J. Phys. Chem.* **1993**, *97*, 8495. (g) Sun, L.; Searson,

....

Physical and Materials Chemistry Division, National Chemical Laboratory   61

P. C.; Chien, C. L. *Phys. Rev. B* **2000**, *61*, R6463. (h) Whitney, T. M.; Jiang, J. S.; Searson, P. C.; Chien, C. L. *Science* **1993**, *261*, 1316. (i) Sun, L.; Searson, P. C.; Chien, C. L. *Appl. Phys. Lett.* **1999**, *74*, 2803.

49. (a) Hulteen, J. C.; Martin, C. R. *J. Mater. Chem.* **1997**, *7*, 1075. (b) Jirage, K. B.; Hulteen, J. C.; Martin, C. R. *Science* **1997**, *278*, 655.

50. van der Zande, B. M. I.; Boehmer, M. R.; Fokkink, L. G. J.; Schoenenberger, C. *Langmuir* **2000**, *16*, 451.

51. Schoenenberger, C.; van der Zande, B. M. I.; Fokkink, L. G. J.; Henny, M.; Schmid, C.; Krueger, M.; Bachtold, A.; Huber, R.; Birk, H.; Staufer, U. *J. Phys. Chem. B* **1997**, *101*, 5497.

52. Forrer, P.; Schlottig, F.; Siegenthaler, H.; Textor, M. *J. Appl. Electrochem.* **2000**, *30*, 533.

53. (a) Hou, Z.; Abbott, N. L.; Stroeve, P. *Langmuir* **2000**, *16*, 2401. (b) Wirtz, M.; Martin, C. R. *Adv. Mater.* **2003**, *15*, 455. (c) Sun, Y.; Xia, Y. *Adv. Mater.* **2004**, *16*, 264. (d) Sun, Y.; Wiley, B.; Li, Z. –Y.; Xia, Y. *J. Am. Chem. Soc.* **2004**, *126*, 9399. (e) Cepak, V. M.; Hulteen, J. C.; Che, G.; Jirage, K. B.; Lakshmi, B. B.; Fisher, E. R.; Martin, C. R.; Yoneyama, H. *Chem. Mater.* **1997**, *9*, 1065. (f) Cepak, V. M.; Hulteen, J. C.; Che, G.; Jirage, K. B.; Lakshmi, B. B.; Fisher, E. R.; Martin, C. R.; Yoneyama, H. *J. Mater. Res.* **1998**, *13*, 3070. (g) Sun, Y.; Mayers, B.; Herricks, T. ; Xia, Y. *Nano Lett.* **2003**, *3*, 955.

54. (a) Johansson, A. ; Widenkvist, E. ; Lu, J. ; Boman, M. ; Jansson, U. *Nano Lett.* **2005**, *5*, 1603. (b) Hernandez-Sanchez, B. A.; Chang, K-S. ; Scancella, M. T. ; Burris, J. L. ; Kohli, S. ; Fisher, E. R. ; Dorhout, P. K.; *Chem. Mater.* **2005**, 17, 5909. (c) Jin, C. G.; Jiang, G. W.; Liu, W. F.; Cai, W. L.; Yao, L. Z.; Li, X. G. *J. Mater. Chem.* **2003**, *13*, 1743. (d) Zhong, Z.; Ang, T-P.; Luo, J.; Gan, H-C.; Gedanken, A. *Chem. Mater.* **2005**, *17*, 6814. (e) Wang, X. W.; Fei, G. T.; Xu, X. J.; Jin, Z.; Zhang, L. D. *J. Phys. Chem. B* **2005**, *109*, 24326.

55. Esumi, K.; Matsuhisa, K.; Torigoe, K. *Langmuir* **1995**, *11*, 3285.

56. Govindaraj, A.; Satishkumar, B. C.; Nath, M.; Rao, C. N. R. *Chem. Mater.* **2000**, *12*, 202.

57. Fullam, S.; Cottel, D.; Rensmo, H.; Fitzmaurice, D. *Adv. Mater.* **2000**, *12*, 1430.

58. (a) Yu, Y. –Y.; Chang, S. –S.; Lee, C. –L.; Wang, C. R. C. *J. Phys. Chem. B* **1997**,

....

Physical and Materials Chemistry Division, National Chemical Laboratory   62

Ph. D. Thesis   *Chapter 1*   *University of Pune, May 2006*

101, 6661. (b) Chang, S. –S.; Shih, C. –W.; Chen, C. –D.; Lai, W. –C.; Wang, C. R. C. *Langmuir* **1999**, *15*, 701.

59.   (a) Reetz, M. T.; Helbig, W. *J. Am. Chem. Soc.* **1994**, *116*, 7401. (b) Reetz, M. T.; Helbig, W.; Quaiser, S. A.; Stimming, U.; Breuer, N.; Vogel, R. *Science* **1995**, *267*, 367. (c) R. Schuster *Chem. Phys. Chem.* **2001**, *2*, 411.

60.   Zach, M. P.; Ng, K. H.; Penner, R. M. *Science* **2000**, *290*, 2120.

61.   (a) Mulvaney, P.; Giersig, M.; Henglein, A. *J. Phys. Chem*, **1993**, *97*, 7061. (b) Henglein, A.; Giersig, M. *J. Phys. Chem.* **1994**, *98*, 6931.

62.   Brown, K. R.; Walter, D. G.; Natan, M. J. *Chem. Mater.* **2000**, *12*, 306.

63.   Jana, N. R.; Gearheart, L.; Murphy, C. J. *Chem. Mater.* **2001**, *13*, 2313.

64.   (a) Frens, G. *Nature* **1973**, *241*, 20. (b) Brown, K. R.; Lyon, L. A.; Fox, A. P.; Reiss, B. D.; Natan, M. J. *Chem. Mater.* **2000**, *12*, 314. (c) Jana, N. R.; Gearheart, L.; Murphy, C. J. *Langmuir* **2001**, *17*, 6782.

65.   Jana, N. R.; Gearheart, L.; Murphy, C. J. *J. Phys. Chem. B* **2001**, *105*, 4065.

66.   Busbee, B. D.; Obare, S. O.; Murphy, C. J. *Adv. Mater.* **2003**, *15*, 414.

67.   Pérez-Juste, J.; Liz-Marzán, I. M. ; Carnie, S.; Chan, D. Y. C.; Mulvaney, P. *Adv. Functl. Mater.* **2004**, *14*, 571.

68.   (a) Biggs, S.; Mulvaney, P. *J. Chem. Phys.* **1994**, *100*, 8501. (b) Huang, X.; Yang, J.; Zhang, W.; Zhang, Z.; An, Z. *J. Chem. Educ.* **1999**, *76*, 93.

69.   Gao, J.; Bender, C. M.; Murphy, C. J. *Langmuir* **2003**, *19*, 9065.

70.   Wu, H. –Y.; Chu, H. –C.; Kuo, T. –J. Kuo, C. –L. Huang, M. H. *Chem. Mater.* **2005**, *17*, 6447.

71.   (a) Nikoobakt, B.; Wang, Z. L.; El-Sayed, M. A. *J. Phys. Chem. B* **2000**, *104*, 8635. (b) Nikoobakt, B.; El-Sayed, M. A. *Langmuir* **2001**, *17*, 6368. (c) Johnsson, C. J.; Dujardin, E.; Davis, S. A.; Murphy, C. J.; Mann, S. *J. Mater. Chem.* **2002**, *12*, 1765.

72.   Jana, N. R.; Gearheart, L. Murphy, C. J. *Adv. Mater.* **2001**, *13*, 1389.

73.   (a) Jana, N. R.; Gearheart, L.; Obare, S. O.; Murphy, C. J. *Langmuir* **2002**, *18*, 922. (b) Pal, T.; De, S.; Jana, N. R.; Pradhan, N.; Mandal, R.; Pal, A.; Beezer, A. E.; Mitchell, J. C. *Langmuir* **1998**, *14*, 4724. (c) Wang, Z. L.; Gao, R. P.; Nikoobakht, B.; El-Sayed M. A. *J. Phys. Chem. B* **2000**, *104*, 5417.

74.   (a) Nikoobakht, B.; El-Sayed, M. A. *Chem. Mater.* **2003**, *15*, 1957. (b) Pérez-Juste, J. ; Correa-Durate, M. A. ; Lz-Marzán, L. M. *Appl. Surf. Sci.* **2004**, *226*, 137. (c) Sau,

T. K.; Murphy, C. J. *Langmuir* **2004**, *20*, 6414. (d) Alivisatos, A. P. *J. Phys. Chem.* **1996**, *100*, 13226.

75. Kim, F.; Song, J. H.; Yang, P. *J. Am. Chem. Soc.* **2002**, *124*, 14316.

76. (a) Esumi, K.; Hara, J.; Aihara, N,; Usui, K.; Torigoe, K. *J. Colloid. Interface Sci.* **1998**, *208*, 578. (b) Leontidis, E.; Kleitou, K.; Kyprianidou-Leodidou, T.; Bekiari, V.; Lianos, P. *Langmuir* **2002**, *18*, 3659.

77. Niidome, Y.; Nishioka, K.; Kawasaki, H.; Yamada, S. *Chem. Commun.* **2003**, 2376.

78. (a) Taub, N.; Krichevski, O.; Markovich, G. *J. Phys. Chem. B* **2003**, *107*, 11579. (b) Wei, Z.; Mieszawska, A. J.; Zamborini, F. P. *Langmuir* **2004**, *20*, 4322.

79. Kim, J-U.; Cha, S-H.; Chin, K.; Jho, J. Y.; Lee, J-C. *Adv. Mater.* **2004**, *16*, 459.

80. Pérez-Juste, J.; Pastoriza-Santos, I.; Liz-Marzán, L. M.; Mulvaney, P. *Coord. Chem. Rev.* **2005**, *249*, 1870.

81. Gao, P.; Zhang, C.; Liu, M. *Langmuir* **2006**, *22*, 775.

82. (a) Liu, S.; Yue, J.; Gedanken, A. *Adv. Mater.* **2001**, *13*, 656. (b) Zhu, j. j.; Liu, S. W.; Palchik, O.; Koltypin, Y.; Gedanken, A. *Langmuir* **2000**, *16*, 6396.

83. ai, Hu, Z.; Xu, T.; Liŭ, R. j.; Iin Li, H. *Mater. Sci. Eng. A* **2004**, *371*, 237.

84. Hong, B. H.; Bae, S. C.; Lee, C-W. Jeong, S.; kim, K. S. *Science* **2001**, *294*, 348.

85. Edmondson, M. J.; Zhou, W.; Sieber, S. A.; Jones, I. P.; Gameson, I.; Anderson, P. A.; Edwards, P. P. *Adv. Mater.* **2001**, *13*, 1608.

86. Bhattacharyya, S.; Saha, S. K.; Chakravorty, D. *Appl. Phys. Lett.* **2000**, *77*, 3770.

87. Sauer, G.; Brehm, G.; Schneider, S.; Nielsch, K.; Wehrspohn, R. B.; Choi, J.; Hofmeister, H.; Gösele, U. *J. Appl. Phys.* **2002**, *91*, 3243.

88. Choi, J.; Sauer, G.; Nielsch, K.; Wehrspohn, R. B.; Gösele, U. *Chem. Mater.* **2003**, *15*, 776.

89. Lahav, M.; Sehayek, T.; Vaskevich, A.; Rubinstein, I. *Angew. Chem. Int. Ed.* **2003**, *42*, 5576.

90. Qu, L.; Shi, G.; Wu, X.; Fan, B. *Adv. Mater.* **2004**, *16*, 1200.

91. (a) Ajayan, P. M.; Iijima, S. *Nature* **1993**, *361*, 333. (b) Ajayan, P. M.; Stephan, O.; Redlich, P.; Colliex, C. *Nature* **1995**, *375*, 564. (c) Chen, Y. K.; Tsang, S. C.; Green, M. L. H. *Chem. Commun.* **1996**, 2489.

92. Sloan, J.; Wright, D. M.; Woo, H. –G.; Bailey, S.; Brown, G.; York, A. P. E.; Coleman, K. S.; Huchinson, J. L.; Green, M. L. H. *Chem. Commun.* **1999**, 699.

93. Kijima, T.; Yoshimura, T.; Uota, M.; Ikeda, T.; Fujikawa, D.; Mouri, S.; Uoyama, S. *Angew. Chem. Int. Ed.* **2004**, *43*, 228.

94. Zhu, Y-J. ; Hu, X-L. *Mater. Letts.* **2004**, *58*, 1517.

95. Viau, G.; Piquemal, J-Y.; Esparrica, M.; Ung, D.; Chakroune, N.; Warmont, F.; Fiévet, F. *Chem. Commun.* **2003**, 2216.

96. Zheng, X.; Zhu, L.; Yan, A.; Wang, X.; Xie, Y. *J. Colloid. Interface Sci.* **2003**, *268*, 357.

97. (a) Chen, A.; Wang, H.; Li, X. *Chem. Commun.* **2005**, 1863. (b) Chen, A.; Kamata, K.; Nakagawa, M.; Iyoda, T.; Wang, H.; Li, X. *J. Phys. Chem. B* **2005**, *109*, 18283.

98. Zhao, Q.; Qiu, J.; Zhao, C.; Hou, L.; Zhu, C. *Chem. Lett.* **2005**, *34*, 30.

99. Sun, X.; Li, Y. *Adv. Mater.* **2005**, *17*, 2626.

100. Kong, R.; Yang, Q.; Tang, K. *Chem. Lett.* **2006**, *35*, 402.

101. (a) Fiévet, F.; Lagier, J. P.; Figlarz, M. *MRS Bull.* **1989**, *14*, 29. (b) Fiévet, F.; Lagier, J. P.; Blin, B.; Beaudoin, B.; Figlarz, M. *Solid State Ionics* **1989**, *32/33*, 198. (c) Viau, G.; Fiévet-Vincent, F.; Fiévet, F. *Solid State Ionics* **1996**, *84*, 259. (d) Toneguzzo, P.; Via, G.; Acher, O.; Fiévet-Vincent, F.; Fiévet, F. *Adv. Mater.* **1998**, *10*, 1032. (e) Bonet, F.; Delmas, V.; Grugeon, S.; Urbina, R. H.; Silvert, P. Y.; Tekaia-Elhsissen, K.; Nanostr. Mater. **1999**, *11*, 1277. (f) Ducamp-Sanguesa, C.; Herrera-Urbina, R.; Figlarz, M. *J. Solid. State Chem.* **1992**, *100*, 272.

102. (a) Sun, Y.; Gates, B.; Mayers, T.; Xia, Y. *Nano. Lett.* **2002**, *2*, 165. (b) Sun. Y.; Xia, Y. *Adv. Mater.* **2002**, *14*, 833. (c) Gao, Y.; Jiang, P.; Liu, D. F.; Yuan, H. J.; Yan, X. Q.; Zhou, Z. P.; Wang, J. X.; Song, L.; Liu, L. F.; Zhou, W. Y.; Wang, G.; Wang, C. Y.; Xie, S. S. *Chem. Phys. Letts.* **2003**, *380*, 146. (d) Graff, A.; Wagner, D.; Ditlbacher, H.; Kreibig, U. *Eur. Phys. J. D* **2005**, *34*, 263.

103. Jones, W. S.; Tamplin, W. S. in *Glycols* (Editors: G. O. Curme, Jr., F. Johnston), Reinhold, New York, **1952** p. 38.

104. Kirkland, A. I.; Jefferson D. A; Duff D. G; Edward P. P; Gamerson I; Johnson B. F. G; Smith, D. G. *Proc. R. Soc. London A* **1993**, *440*, 589.

105. Klasu, T.; Joerger, R.; Olsson, E.; Granqvist, C. -G. *Proc. Natl. Acad. Sci. USA.* **1999**, *96*, 13611.

106. Zhou, Y.; Wang, C. Y.; Zhu, Y. R.; Chen, Z. Y. *Chem. Mater.* **1999**, *11*, 2310.

107. Métraux, G. S.; Cao, Y. C. ; Jin, R.; Mirkin, C. A. *Nano Lett.* **2003**, *3*, 519.

....

Physical and Materials Chemistry Division, National Chemical Laboratory   65

108. Sun, Y.; Xia, Y. *Adv. Mater.* **2003**, *15*, 695.

109. Shankar, S. S.; Rai, A.; Ankamwar, B.; Singh, A.; Ahmad, A.; Sastry, M. *Nature Materials* **2004**, *3*, 482.

110. Liu, B.; Xie, J.; Lee, J. Y.; Ting, Y. P.; Chen, J. P. *J. Phys. Chem. B* **2005**, *109*, 15256.

111. Malikova, N.; Pastoriza-Santos, I.; Schierhorn, M.; Kotov, N. A.; Liz-Marzán, L. M. *Langmuir* **2002**, *18*, 3694.

112. (a) Shao, Y.; Jin, Y.; Dong, S. *Chem. Commun.* **2004**, 1104. (b) Tsuji, M.; Hashimoto, M.; Nishizawa, Y.; Tsuji, T. *Chem. Lett.* **2003**, *32*, 1114. (c) Ibano, D.; Yokota, Y.; Tominaga, T. *Chem. Lett.* **2003**, *32*, 574.

113. (a) Porel, S.; Singh, S.; Radhakrishnan, T. P. *Chem. Commun.* **2005**, 2387. (b) Sakai, T.; Alexandridis, P. *Nanotechnology* **2005**, *16*, S344.

114. Sun, X.; Dong, S.; Wang, E. *Angew. Chem. Int. Ed.* **2004**, *43*, 6360.

115. Sun, X.; Dong, S.; Wang, E. *Langmuir* **2005**, *21*, 4710.

116. Kim, F.; Connor, S.; Song, H. Kuykendall, T.; Yang, P. *Angew. Chem. Int. Ed.* **2004**, *43*, 3673.

117. (a) Marks, L. D. *Rep. Prog. Phys.* **1994**, *57*, 603. (b) Cleveland, C.; Landman, U. *J. Chem. Phys.* **1991**, *94*, 7376.

118. (a) Allpress, J. G.; Sanders, J. V. *Surf. Sci.* **1967**, *7*, 1. (b) Marks, L. D.; Smith, D. J. *J. Cryst. Growth* **1981**, *54*, 425. (c) Solliard, C. *Surf. Sci.* **1981**, *106*, 58. (d) Yang, C. Y. *J. Cryst. Growth* **1979**, *47*, 274. (e) Wayman, C. M.; Darby, T. P. *J. Cryst. Growth* **1975**, *28*, 53. (f) Napijko, S. A.; Styopkin, V. I.; Hofmeister, H.; Scholtz, R. *J. Cryst. Growth* **1986**, *76*, 501.

119. (a) Wang, Z. L. *J. Phys. Chem. B* **2000**, *104*, 1153. (b) Petroski, J. M.; Wang, Z. L.; Green, T. C.; El-Sayed, M. A. *J. Phys. Chem. B* **1998**, *102*, 3316.

120. (a) Puntes, V. F.; Krishnan, K. M.; Alivisato, A. P. *Science* **2001**, *291*, 2115. (b) Bradley, J. S.; Tesche, B.; Busser, W.; Maase, M.; Reetz, M. T. *J. Am. Chem. Soc.* **2000**, *122*, 4631.

121. Ah, C. S.; Yun, Y. J.; Park, H. J.; Kim, W-J.; Ha, D. H.; Yun, W. S. *Chem. Mater.* **2005**, *17*, 5558.

122. Sau, T. K.; Murphy, C. J. *J. Am. Chem. Soc.* **2004**, *126*, 8648.

123. (a) Jin, R.; Cao, Y. C.; Hao, E.; Métraux, G. S.; Schatz, G. C.; Mirkin, C. A. *Nature*

....

Physical and Materials Chemistry Division, National Chemical Laboratory   66

2003, *425*, 487. (b) Callegari, A.; Tonti, D.; Chergui, M. *Nano Lett.* **2003**, *3*, 1565.

124. Sun, Y.; Xia, Y. *Analyst* **2003**, *128*, 686.

125. Jiang, L-P.; Xu, S.; Zhu, J-M.; Zhang, J-R.; Zhu, J-J.; Chen, H-Y. *Inorg. Chem.* **2004**, *43*, 5877.

126. Pastoriza-Santos, I.; Liz-Marzán, L. M. *Nano Lett.* **2002**, *2*, 903.

127. Sarkar, A.; Kapoor, S.; Mukherjee, T. J. *Colloid interface Sci.* **2005**, *287*, 496.

128. (a) Deivaraj, T. C.; Lala, N. L.; Lee, J. Y. *J. Colloid interface Sci.* **2005**, *289*, 402. (b) Machulek Jr., A.; Moisés De Oliveira, H. P.; Gehlen, M. H. *Photochemical Photobiological Sci.* **2003**, *2*, 921.

129. Chen, S.; Caroll, D. L. *Nano Lett.* **2002**, *2*, 1003.

130. Chen, S.; Carroll, D. L. *J. Phys. Chem. B* **2004**, *108*, 5500.

131. Pillai, Z. S.; Kamat, P. V. *J. Phys. Chem. B* **2004**, *108*, 945.

132. (a) Maillard, M.; Giorgio, S.; Pileni, M. P. *Adv. Mater.* **2002**, *14*, 1084. (b) Germain, V.; Li, J.; Ingert, D.; Wang, Z. L.; Pileni, M. P. *J. Phys. Chem. B* **2003**, *107*, 8717.

133. Sun, Y.; Mayers, B.; Xia, Y. *Nano Lett.* **2003**, *3*, 675.

134. Métraux, G. S.; Mirkin, C. A. *Adv. Mater.* **2005**, *17*, 412.

135. Chen, S.; Wang, Z. L.; Ballato, J.; Foulger, S. H.; Carroll, D. L. *J. Am. Chem. Soc.* **2003**, *125*, 16186.

136. Hao, E.; Bailey, R. C.; Schatz, G. C.; Hupp, J. T.; Li, S. *Nano Lett.* **2004**, *4*, 327.

137. (a) Yamamoto, M.; Kashiwagi, Y.; Sakata, T.; Mori, H.; Nakamoto, M. *Chem. Mater.* **2005**, *17*, 5391. (b) Sun, Y.; Mayers, B. T.; Xia, Y. *Nano Lett.* **2002**, *2*, 481. (c) Yu, D.; Yam, V. W-W. *J. Am. Chem. Soc.* **2004**, *126*, 13200. (d) Jin, Y.; Dong, S. *J. Phys. Chem. B* **2003**, *107*, 12902. (e) Hao, E.; Li, S.; Bailey, R. C.; Zou, S.; Schatz, G. C.; Hupp, J. T. *J. Phys. Chem. B* **2004**, *108*, 1224. (f) Nehl, C. L. ; Liao, H. ; Hafner, J. H. *Nano Lett.* **2006, 6, 683**

138. (a) Hao, E.; Kelly, L.; Hupp, J. T.; Schatz, G. C. *J. Am. Chem. Soc.* **2002**, *124*, 15182. (b) Chen, S.; Fan, Z.; Carroll, D. L. *J. Phys. Chem. B* **2002**, *106*, 10777.

139. Sun, Y.; Xia, Y. *Science* **2002**, *298*, 2176.

140. Wiley, B.; Sun, Y.; Mayers, B.; Xia, Y. *Chem. Eur. J.* **2005**, *11*, 454.

141. Liu, M.; Guyot-Sionnest, P. *J. Phys. Chem. B* **2005**, *109*, 22192.

142. (a) Kolb, D. M. In *Advances in electrochemistry and electrochemical engineering*; Gerisher, H.; Tobias, C. W. Eds.; Wiley: New York, 1978, vol.11. (b) Herrero, E.;

Buller, L. J.; Abruna, H. D. *Chem. Rev.* **2001**, *101*, 1897.

143. Kolb, D. M.; Przasnyski, M.; Gerischer, H. *J. Electroanal. Chem.* **1974**, *54*, 25.

144. Anacker, E. W. In *Cationic Surfactants*; Jungermann, E., Ed.; Marcel Dekker: New York, **1970**.

145. Lofton, C.; Sigmund, W. *Adv. Funct. Mater.* **2005**, *15*, 1197.

146. Kreibig, U.; Vollmer, M. *Optical properties of metal clusters* Berlin: Springer, **1995**.. (b) Kerker M. *The scattering of Light and Other Electromagnetic Radiation* New York: Academic, **1969**. (c) Bohren C. F.; Huffman, D. R.; *Absorption and Scattering of Light by Small Particles*. 1983, New York: Wiley. (d) Papavassiliou, G. C. Prog. *Solid State Chem.* **1979**, *12*, 185.

147. (a) Ghosh, S. K.; Nath, S.; Kundu, S.; Esumi, K.; Pal, T. *J. Phys. Chem. B* **2004**, *108*, 13963. (b) Link, S.; El-Sayed, M. A. *J. Phys. Chem. B* **1999**, *103*, 4212.

148. (a) Wilcoxon, J. P.; Martin, J. E.; Provencio, P. *Langmuir* **2000**, *16*, 9912. (b) Wilcoxon, J. P.; Martin, J. E.; Provencio, P. *J. Chem. Phys.* **2001**, *115*, 998. (c) Wilcoxon, J. P.; Provencio, P. *J. Phys. Chem. B* **2003**, *107*, 12949.

149. Creigton, J. A.; Eadon, D. G. *J. Chem. Soc. Faraday trans.* **1991**, *87*, 3881.

150. Asheroff, N. W.; Mermin, N. D. *Solid State physics*. 1976, Philadelphia: Sauders College.

151. (a) Gans, R. *Ann. Phys.* **1915**, *47*, 270. (b) Gans, R. *Ann. Phys.* **1912**, *37*, 881.

152. (a) Mohamed, m. B.; Ismael, K. Z.; Link, S.; El-Sayed, M. A. *J. Phys. Chem. B* **1998**, *102*, 9370. (b) van der Zande, B. M. I.; Bohmer, M. R.; Fokkink, L. G. J.; Schonenberger, C. *J. Phys. Chem. B* **1997**, *101*, 852.

153. Williams, D. B.; Carter, C. B. *Transmission Electron Microscopy*, Vol I-III, Kluwer Academic, Plenum Publishers, **1996**.

154. Chen, H.; Gao, Y.; Zhang, H.; Liu, L.; Yu, H.; Tian, H.; Xie, S.; Li, J. *J. Phys. Chem. B* **2004**, *108*, 12038.

155. Martin, J. E.; Odinek, J.; Wilcoxon, J. P.; Anderson, R. A.; Provencio, P. *J. Phys. Chem. B* **2003**, *107*, 430.

156. (a) Duan, J.; Yang, S.; Liu, H.; Gong, J.; Huang, H.; Zhao, X.; Zhang, R.; Du, Y. *J. Am. Chem. Soc.* **2005**, *127,* 6180. (b) Ding, Y.; Wang, Z. L. *J. Phys. Chem. B.* **2004**, *108*, 12280.

157. Goldstein, J. I. et al., *Scanning Electron Microscopy and X-ray Microananalysis,*

....

Physical and Materials Chemistry Division, National Chemical Laboratory   68

Kluwer Academic/ Plenum Publishers, New York, 3rd ed., **2003**.

158. Cullity, B. D.; Stock, S. R. *Elements of X-ray Diffraction*, 3rd Ed., Prentice Hall Pub. New Jersey. **2001**.

159. Zanchet, D.; Hall, B. D.; Ugarte, D. *J. Phys. Chem. B* **2000**, *104*, 11013.

160. (a) Sandhyarani, N.; Pradeep, T. *Chem. Mater.* **2000**, *12*, 1755. (b) Sandhyarani, N.; Resmi, M. R.; Unnikrishnan, R.; Vidyasagar, K.; Ma, S.; Antony, M. P.; Selvaam, G. P.; Visalakshi, V., Kumar, N. C.; Pandian, K.; Tao, Y. T.; Pradeep, T. *Chem. Mater* **2000**, *12*, 104.

161. (a) Nyffenegger, R. M.; Penner, R. M. *Chem. Rev.* **1997**, *97*, 1195. (b) Kossakovski, D.; Beauchamp, J. L. *Anal. Chem.* **2000**, *72*, 4731. (c) Durig, U.; Pohl, D. W.; Rohner, F. *J. Appl. Phys.* **1986**, *59*, 3318. (d) Rugar, D.; Budakian, R.; Mamin, H. J.; Chui, B. W. *Nature* **2004**, *430*, 329. (e) Schonenberger, C.; Alvarado, S. F.; Lambert, S. E.; Sanders, I. L. *J. Appl. Phys.* **1990**, *67*, 7278. (f) Martin, Y.; Wickramasinghe, H. K. *Appl. Phys. Lett.* **1987**, *50,* 1455. (g) Zhong, Q.; Innis, D.; Kjoller, K.; Elings, V. B. *Surf. Sci. Lett.* **1993**, *290*, L888. (h) Garcia, R.; Martinez, R. V.; Martinez, J. *Chem. Soc. Rev.* **2006**, *35*, 29. (i) http://en.wikipedia.org/wiki/Scanning_probe_microscopy

162. (a) Kaiser, W. J.; Jaklevic, R. C. *Surf. Sci.* **1987**, *181*, 55. (b) Binning, G.; Smith, D. P. E. *Rev. Sci. Instrum.* **1986**, *57*, 1688. (c) Dharmadhikari, C. V. In *Encyclopedia of Analytical Chemistry: Instrumentation and Applications*; Meyers, R. A.; Ed.; John Wiley, UK, **2000**.

163. Hosaka, S.; Koyanagi, H.; Kikukawa, A.; Miyamoto, M.; Imura, R.; Ushiyama, J. *J. Vac. Sci. Technol. B* **1995**, *13*, 1307.

164. (a) Sze, S. M. *VLSI Technology*, AT&T Bell Laboratories, Murray Hill, New Jersey. (b) Wieder, H. H. *Four Terminal Nondestructive Electrical and Galvanomagnetic Measurements* in *Nondestructive Evaluation of Semiconductor Materials and Devices* (J.N. Zemel, ed.), Plenum Press, New York, NY, **1979**, 67-104.

165. (a) Ingram, R. S.; Murray, R. W. *Langmuir* **1998**, *14*, 4115. (b) Pietron, J. J.; Hicks, J. F.; Murray, R. W. *J. Am. Chem. Soc.* **1999**, *121*, 5565. (c) Ingram, R. S.; Hostetler, M. J.; Murray, R. W.; Schaaff, T. G.; Khoury, J. T.; Whetten, R. L.; Bigioni, R. L.; Guthrie, D. K.; First, P. N. *J. Am. Chem. Soc.* **1997,** *119*, 9279. (d) Chen, S.; Ingram, R. S.; Hostetler, M. J.; Pietron, J. J.; Murray, R. W.; Schaaff, T. G.; Khoury, J. T.; Alvarez, M. M.; Whetten, R. L. *Science* **1998**, *280*, 2098. (e) Guo, R.;

....

Physical and Materials Chemistry Division, National Chemical Laboratory   69

Georganopoulou, D.; Feldberg, S. W.; Donkers, R.; Murray, R. W. *Anal. Chem.* **2005**, *77*, 2662. (f) Quinn, B. M.; Lijeroth, P.; Ruiz, V.; Kaaksonen, T.; Kontturi, K. *J. Am. Chem. Soc.* **2003**, *125*, 6644. (g) Hicks, J. F.; Miles, D. T.; Murray, R. W. *J. Am. Chem. Soc.* **2002**, *124*, 13322.

166. Terril, R. H.; Postlethwaite, T. A.; Chen, C. H.; Poon, C. D.; Terzis, A.; Chen, A.; Hutchison, J. E.; Clark, M. R.; Wignall, G.; Londono, J. D.; Superfine, R.; Falvo, M.; Johnson Jr., C. S.; Samulski, E. T.; Murray, R. W. *J. Am. Chem. Soc.* **1995**, *117*, 12537.

167. Hostetler, M. J.; Wingate, J. E.; Zhong, C.-J.; Harris, J. E.; Vachet, R. W.; Clark, M. R.; Londono, J. D.; Green, S. J.; Stokes, J. J.; Wignall, G. D.; Glish, G. L.; Porter, M. D.; Evans, N. D.; Murray, R. W. *Langmuir* **1998**, *14*, 17.

168. (a) Ulman, A. *Chem. Rev.* **1996**, *96*, 1533. (b) Badia, A.; Gao, W.; Singh, L.; Demers, L.; Cuccia, L.; Reven, L. *Langmuir* **1996**, *12*, 1262.

169. Arons, A. B.; Peppard, M. B.; *Einstein's Proposal of the Photon Concept - a Translation of the Annalen der Physik Paper* of 1905, Am. J. Phys. **1965**, 33, 367.

170. (a) Wagner, C. D.; Riggs, W. M.; Davis, L. E.; Moulder, J. E. *Handbook of X-ray Photoelectron Spectroscopy*; Perkin-Elmer Corp.: **1979**. (b) Sherwood, P. M. A. In *Surface Analysis by Auger and X-ray Photoelectron Spectroscopy*; Briggs, D., Grant, J. T., Eds. Surface Spectra Ltd. and IM Publications: Chichester, **2003**.

171. Kohlmann, O.; Steinmetz, W. E.; Mao, X.-A.; Wuelfing, W. P.; Templeton, A. C.; Murray, R. W.; Johnson, C. S., Jr. *J. Phys. Chem. B* **2001**, *105*, 8801.

172. (a) Brown, L. O.; Hutchison, J. E. *J. Phys. Chem. B* **2001**, *105*, 8911. (b) Bodkev, F.; Hansen, M. F.; Koch, C. B.; Leffman, K.; Steen, M. *Phy. Rev. B* **2000**, *61*, 6826. (c) Hutter, E.; Fendler, J. H.; Roy, D. *J. Phys. Chem. B* **2001**, *105*, 11159. (d) Freeman, R. G.; Grabar, K. C.; Allison, K. J.; Bright, R. M.; Davis, J. A.; Guthrie, A. P.; Hommer, M. B.; Jackson, M. A.; Smith, P. C.; Walter, D. G.; Natan, M. J. *Science* **1995**, *267*, 1629. (e) Chen, S.; Yang, Y. *J. Am. Chem. Soc.* **2000**, *124*, 5280. (f) Yang, Y.; Grant, K. M.; White, H. S.; Chen, S. *Langmuir* **2003**, *19*, 9446. (g) Chen, Y.; Palmer, R. E.; Shelley, E. J.; Preece, J. *Surf. Sci.* **2002**, *502-503*, 208. (h) Otsuka, H.; Akiyama, Y.; Nagasaki, Y.; Kataoka, K. *J. Am. Chem. Soc.* **2001**, *123*, 8226. (i) Armelao, L.; Colombo, P.; Fabrizio, M.; Gross, S.; Silvia, T. E. *J. Mat. Chem.* **1999**, *9*, 2893. (j) Georganopoulou, D. G.; Mirkin, M. V.; Murray, R. W. *Nano*

....

Physical and Materials Chemistry Division, National Chemical Laboratory   70

Lett. **2004**, *4*, 1763.

173. (a) Daniel, M-C.; Astruc, D. *Chem. Rev.* **2004**, *104*, 293. (b) Mulvaney, P. *Langmuir* **1996**, *12*, 788.

174. *Light Scattering by Nonspherical Particles* (Eds.: Mishchenko, M. I.; Hovenier, J. W.; Travis, L. D.), Academic Press, San Diego, **2000**.

175. (a) Sun, Y.; Yin, Y.; Mayers, B. T.; Herricks, T.; Xia, Y. *Chem. Mater.* **2002**, 14, 4736. (b) Caswell, K. K.; Bender, C. M.; Murphy, C. J. *Nano Lett.* **2003**, 3, 667.

176. (a) Bhattacharrya, S.; Saha, S. K.; Chakravorty, D. *Appl. Phys. Lett.* **2000**, *76*, 3896. (b) Zhu, J. –J.; Lia, X. –H.; Zhao, X. –N.; Chen, H. –Y. *Mater. Lett.* **2001**, *49*, 91.

177. Millstone, J. E.; Park, S.; Shuford, K. L.; Qin, L.; Schatz, G. C.; Mirkin, C. A. *J. Am. Chem. Soc.* **2005**, *127*, 5312.

178. (a) Cuenot, S.; Frétigny, C.; Demoustier-Champagne, S.; Nysten, B. *Phys. Rev. B* **2004**, *69*, 165410. (b) Levitt, A. P. *Whisker Technology*, Levitt, A. P., Ed.; Wiley-Interscience: New York, 1970. (c) Wong, E. W.; Sheehan, P. E.; Lieber, C. M. *Science* **1997**, *277*, 1971.

179. Segall, D. E.; Ismail-Beigi, S.; Arias, T. A. *Phys. Rev. B* **2002**, *65*, 214109.

180. Wu, B.; Heidelberg, A.; Boland, J. J. *Nature Materials* **2005**, *4*, 525.

181. Wu, B.; Heidelberg, A.; Boland, J. J.; Sader, J. E.; Sun, X.; Li, Y. *Nano Lett.* **2006**, *6*, 468.

182. Li, X.; Gao, H.; Murphy, C. J.; Caswell, K. K. *Nano Lett.* **2003**, *3*, 1495.

183. (a) Rubio-Bollinger, G.; Bahn, S. R.; Agraït, N.; Jacobsen, K. W.; Vieria, S. *Phys. Rev. Lett.* **2001**, *87*, 026101. (b) Rubio, G. Agraït, N.; Vieria, S. *Phys. Rev. Lett.* **1996**, *76*, 2302.

184. Scheer, E.; Agráit, N.; Cuevas, J. C.; Veuati, A. L.; Ludoph, B.; Martin-Rodero, A.; Rubio-Bollinger, G.; van Ruitenbeek, J. M.; Urbina, C. *Nature* **1998**, *394*, 780.

185. Rodrigues, V.; Fuhrer, T.; Ugarte, D. *Phys. Rev. Lett.* **2000**, *85*, 4124.

186. Gall, K.; Dia, J.; Dunn, M. L. *Nano Lett.* **2004**, *4*, 2431.

187. Marszalek, P. E.; Greenleaf, W. J.; Li, H.; Oberhauser, A. F.; Fernandez, J. M. *Proc. Natl. Acad. Sci. USA.* **2000**, *97*, 6282.

188. (a) He, H. X.; Tao, N. J. *Adv. Mater.* **2002**, *14*, 161. (b) Bogozi, A.; Lam, O.; He, H. X.; Li, C. J.; Tao, N. J.; Nagahara, L. A.; Amlani, I.; Tsui, R. *J. Am. Chem. Soc.* **2001**, *123*, 4585. (c) Takayanagi, K.; Kondo, Y.; Ohnishi, H. JSAP International, **2001**, *3*, 3.

Ph. D. Thesis   *Chapter 1*   *University of Pune, May 2006*

(d) Costa-Krämer, J. L.; García, N.; garcía-Mochales, P.; Serena, P. A.; Marqués, M. I.; Correia, A. Phys. Rev. B **1997**, *55*, 5416.

189. (a) Link, S.; Burda, C.; Mohamed, M. B.; Nikoobakht, B.; El-Sayed, M. A. *Phys. Rev. B* **2000**, *61*, 6086. (b) Link, S.; El-Sayed, M. A. *Annu. Rev. Phys. Chem.* **2003**, *54*, 331.

190. (a) Xiao, S.; Hu, W.; Yang, J. *J. Phys. Chem. B* **2005**, *109*, 20339. (b) Buffat, P.; Borel, J. –P. *Phys. Rev. A* **1976**, *13*, 2287. (c) Castro, T.; Reifenberger, R.; Choi, E.; Andres, R. P. *Phys. Rev. B* **1990,** *42*, 8548.

191. (a) Lakowicz, J.; Geddes, C.; Gryczynski, I.; Malicka, J.; Gryczynski, Z.; Aslan, K. Lukomska, J.; Matveeva, E.; Zhang, J.; Baduga, R.; Huang, J. *J. Fluresc.* **2004**, *14*, 425. (b) Thomas, K. G.; Kamat, P. V. *Acc. Chem. Res.* **2003**, *36*, 888.

192. Podolskiy, V. A. *Optics Express* **2003**, *11*, 735.

193. Narayanan, R.; El-Sayed, M. A. *J. Phys. Chem. B* **2005**, *109*, 12663.

194. Vo-Dinh, T. *Trends Anal. Chem.* **2002**, *74*, 504.

195. Tao, A.; Kim, F.; Hess, C.; Goldberger, J.; He, R.; Sun, Y.; Xia, Y. Yang, P. *Nano Lett.* **2003**, *3*, 1229.

196. (a) Maier, S. A.; Brongersma, M. L.; Kik, P. G.; Meltzer, S.; Requicha, A. A. G.; Atwater, H. A. *Adv. Mater.* **2001**, *13*, 1501. (b) 'Bright New World' *NewScientist* **2003**, 31 (www.newscientis.com).

197. (a) Murray, B. J.; Walter, E. C.; Penner, R. M. *Nano Lett.* **2004**, *4,* 665. (b) Walter, E. C.; Favier, F.; Penner, R. M. *Anal. Chem.* **2002**, *74*, 1546.

198. Alivisatos, P. *Nat. Biotechnol.* **2004**, *22,* 47.

199. (a) Mock, J. J.; Barbic, M.; Smith, D. R.; Schultz, D. A.; Schultz, S. *J. Chem. Phys.* **2002**, *116*, 6755. (b) Schultz, S.; Smith, D. R.; Mock, J. J.; Schultz, D. A. *Proc. Natl. Acad. Sci. USA* **2000,** *97*, 996. (c) Mock, J. J.; Oldenburg, S. J.; Smith, D. R.; Schultz, D. A. Schultz, S. *Nano Lett.* **2002**, *2*, 465.

200. Haes, A. J.; Hall, W. P.; Chang, L.; Klein, W. L.; van Duyne, R. P. *Nano Lett.* **2004**, *4,* 1029.

201. Zheng, G.; Patolsky, F.; Cui, Y.; Wang, W. U.; Lieber, C. M. *Nat. Biotechnol.* **2005**, *23,* 1294.

202. Takahashi, H.; Niidome, T.; Nariai, A.; Niidome, Y.; Yamada, S. *Chem. Lett.* **2006**, *35,* 500.

....

Physical and Materials Chemistry Division, National Chemical Laboratory   72

203. Li, Y.; Hong, X. M.; Collard, D. M.; El-Sayed, M. A. *Org. Lett.* **2000**, *2*, 2385.

204. (a) Chen, M. S.; Goodman, D. W. *Science* **2004**, *306*, 252. (b). Valden, M.; Lai, X.; Goodman, D. W. *Science* **1998**, *281*, 1647.

205. (a) Wu, Y.; Xiang, J.; Yang, C.; Lu, W.; Lieber, C. M. *Nature* **2004**, *430*, 61. (b) Friedman, R. S.; McAlpine, M. C.; Ricketts, D. S.; Ham, D.; Lieber, C. M. *Nature* **2005**, *434*, 1085.

206. Husain, A.; Hone, J.; Ch Postma, H. W.; Huang, X. M. H.; Drake, T.; Barbic, M.; Scherer, A.; Roukes, M. L. *App. Phys. Lett.* **2003**, *83*, 1240.

207. (a) Lieber, C. M. *Sol. State Commun.* **1998**, *107*, 607. (b) Chen, j.; Saeki, F.; Wiley, B. J.; Cang, H.; Cobb, M. J.; Li, Z-Y.; Au, L.; Zhang, H.; Kimmey, M. B. Li, X.; Xia, Y. *Nano Lett.* **2005**, *5*, 473.

Chapter 2

A Comparative Study on Nanoparticles and Nanowires of Silver*

The present chapter describes a study on silver nanowire synthesized by using 4-aminothiophenol as a new capping and reducing agent. These nanowires (NWs)
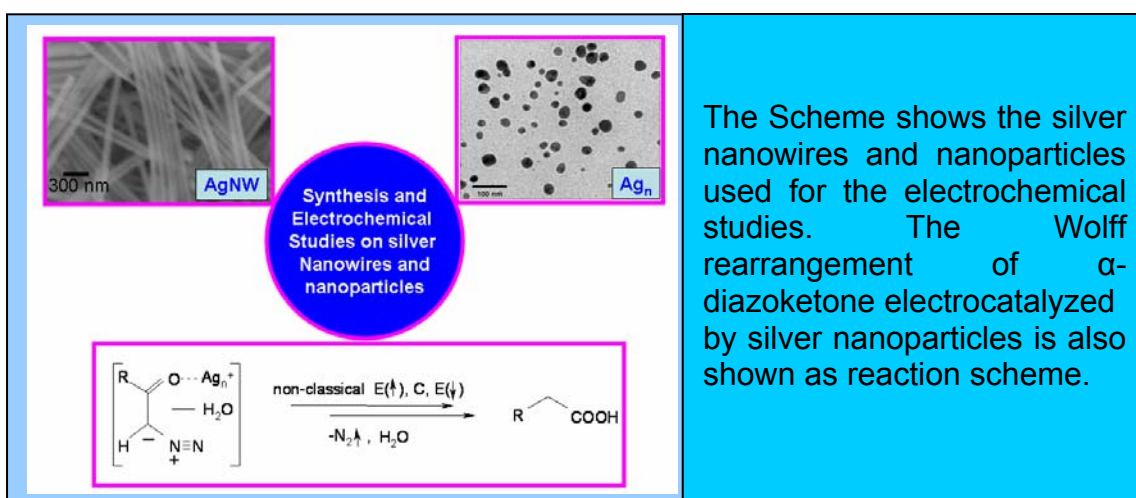
The Scheme shows the silver nanowires and nanoparticles used for the electrochemical studies. The Wolff rearrangement of α-diazoketone electrocatalyzed by silver nanoparticles is also shown as reaction scheme.

possess a diameter of about 60-80 nm and length of several micrometers revealing many interesting properties as a function of their aspect ratio. Electrochemical behavior of well defined NWs has been compared with that of spherical silver nanoparticles (Ag NPs) of similar sizes and capping agents. Interestingly, Ag NWs have been found to show quasi-reversible electron transfer process at smaller rate constant as compared to the electron transfer features of NPs. Finally, electrocatalytic activity of Ag NPs during the Wolff rearrangement of α-diazoketone has been demonstrated to reveal a remarkable application of these nanoclusters for electro-organic synthesis following a unique E(↑), C, E(↓) mechanism.

2.1 Introduction

After many decades of sustained efforts, different methods have been developed to synthesize nanoparticles/nanoclusters with fairly controlled shape and size. Consequently, different types of nanostructures including spherical nanoparticles, nanorods, nanowires, nanotubes, etc. have been synthesized by both high temperature and low temperature methods.[1] These materials with at least one dimension in the length scale of 1-100 nm show fascinating size and shape dependent properties arising from the quantum confinement.[2] For example, the lattice constant of the face-centered-cubic (fcc) unit cell of silver is contracted by as much as 9% for nanoparticles and the melting point is depressed by as much as up to 700 ^{0}C compared to that of bulk value (960 ^{0}C).[3] Similarly, the measured elastic modulus of the nanomaterials with smaller diameter is significantly higher than that of the larger ones comparable to macroscopic modulus of the material.[4a] Moreover, electronic properties including the photoelectron yield and the energy of the plasmon resonance absorption also exhibit similar size dependence.[4] These observations lead to the expectation that the electrochemical properties of nanoparticles should also be size dependent. Many experimental studies indeed show the size dependent electrochemical properties. According to Plieth, the standard redox potential (E^0) of the nanoclusters of silver shifts negatively from the corresponding bulk E^0, provided that the surface free energy (g) is the same for both.[5] This is further confirmed by the pulse radiolysis experiment of Henglein et al., where a single Ag atom exhibits an E^0 of -1.8 V vs. NHE (+0.799 V for bulk Ag), while the silver trimer (i.e. Ag_3) is found to have an E^0 near -1.0 V.[6, 7]

Similarly, Mulvani et al. have investigated the surface plasmon resonance (SPR) absorption of small polyacrylic acid coated silver nanoclusters using an optically transparent thin layer electrode by spectroelectrochemistry revealing the dependence of the SPR band on the applied potential and shape and size.[8] Interestingly, metal nanoparticles also exhibit interesting size and shape dependent catalytic activity.[9] Several reactions such as electron-transfer reaction, cross-coupling reaction, hydrogenation, oxidation, have been investigated using various colloidal and supported metal nanoparticles.[10] In many cases, metal nanoparticles show unusual catalytic activity due to high surface-to-volume ratio and high surface energy, not observed for their bulk counterparts. El-Sayed and co-workers have recently demonstrated the effect of

....

Physical and Materials Chemistry Division, National Chemical Laboratory   75

catalyst size and shape on the energetics and dynamics of electron transfer processes.[10d, 11] During the course of the reactions, shape changes occur due to the dissolution of atoms from the corners and edges leading to a change in activation energy. These shape changes also cause reduction in catalytic activity for few cases, such as Suzuki cross-coupling reaction catalyzed by tetrahedral platinum nanoparticles.[12]

Among different types of nanomaterials, high aspect ratio nanostructures are of particular interest, since their shape anisotropy offers additional degrees of freedom for manipulation of their properties as compared to spherical particles.[13] The feasibility studies of molecules on anisotropic metal surfaces have been carried out with techniques such as surface enhanced Raman spectroscopy and various such geometries have been proposed for molecular recognition.[13b-d] Another fact of general interest is that they provide experimental confirmation of theoretical predictions, which describes the unique properties of high aspect ratio nanomaterials based on few theoretical approaches such as the discrete dipole approximation (DDA), finite difference time domain methods (FDTD), and the modified long wavelength approximation (MLWA).[14] However, a precise control of their size, shape, composition, crystallinity and structure is desired to resolve some of the key issues regarding their possible applications in catalysis, photonics, optoelectronics, etc. with unique physico-chemical properties.

One of the exciting and important high aspect ratio nanostructures is silver nanowires. Silver nanowires have received a special interest because bulk silver exhibits highest electrical and thermal conductivities. Accordingly, several methods have been developed for the synthesis of silver nanowires and nanorods. For example, a glucose reduction route for the large scale synthesis of silver nanowires has been demonstrated recently.[15] The synthesis procedure involves the addition of aqueous silver nitrate to a vigorously agitated aqueous solution of glucose and PVP, which was then heated at 450 K in a Teflon-sealed autoclave. Similarly, capillarity of carbon nanotubes (CNTs) offers a unique template for the growth of metallic and semiconductor nanowires.[16] However, the best known method so far, for silver nanowires is the polyol synthesis, where liquid polyols such as diethylene glycol (DG) and ethylene glycol (EG) are used as both solvent medium and reducing agents.[17, 18] Xia and co-workers have extensively

....

Physical and Materials Chemistry Division, National Chemical Laboratory   76

investigated the polyol synthesis of silver nanowires establishing the critical role of Pt nanoparticle seeds in determining the morphological evolution.[19] However, subsequent developments have clearly established that Pt seed is not a prerequisite for the growth of silver nanowires as it can be formed even by a simple self seeding process.[20] Ethylene glycol serves as a good solvent for both $AgNO_3$ and PVP, because of its relatively high dielectric constant (~ 37).[19-21] Several such methods have been described in the previous chapter.[22, 23] However, most of the existing methods suffer from lack of selectivity, since it is almost impossible to get pure (100%) nanowires. Similarly, another major draw back of these generic synthetic methods is the difficulty regarding the reproducibility of nanowires with similar diameter and length. Therefore it is widely accepted that further investigations would be of great value if we can understand the growth mechanism and role of various growth controlling factors such as solvent properties, which could solve few of these present limitations.[24]

In the present chapter, a new method of silver nanowire synthesis by 4-aminothiophenol (4-ATP) in aqueous acetonitrile is discussed. 4-ATP is chosen because it spontaneously organizes into rod-shaped micelles (or inverse micelles) when their concentration reaches a critical value. These anisotropic structures immediately act as soft templates to promote the formation of nanowire when coupled with appropriate chemical reactions.[25] Consequently, 4-ATP plays the multiple role of acting both as a soft-template and reducing agent. These nanowires are characterized by different techniques such as TEM, XRD, FTIR, TGA. Further, systematic investigations of the electrochemical properties of PVP capped silver nanowires and nanoparticles of similar diameter have been presented. More specifically, electrochemical properties of well defined silver nanowires and spherical nanoparticles synthesized by standard polyol process are investigated using cyclic voltammetry in different electrolytic conditions. We compare present electrochemical studies with our recent investigations on redox behavior of dodecanethiol protected silver nanoparticles with the systematic variation in size (2–7 nm). Previous investigations have revealed multiple redox responses for gold nanoparticles in non-aqueous medium, while silver nanoparticles showed irreversible redox behavior in aqueous KCl solution.[26a] More interestingly, we have found that redox properties are affected by the size and shape as in agreement with the theoretical calculations.[5,6] Finally, electro-catalytic activity of silver nanoparticles is discussed

considering the Wolff rearrangement of α-diazoketones as a typical example. We have developed a simple preparatory method for the Wolff rearranged carboxylic acids involving ketocarbenes as intermediates, demonstrating an important catalytic application of silver nanoparticles. We propose a mechanism for Wolff rearrangement based on the electrochemical results.

2.2 Experimental Section

2.2.1 Materials: 4-aminothiophenol (4-ATP, 90%), Hydrogen Hexachloroplatinate(IV) Hydrate ($H_2PtCl_6.6H_2O$. 99.9 %), and Poly(N-vinyl pyrrolidone) (PVP, MW 55,000) were purchased from Aldrich Chemicals, while silver nitrate ($AgNO_3$, 99.9 %) and all other chemicals were procured from Merck, India. All these chemicals were used without further purification. Water used for these experiments was de-ionized with Milli-Q reagent system (18 MΩ cm).

2.2.2 Synthesis of Silver Nanowires by 4-ATP: Three different samples were prepared by mixing 0.01M (2 ml) aqueous solution of $AgNO_3$ and 0.01 M ATP solution in acetonitrile with mixing ratio each of 1:2 (sample 1), 1:5 (sample 2) and 1:10 (sample 3). For sample 1, solution was diluted to make the final ratio of water to acetonitrile (a) 1:5 and (b) 5:1 respectively. These mixtures were stirred gently for few seconds to get yellow solutions, except for sample 1, which was red. To study the effect of solvent, various samples were prepared as a function of the mole fraction of acetonitrile in water keeping the final concentrations of $AgNO_3$ and ATP both constant at 1 mM (the total volume of all these samples was 10 ml each).

2.2.3 Synthesis of Silver Nanowires by Polyol Process: Silver nanowires were synthesized by polyol method with minor modifications.[20] Briefly, 1 mM H_2PtCl_6 solution in 5 mL of ethylene glycol was heated for 1 h under refluxing condition at 150 ^{0}C in a three necked round bottom flask fitted with a condenser. In the next step, 5 mL 0.06 g $AgNO_3$ and another 5 mL of 0.20 g PVP in ethylene glycol were simultaneously added slowly to the reaction flask. Heating was continued for another 1 h under vigorous stirring at 170 ^{0}C. The solution color turned yellow to grey, indicating the formation of silver nanowires. After cooling the solution to room temperature, silver nanowires were

....

Physical and Materials Chemistry Division, National Chemical Laboratory   78

separated by adding excess amount of acetone.

2.2.4 Synthesis of Silver Nanoparticles: Silver nanoparticles (for convenience, Ag NPs or sometimes Ag_n) with average size 40 ($\pm$ 10) nm were synthesized following a similar process adopted for preparing silver nanowires by polyol process, but with a major modification in the procedure. Briefly, 10 mL of 0.2 g PVP in ethylene glycol was heated for 1 h at 80 ^{0}C in a round bottom flask fitted with a condenser. A homogenous solution was achieved, and then 0.05 g $AgNO_3$ was added at a time and heating was continued for another 2 h under vigorous stirring. The solution slowly turned yellow and was cooled to room temperature and was mixed with excess amount of acetone (100 mL) and kept undisturbed for 24 h. Silver nanoparticles were precipitated at the bottom of the flask and washed several times with acetone before cyclic voltammetric experiments.

2.2.5 Characterization Techniques

The finer details of characterization techniques have been discussed in the previous chapter. Therefore, a brief discussion about all instruments used for the present study has been given here.

2.2.5.1 UV-visible Spectroscopy: All UV-visible absorption measurements were recorded using UV-2101PC double beam spectrometer, Shimadzu with quartz cells of 1 cm path length. The spectra were background subtracted using the solvent used for nanoparticle dispersion.

2.2.5.2 TEM Analysis: The TEM micrographs were taken on a JEOL model 1200EX instrument operated at an accelerating voltage of 120 KV. The TEM samples were prepared by drop-casting the respective solutions on a carbon coated Cu grids (3 nm thick, deposited on a commercial copper grid) and air dried at room temperature.

2.2.5.3 SEM Analysis: Scanning electron microscopic (SEM) measurements were carried out on a Leica Stereoscan-440 instrument equipped with Phoenix energy dispersive analysis of X-ray (EDAX) attachment.

2.2.5.4 XRD Analysis: X-ray diffraction was carried out on a Philip1730 machine using

....

Physical and Materials Chemistry Division, National Chemical Laboratory   79

CuKα radiation (λ = 1.54 A^0) at a step of 0.02° (2θ) at room temperature. The background was subtracted with the linear interpolation method. Samples were prepared by making thin films on glass substrates.

2.2.5.5 FTIR Analysis: Fourier transform infra-red (FTIR) spectroscopic measurements were recorded on Shimadzu 8201-PC. Spectra were recorded in the diffuse reflectance mode at a resolution of 4 cm^{-1} at room temperature. Samples were drop casted (from dispersions in acetonitrile) on silicon substrates to form thin films and then vacuum dried.

2.2.5.6 Thermogravimetric Analysis: The TGA-7, Perkin Elmer thermal analysis system was used to determine the thermal stability of nanoparticles. The samples were heated under constant nitrogen flow from 323 to 1170 K (or desired temperature range) with a scanning rate of 5 K/min and the resultant weight loss was recorded.

2.2.5.7 Electrochemical Measurements: Electrochemical measurements were carried out on an Autolab PGSTAT30 (ECO CHEMIE) instrument using sample coated on Pt (2 mm) disk as a working electrode, Pt flag as counter electrode and Ag/AgCl as reference electrode under different electrolytic media. The working electrode was prepared by drop-casting the respective solutions containing nanoparticles several times on the electrode followed by careful drying in air. All experiments were carried out with above specifications, unless mentioned separately.

2.2.5.8 Procedure for Controlled Potential Coulometry of α-Diazoketones: The controlled potential coulometry (CPC) of the α-diazoketone was carried out on an EG & G Potentiostat using a divided cell assembly (Figure 2.1). Ag$_2$O coated on Pt-plate (1 cm^2) was used as the anode, while a graphite plate (area 4 cm^2) was used as the cathode. Experiments were carried out using Ag/AgCl as reference electrode (wherever required) in aqueous acetonitrile (H$_2$O: CH$_3$CN, 1:10 v/v), 200 mL (this mixing ratio was maintained for all electrochemical experiments involving Wolff rearrangement). 1.2 g LiClO$_4$ was used as electrolyte for the coulometry at 0.4 V in presence of 0.510 g of respective α-diazoketones at 300 K.

The electrochemical reaction begins after the application of an anodic potential and the coulometry was continued till the evolution of nitrogen from the anode surface ceased; at this time the cell current attained a constant value. Additionally, thin layer

....

Physical and Materials Chemistry Division, National Chemical Laboratory   80

chromatographic analysis indicated the complete disappearance of starting α-diazoketones. The resulting solution was concentrated in vacuum and the residues were worked- up to get the rearranged carboxylic acids. The residues were dissolved in ethyl
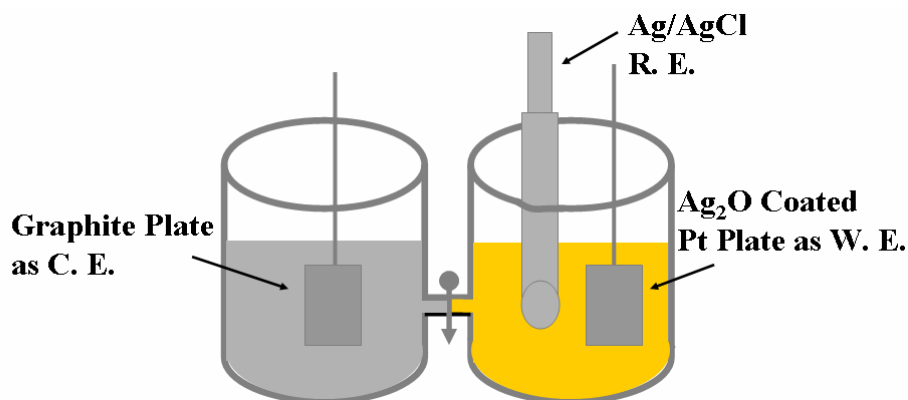
Figure 2.1: Schematic of coulometric set up (not to scale).

acetate (50 mL) and extracted with aqueous sodium bicarbonate (1M in H_2O, 3 x 10 mL). The alkaline extracts were acidified to pH 4 using hydrochloric acid (1M) at 273 K and the liberated carboxylic acids were extracted using chloroform (3 x 20 mL). The organic layers were dried over anhydrous sodium sulfate and were concentrated under reduced pressure to analyze the Wolff-rearranged products. The crude products were further purified by crystallization to give the pure carboxylic acids.

2.3 Results and Discussion

The high positive redox potential of the Ag/Ag^+ couple (+0.799 V vs. NHE) implies the possibility of facile reduction of Ag^+ ion by a wide range of reducing agents such as triethylamine and N,N-dimethyl formamide and triethylamine.[26b] Therefore, it is of general interest to see the reducing capability of other amino group containing polyfunctional organic molecules and to find their role on controlling the growth of nanoparticles. We have found that 4-ATP can also be used for the reduction of Ag^+ ions to form silver nanoparticles and nanowires. Accordingly, we have investigated the 4-ATP concentration as well as the mole fraction of acetonitrile/water to control the aspect ration of silver nanoparticles.

2.3.1.1 Effect of 4-ATP Concentration and Solvent Mixing Ratio

The formation of silver nanoparticles by 4-ATP is manifested by the instantaneous appearance of a deep yellow color, which is verified by UV-visible absorption spectroscopy. In general, UV-visible absorption peak position of silver nanoparticles varies with the shape, size and distribution and also with the solvent properties like dielectric constant.[27] Figure 2.2(a) shows the UV-visible spectra of samples 1(a) and 1(b) (recorded after 1h of mixing), where the surface plasmon absorptions can be seen as two shoulders at (i) ca. 415 and (ii) ca. 460 nm respectively, confirming the formation of silver nanoparticles. The shift in their peak positions observed for the above samples is rationalized by the variation in particle size as well as the change in dielectric constant of the dispersing medium. Nevertheless, a pronounced red shifted peak position of sample 1(b) could also be attributed to the possibility of assembly formation.
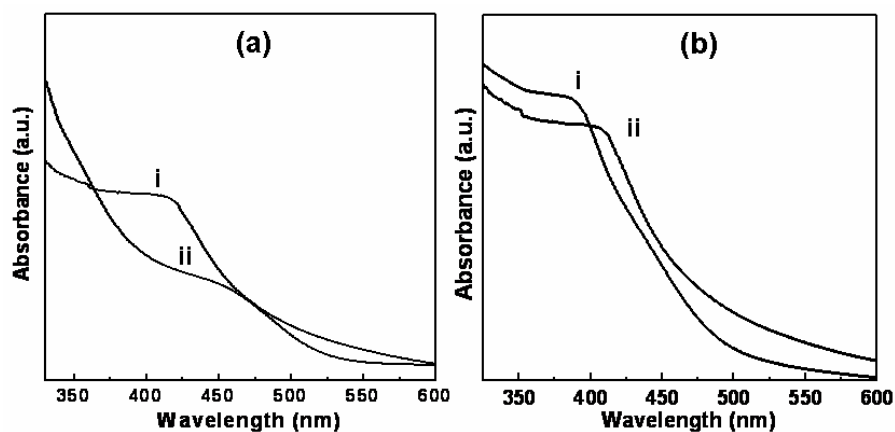
Figure 2.2 (a) UV-Visible absorption spectra of AgNPs prepared by mixing 0.01 M aqueous solution of AgNO$_3$ (2ml) and 0.01 M 4-ATP (4ml) in acetonitrile with the final ratio of water and acetonitrile (i) 1:5 (ii) 5:1. (b) UV-Visible absorption spectra of silver nanowires (i) sample 3 with mixing ratio 1:10, (ii) sample 2 with mixing ratio 1:5.

The plasmon absorption for nanorods/nanowires splits into two distinct peaks corresponding to the perpendicular and longitudinal oscillations of the free electrons along the nanowire axis.[28] However, as the aspect ratio exceeds 5, the plasmon absorption corresponding to longitudinal oscillations is not observed.[28b, 19, 29] For example, Figure 2.2.b (i) shows only a shoulder at ca. 390 nm in the UV-visible spectrum of the sample 3. Similarly, Figure 2.2.b (ii) shows a weak surface plasmon feature at ca. 405 nm for sample 2, depicting the formation of high aspect ratio silver nanowires.

These results are in agreement with reported values corresponding to the formation of high aspect ratio silver nanostructures.[19, 29a,b, 30] However, the well-resolved sharp peak for silver nanoparticles is absent for 4-ATP capped silver nanostructures, presumably due to the attached π-system containing the -NH$_2$ group which flattens the surface plasmon absorption peak.[6a, 31]
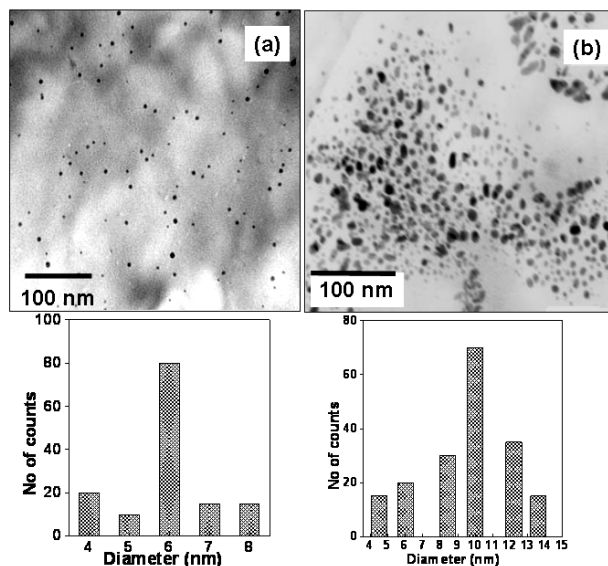
Figure 2.3 TEM images of silver nanoparticles, prepared by mixing 0.01 M aqueous solution of AgNO$_3$ and 0.01 M 4-ATP solution in acetonitrile with the final ratio of water and acetonitrile (a) 1:5 (b) 5:1 along with the respective histograms given below the images. Particles were counted for a particular area by an arbitrary unit (a.u.).

Figures 2.3(a) and 2.3(b) show TEM images of samples 1(a) and 1(b), where nanoparticles of 6 and 10 nm respectively can be seen. More specifically, Figure 2.3(a) shows a uniform distribution of smaller sized nanoparticles, whereas Figure 2.3(b) shows polydispersity, as is evident from the corresponding histograms. In comparison, however, Figure 2.4(a) shows the formation of low aspect ratio (R<30) silver nanowires from sample 2. These nanowires are not uniform in length and width due to the low ATP concentration. For example, high ATP concentration in sample 3 produces very high aspect ratio nanowires (up to 100) as shown by the TEM image in Figure 2.4(b). Interestingly, the length of these nanowires is found to vary from ~1 to ~8 μm, with a diameter of 60-80 nm. Moreover, the selected area electron diffraction pattern shown in the inset of Figure 2.4(b), depicts that these wires are crystalline, which could be

indexed to fcc silver.
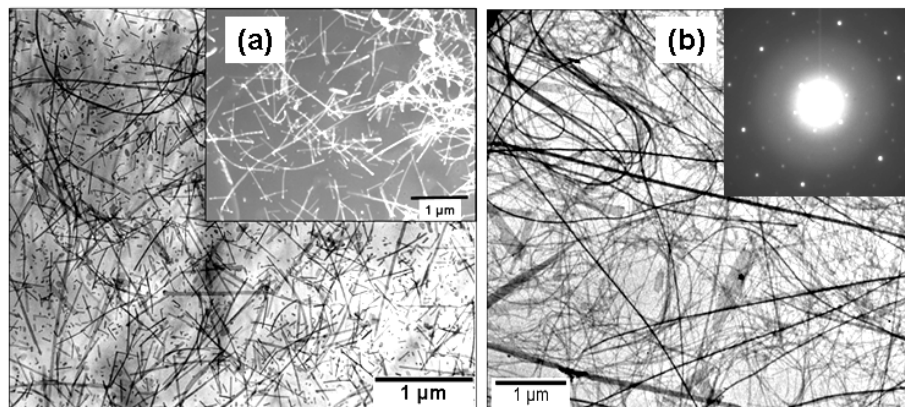
Figure 2.4 TEM images of silver nanowires, prepared by mixing 0.01 M aqueous solution of $AgNO_3$ and 0.01 M ATP solution in acetonitrile with the mixing ratios (a) 1:5 and (b) 1:10. Inset of 'a' shows the dark field image of nanowires, while inset of 'b' shows the SAED pattern.

The crystal structure of these nanowires is further verified by powder X-ray diffraction for a large quantity of the sample. Figure 2.5(a) shows the XRD pattern of as prepared silver nanowires (sample 3), which shows peaks corresponding to diffraction from (111), (200), (220), (311) crystal planes of bulk fcc silver. In comparison, Figure 2.5(b), shows the XRD pattern for the sample 1(a), where predominant (200) crystal plane is evident. The lattice constants from these patterns are 4.089 and 4.078 Å for samples 1(a) and 3 respectively.
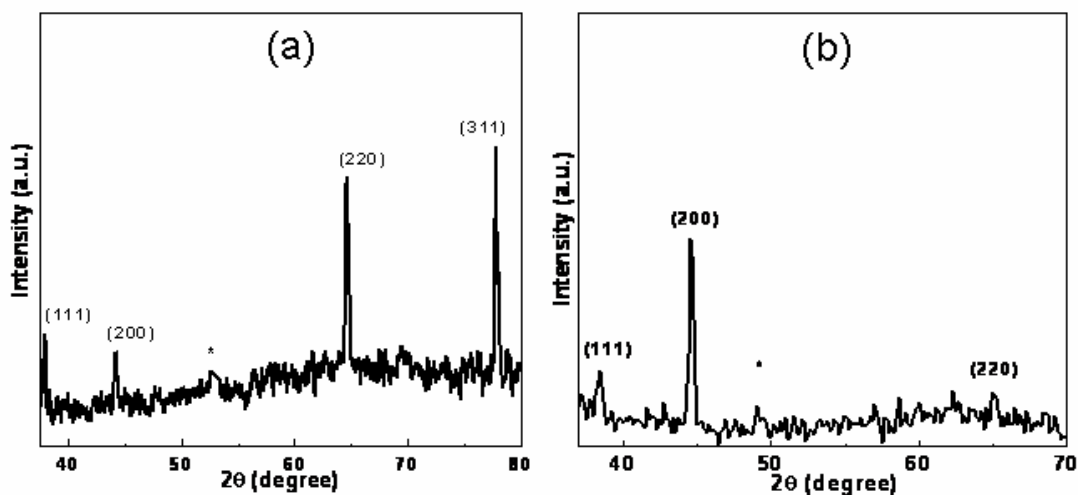
Figure 2.5 XRD pattern of as synthesized silver (a) nanowires from sample 3 and (b) nanoparticles from sample 1.a; corresponding lattice planes are also shown.

....

Physical and Materials Chemistry Division, National Chemical Laboratory   84

2.3.1.2 Effect of Solvent Mole Fraction

A significant effect of solvent on the aspect ratio is also observed by varying the mole fraction of acetonitrile in water systematically. Surprisingly, no nanoparticles are formed when the mole fraction is close to 1 as confirmed by the absence of surface plasmon peak in the UV-visible spectrum. However, the addition of ca. 0.5 ml water instantaneously turns the solution yellow and the surface plasmon feature appears as a shoulder at ca. 400 nm. This observation further indicates the importance of water content during the reduction process. For the other extreme case, i.e., when the mole fraction is close to 0, only spherical nanoparticles are formed as confirmed from the TEM analysis. TEM images of the nanowires prepared by varying the mole fraction are given in Figure 2.6. Formation of only spherical nanoparticles can be seen from the sample having the mole fraction close to 0, which is evident from the TEM image given in Figure 2.6(a). In the intermediate range (i.e., mole fractions corresponding to 0.4, 0.7 and 0.9) different aspect ratio nanowires are formed as shown in Figure 2.6(b-d) respectively. More specifically, high aspect ratio silver nanowires are seen in Figure 2.6(b) whereas Figure 2.6(d) shows low aspect ratio silver nanowires. In Figure 2.6(c), silver nanowires of an intermediate aspect ratio are seen.
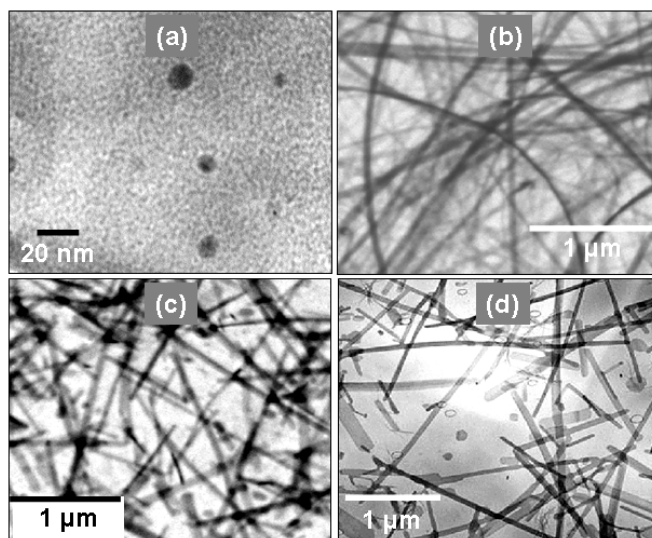
Figure 2.6 TEM images of nanostructures formed under different mole fractions (a) 0, (b) 0.4, (c) 0.7 and (d) 0.9. In all these cases final concentration of $AgNO_3$ and ATP were kept constant at 0.001M.

Interestingly, water accelerates reduction process because of its high dielectric

----

constant (~ 78). Therefore, in water, only spherical particles are formed. If 4-ATP concentration is too high, the effect of water is perhaps masked by the presence of high concentration of the reducing agent. The actual growth mechanism is still not established. One assumption is that hydrogen bonding character of water and acetonitrile at various mole fractions could play a major role during the growth of nanoparticles. However, it is clear from the present investigation that surfactant molecule (4-ATP) plays one of the key factors, by spontaneously organizing into rod-shaped micelles (or inverse micelle) when their concentration reaches a critical value. Figure2.7(a) shows the TEM image of such templates, while inset depicts TEM image of the linear organization of silver nanoparticles on such templates. These anisotropic structures immediately act as soft templates to promote the formation of nanowire when coupled with appropriate chemical reaction. 4-ATP exists as 4-ammmonio-1-benzenethiolate so that there is hydrogen bonding between S-H and N$^+$ where sulfur act as the donor.[25] This bridging between 4-ATP molecules helps it to form the soft template. Consequently, 4-ATP plays the double role both as a soft-template and reducing agent. This conclusion is supported by the recent findings, where the formation of nanowires from silver nitrate has been demonstrated following a similar approach.[32]
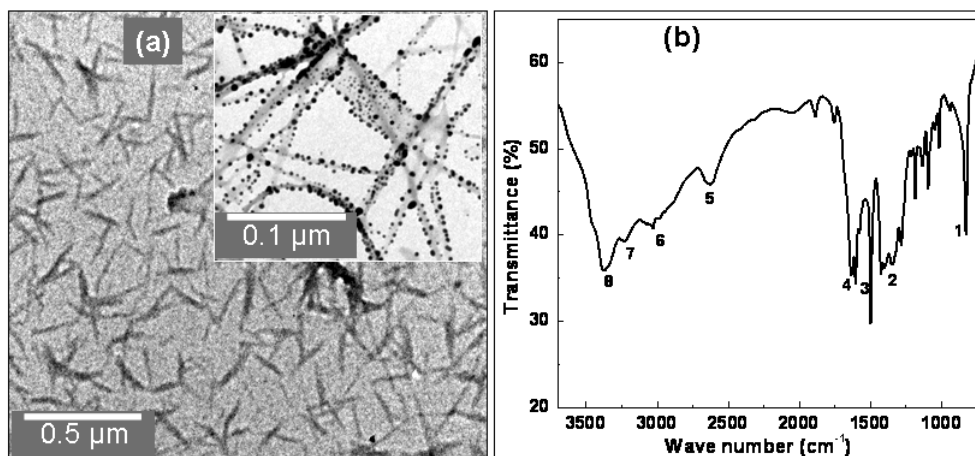
Figure 2.7 (a) TEM image of 4-ATP recorded from the solution in acetonitrile/water. (b) FTIR spectrum of the silver nanowires showing the presence of 4-ATP on the surface of nanowires, (peak positions are marked as 1-8 for different functional groups). Inset: TEM image of spherical silver nanoparticles organized on templates of 4-ATP.

In order to understand the molecular level interactions of 4-ATP with nanostructures, we further investigate all samples by FTIR spectroscopy. Similar results are obtained for

both nanowires and spherical nanoparticles suggesting that the nature and function of the monolayer protection is invariant to the aspect ratio. Figure 2.7(b) shows a typical FTIR spectrum, where band at (1) 825 cm^{-1} arises due to =C-H deformations of benzene ring. The bands arising due to the aromatic C=C in-plane vibrations at (4) 1625 and (3) 1497 cm^{-1} respectively, give valuable proof for the presence of benzene ring. Another peak at 3026 (6) cm^{-1} could be attributed to the stretching of aromatic =C-H bond. The occurrence of a very weak band at (5) 2624 cm^{-1} of S-H stretching indicates the presence of excess 4-ATP, which is not removed despite extensive washing. The spectrum also shows the appearance of an S=O stretch at (2) 1338 cm^{-1}, suggesting the oxidation of thiol. Interestingly, a medium absorption band of N-H at (8) 3375 cm^{-1} can be seen in the spectrum corresponding to the stretching of charged amine (-NH$_3^+$). This is followed by a weak band at (7) 3225 cm^{-1}, which corresponds to the stretching of
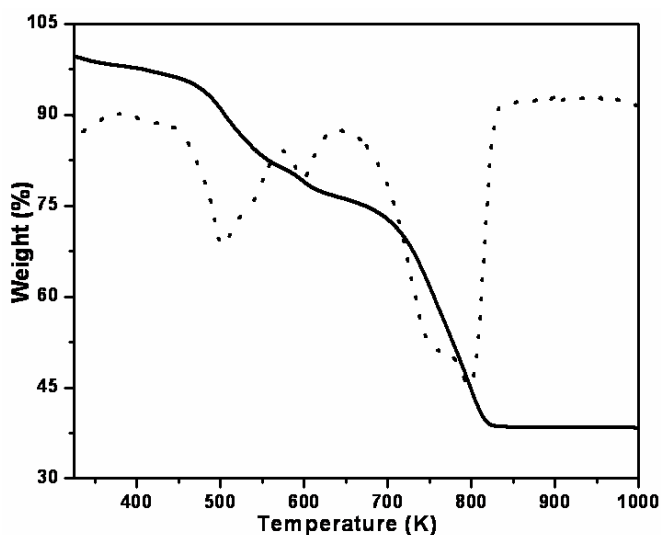
Figure 2.8 TG profile of 4-ATP capped silver nanowires along with its derivative (dotted line).

bonded N-H. Thus, FTIR spectrum gives conclusive evidence regarding the chemical nature of the protective molecular layer on silver surface. Thermo gravimetric analysis shows nearly 70 % organic molecules on nanowire surface, possibly due to the presence of several layers of 4-ATP on its surface by virtue of hydrogen bond. Figure 2.8 shows the TG profile for silver nanowires, indicating the onset of mass loss at 500 K, which finally completes at 820 K. More specifically, the thermogram shows major mass loss at three different temperatures i.e., 500, 600, and 790 K respectively indicating

different layers of organic molecules (it is expected that polymeric material can form as a result of oxidation of 4-ATP) attached on the surface.

The above experimental results suggest that the protecting molecule (i.e., 4-ATP) and the solvent mole fraction play a critical role in controlling the aspect ratio of these nanostructures. The presence of S=O stretching peak suggests that –SH group undergoes oxidation during the reaction. Moreover, the involvement of NH_2 group cannot be precluded especially because IR spectrum suggests the presence of charged species. TG analysis shows excess amount of 4-ATP on silver nanowires, which does not remove despite the extensive washing. The presence of excess amount of 4-ATP protects silver nanowires from external perturbations or reagents, which also limits the study of electrochemical properties of core. Significantly, these nanowires are electrically resistive (~10 MΩ). This is also a major disadvantage for practical applications of these nanowires, since 4-ATP is electrochemically active and sensitive towards air and undergoes further chemical reactions to form sulfide (chapter 3). To investigate the electrochemical properties of core, capping layer should be electrochemically inactive for a considerably large potential window. One of such capping agents is PVP, since it is electrochemically inactive and stable under normal experimental conditions. Therefore, in the following section, we have investigated the electrochemical properties of PVP capped silver nanowires and compared their properties with similar sized spherical silver nanoparticles.

2.3.2 Comparison of Electrochemical Properties of Silver Nanoparticles and Nanowires

Our recent investigation on the redox properties of dodecanethiol protected silver nanoparticles in the size range 2-7 nm has revealed the strong size dependent peak potentials and the occurrence of plateau type redox peaks, due to the effective surface passivation. However, electrochemical properties of silver nanoparticles beyond this size range and particularly of silver nanowires are not known. To fill this gap and compare the electrochemical properties of silver nanoparticles with nanowires, we have synthesized PVP capped 40 nm Ag NPs and 70 nm diameter nanowires and investigated their electrochemical properties. Figures 2.9(a) and 2.9(b) show the SEM and TEM images of Ag

....

Physical and Materials Chemistry Division, National Chemical Laboratory　　　　　　　88
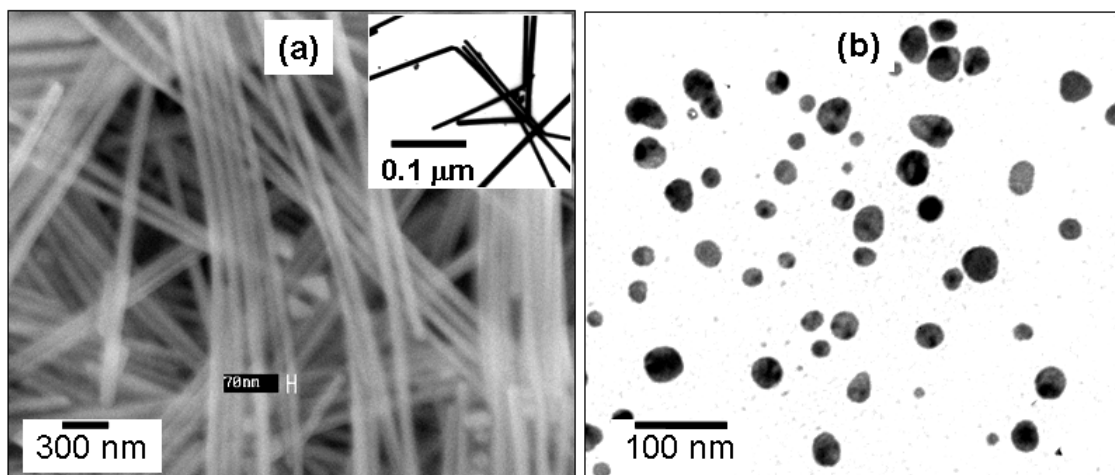
Figure 2.9 (a) SEM image of silver nanowires synthesized by polyol process; the inset shows TEM image of these silver nanowires. (b) TEM image of silver nanoparticles synthesized by polyol process at 80 ^{0}C.

NWs and NPs employed for the electrochemical investigations. Silver nanowires are relatively free from impurities such as spherical nanoparticles, while we could not control the growth to a particular size for spherical silver nanoparticles despite maintaining a critical reaction condition. However, the average size of these particles is around 40 nm which fortuitously serves our purpose to investigate the electrochemical properties of larger sized silver nanoparticles. Although, we tried to synthesize Ag NPs beyond this size range with polyol process, all our efforts to synthesize 70 nm particles resulted only in the formation of 40-50 nm particles.

(a) 0.1 M Aqueous KCl Solution: Figures 2.10(a) and 2.10(b) show the cyclic voltammograms of Ag nanowires and Ag nanoparticles in 0.1 M aqueous KCl solution at 0.05 Vs^{-1}. Interestingly, oxidation peaks are observed at 0.10 and 0.11 V for Ag NWs and Ag NPs respectively, while reduction takes place at -0.05 and -0.01 V. No significant variation of the peak potential with scan rate is observed for silver nanoparticles, while silver nanowires show moderate variation of peak potential with scan rate. Accordingly, the values of ΔEp are 0.15 and 0.12 V for Ag NWs and Ag NPs respectively, apparently indicating the change in electrochemical properties with diameter /size. The origin of an additional reduction peak (post peak) for nanoparticles is not clear. However, one

....

Physical and Materials Chemistry Division, National Chemical Laboratory   89
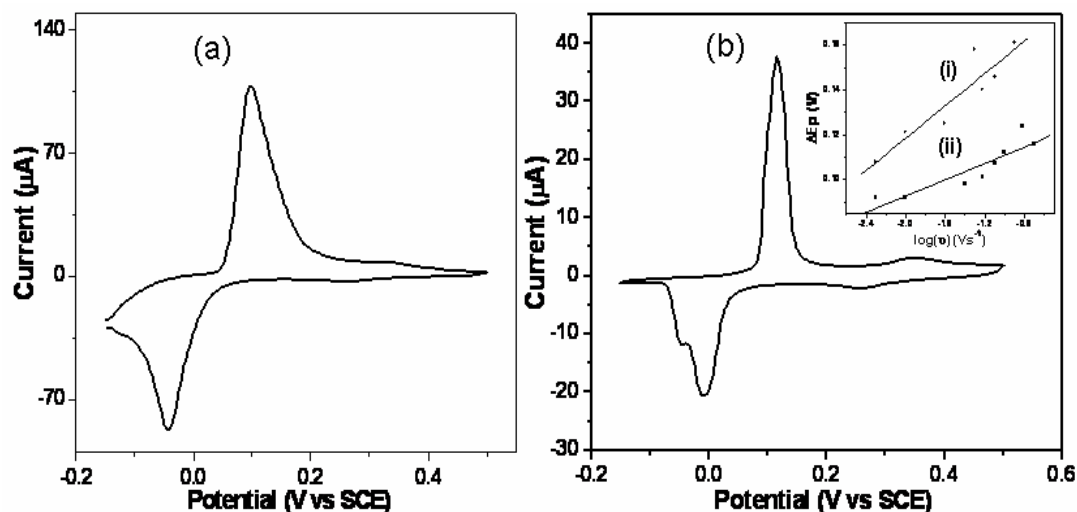
Figure 2.10 Cyclic voltammograms of silver nanowires (a) and silver nanoparticles (b) in 0.1 M aqueous KCl solution. Respective samples were drop-coated on an Au disk electrode (2mm) and were used as working electrode. A large Pt flag was used as counter and saturated calomel (SCE) was used as reference electrode. Inset of 'b' shows the variation of ΔEp with logarithm of scan rate for silver nanowires (i) and silver nanoparticles (ii).

possible explanation is due to the adsorption of Cl^- ion on Ag NPs. It does not happen in the case of Ag NWs because: (i) Ag NWs are more resistant to reduction (-0.05 V) than that of Ag NPs (-0.01 V) and (ii) perhaps capping is more effective for Ag NWs. Inset of Figure 2.10(b) shows the variation of ΔEp with logarithm of scan rates for silver nanowires (a) and nanoclusters (b). More abrupt changes of ΔEp values are observed for Ag NWs compared to that of Ag NPs as is evident from graph 'i' and 'ii'.

(b) 0.1 M Aqueous KNO$_3$ Solution: Figures 2.11(a) and 2.11(b) show the cyclic voltammograms of Ag NWs and Ag NPs recorded in 0.1 M aqueous solution of KNO$_3$ at a scan rate of 0.05 Vs^{-1}. The oxidation peaks are observed at 0.24 and 0.39 V for Ag NWs and Ag NPs respectively, while respective reduction processes occur at 0.09 and 0.29 V. Interestingly, the redox couple of Ag NWs is more symmetric in nature as compared to that of Ag NPs, where the reduction peak is observed as a plateau. Similar to earlier observation, the peak potential does not change significantly with scan rate for silver nanoparticles, while a moderate change is observed for silver nanowires. The ΔEp value is higher in case of Ag NWs (0.15 V) as compared to Ag NPs (0.10 V) indicating a
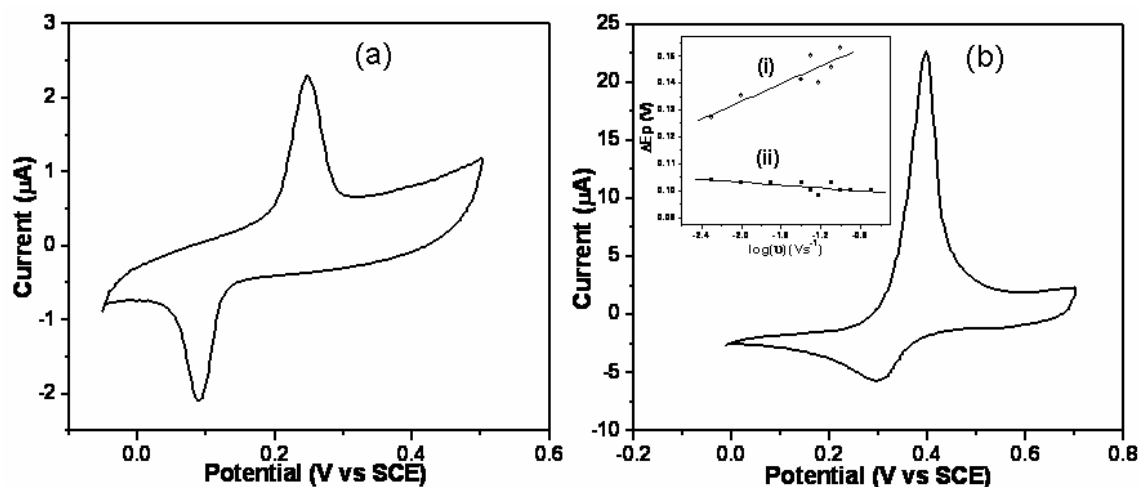
Figure 2.11 Cyclic voltammograms of silver nanowires (a) and silver nanoparticles (b) in 0.1 M aqueous KNO_3 solution. Respective samples were drop-casted on an Au disk electrode (2mm) to use as working electrode. A large Pt flag was used as counter and saturated calomel (SCE) was used as reference electrode. Inset of 'b' shows the variation of ΔEp with logarithm of scan rate for silver nanowires (i) and silver nanoparticles (ii).

variation of about 50 mV. Accordingly, inset of Figure 2.11(b) shows the variation of ΔEp with logarithm of scan rates for Ag NWs (i) and Ag NPs (ii). The more prominent variation of ΔEp for Ag NWs as compared to the Ag NPs with scan rate could be attributed to the dynamics of defects present on high aspect ratio structures due to more strain and enhanced surface energy. This is also in agreement with the thermodynamic finding that the half wave potential $E_{1/2}$ is greater for Ag NPs (0.34 V) as compared to that of Ag NWs (0.13 V).

(c) 0.1 M Aqueous LiClO$_4$ Solution: We have investigated the electrochemical properties of Ag NWs and Ag NPs in aqueous $LiClO_4$ solution to get more general information of electrochemical properties. Accordingly, Figures 2.12(a) and 2.12(b) show the cyclic voltammograms of Ag NWs and NPs recorded in 0.1 M aqueous $LiClO_4$ solution at a scan rate of 0.05 Vs^{-1}. Significantly, redox behavior is almost similar with respect to peak symmetry for both silver nanowires and silver nanoparticles, where oxidation peak is more intense as compared to the plateau like reduction peak. The oxidation takes place at 0.20 and 0.39 V for Ag NWs and Ag NPs respectively, while respective reduction processes occur at 0.05 and 0.28 V. Interestingly, the ΔEp value is again higher in case of Ag NWs (0.15 V) compared to that of Ag NPs (0.11 V) indicating

a moderate change (40 mV). The plot of ΔEp vs. logarithm of scan rate shows [inset of Figure 2.12(b)] an abrupt variation of ΔEp for Ag NWs as compared to that of Ag NPs. Similar electrochemical properties in 0.1 M $HClO_4$ solution are also observed. The present experimental results show that the relative magnitude of ΔEp is more for Ag NWs as compared to Ag NPs in all electrolytic media investigated. This feature indicates
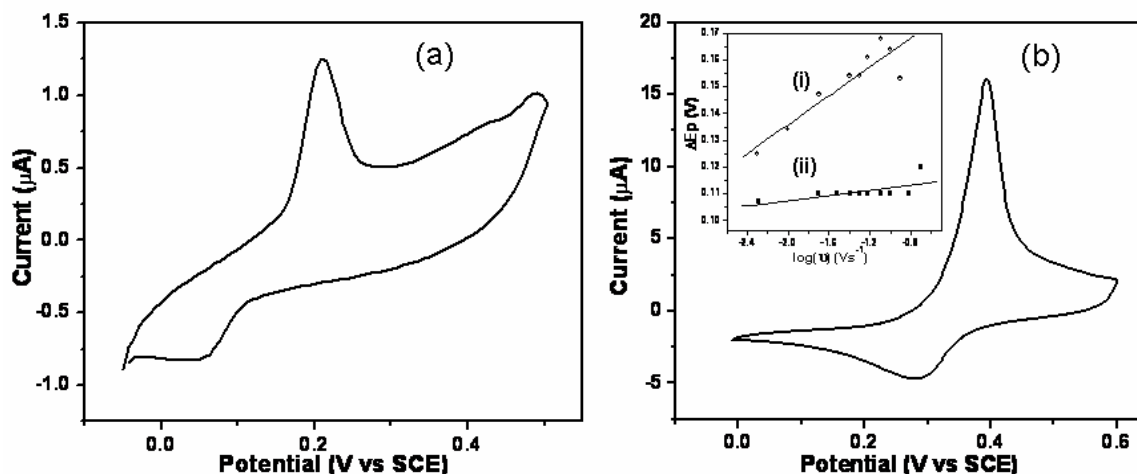
Figure 2.12 Cyclic voltammograms of silver nanowires (a) and silver nanoparticles (b) in 0.1 M aqueous $LiClO_4$ solution; respective samples were drop-coated on an Au disk electrode (2mm) and were used as working electrode. A large Pt flag was used as counter and saturated calomel (SCE) was used as reference electrode. Inset of 'b' shows the variation of ΔEp with logarithm of scan rate for silver nanowires (i) and silver nanoparticles (ii).

that Ag NWs will promote quasi-reversible electron transfer process occurring at smaller rate constant (k^0) as compared to Ag NPs.

The overall electrochemical experiments suggest that, Ag NWs and NPs show redox activity at a moderate potential window of -0.1 to 0.70 V. The electrochemical reaction can be represented by,

$$Ag_n^+ + e^- \;\; \rightarrow \;\; Ag_n^0 \qquad\qquad (2.1)$$
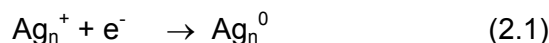
The oxidized species undergoes further chemical reactions depending on the electrolytic medium. The broad nature of redox peaks might arise due to a distribution of redox potentials corresponding to cluster dispersion, while the plateau type behavior of both oxidation and reduction peaks, as observed earlier for smaller nanoparticles, can be attributed to the microelectrode type behavior. Table 2.1 summarizes the $E_{1/2}$ values at different electrolytic conditions for Ag NWs and AgNPs. The half wave potential ($E_{1/2}$) is

fairly double for Ag NPs as compared to Ag NWs in all electrolytic media, i.e., KCl, KNO$_3$ and LiClO$_4$. The electrochemical study clearly demonstrates that electron transfer features, as revealed by the half wave potential (E$_{1/2}$) and ΔEp, are dependent on the shape and size of silver nanoparticles. Significantly, the E$_{1/2}$ values of silver nanowires and larger sized nanoparticles are relatively higher than that of the smaller sized DDT capped Ag NPs (2-7 nm). This is in agreement with the reported observation that for smaller sized nanoparticles, E^0 ($\approx$ E$_{1/2}$ for ideal reversible system) should shift negatively to that of larger counterparts.

Table 2.1 E$_{1/2}$ values under different electrolytic media

E$_{1/2}$ (V) vs. SCE	KCl	KNO3	LiClO4
AgNWs (dia. 70 nm)	0.03	0.16	0.13
AgNPs (40 nm)	0.05	0.34	0.33
AgNPs (DDT capped, 4.7 nm)	0.012	-	-

2.3.3 Electrocatalytic Role of Silver Nanoparticles on Wolff Rearrangement

The Wolff-rearrangement of α-diazocarbonyl compounds has been of tremendous synthetic utility for over a hundred years.[33] The rearrangement involves a stereospecific 1,2-carbon shift leading to the formation of ketene via a short lived α-ketocarbene intermediate following the expulsion of a nitrogen molecule.[34] This α-elimination of dinitrogen can be initiated under the influence of thermal energy, ultraviolet light, transition-metal catalyst or microwave radiation.[35] Although, many explicit suggestions, like the reduction of activation energy and the stabilization of reaction intermediates have been made, the mechanistic role of transition-metal catalyst remains enigmatic.[36] In the present section, we show that *in situ* generated silver nanoparticles from Ag$_2$O acts as electron   mediator during the Wolff rearrangement.

Attempts to trigger the α-elimination of nitrogen from α-diazocarbonyl compounds either by the removal or the addition of an electron using conventional electrodes, like platinum, glassy carbon lead to the realization of products arising from carbene cation

radical (CCR) or carbene anion radical (CAR) intermediates respectively.[37] However, the formation of products arising from α-ketocarbene intermediates is significantly missing. Similarly, efforts to induce the rearrangement by removing an electron from α-diazoacetophenone using triarylamine radical cation have failed, probably due to the non-occurrence of back donation of electron to the intermediate product. Significantly, a redox electrocatalyst offers a unique possibility to simultaneously remove one electron and to back donate following the α-elimination of dinitrogen from the diazo compounds or vice versa. [38]
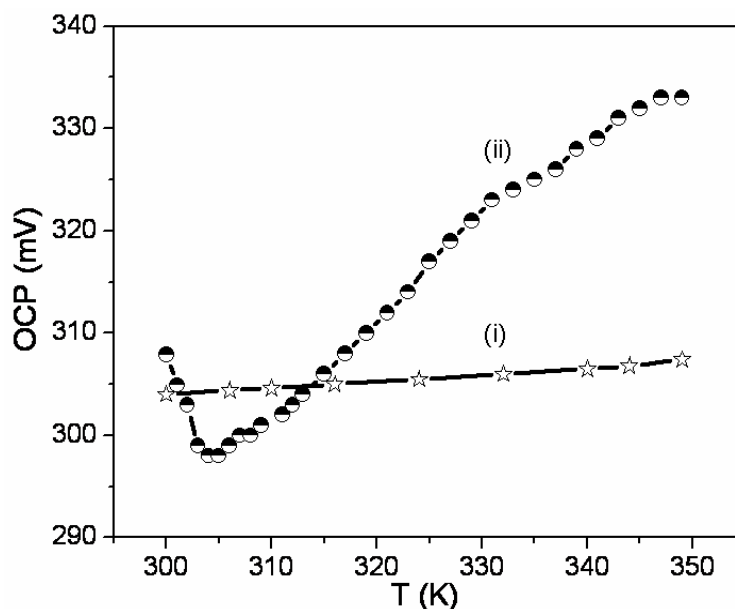
Figure 2.13 Plot of open circuit potential (OCP) as a function of temperature for the cell made up of silver (I) oxide coated on platinum wire as the working electrode and Ag/AgCl as the reference electrode in aqueous acetonitrile (H_2O : CH_3CN; 1 : 10 v/v) solution (i) and following the addition of the 1-Diazo-2-tridecanone '1a' (ii).

The preliminary information of the involvement of silver nanoparticles is acquired by monitoring open circuit potential (OCP, between Ag_2O coated working electrode and Ag/AgCl reference electrode) as a function of temperature following the addition of $CH_3(CH_2)_{10}COCH_2N_2$ (1-Diazo-2-tridecanone, 1a).[39] Figure 2.13 shows the plot of variation of OCP against temperature. Initially, the OCP decreases (curve ii) from 310 mV (300 K) to 299 mV (306 K) and then begins to rise along with copious evolution of nitrogen from the working electrode with a shift of about 34 mV in the anodic direction.

The initial shift of OCP in cathodic direction during the induction period (before the onset of nitrogen evolution) indicates the reduction of Ag_2O. This *in situ* formation of Ag_n triggers the decomposition of α-diazoketone, 1a and hence the OCP moves rapidly to more positive values. The anodic direction of the OCP change and the nature of the electrocatalyst together indicate the oxidation of α-diazoketone, 1a, as one of the important steps during the sequential generation of ketene (Scheme 2.1). In contrast, experiments performed in the absence of diazo compounds shows no such noteworthy change in OCP (Figure 2.13, curve 'i').
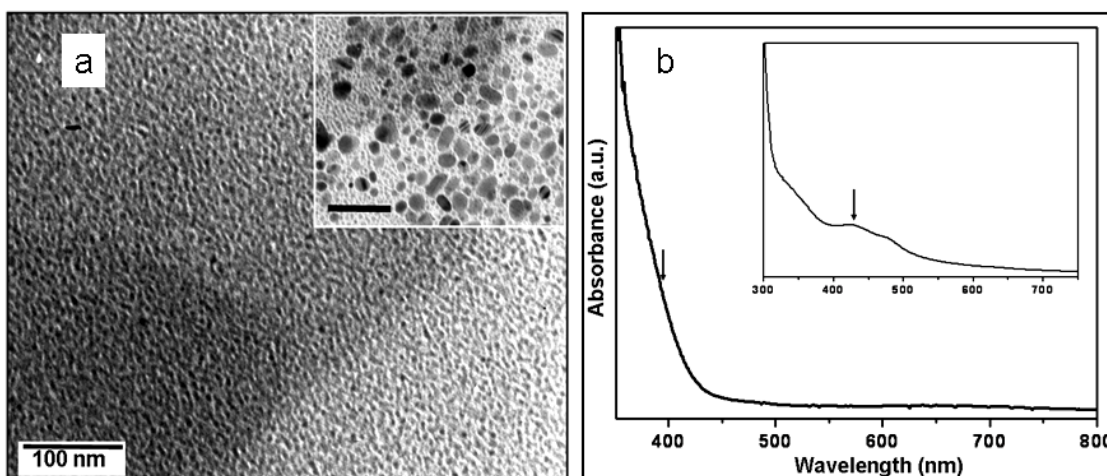
Figure 2.14 (a) TEM image of *in situ* generated Ag_n from Ag_2O on the addition of α-diazoketone, 1a. Inset shows TEM image taken after 1 h of the reaction exhibiting particle size growth, with time (scale bar is 100 nm). (b) UV-visible absorption spectrum of *in situ* generated Ag_n in aqueous acetonitrile (1:10 v/v), while inset shows the UV-visible spectrum recorded in toluene.

Figure 2.14 shows the TEM and UV-visible spectra of silver nanoparticles generated during the electrochemical reactions. More specifically, UV-visible analysis shows the presence of a surface plasmon absorption band at *ca.* 400 nm, a distinct characteristic of Ag_n.[6a] Accordingly, Figure 2.14(b) shows the UV-visible spectrum of silver nanoclusters formed after the addition of diazoketone to a dispersion of Ag_2O in both aqueous acetonitrile and toluene (inset). It is interesting to note that UV-visible spectrum of silver nanocluster in aqueous acetonitrile fails to show distinct surface plasmon peak due to solvent effect, while spectrum in toluene shows a distinct absorption at 415 nm. Further, transmission electron microscopy (TEM) also confirms the presence of nearly mono-

dispersed Ag nanoclusters (2- 4 nm). Accordingly, Figure 2.14(a) shows the TEM image of silver nanoclusters formed in aqueous acetonitrile after addition of diazoketone.

The electrochemical behavior of Ag_2O in the absence of α-diazoketone also reveals the *in-situ* formation of Ag_n,

$$Ag_2O + H_2O + 2e^- \rightarrow 2Ag^\circ + 2OH^- \quad (E^\circ = 0.342 \text{ V vs. NHE}) \text{------------ (1)}$$
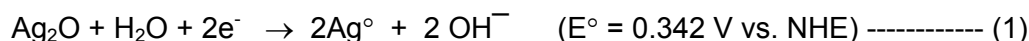
Voltammetric analysis of these *in situ* generated Ag_n clusters in aqueous acetonitrile reveals the presence of a distinct redox couple with unique electron transfer properties as represented by voltammogram 'i' in Figure 2.15. The redox couple is centered at *ca.* 0.27 V with anodic and cathodic peaks at *ca.* 0.34 and 0.2 V respectively. Furthermore, the ratio of areas of anodic to cathodic peaks is fairly close to unity (1.13), while individual peak potential shows marginal variation as a function of the scan rate. Interestingly, the presence of capping agents stabilizes and guides electron transfer
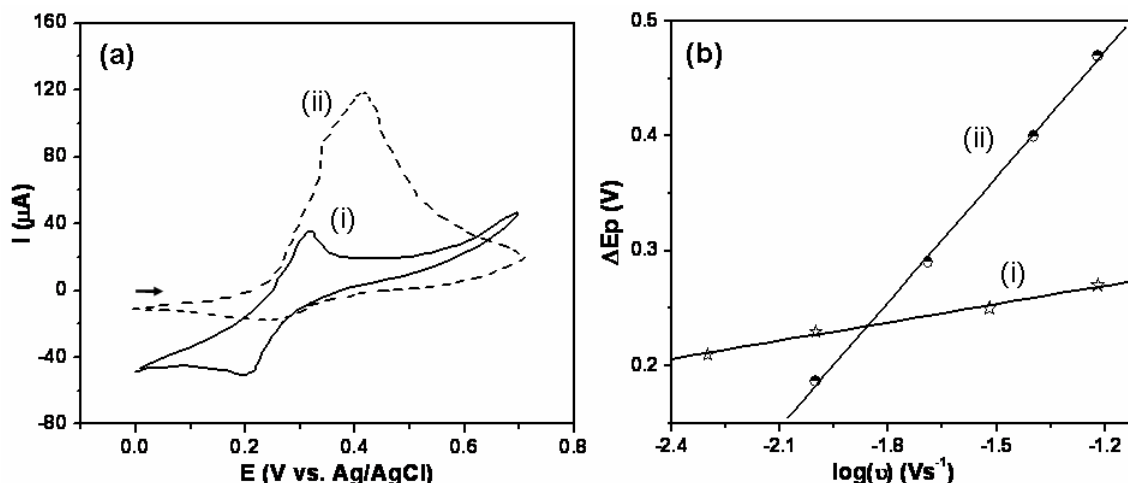
Figure 2.15 (a) Superimposed cyclic voltammograms of *in situ* generated silver nanoclusters from silver (I) oxide in aqueous acetonitrile (H_2O : CH_3CN, 1:10 v/v) containing 0.1 M n-Bu_4NClO_4 as supporting electrolyte with reference to Ag/AgCl electrode at the scan rate of 0.01 Vs^{-1}; (i) in the absence of α-diazoketone, (ii) in the presence of α-diazoketone '1a'. (b) Relationship between ΔEp and logarithm of scan rate. (i) *In situ* generated Ag_n, (ii) Ag_n in the presence of α-diazoketone, 1a.

behavior. For example, benzoic acid protected Ag clusters exhibit redox behavior over a wide range of scan rate (1.0×10^{-3} to 30.0 Vs^{-1}).[35c] However, the present nanoclusters lack the surface capping layer. More significantly, voltammogram reveals the larger magnitude of separation between anodic and cathodic peaks ($\Delta Ep \approx 0.14$ V), which

----

plays a decisive role for the occurrence of coupled chemical reaction (vide infra) due to the enhancement of time interval between two electron transfer steps.[40] Origin of the redox couple could be attributed to the occurrence of an electron transfer process represented by the following equation:

$$Ag_n^+ + e^- \quad \rightarrow \quad Ag_n^\circ \text{ ------------------- (2)}$$
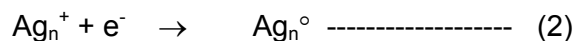
An estimation of the rate constant k^0 for this process based on the magnitude of ΔEp is ca. 4.14×10^{-4} s^{-1}.[41] The variation of ΔEp with logarithm of scan rate is shown in Figure 2.15(b). Importantly, individual peak potential of *in situ* generated Ag_n does not vary with either the nature or the concentration of the supporting electrolyte, although they are strongly influenced by both solvent and substrate nature.
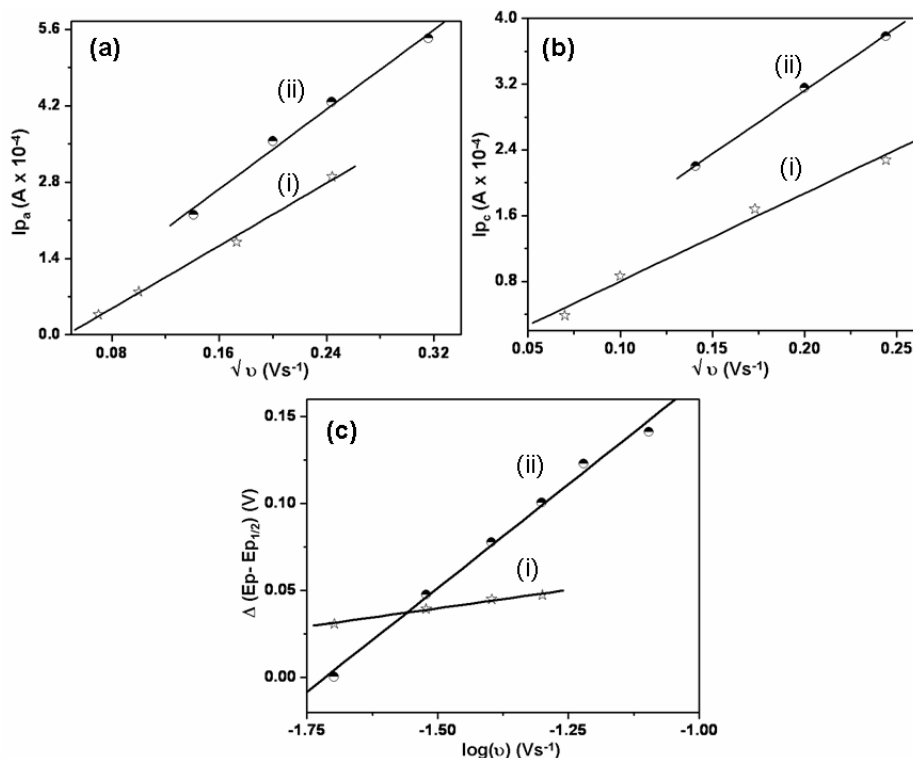
Figure 2.16 (a) Relationship between peak current (anodic) and square root of scan rate. (i) *In situ* generated Ag_n, (ii) Ag_n in the presence of α-diazoketone, 1a. (b) Relationship between peak current (cathodic) and square root of scan rate. (i) *In situ* generated Ag_n, (ii) Ag_n in the presence of α-diazoketone, 1a. (c) Relationship between $\Delta(Ep-Ep/2)$ and logarithm of scan rate. (i) *in situ* generated Ag_n, (ii) Ag_n in the presence of α-diazoketone, 1a.

In comparison, cyclic voltammogram of Ag_n in the presence of α-diazoketone, 1a shows drastic changes suggesting the occurrence of a remarkable coupled chemical

reaction as can be seen in voltammogram 'ii' in Figure 2.15. For example, forward scan of the first cycle (v = 0.01 Vs^{-1}) shows more anodically shifted, steeply descending oxidation peak at around 0.4 V with a higher peak current. The nature of this peak is reminiscent of an electron transfer followed by a chemical reaction. In comparison, the reverse scan depicts substantially suppressed cathodic peak exhibiting a plateau around 0.2 V. More importantly, the forward scan of the second cycle shows anodically shifted
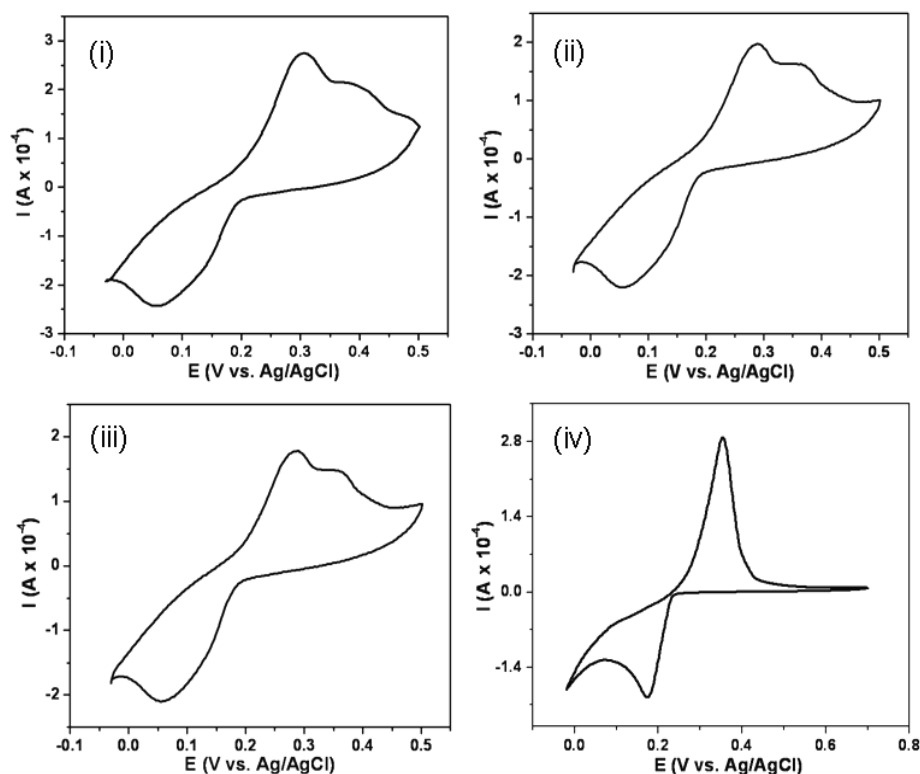
Figure 2.17 (i-iii) Cycle dependent voltammograms (1st three cycles) of α-diazoketone, 1a, over *in situ* generated Ag$_n$ from Ag$_2$O at the scan rate of 0.03 Vs^{-1}. We have coated relatively higher quantity of Ag$_2$O in order to increase the concentration of Ag$_n$. (iv) Cyclic voltammograms of blank Ag$_2$O at 0.03 Vs^{-1} (2nd cycle).

descending peak around 0.40 V with a pre-peak around 0.35 V. Interestingly, both anodic and cathodic peak currents increase with increasing scan rate, while plot of Δ(Ep-Ep/$_2$) vs. log (υ) is also linear. Figures 2.16(a) and 2.16(b) show variation of peak currents with square root of scan rate, while Figure 2.16(c) shows the variation of Δ(Ep-Ep/$_2$) with logarithm of scan rate. The linear nature of plots of Ip vs. square root of scan rate indicates that diffusion of electroactive species towards the electrode surface can be

----

estimated by using the Cottrell equation. Slope of the plot $\Delta(Ep-Ep/_2)$ vs. log (υ) in the presence (curve ii) of α-diazoketone, 1a is higher than that of in the absence (curve i) of α-diazoketone, 1a, indicating a decrease in the energy transfer coefficient (α) for the former (Figure 2.16).

The rise in peak current along with the retention of voltammetric pattern following the addition of more amount of the compound indicates the involvement of the
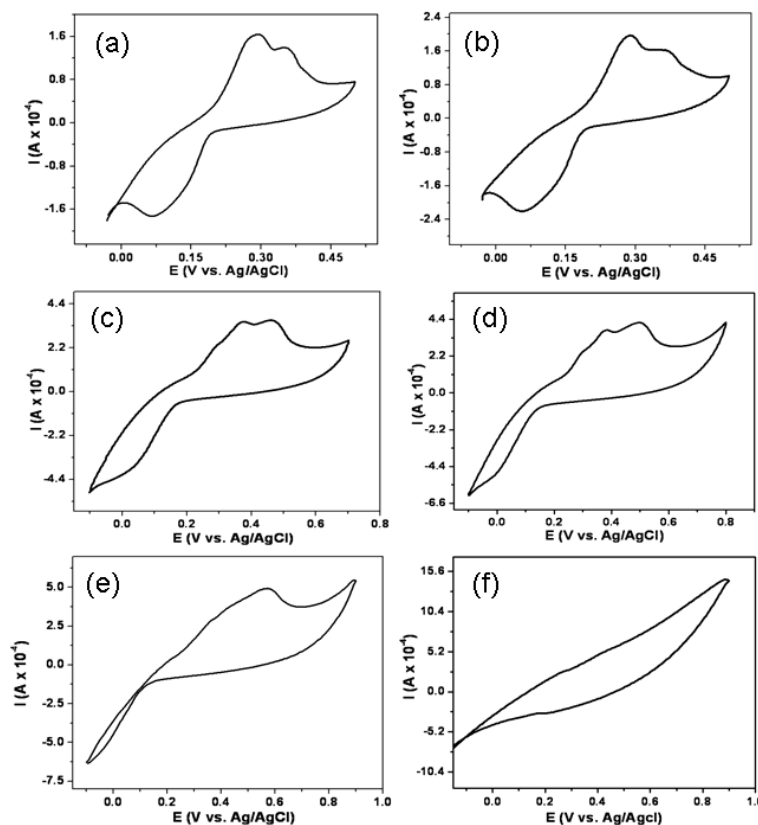
Figure 2.18 Scan rate dependent voltammetric behavior (a. 0.02, b. 0.03, c. 0.04, d. 0.06, e. 0.1, and f. 0.5 Vs^{-1}) of α-diazoketone, 1a over *in situ* generated Ag_n in aqueous acetonitrile with respect to Ag/AgCl electrode (other conditions are identical as earlier).

electrochemical reaction, while the position of new pre-peak at 0.35 V in close proximity with the anodic peak of the original redox couple reveals the regeneration of electrocatalytic species, Ag_n^+. This is further confirmed by increasing the amount of Ag_2O coating on the working electrode, where rise in peak current with the retention of voltammetric pattern is observed. Figure 2.17 shows the corresponding voltammograms

----

at 0.03 Vs^{-1} for the first three cycles (i-iii) in presence of the compound, while cyclic voltammogram in its absence is also shown (iv). However, reverse scan of the second cycle is unable to show two cathodic peaks corresponding to respective anodic peaks due to the plateau like nature of the cathodic response. Successive cycles show a similar voltammetric pattern with decreased peak current. The anodic peaks move in more positive direction, while cathodic plateau shifts more negatively with increasing scan rate. However, voltammograms beyond $\nu >> 0.1\ Vs^{-1}$ are electrochemically silent. For example, Figure 2.18(a-f) shows cyclic voltammograms at different scan rates exhibiting featureless voltammograms appearing beyond the scan rate 0.1 Vs^{-1}. Qualitative comparison between the nature of anodic (peak) and cathodic (plateau) peaks indicates the occurrence of kinetically faster oxidation process. This analysis is in agreement with the shift of OCP to more positive values following the onset of the Wolff rearrangement (vide supra). Significantly, the zero current curve crossing phenomenon with thermodynamically more facile second electron transfer step than the first is absent collectively suggesting the occurrence of a non-classical electron transfer process.[42]

Table 2.2 Cyclic voltammetric features of the Ag°_n/Ag_n^+ redox couple in the absence and presence of α- diazoketones, 1a-f at 0.01 Vs^{-1}.

α-Diazoketones (1) $(RCOCH_2N_2)$ R	Ep_a (V)	Ep_c (V)	ΔEp (V)	$E_{1/2}$ (V)	Yield (%)
i -	0.34	0.20	0.14	0.27	-
ii 1a, $CH_3(CH_2)_{10}$ -	0.40	0.23	0.17	0.31	94
iii 1b, $Ph-CH_2$-	0.40	0.18	0.22	0.29	95
iv 1c, Ph-	0.47	0.17	0.30	0.32	92
v 1d, 2-I-Ph-	0.41	0.18	0.23	0.29	96
vi 1e, 4-MeO-Ph-	0.59	0.11	0.48	0.35	87
vii 1f, 3-Diazocamphor	0.43	0.19	0.24	0.31	Tricyclic ketone

....

Physical and Materials Chemistry Division, National Chemical Laboratory   100
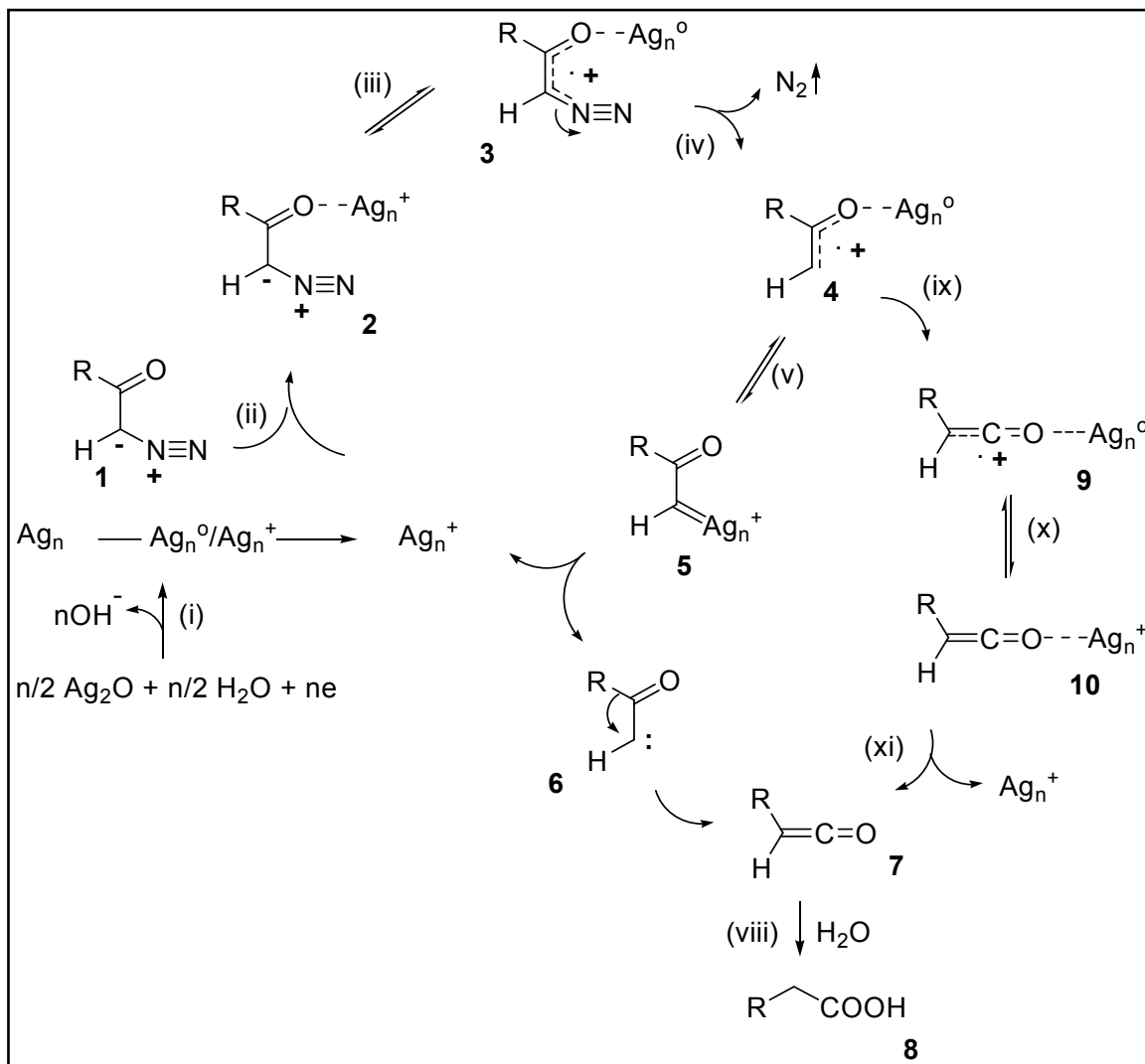
Scheme 2.1 Schematic representation of the electrocatalytic role of *in situ* generated silver nanoclusters (Ag$_n$, size 2-4 nm) during the Wolff rearrangement of α-diazoketones, 1a-e (Table 2.2), involving two nonclassical electron-transfer pathways.

The voltammograms of various α-diazoketones, 1b-f evoke subtle, yet informative features leading to the understanding of stereo-electronic effects associated with the non-classical electron transfer process. Table 2.2 summarizes the voltammetric analysis of different diazoketones under similar experimental conditions. For example, among aromatic diazoketones, the anodic peak potential (Ep$_a$) increases from the iodo (1d) (0.41V) through 1c (0.47 V) to 1e (0.59 V) indicating the relative order of thermodynamic difficulty to oxidize the respective α-diazoketones. Furthermore, the magnitude of ΔEp as well as the difference of the half-wave potential (E$_{1/2}$) of Ag$_n^0$/Ag$_n^+$ redox couple in the presence and absence of respective α-diazoketeones also increase in the similar

manner, leading to a decrease in the rate of non-classical electron transfer process. The magnitude of ΔEp in the absence of α-diazoketone, 1a is independent of scan rate, while on addition of α-diazoketones, ΔEp inceases as a function of scan rate. The rate constant for electron transfer process k^0 decreases following the addition of α-diazoketones as compared to that for the unperturbed Ag_n^0/Ag_n^+ redox couple, probably due to the involvement of a chemical reaction. These results are in good agreement with the previous reports.[43] Significantly, the CPC of 3-diazocamphor results in the exclusive formation of the tricyclic ketone, arising from an intra molecular insertion of α-ketocarbene intermediate into the C-H bond (Scheme 2.2).[35a & b] This substantiates the characteristic evidence of involvement of non-classical E($\uparrow$), C, E($\downarrow$) pathway (vide infra).

Application of an anodic bias on Ag_n coated platinum electrode (0.5 V vs. Ag/AgCl) in aqueous acetonitrile solution of α-diazoketone, 1a, containing pyridine as the nucleophilic probe gives rise to a UV-visible absorption band around λ = 422 nm indicating the formation of α-ketocarbene intermediate 6 and /or ketene 7 (Scheme 2.1). However, it is difficult to discriminate between these two intermediates due to their similar peak positions in the UV- visible absorption band arising from pyridine-α-ketocarbene ylide and pyridine-ketene ylide.[34a & b, 44]
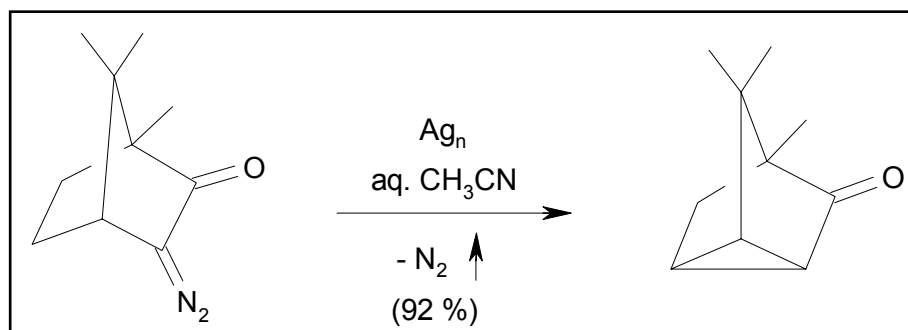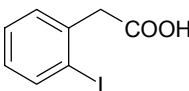
Scheme 2.2 CPC of 3-diazocamphor gives tricyclic ketone.

Two non-classical electron transfer pathways have been proposed for the Wolff rearrangement (Scheme 2.1). The E($\uparrow$), C, E($\downarrow$) pathway represented by steps (iii), (iv) and (v) respectively, leading to the formation of α-ketocarbene 6 (involving structure 5,

Table 2.3 Characterization data of various α- diazoketones, 1a-f and products arising from CPC.

Reactants	Characterization Data	Products	Characterization Data
$CH_3(CH_2)_{10}$ $COCH_2N_2$ MW 224.34	FTIR (cm^{-1}): 2106(s),1640(s)	$CH_3(CH_2)_{10}CH_2CO$ OH MW: 214.35	1709
	^{1}H NMR: 0.88(t, 3H, j=7.0 Hz), 1.2-1.45 (m,16H), 1.6 (m, 2H), 2.0 (t, 2H, C3-CH_2-), 5.18 (s, 1H, C1-CH)		0.89(t, J=7Hz, 3H), 1.27(m, 18H), 1.64(t, J=7Hz, 3H), 2.36(t, J=7Hz, 3H)
	MS M/z (%): 224(M^+, 3),196(1), 183(5), 167(1), 153(2), 125(4), 111(18), 97(75), 84(100), 69(55).		214(M^+,12), 185(12), 171(24), 157(14), 149(12), 129(70), 115(33), 85(50), 73(98), 61(80), 60(98), 57(96), 55(96), 41(100).
Ph-CH_2-$COCH_2N_2$ MW 160.17	FTIR (cm^{-1}): 2099, 1625	Ph-CH_2-CH_2-COOH	3500-2545, 1708
	^{1}H NMR: 3.55(s, 2H), 5.2(s, 1H) 7.3 - 7.6(m, 5H)		2.7 (t, 2H), 3 (t, 2H), 7.15 - 7.7 (m, 5H), 10.45 (s, 1H)
	MS M/z (%): 160(M^+,1), 132(5) 104(94), 119, 91(100) 77(25), 65(34)		
Ph-$COCH_2N_2$ MW 146.14	FTIR (cm^{-1}): 1620, 2104	Ph-CH_2-COOH	1711
	^{1}H NMR: 6.0(s, 1H), 7.4 - 8.1(m, 5H).		3.61 (s, 2H), 7.3 - 7.71 (m, 5H), 9.4 (s, 1H, -COOH
	146(M^+, 41), 118(16), 105(55), 90(100), 77(60) 63(90)		136 (M^+, 90) 91 (100)
2-I-Ph-	FTIR (cm^{-1}):		

$COCH_2N_2$ MW 272.04	2102(s), 1612(s)	(structure: benzyl with COOH and I) MW 262.04	1711
	^{1}H NMR: 5.71(s, 1H), 7.05 - 7.15(m, 1H), 7.3 - 7.5(m, 2H), 7.9(m, 1H)		3.85(s, 2H), 6.85-7.0(m, 1H), 7.1-7.4(m, 2H), 7.75-7.95 (m,1H), 9.25(s, -COOH)
	MS M/z (%): 272 (M^+, 4), 244 (M^+, -N2), 231(12), 203(10), 127(20), 90(10), 89(100), 74(15), 63(95).		262(M^+, 45), 248(10), 231(98), 217(48), 135(100), 127(22), 107(30), 90(16), 89(20), 79(5), 77(5).
4-MeO- PhCOCH$_2$N$_2$	FTIR (cm^{-1}): 2103(s), 1602(s).	MeO-Ph-CH$_2$- COOH	1720
	^{1}H NMR: 3.86(s, 3H), 5.85(s, 1H) 6.91(m, 2H), 7.739(m, 2H)		7.2 (d, 2H), 6.8 (d, 2H), 3.8 (s, 3H), 3.6 (s, 2H)
	MS M/z (%): 176(M^+, 50), 148(18), 135(90) 120(38), 105(20), 91(80), 89(40), 77(100)		167 (M^+, 122), 166 (M^+, 28), 137(8), 135 (12), 122 (92), 91 (48), 79(28)
	C^{13} NMR:		178, 158, 132, 125, 116, 55, 40
3- Diazocamphor	FTIR (cm^{-1}): 2069(s), 1671(s)	Tricyclic ketone MW: 150	1746
	^{1}H NMR: 0.93 (S, 3H, -CH3), 0.97 (S, 6H, 2 -CH3), 2.0 - 2.2 (m,1H), 2.96(d, J = 4Hz, 1H, C4-H).		0.8 (s, 3H), 0.89(s, 3H), 0.96 (s, 3H), 1.45 - 1.55 (m, 1H), 1.7 - 1.8 (m, 1H), 1.9 - 2.1 (m, 3H).
	MS M/z (%): 179(M^+ .1, 4), 178(5) 150(10), 107(96), 105(40), 93(35), 91(94)		150(M^+, 12), 135(30), 122(20), 107 (100), 95(32), 91(72), 79(58), 67(10).

....

Physical and Materials Chemistry Division, National Chemical Laboratory   104

	81(12), 79(100), 77(20), 66(35), 65(35), 55(10), 35(30)		
	^{13}C NMR: 9.47, 18.54, 20.09, 27.07, 30.60, 48.47, 49.60, 58.10, 61.11 (s, C3), 202.41(s, C2)		5.64, 20.31, 20.67, 21.22, 33.69, 35.96 (t), 43.46 (s), 48.21(s), 215.54 (s)

which is more or less similar to the Fischer carbene intermediate) followed by the instantaneous generation of ketene 7. We strongly believe that relative stability of conformation of adsorbed α-ketocarbene over Ag$_n$ will play a decisive role in selecting the reaction pathway. Two possible pathways for the rearrangement from intermediate 5 are decomplexation of Ag$_n$ followed by the rearrangement of free α-ketocarbene 6 (Scheme 2.1) and rearrangement of α-ketocarbene followed by the decomplexation of Ag$_n$.[45] Alternatively, the E($\uparrow$), C, C, E($\downarrow$) pathway represented by steps (iii), (iv), (ix) and (x) respectively, involves the rearrangement of carbene cation radical, ultimately leading to ketene 7. It is worth mentioning that mass spectroscopy detects the formation of carbene cation radicals from α-diazocarbonyl compounds in the gas phase. Interestingly, mass spectroscopic detection of charged Fischer-type copper and silver α-heterocarbenoid intermediates during the metal mediated Wolff-rearrangement of diazomalonate has been reported recently.[37d]

Another remarkable evidence for these mechanistic features (Scheme 2.1) arises from CPC by the application of an appropriate oxidation potential at room temperature (303 K), which leads to the realization of Wolff rearranged carboxylic acids from diazoketones, 1a-e, in excellent yield (Table 2.2). On the other hand, CPC of the α-diazoketone, 1a, using Pt as anode (1.2 V vs. Ag/AgCl) gives merely a mixture of neutral reaction products. Table 2.3 summarizes different characterization data of various α-diazoketones, 1a-f and products arising from CPC.

2.4 Conclusions

The present chapter describes a new method of silver nanowire synthesis by 4-

....

Physical and Materials Chemistry Division, National Chemical Laboratory   105

aminothiophenol with varied aspect ratio. 4-aminothiophenol instantaneously reduces silver nitrate to form nanoparticles, which grow as nanowires on rod shaped template of 4-ATP existed in solution. In addition, the electrochemical study clearly demonstrates that electron transfer features, as revealed by the half wave potential ($E_{1/2}$) and ΔEp, are dependent on the shape and size of silver nanoparticles. Significantly, the $E_{1/2}$ values of silver nanowires (70 nm) and larger sized nanoparticles (40 nm) are relatively higher than that of the smaller sized DDT capped AgNPs (2-7 nm). This is in agreement with the reported observation that for smaller sized nanoparticles, E^0 ($\approx E_{1/2}$ for ideal reversible system) should shift negatively to that of larger counterparts.

Finally, electrocatalytic activity of silver nanoparticles has been demonstrated for Wolff rearrangement of α-diazoketones revealing ECCE or ECE reaction mechanism. In particular, the addition of Ag(I) oxide to a solution of α-diazoketone results in the *in situ* generation of silver nanoclusters which function as electron mediators in Wolff rearrangement. More importantly, this work provides an efficient preparative electrochemical route to realize Wolff rearranged products in excellent yields at room temperature. The technique can be advantageously utilized in the homologation of naturally occurring α- amino acids to β-aminoacids, some of the key building blocks of protenogenic β-peptides.[46]

2.5 References

1.   (a) Sun, Y.; Xia, Y. *Science*   **2002**, *298*, 2176. (b) Sau, T. P.; Murphy, C. J. *J. Am. Chem. Soc.* **2004**, *126*, 8648. (c) Milliron, D. J.; Hughes, S. M.; Cui, Y.; Manna, L.; Li, J.; Wang, L-W.; Alivisators, A. P. *Nature* **2004**, *430*, 190. (d) Hao, E.; Kelly, K. L.; Hupp, J. T.; Schatz, G. C. *J. Am. Chem. Soc.* **2002**, *124*, 15182. (e) Chen, S.; Wang, Z. L.; Ballato, J.; Foulger, S. H.; Carroll, D. L. *J. Am. Chem. Soc.* **2003**, *125*, 16186. (f). Kim, F., Connor, S.; Song, H.; Kuykendall, T.; Yang, P. *Angew. Chem. Int. Ed.* **2004**, *43*, 3673. (g) Millstone, J. E.; Park, S.; Shuford, K. L.; Qin, L.; Schatz, G. C.; Mirkin, C. A. *J. Am. Chem. Soc.* **2005**, *127*, 5312. (h) Jin, R.; Cao, Y. W.; Mirkin, C. A.; Kelly, K. L.; Schatz, G. C.; Zheng, J. G. *Science* **2001**, *294*, 1901. (i) Jin, R.; Cao, C.; Hao, E.; Métraux, G. S.; Schatz, G. C.; Mirkin, C. A. *Nature* **2003**, *425*, 487. (j) Chen, S.; Carroll, D. L. *Nano Lett.* **2002**, *2*, 1003. (k) Jiang, L-P.; Xu, S.; Zhu, J-M.; Zhang, J-R.; Zhu, J-J.; Chen, H-Y. *Inorg. Chem.* **2004**, *43*, 5877. (l) Métraux, G. S.; Mirkin, C. A. *Adv. Mater.* **2005**, *17*, 412.

2.   (a) Schmid, G.; Baumle, M.; Greekens, M.; Heim, I.; Osemann C.; Sawitwoski, T. *Chem. Soc. Rev.* **1999,** *28*, 179. (b) Colvin, V. L.; Schlamp, M. C.; Alivisatos, A. P. *Nature* **1994**, *370*, 354. (c) Shipway, A. N.; Katz, E.; Willner, I. *Chem. Phys. Chem.* **2000**, *1*, 18. (d) Rao, C. N. R.; Kulkarni, G. U.; Thomas, P. J.; Edwards, P. P. *Chem. Soc. Rev.* **2000**, *29*, 27. (e) Pileni, M. P. *J. Phy. Chem. B* **2001**, *104*, 3358. (f) Schmid, G.; Chi, L. F. *Adv. Mater.* **1998**, *10*, 515. (g) Henglein, A. *Chem. Rev.* **1989**, *89*, 1861.

3.   (a) Montano, P. A.; Purdum, H.; Shenoy, G. K.; Morrison, T. I.; Schulze, W. *Surf. Sci.* **1985**, *156*, 228. (b) Buffat, P.; Borel, J. –P. *Phys. Rev. A* **1976**, *13*, 2287. (c) Castro, T.; Reifenberger, R.; Choi, E.; Andres, R. P. *Phys. Rev. B* **1990**, *42*, 8548.

4.   (a) Cuenot, S.; Frétigny, C.; Demoustier-Champagne, S.; Nysten, B. *Phys. Rev. B* **2004**, *69*, 165410. (b) Mueller, U.; Schmidt-Ott, A.; Burtscher, H. Z. *Phys. B.* **1988**, *73*, 103. (c) Schleicher, B.; Burtscher, H.; Siegmann, H. C. *Appl. Phys. Lett.* **1993**, *63*, 1191. (d) Schmidt-Ott, A.; Schurtenberger, P.; Siegmann, H. C. *Phys. Rev. Lett.* **1980**, *45*, 1284. (e) Link, S.; El-Sayed, M. A. *Annu. Rev. Phys. Chem.* **2003**, *54*, 331.

5.   (a) Plieth, W. J. *Phys. Chem.* **1982**, *86*, 3166. (b) Plieth, W. J. *Surf. Sci.* **1985**, *156*,

....

Physical and Materials Chemistry Division, National Chemical Laboratory   107

530. (c) Fisher, L. R.; Israelachvili, J. N. *J. Colloid Interface Sci.* **1981**, *80*, 528.

6.   (a) Henglein, A. *J. Phys. Chem.* **1993**, *97*, 5457. (b) Henglein, A. *Top. Curr. Chem.* **1988**, *141*, 113. (c) Henglein, A.; Mulvaney, P.; Linnert, T. *Faraday Dis. Chem. Soc.* **1991**, 92, 31. (d) Henglein, A. in *Modern Trends of Colloid Science in Chemistry and Biology*; Eicke, H.-F., Ed.; Berkhäuser-Verlag: Basel, Switzerland, **1985**, p 126.

7.   (a) Henglein, A. *Ber. Bunsen-Ges. Phys. Chem.* **1977**, 81, 556. (b) Henglein, A. *Chem. Phys. Lett.* **1989**, 154, 473. (c) Tausch-Treml, R.; Henglein A.; Lilie, J. *Ber. Bunsen-Ges. Phys. Chem.* **1978**, 82, 1335.

8.   Ung, T.; Giersig, M.; Dunstan, D.; Mulvaney, P. *Langmuir* **1997**, 13, 1773.

9.   Narayanan, R.; El-Sayed M. A. *J. Phys. Chem. B* **2005**, *109*, 12663.

10.   (a) Freund, P.L.; Spiro, M. *J. Phys. Chem.* **1985**, *89*, 1074. (b) Li, Y.; Petroski, J.; El-Sayed, M. A. *J. Phys. Chem. B* **2000**, *104*, 10956. (c) Narayanan, R.; El-Sayed, M. A. *J. Phys. Chem. B* **2003**, *107*, 12416. (d) Narayanan, R.; El-Sayed, M. A. *J. Am. Chem. Soc.* **2004**, *126*, 7194. (e) Li, Y.; Hong, X. M.; Collard, D. M.; El-sayed, M. A. *Org. Lett.* **2000**, *2*, 2385. (f) Kogan, V.; Aizenshtat, Z.; Popovitz-Biro, R.; Neumann, R. *Org. Lett.* **2002**, *4*, 3529. (g) Calo, V.; Nacci, A.; Moopoli, A.; Laera, S.; Cioffi, N. *J. Org. Chem.* **2003**, *68*, 2929. (h) Na, Y.; Park, S.; Han, S. B.; Han, H.; Ko, S.; Chang, S. *J. Am. Chem. Soc.* **2004**, *126*, 250. (i) Gopidas, K. R.; Whitesell, J. K.; Fox, M. A. *Nano Lett.* **2003**, *3*, 1757. (j) Yeung, L. K.; Crooks, R. M. *Nano Lett.* **2001**, *1*, 14.

11.   (a) Narayanan, R.; El-Sayed, M. A. *J. Phys. Chem. B* **2004**, *108,* 5726. (b) Narayanan, R.; El-Sayed, M. A. *Nano. Lett.* **2004**, *4*, 1343.

12.   Narayanan, R.; El-Sayed, M. A. **Langmuir** *2005*, *21*, 2027.

13.   (a) Chen, M.; Sun, L.; Bonevich, J. E.; Reich, D. H.; Chien, C. L.; Searson, P. C. *Appl. Phys. Lett.* **2003**, *82*, 3310. (b) Alivisatos, P. *Nat. Biotechnol.* **2004**, *22*, 47. (c) Schultz, S.; Smith, D. R.; Mock, J. J.; Schultz, D. A. *Proc. Natl. Acad. Sci. USA* **2000,** *97*, 996. (d) Lee, S. J.; Morrill, A. R.; Moskovits, M. *J. Am. Chem. Soc.* **2006**, *128*, 2200.

14.   Hao, E.; Schatz, G. C.; Hupp, J. T. J. Fluorescence **2004**, *14*, 331.

15.   Sun, X.; Li, Y. *Adv. Mater.* **2005**, *17*, 2626.

16.   (a) Ajayan, P. M.; Iijima, S. *Nature*, **1993**, *361*, 333. (b) Ajayan, P. M.; Stephan, O.;

....

Physical and Materials Chemistry Division, National Chemical Laboratory   108

Redlich, P.; Colliex, C. *Nature*, **1995**, 375, 564. (c) Chen, Y. K.; Tsang, S. C.; Green, M. L. H. *Chem. Commun.* **1996**, 2489. (d) Sloan, J.; Wright, D. M.; Woo, H. –G.; Bailey, S.; Brown, G.; York, A. P. E.; Coleman, K. S.; Huchinson, J. L.; Green, M. L. H. *Chem. Commun.* **1999**, 699. (e) Govindaraj, A.; Satishkumar, B. C.; Nath, M.; Rao, C. N. R. *Chem. Mater.* **2000**, *12*, 202.

17. (a) Fiévet, F.; Lagier, J. P.; Figlarz, M. *Mater. Res. Soc. Bull.* **1989**, *14*, 29. (b) Fiévet, F.; Lagier, J. P.; Blin, B.; Beaudoin, B.; Figlarz, M. *Solid State Ionics* **1989**, *32/33*, 198. (c) Viau, G.; Fiévet-Vincent, F.; Fiévet, F. *Solid State Ionics* **1996**, *84*, 259. (d) Toneguzzo, P.; Via, G.; Acher, O.; Fiévet-Vincent, F.; Fiévet, F. *Adv. Mater.* **1998**, *10*, 1032. (e) Bonet, F.; Delmas, V.; Grugeon, S.; Urbina, R. H.; Silvert, P. Y.; Tekaia-Elhsissen, K. *Nanostr. Mater.* **1999**, *11*, 1277.

18. Ducamp-Sanguesa, C.; Herrera-Urbina, R.; Figlarz, M. *J. Solid. State Chem.* **1992**, *100*, 272.

19. Sun, Y.; Gates, B.; Mayers, T.; Xia, Y. *Nano. Lett.* **2002**, *2*, 165.

20. (a) Sun. Y.; Xia. Y. *Adv. Mater.* **2002**, *14*, 833. (b) Gao, Y.; Jiang, P.; Liu, D. F.; Yuan, H. J.; Yan, X. Q.; Zhou, Z. P.; Wang, J. X.; Song, L.; Liu, L. F.; Zhou, W. Y.; Wang, G.; Wang, C. Y.; Xie, S. S. *Chem. Phys. Letts.* **2003**, *380,* 146.

21. (a) Jones, W. S.; Tamplin W. S. in *Glycols* (Editors: Curme, G. O. Jr.; Johnston, F.) Reinhold, New York, **1952**, p. 38. (b) Marcus, Y. *Introduction to Liquid State Chemistry*: New York, Wiley Interscience, **1997**, p110.

22. (a) Chen, A.; Wang, H.; Li, X. *Chem. Commun.* **2005**, 1863. (b) Chen, A.; Kamata, K.; Nakagawa, M.; Iyoda, T.; Wang, H.; Li, X. *J. Phys. Chem. B* **2005**, *109*, 18283.

23. Zhao, Q.; Qiu, J.; Zhao, C.; Hou, L.; Zhu, C. *Chem. Letts.* **2005**, *34*, 30.

24. Lofton, C.; Sigmund, W. Adv. Funct. Mater. **2005**, *15*, 1197.

25. Jetti, R. K. R.; Boese, R.; Thakur, T. S.; Vangala, V. R.; Desiraju, G. R. *Chem. Commun.* **2004**, 2526.

26. (a) Chaki, N. K.; Sharma, J.; Mandle, A. B.; Mulla, I. S.; Pasricha, R.; Vijayamohanan, K. *Phys. Chem. Chem. Phys.* **2004,** *6,* 1304. (b) Chaki, N. K.; Sudrik, S. G.; Sonawane, H. R.; Vijayamohanan, K. *Chem. Commun.* **2002**, 76.

27. Kelly, K. L.; Coronado, E.; Zhao, L. L.; Schatz, G. C. J. Phys. Chem. B, **2003**, *107*, 668.

28. (a) Link, S.; El-Sayed, M. A. *J. Phys. Chem. B,* **1999**, *103*, 8410. (b) Ah, C. S.;

Hong, S. D.; Jang, D. J. *J. Phys. Chem. B*, **2001**, *105*, 7871. (c) Link, S.; Mohamed, M. B.; El-Sayed, M. A. *J. Phys. Chem. B*, **1999**, *103*, 3073.

29. (a) Sun, Y.; Yin, Y.; Mayers, B. T.; Herricks, T.; Xia, Y. *Chem. Mater.* **2002**, 14, 4736. (b) Caswell, K. K.; Bender, C. M.; Murphy, C. J. *Nano Lett.* **2003**, 3, 667.

30. (a) Jhu, J.; Liu, S.; Palchik O.; Koltypin, Y.; Gedanken, A. *Langmuir* **2000**, *16*, 6396. (b) Zhang, D.; Limin Ma, Qi. J.; Cheng, H. *Chem. Mater.* **2001**, *13*, 2753.

31. (a) Linnert, T.; Mulvaney, P.; Henglein, A. *J. Phys. Chem.* **1993**, *97*, 679. (b) Thomas, K. G.; Zajicek, J.; Kamat, P. V. *Langmuir* **2002**, 18, 3722.

32. Viau, G.; Piquemal, J. –Y.; Esperrica, M.; Ung, D.; Chakroune, N.; Warmont, F. Fiévet, F. *Chem. Commun.* **2003**, 2216.

33. (a) Doyle, M. P.; Mckervey, M. A.; Ye, T. *Modern Catalytic Methods for Organic Synthesis with Diazo compounds*, Wiley, New York, 1998. (b) Kirmse, W. *Eur. J. Org. Chem.* **2002**, *2002*, 2193.

34. (a) Toscano, J. P.; Platz, M. S.; Nikolaev, V. *J. Am. Chem. Soc.* **1995**, *117*, 4712. (b) Likhotvorik, I.; Zhu, Z.; Tae, E. L.; Tippmann, E.; Hill, B. T.; Platz, M. S. *J. Am. Chem. Soc.* **2001,** *123*, 6061.

35. (a) Sudrik, S. G. Chavan, S. P.; Chandrakumar, K. R. S.; Pal, S.; Date, S. K.; Chavan, S. P.; Sonawane, H. R. *J. Org. Chem.* **2002,** *67*, 1574. (b) Zeller, K. P.; Blocker, A.; Haiss, P. *Mini-Rev. Org. Chem.* **2004**, *1*, 291. (c).. Sudrik, S. G.; Chaki, N. K.; Chavan, V. B.; Chavan, S. P.; Chavan, S. P.; Sonawane, H. R.; Vijayamohanan, K. *Chem. Eur. J.* **2006**, *12*, 859.

36. Newman, M. S.; Beal, P. F. *J. Am. Chem. Soc.* **1950**, *72*, 5163.

37. (a) Zuev, P. S.; Nefedov, O. M. *Russ. Chem. Rev.* **1989**, *58*, 636. (b) *The Chemistry of Diazonium and Diazo Groups, Part 2*, (Ed.: S. Patai), Wiley-Interscience, Chichester, **1978**. (c) Bethel, D.; Parker, V. D. *Acc. Chem. Res.* **1988**, *21*, 400. (d) Julian, R. R.; May, J. A.; Stoltz, B. M.; Beauchamp, J. L.; *J. Am. Chem. Soc.* **2003**, *125,* 4478.

38. Jones, C. R. *J. Org. Chem.* **1981**, *46*, 3370.

39. Paik, W-k.; Eu, S.; Lee, K.; Chon, S.; Kim, M. *Langmuir* **2000**, *16*, 10198.

40. (a) Feldberg, S. W.; Jeftic, L. *J. Phys. Chem.* **1972**, *76*, 2439. (b) Evans, D. H. *Chem. Rev.* **1990**, *90*, 739.

41. Cheng, W.; Dong, S.; Wang, E. *Electrochem. Commun.* **2002**, *4*, 412.

42. (a) Feldberg, S. W.; Jeftic, L. *J. Phys. Chem*. **1972**, *76*, 2439. (b) Evans, D. H. *Chem. Rev.* **1990**, *90*, 739.

43. Yukawa, Y.; Tsuno, Y.; Ibata, T. *Bull. Chem. Soc. Jpn.* **1967**, *40*, 2613.

44. Chiang, Y.; Kresge, A. J.; Popik, V. V. *J. Am. Chem. Soc.* **1999**, *121*, 5930.

45. Bogdanova, A.; Popik, V. V. *J. Am. Chem. Soc.* **2004**, *126*, 11293.

46. Moreno-Manas, M.; Pleixats, R. *Acc. Chem. Res.* **2003**, *36,* 638.

Chapter 3

Shape Selective Preparation of Gold Nanoparticles: Role of Polyfunctional Organic Molecules as Capping and Reducing Agents[*]

The role of poly functional organic molecules on the shape controlled synthesis of nanoparticles has been investigated in this chapter. In particular, three different organic molecules, viz. 4-aminothiophenol, Bismarck Brown R, and Bismarck brown Y have been employed to investigate

The scheme shows different shapes of gold nanoparticles synthesized by various poly-functional molecules (TEM and AFM images, not to scale).

their role in achieving shape control during the synthesis. Although spherical aggregates (70-80 nm) of gold nanoparticles (3 nm) are formed by 4-aminothiophenol as the capping agent, the use of more intricate multifunctional dye molecules like Bismarck brown R and Y, interestingly, gives gold nanoplates in good yield. These gold plates are of 500 nm to micrometer size with a thickness of around 80-108 nm. All these nanostructures are electrochemically active and their electron transfer properties have been studied by cyclic voltammetry along with their optical properties.

3.1 Introduction

Shape and size selective synthesis of inorganic nanoparticles and their inherent properties have received immense interest recently.[1] This is mainly because the precise tuning of size and shape provides good control over different physical and chemical properties of nanoscale materials. For example, some of these particles like gold and silver show strong size and shape dependent surface plasmon resonance absorption exhibiting different colors. Similarly their melting point and mechanical properties also change with size as has been reported recently.[1c,d] In addition, due to their large effective scattering cross section and their non-bleaching properties, these particles also act as potential candidates in the field of single molecular labeling based biological assays and as output signal enhancers in near field optical microscopy applications.[2]

A convenient way to produce noble metal nanoparticles is the reduction of metal halides or anionic metal precursors with alcohols, amines, $NaBH_4$, or H_2 in the presence of surfactants such as poly(N-vinyl pyrrolidone) (PVP), polyacrylate etc.[3, 4] The role of the capping agents is not only to protect the nanoparticles against aggregation but also to influence the final shape and size of the particles. In particular, organic molecules, such as long chain thiols, amines and carboxylic acids are frequently used to passivate their surfaces, which also control their dispersion, size, shape, and stability depending on the metal ion to capping molecule ratio. However, other procedures have been developed to overcome the drawbacks of bi-phasic methods and to prepare and assemble nanoparticles in a single phase without using external reducing agents. For example, Brust et al. have developed a synthesis involving p-mercaptophenol-stabilized gold nanoparticles in a single phase, which can be used for the preparation of various monodispersed nanoparticles stabilized by a variety of functional ligands.[5]

Among those ligands, multi-functional molecules are of special interest in interconnected nanoparticle synthesis since their role in directed nano-assembly formation can be manipulated with respect to inter-particle spacing.[5i, 6] Accordingly, one of the important aspects of nanoparticle research is to develop self-assembly strategies based on wet soft solution methods, so that attractive "bottom up" approaches to construct assemblies (so called 'meta-materials') of perfect nano-crystallites, identically

Ph. D. Thesis   *Chapter 3*   *University of Pune, May 2006*

----

replicated in unlimited quantities could be implemented.[7] For example, the planar array of small metal islands separated from each other by tunnel barriers is of great interest for developing nanoscale electronic circuits. The electronic conduction in such structures is said to be varied from metallic to insulating limit by controlling the size and strength of coupling.[8] Several such molecules, like 4-aminothiophenol (4-ATP) have also been used for 2D/3D assembly of nanoparticles using covalent or electrostatic interactions.[9] Further, these molecules are used to assemble nanoparticles advantageously by chemical reactions of terminal functional groups, such as thiolates adsorbed on the surfaces of nanoparticles.[10]

Similarly, the precise control of shape provides unique control over different physical and chemical properties of nanoscale materials with technologically important applications.[11] The challenging task, however, is to design and synthesize metal nanoparticles with well-defined and finely tunable size, surface structure, and composition. This has attracted the attention of the current researchers on nanomaterials and has subsequently led to several discoveries of how to control the shape of nanoparticles. Consequently monodispersed inorganic nanocrystals with various shapes such as spherical, rod, cubic, octahedral, prism, tetrapod, and other branched structures have been successfully synthesized and characterized recently with respect to their optical, electronic, magnetic, and catalytic properties.[12] Despite these studies on several advanced methods to control the shape and size, the use of multifunctional organic molecules, such as azo dyes in achieving such structures has been sparsely investigated. Azo dyes have attracted significant research interest for polymer based large-scale optical storage device applications.[13, 14] These molecules are also important in biophotonics through radiative decay engineering (RDE) of organic dyes in the close vicinity of conducting metal surfaces or covalently attached to them.[15] It has been demonstrated that fluorescence intensity can be enhanced many orders of magnitude, when organic dyes are near the metal thin films and nanoparticles.[16] Moreover, organizing these chromophores with specific optical properties can interestingly yield photoresponsive organic-inorganic hybrid materials to tailor the optoelectronic properties of metal nanoparticles offering exciting opportunities for the design of novel photonic devices for sensing, switching, light energy harvesting, and

....

Physical and Materials Chemistry Division, National Chemical Laboratory   114

biomolecular labeling etc.[17]

Few of these issues have been addressed in the present chapter. In the preceding chapter, we have already discussed the role of 4-ATP on silver nanowire synthesis and electrochemical properties of well-defined nanoparticles and nanowires. The present chapter extends the study on the role of poly functional organic molecules in nanoparticle synthesis focusing on the versatility of poly-functional organic molecules in achieving shape control apart from their use as molecular interconnects. A new approach to achieve shape control via selective organic molecules with specific functionalities has been established, where these molecules also control the degree of self-assembly formation. First part of the chapter demonstrates the synthesis of spherical gold nanoparticles by 4-ATP in N, N-dimethylformamide, while the later section describes the explicit preparation of gold nanoplates by Bismarck brown R and Bismarck brown Y in presence of PVP. In essence, we have demonstrated differently-shaped nanoparticles such as spherical particles, nanowires (discussed in the previous chapter), and triangular and hexagonal nanoplates of gold and silver using various poly functional organic molecules.

3.2 Self-assembled Monolayer and Electrochemical Properties of 4-ATP

The electrochemical properties of the 4-ATP have been elaborately studied by cyclic voltammetry as self-assembled monolayer (SAM) on polycrystalline gold electrodes by different researchers. Pioneering work on the adsorption of purely aromatic thiols was carried out by Hubbard et al.[22] These studies have shown that adsorption takes place through sulphur, with the pendant aromatic moiety assuming a perpendicular orientation with respect to the surface when adsorbed from dilute solutions. The formed monolayers did not, however, posses long-range order, except on Ag(111). Similarly, no long-range order was observed in 4-nitro- and 4-aminothiophenol SAMs on silver electrodes studied by surface-plasmon-polariton-enhanced Raman spectroscopy (SPPERS).[23] Although SAMs of thiophenol do not show long-range ordering on gold electrode, SAMs of 4-ATP exhibit relatively well-ordered monolayers.[24] Scanning tunnelling microscopy (STM) studies suggest that it forms a ($\sqrt{3}$ x $\sqrt{3}$) R30^0 monolayer on Au(111) electrodes, with the nearest and next nearest neighbour spacing of 4.9 ± 0.3 and 8.9 ± 0.5 Å, respectively.[25] Further, self-assembled monolayer of 4-ATP can carry out certain

....

Physical and Materials Chemistry Division, National Chemical Laboratory   115

functions because of the presence of specific chemical groups at the SAM/electrolyte interface.[26] This SAM can be used to bind negatively charged solution-phase probe molecules when solution pH is low enough so that the surface-bound amino group is protonated.[27] The pKa value of 4-ATP on gold surface has been determined by differential capacitance measurements to be 6.9 ± 0.5 (at +0.2 V versus Ag/AgCl).[28] The modification of the electrode with 4-ATP SAM has been shown to have an advantageous effect during the polymerization of polyaniline with improved density, adhesion, optical, and electrochemical properties.[29]

Interestingly, monolayer of 4-ATP on gold electrode shows more than one pH dependent distinct peaks due to the formation of several redox active species with time. Initially, Hayes et. al. have proposed the involvement of an ECE mechanism where, the formation of redox active 2-(4′-mercaptophenylamino) benzoquinone is the intervening chemical step.[30] However, Lukkari et. al. have later opposed the above explanation and demonstrated that the product of SAM oxidation can not be aminoquinone using aminoquinone modified electrodes as probe.[31]

In general, 4-ATP can undergo following electrochemical reactions:

$$HS-\!\!\left\langle\!\!\bigcirc\!\!\right\rangle\!\!-NH_2^{+\cdot} + H^+ + e^- \longrightarrow HS-\!\!\left\langle\!\!\bigcirc\!\!\right\rangle\!\!-NH_3^+$$

$$(3.1)$$

$$(E^0 = 0.83 \text{ V vs. NHE; gas phase, aniline) }[32]$$
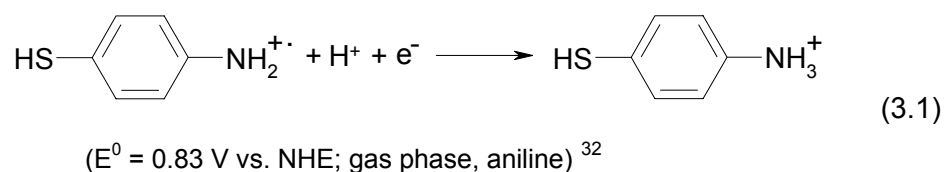
This is a (1e⁻, 1H⁺) process and is highly pH dependent.[30] The radical cation is stabilized by delocalization on the gold surface for both the cases, i.e. 4-ATP SAM and Au NPs. The oxidation does not lead to the cleavage of the gold-sulfur bond[31] since it can react with the neighbouring radical cation bound to another nanoparticle forming a dimer. However, the carbon sulphur bond cleavage can occur either concertedly or after the coupling reaction. Further, the dimerized product can undergo following two electron transfer process:[33]

$$-\!\!\left\langle\!\!\bigcirc\!\!\right\rangle\!\!-NH-\!\!\left\langle\!\!\bigcirc\!\!\right\rangle\!\!-NH_3^+ \underset{\text{reduction}}{\overset{\text{oxidation}}{\rightleftharpoons}} -\!\!\left\langle\!\!\bigcirc\!\!\right\rangle\!\!-N=\!\!\left\langle\!\!\bigcirc\!\!\right\rangle\!\!=NH + 2H^+ + 2e^-$$

$$(3.2)$$

....

Physical and Materials Chemistry Division, National Chemical Laboratory   116
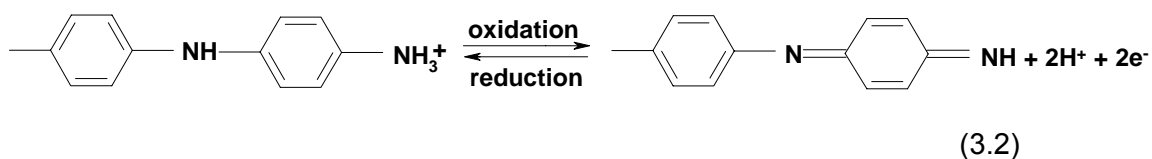
Another possibility is:[31]

$$(3.3)$$
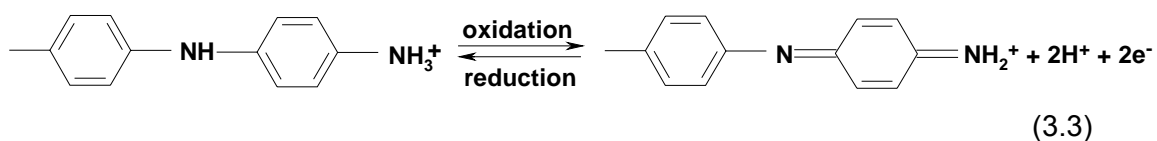
The aniline dimmer can undergo hydrolytic cleavage of the imine moiety to give the corresponding surface bound (in case of SAM) quinine monoamine, which can further undergo reversible redox reaction ($2e^-$, $2H^+$) as represented by:

$$(3.4)$$
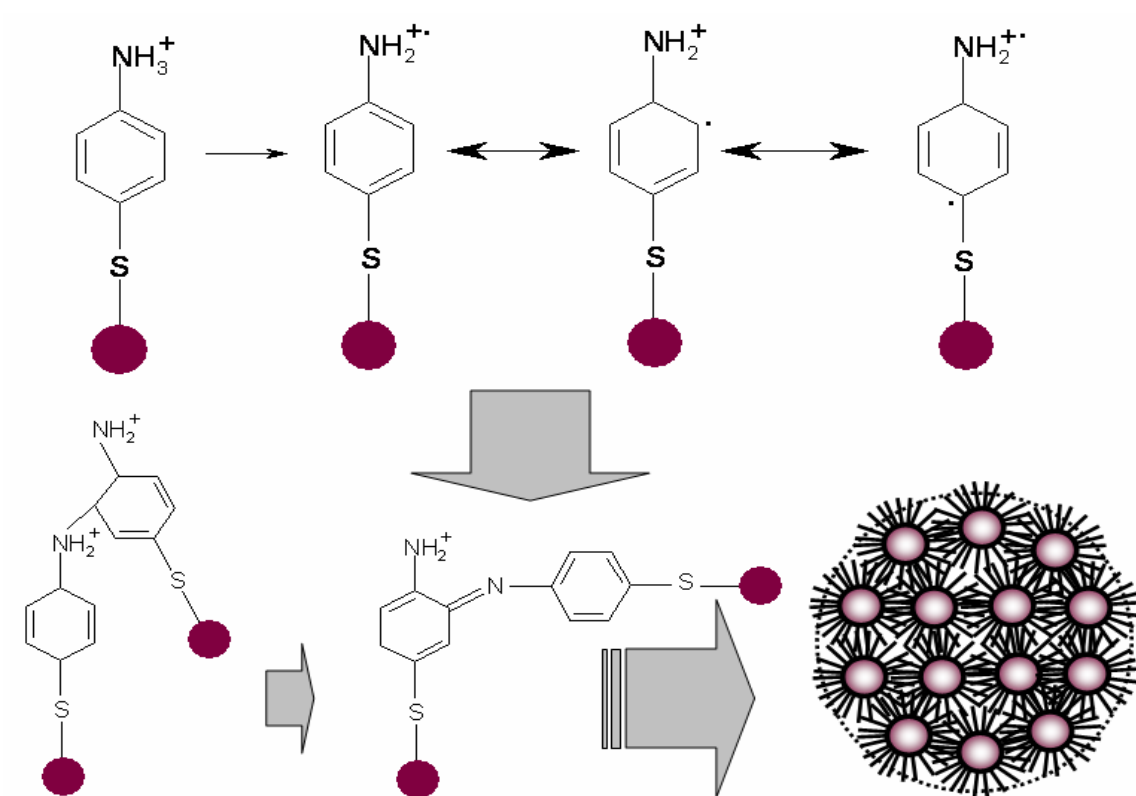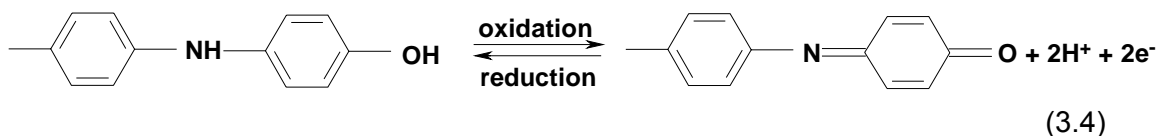
Scheme 3.1: Assembly of gold nanoparticles by 4-ATP at low pH.

Interestingly, initial dimerization step can occur by the chemical route also, provided

that 4-ATP is oxidized in the preceding chemical reaction in acidic medium.[34] The oxidizing ability of Au^{3+} ions and the low pH of chloroauric acid solution can initiate the dimerization step. Indeed, we will see later (section 3.4.1) that this type of polymerization leads to the formation of spherical aggregates of gold nanoparticles. The overall mechanism is given as Scheme 3.1.

However, at high pH (≥6), deprotonation of the amino group and its resultant radicals lead to the decreased efficiency of above coupling reaction, concomitantly altering the reaction mechanism to a head-to-head coupling to form an azobenzene structure.[35, 36] Another indirect evidence for the above scheme arises from their interesting optical properties ascribed to the inter-particle coupling. As explained in the introductory chapter (Chapter 1) the surface plasmon absorption of such nanoparticles strongly depends on the electronic state.[37-40]

3.3 Experimental Section

3.3.1 Materials: Hydrogen tetrachloroaurate(III) trihydrate ($HAuCl_4.3H_2O$, 99.9 %), 4-aminothiophenol (4-ATP, 90%), Bismarck Brown R (BBR, dye content 40%), Bismarck Brown Y (BBY, dye content 50%), Poly(vinyl pyrrolidone) (MW 55,000, PVP) were purchased from Aldrich Chemicals. N,N-dimethylformamide (DMF), and perchloric acid ($HClO_4$) were purchased from Merck, India. All these chemicals were used without further purification. Water used for these experiments was de-ionized with Milli-Q Reagent system (18 MΩ cm).

3.3.2 Synthesis of 4-ATP Capped Au NPs: 20 mL of 10 mM 4-ATP solution in DMF was added to 30 mL aqueous solution of $HAuCl_4$ (1 mM) followed by continuous stirring for 1 h at room temperature. The color turns wine-red immediately and finally becomes brownish blue. Sampling was done by taking each time 5 mL aliquot from the parent solution at different intervals for UV-visible measurement and transmission electron microscopy. Finally, Au NPs were separated by centrifugation at 5000 rpm and purified by successive washing with acetonitrile-water followed by dry acetonitrile.

3.3.3 Synthesis of Au Nanoplates: In a typical synthesis, 40 mL of aqueous 0.1 mM BBR/BBY solution (pH ~ 4.11) was added slowly to 20 mL of aqueous 1 mM $HAuCl_4$ in

....

Physical and Materials Chemistry Division, National Chemical Laboratory   118

presence of 400 mg of PVP in 100 mL round bottom flask (equipped with a magnetic stirring bar embedded in Teflon) under continuous stirring (final pH ~ 3.2), the intense brown color of the solution changed to pale green, indicating probably the reduction of Au^{+3} to Au^0 and/or the formation of an amine complex.[5c] After 2 h, stirring was stopped and the solution was kept undisturbed for 24 h. The bluish crystals of gold nanoplates accumulated at the bottom of the round bottom flask were separated by decanting and washed several times with water. Final product was separated by centrifugation at 7000 rpm. Later, this procedure was repeated for several times to gather large amount of sample.

3.3.4 Characterization Techniques

An elaborate description of different characterization techniques along with their advantages and limitations has been given in the Chapter 1. Briefly, following techniques were used for the present work.

3.3.4.1 UV-visible Spectroscopy: UV–visible (NIR) spectroscopic measurements were carried out on a JASCO dual-beam spectrophotometer (model V-570, using quartz cells of 1 cm path length) operated at a resolution of 1 nm with quartz cells of 1 cm path length. The spectra were background subtracted for the solvent used for nanoparticle dispersion.

3.3.4.2 TEM Analysis: The TEM micrographs were taken on a JEOL model 1200EX instrument operated at an accelerating voltage of 120 kV. The TEM samples were prepared by drop-casting the respective solutions on a carbon coated Cu grids (3 nm thick, deposited on a commercial copper grid) and air dried at room temperature.

3.3.4.3 SEM Analysis: Scanning electron microscopic (SEM) measurements were carried out on a Leica Stereoscan-440 instrument equipped with Phoenix energy dispersive analysis of X-ray (EDAX) attachment.

3.3.4.4 AFM Analysis: Atomic force microscopic images were recorded in the contact mode on a VEECO digital instruments multimode scanning probe microscope equipped

with a nanoscope IV controller. Samples were prepared by drop-casting the respective solution onto silicone (111) substrate.

3.3.4.5 XRD Analysis: X-ray diffraction was carried out on a Philip1730 machine using CuKα radiation (λ = 1.54 Å) at a step of 0.02 degree (2θ) at room temperature. The background was subtracted with the linear interpolation method.

3.3.4.6 FTIR Analysis: Fourier transform infra-red (FTIR) spectroscopic measurements were recorded on Shimadzu 8201-PC. Spectra were recorded in the diffuse reflectance mode at a resolution of 4 cm^{-1} at room temperature.

3.3.4.7 Thermogravimetric Analysis: The TGA-7, Perkin Elmer thermal analysis system was used to determine the thermal stability of samples. The samples were heated under constant nitrogen flow from 50 to 900 ^{0}C (or a desired range) with a scanning rate 5 ^{0}C/min and the resultant weight loss was recorded.

3.3.4.8 Electrochemical Measurements: All the electrochemical measurements were carried out on an Autolab PGSTAT30 (ECO CHEMIE) instrument using sample coated Pt (2 mm) or glassy carbon (3 mm) disk as working electrode, Pt flag as counter electrode and Ag/AgCl as reference electrode. 0.1 M HClO$_4$ was used as electrolyte for all experiments. The working electrode was prepared by drop-casting the respective solutions containing nanoparticles several times on the Pt disk followed by careful drying in air.

3.4 Results and Discussion

We have investigated the role of series of organic molecules: 4-aminothiophenol (4-ATP), Bismarck brown R (BBR), Bismarck brown Y (BBY), Chrysoidine (CD, basic orange), Mordant brown (MB), and Fat brown (FB) on shape-controlled synthesis of gold nanoparticles. However, nanoparticles synthesized by first three compounds are described in details mainly because of their role to achieve well-defined shape.

3.4.1 Gold Nanoparticles by 4-Aminothiophenol

Figure 3.1 shows the time dependent UV-visible spectrum of as synthesized gold

....

Physical and Materials Chemistry Division, National Chemical Laboratory   120

nanoparticles in DMF/water. The appearance of surface plasmon band at 550 nm confirms the formation of Au NPs.[41] A relatively sharp peak is observed, which decreases progressively with time. Generally, a solution of gold nanoparticles (2-20 nm) shows the characteristic surface plasmon absorption at 520 nm in UV-visible absorption spectrum, which strongly depends on the dielectric medium, particles size, shape and dispersity.[42] Moreover, the SPR band may be red shifted if nanoparticles are interlinked due to the intercrystal coupling of SPR band.[43] Accordingly, if the interconnected or assembly of nanoparticles are to be formed, one would observe significant broadening of the surface plasmon band or the appearance of a red-shifted absorption band due to coupling of the individual surface plasmon of nanoparticles in the aggregated structures.[5i, 44] Therefore, we could assign SPR band at 550 nm as due to the inter-crystal coupling of the surface plasmon band arising from the interaction of gold nanoparticles among each other through 4-ATP.[45] This is also clear from the decreasing intensity of UV-visible spectrum with time, obviously caused by the self-assembly
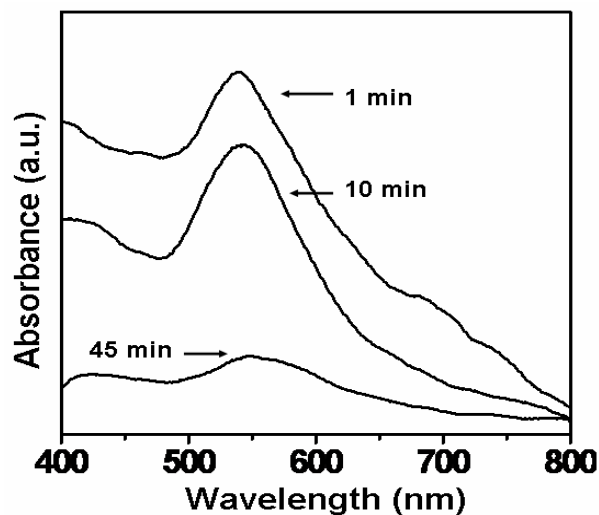
Figure 3.1 Time dependent UV-visible spectra of gold nanoparticles synthesized by 4-ATP DMF/water. Intensity of the SPR peak slowly decrease and red shifted with time. Also, 4-ATP capped nanoparticles undergo aggregation and precipitation, finally leading to a clear solution.

formation. Significantly, the initial wine red color of the solution slowly turns to brownish blue after 3-4 min signifying the formation of self-assembly.[40e] 4-ATP is expected to

behave as molecular interconnect, because both thiol and amino groups are known to show coordination ability on a metal surface. The role of amine as reducing agent is well established and occurs through the initial formation of gold-amine complex followed by the reduction.[4e, 5c]

TEM measurements can provide deeper insight into the assembly formation during the synthesis of gold nanoparticles.[46] Figure 3.2(a) shows the TEM image of Au NPs taken from the DMF/water dispersion immediately after mixing. The micrograph clearly indicates the formation of nearly mono-dispersed smaller sized nanoparticles with an average size of 3 nm. These nanoparticles tend to aggregate easily owing to the presence of bi-functional 4-ATP and indeed they settle down progressively with time forming self-assembly. This tendency of assembly formation can be seen from the TEM image, where portions of aggregates are marked by white circles. This is further
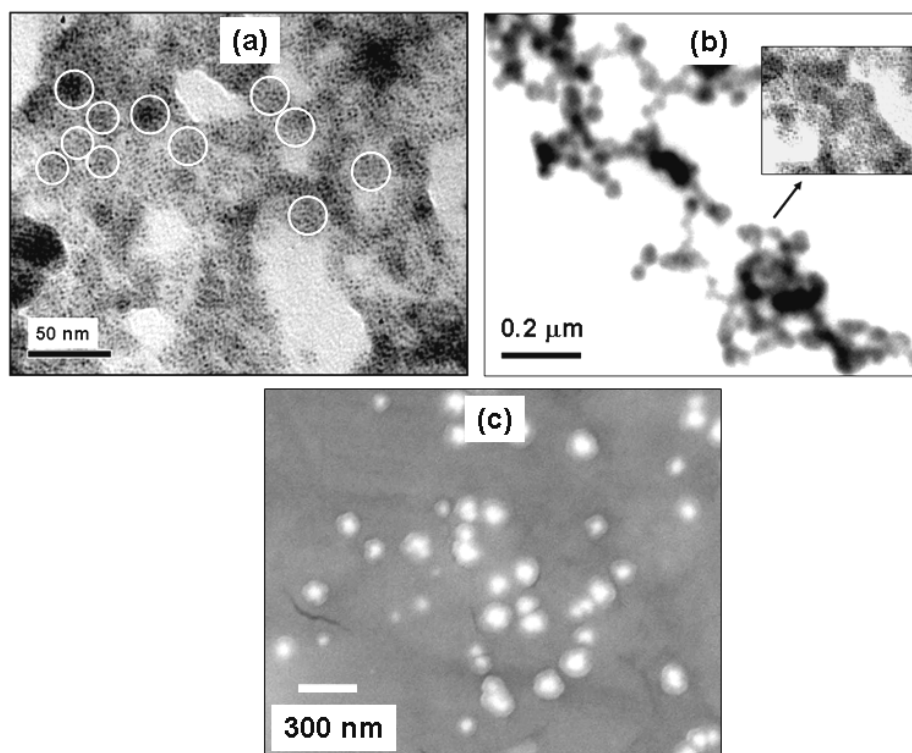
Figure 3.2 TEM images of gold nanoparticles by mixing 30 mL aqueous solution of HAuCl$_4$ (1 mM) and 20 mL ATP (10 mM) solution in DMF recorded immediately (a) and recorded after 1 h (b). Inset shows the high magnification micrograph of a particular portion (scale bar is 50 nm). (c) SEM image of such aggregates recorded for the precipitates formed on prolonged standing.

confirmed by recording the TEM image of the aggregates on their re-dispersion by sonication. Accordingly, Figure 3.2(b) shows the TEM image recorded for the sample after 1 h of the reaction. The chain like arrangement of nearly spherical aggregates of gold nanoparticles is clear from the image indicating the assembly formation. The size of these aggregates is in the range of 70-80 nm. However, the TEM micrograph shows randomness of the aggregates depicting crystalline assembly with the individual clusters placed in random locations. The high magnification TEM image of a portion of these aggregates confirms that these aggregates are constituted by close-packed smaller sized AuNPs, as is given in the inset of Figure 3.2(b), while SEM image also clearly depicts the formation of spherical aggregates [Figure 3.2(c)]. Further, the crystal structure of these particles is confirmed by XRD analysis as shown in Figure 3.3(a), where (111), (200), (220) and (311) crystal planes of bulk fcc structure are identified with a lattice constant of 4.072 A^0. [47] The thermo-gravimetric study of the 'as prepared' nanoparticles shows that AuNPs are stable up to 480 K. For example, Figure 3.3(b) shows the typical thermogram of AuNPs showing the onset of desorption of organic molecules at around 480 K and the process is completed at around 820 K with the maximum mass loss at 520 K. No significant mass loss is seen beyond this temperature
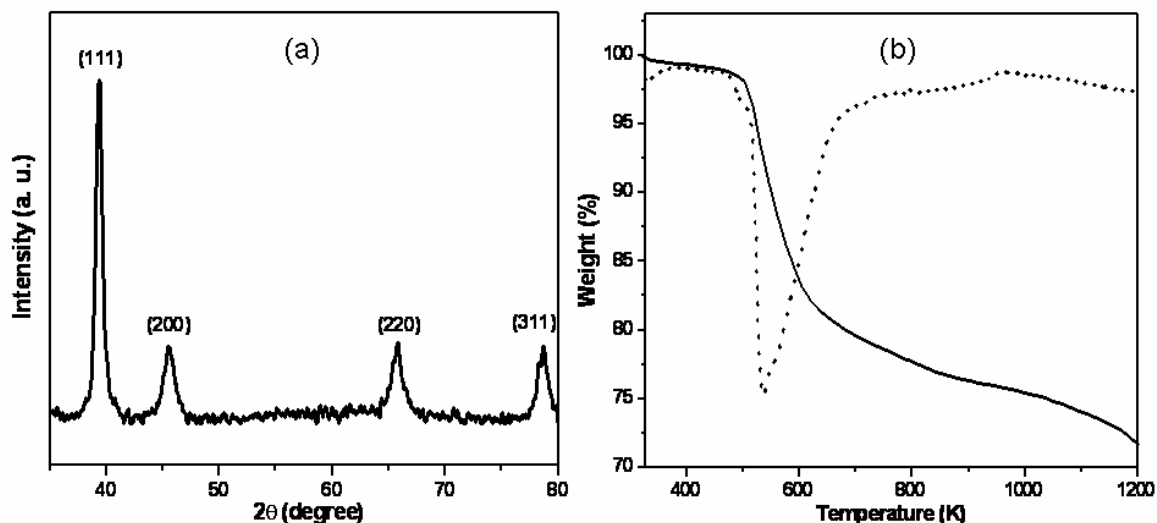
Figure 3.3 (a) XRD pattern of as synthesized gold nanoparticles. Corresponding lattice planes are marked. (b) Thermogram of as synthesized gold nanoparticles. Dotted line represents the differential curve. Thermogram was recorded at a heating rate of 10 K/min under continuous N_2 flow.

up to 1000 K. The total weight loss is ca. 22 % and occurs predominantly through a single step process.[48] The composition of AuNPs is qualitatively determined from the approximated average size of 3 nm and assuming their shape as spherical with perfect fcc packing, 2S or 2N atoms per 3 Au atoms (radius 144 pm) on the surface as reported for two dimensional SAM; which gives a composition of $\sim Au_{923}ATP_{241}$ and is in close agreement with the thermal analysis.[49] The FTIR spectral analysis was carried out to understand the molecular level interactions of 4-ATP with gold. FTIR spectrum of the 4-ATP capped gold nanoparticles is similar to that of bulk 4-ATP and thus only significant differences are discussed.[50] Figure 3.4 shows the typical FTIR spectrum of AuNPs taken in diffused reflectance mode. A notable difference is the appearance of –S=O stretching in the case of AuNPs, which is categorically absent in the spectrum of pure 4-ATP. For better clarity, the magnified FTIR spectra of the –S=O stretching regions (1330-1420 cm-1) for pure 4-ATP (upper curve) and 'as synthesized' gold nanoparticles (lower curve) is given in the inset. This band appears from the oxidized product of –SH indicating the
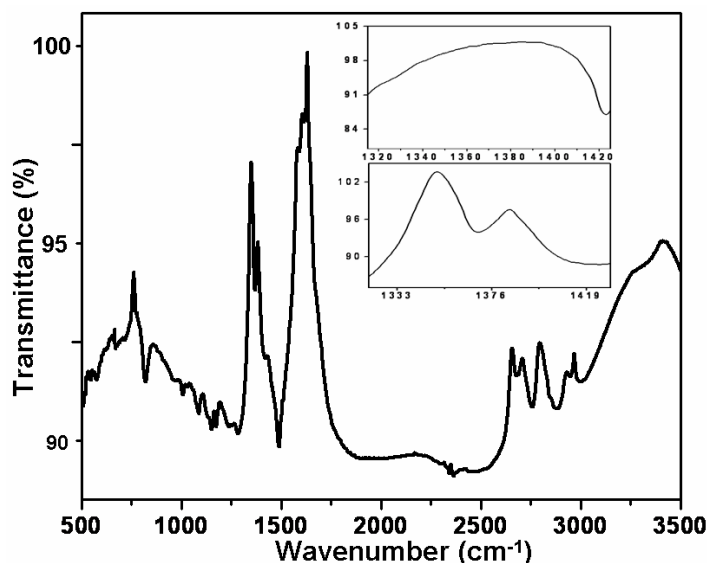
Figure 3.4 FTIR spectra of powdered sample of as synthesized 4-ATP capped gold nanoparticles. Inset shows the magnified FTIR spectra of the –SO stretching regions for pure 4-ATP (upper curve) and as synthesized gold nanoparticles (lower curve).

involvement of thiol group in the reduction process. Further confirmation of the oxidation of –SH group comes from the analysis of X-ray photoelectron spectra of AuNPs.[51]

Figure 3.5(a) shows the XP spectrum for S 2p binding energy (B. E.) region. The S binding energies at 163.2 eV and 164.7 eV correspond to S $2p_{3/2}$ peaks of thiolates and free -SH species respectively. There are two other major peaks of almost equal intensities to that of thiolate species at ca. 168 and 169.7 eV, which could be explained due to the formation of oxidized species. The contribution from the beam-induced
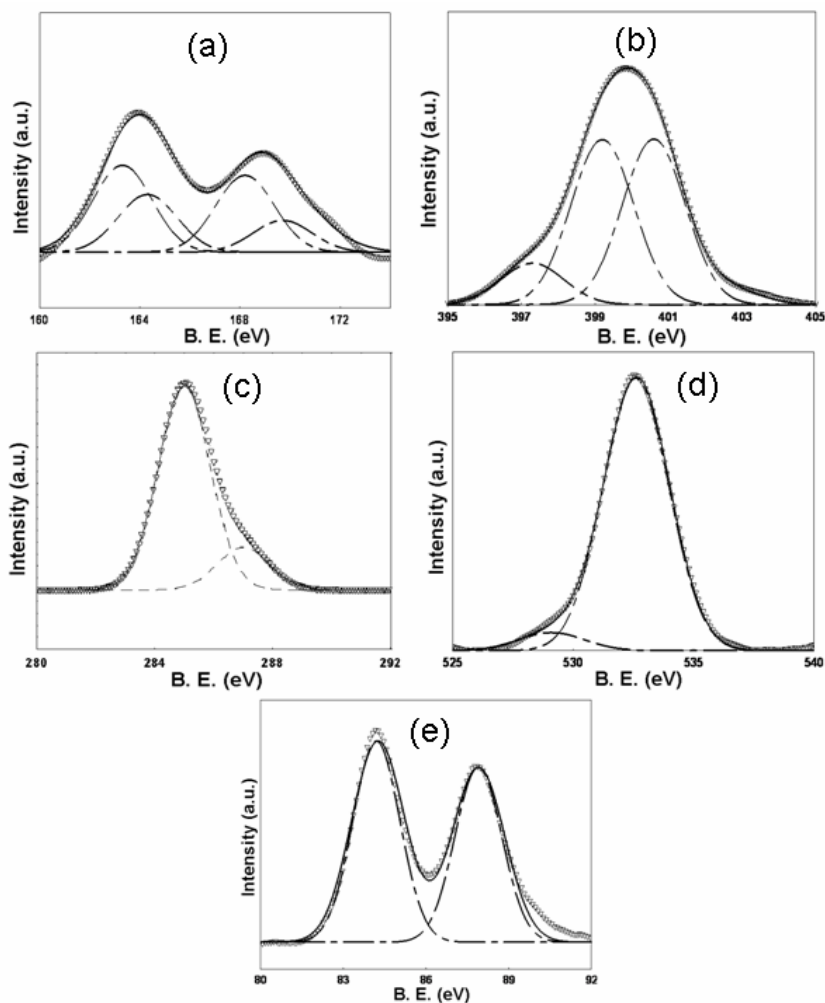
Figure 3.5 Core level XP spectra of (a) S 2 p, (b) N 1s, (c) C 1s, (d) O 2p and (e) Au 4f species present in AuNPs. The triangles represent the experimental data; solid lines represent Gaussian fits to the data. The dotted lines are the de-convoluted individual peaks of different species present in the sample.

damage can be ignored considering the high intensity of these peaks. Figure 3.5(b) is the XP spectrum for N 1s binding energy region, which shows a triplet. There is a minor

contribution from the gold amine complex having a very low intensity peak at 397.3 eV. The B. E. region corresponding to the free amino group or bonded amine falls in the range 398-400 eV. Therefore, the peak at 399.3 eV could be attributed to the bonded or free amine. There is a peak of nearly equal intensity at ca. 401 eV indicating the presence of N as charged species.[52] This peak suggests the involvement of electrostatic interactions, particularly with nanoparticle surface and is in agreement with the earlier reports. [50a, 51a, 53]Similarly, two peaks are observed in the C 1s region [Figure 3.5(c)] corresponding to the carbon atoms within the phenyl ring (major peak at 285 eV) and terminal carbons (a minor peak at ca. 287 eV. [50a] Significantly, Figure 3.5(d) shows the oxygen 1s binding energy region with a prominent peak at 532.2 eV corresponding to the contribution from $NH_2C_6H_4SO_2$- species, while a minor peak of atmospheric oxygen is observed at 529.2 eV. The presence of O 1s peak further strengthens our earlier conclusion that thiol species undergoes oxidation during the reduction of metal ions. However, this oxygen also could be a bicarbonate/carbamate species that formed by reaction with ambient H_2O and CO_2 and was reported earlier for amine terminated SAM.[52]

Table 3.1:   Binding energy positions for the atomic species present within AuNPs.

Species	B. E. (eV)
S 2p (thiolates and free –SH)	163.2, 164.7
Oxidized S	168, 169.7
N 1s	397.3 (minor), 399.3, 401
C 1s	285, 287
O 1s	529.2 (minor), 532.2
Au 4f	84.2, 87.9

Au 4f peaks are slightly shifted towards higher binding energy. This shifting of B. E. values compared to bulk gold infers a shift in the Fermi level. A similar positive shifting in the Au 4f core-level has been reported upon interaction of adsorbed thiol molecules with gold nanoparticles.[54] A maximum shift of 0.41 eV has been reported for smallest particle (~ 1nm) without any line width broadening. This suggests that these changes affect the

whole particle and not only the particle surface, where the actual Au-S or Au-N bond is located. The valence band can undergo similar shifting and change of valence band shape due to the re-hybridization of Au 5d electrons leading to the creation of an Au-S bond. XP spectrum in Figure 3.5(e) shows the $4f_{7/2}$ peak at 84.2 eV and $4f_{5/2}$ peak at 87.9 eV respectively.[47a] Table 3.1 summarizes the XPS results.

Two major conclusions can be drawn from the XPS analysis from the Table 3.1: (a) both -NH$_2$ and -SH groups compete for the attachment on nanoparticle surface and (b) –SH undergoes oxidation during the reduction of AuCl$_4^-$ ions. The presence of free amine and thiol groups on the AuNP surface renders them soluble in polar solvents. Above experimental results suggest that both amino and thiol groups take part in the reduction process. The role of amine as a reducing as well as surface passivating agent is well established and occurs through the initial formation of gold-amine complex followed by the reduction. A plausible explanation for the self-assembly formation can be drawn by considering the similar metal-binding ability of both thiol and amine groups. It can be summarized that the adjacent Au nanoparticles are interconnected either by hydrogen bonding through the direct coupling between amino and thiol groups or by covalent bonding resulting from the chemical reaction as discussed under the section 3.2 in the introduction. The synthetic procedure for Au NPs and their successive self-assembly formation is shown in Scheme 3.1.

It is interesting to investigate the redox properties of as synthesized 4-ATP capped AuNPs, which might have important consequences in manipulating the surface properties of nanoparticles due to the formation of various redox-active functional groups.[31, 33, 55] Accordingly, Figure 3.6(a) shows the cyclic voltammograms of as synthesized AuNPs on Pt electrode in a potential window -0.2 to 0.9 V in 0.1 M HClO$_4$ at a scan rate of 0.1 Vs^{-1}. In particular, two quasi-reversible redox couples are observed centered at 0.32 and 0.11 V vs. Ag/AgCl respectively, of which the couple at 0.32 V is significant one. More specifically, an oxidation and a low intensity reduction peaks can be seen at 0.38 V and 0.25 V respectively in the voltammogram, which decreases with successive cycles [inset, Figure 3.6(a)]. Similarly, Figure 3.6(b) shows the superimposed cyclic voltammograms of the AuNPs at different scan rates: 0.005, 0.04, 0.08, 0.15, 0.40, and 1 Vs^{-1} under identical experimental conditions. The redox peaks are well resolved in the differential pulse voltammograms as can given in inset of Figure 3.6(b). Interestingly,

the redox couples of the present NPs at 0.32 V and 0.11 V are in accordance to the Lukkari's report, considering the shift of potential could be due to the differences in the environment of 4-ATP capped NPs on Pt electrode to that of 4-ATP monolayer on gold.[31] Accordingly, the prominent quasi-reversible redox couple at 0.32 V indicates the presence of the quinone-diimine in these NP assemblies, which probably formed during the synthesis or in a similar dimerization step as predicted in the case of 4-ATP SAM. Interestingly, a small quasi-reversible couple at 0.11 V signifies the hydrolyzed product of the diimine as quinone-monoimine. Granot et. al have attributed this redox couple to bisaniline cross-linked units.[36] In a striking difference, the initial formation of the radical cation step is absent in the cyclic voltammograms of these NPs appeared due to the initial oxidation through protonation, which is reasonable as the XPS results indicate the prior formation of charged -N species during the synthesis. Thus, the presence of these charged species also suggests the formation of these electroactive dimerized products during the reduction of $AuCl_4^-$ ions, which initiates the assembly formation.
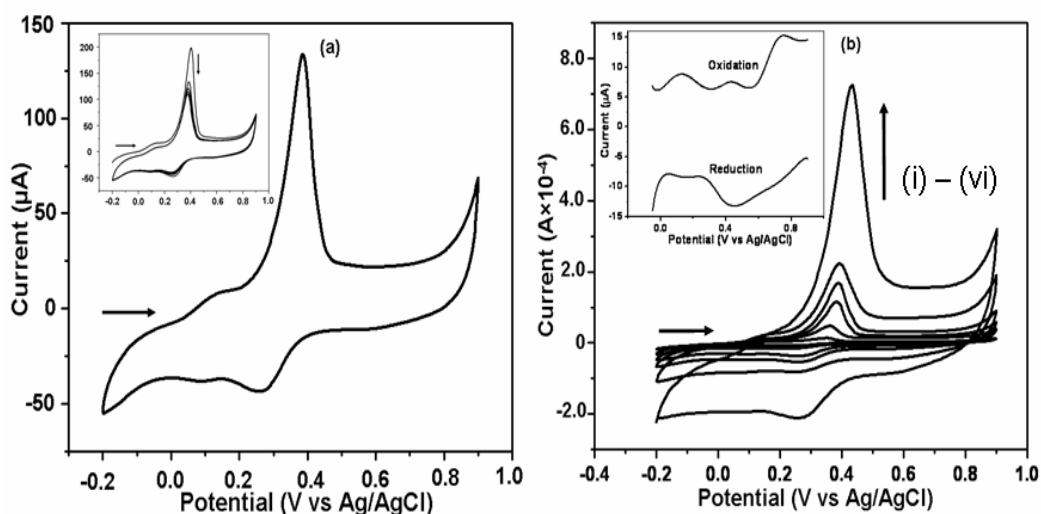
Figure 3.6: Cyclic voltammograms of AuNPs: (a) at a scan rate of 0.1 Vs^{-1} (2nd cycle; inset shows the cyclic voltammograms for first 5-cycles) and (b) at different scan rates: (i) 0.005, (ii) 0.04, (iii) 0.08, (iv) 0.15, (v) 0.4, and (vi) 1.0 Vs^{-1}. The potential was cycled between -0.2 and 0.9 V in 0.1M H_2SO_4. AuNPs modified Pt disc electrode was used as working electrode, Pt flag as counter and Ag/AgCl electrode was used as reference electrode. Inset shows the differential pulse voltammograms at amplitude 0.03 V under the identical potential window.

In essence, a single step method for the synthesis and self-assembly of ca. 3 nm

gold nanoparticles by 4-ATP in DMF/water has been achieved and the size of the nanoparticles can be controlled by keeping a critical $AuCl_4^-$ /4-ATP ratio at controlled pH. An appropriate selection of solvent is very important for the reduction process, since 4-ATP is a weak reducing agent. The reduction of $AuCl_4^-$ ions takes place only in the presence of high dielectric solvents like DMF and dimethylsulfoxide (DMSO).[4b] The high water content (> 80 %) facilitates assembly formation and precipitation occurs within 30 min, although the nanoparticles are neither formed in water nor in DMF alone at room temperature. DMF accelerates the reduction process and its electron donating property has been established at elevated temperature. Amino group of 4-ATP is primarily involved in the reduction process, which is further investigated in the next section where gold nanoplates have been prepared using multifunctional dye molecules containing several amino groups.

3.4.2 Gold Nanoplates by Bismarck Brown R and Bismarck Brown Y

In this section, we discuss a new strategy based on wet chemical techniques to prepare triangular and hexagonal nanoplates using two important poly functional dye molecules, Bismarck brown R (BBR) and Bismarck brown Y (BBY) as reducing/capping agents, demonstrating importance of poly-functional organic molecules in shape control.
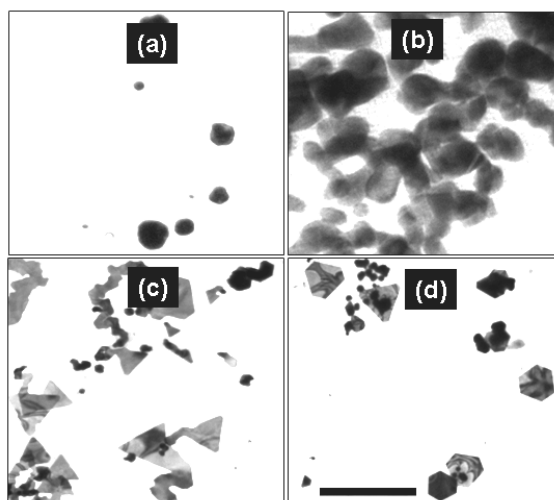
Figure 3.7: TEM images of the various structures formed in the reaction between 40 mL of aqueous BBR and 20 mL of aqueous $HAuCl_4$ solution in presence of 400 mg of PVP at different time intervals: (a) 5 min, (b) 2 h, (c) 7 h, and (d) 15 h. For first three cases scale bar is 50 nm and for the last one it is 1 µm.

....

Physical and Materials Chemistry Division, National Chemical Laboratory   129

Ph. D. Thesis   *Chapter 3*   *University of Pune, May 2006*

The morphological evolution of gold nanoplates is investigated initially by time dependent transmission electron microscopy. Figure 3.7 displays the typical TEM images of various nanostructures obtained from the reaction mixture of 40 mL of aqueous BBR and 20 mL of aqueous $HAuCl_4$ solution in presence of 400 mg of PVP at different time intervals: (a) 5 min, (b) 2 h, (c) 7 h, and (d) 15 h. The images clearly show the evolution of various shaped nanoparticles at different time intervals. Thus, the growth mechanism of gold nanoplates could be speculated as due to the very slow reduction of $AuCl_4^-$ ions by BBR/BBY forming spherical nanoparticles with dynamic surfaces at initial stages, which finally grow into triangular and hexagonal shapes. TEM studies confirm the above speculation as formation of spherical nanoparticles is observed initially, which finally converted into nanoplates (Figure 3.7 a-d). Although few methodologies have been developed to synthesize triangular gold nanoplates, mechanistic details of their growth are still elusive (except for the case of photo-induced conversion[12e]).[11, 12a, 56] The structural dependence of reducing agents on the shape selective growth of nanocrystals is either little known or ignored so far. Significantly, our investigations and other related studies carried out with linear amines have demonstrated that spherical nanoparticles are formed in case of mono functional molecules, while poly functional reducing agents give high aspect ratio nanostructures.[57] From these studies, we conclude that shape control can be achieved by choosing specific reducing agents during the growth of nanocrystals.
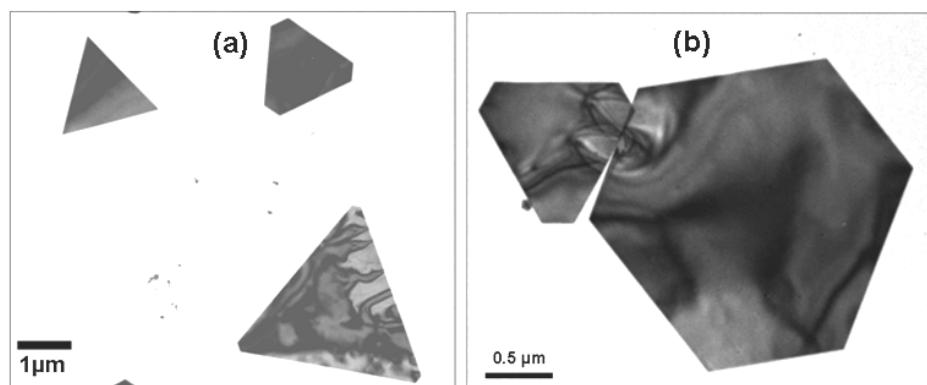
Figure 3.8: (a) TEM image of the triangular gold nanocrystals obtained from the reaction mixture of BBR and $HAuCl_4$. (b) TEM image of a micrometer sized hexagonal plate along with a truncated triangular plate.

....

Physical and Materials Chemistry Division, National Chemical Laboratory   130

Figure 3.8(a) displays a typical TEM image of nanoplates, where both sharp edged and truncated triangular nanoplates are clearly seen with the edge length of 500 nm to several nanometers (micrometer). Since, all these nanoparticles are collected at a particular time period, it is unexpected that all particles would have single shape and instead a mixture of triangular and hexagonal nanoplates can be seen, which is however, commonly observed phenomenon for gold nanoplate synthesis.[11a, 56, 58] Figure 3.8(b) shows TEM image of a micrometer sized hexagonal plate along with a truncated triangular plate. SAED pattern of such a hexagon shows similar pattern to that of a
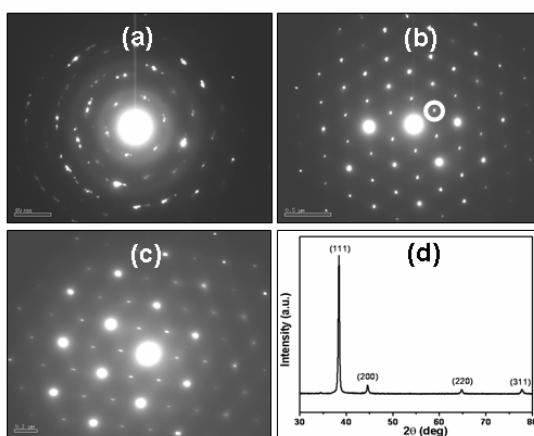
Figure 3.9: SAED patterns of (a) spherical nanoparticles, (b) triangular and (c) hexagonal nanoplates, while (d) is the XRD pattern of a large quantity of the as synthesized gold nanoplates supported on glass plate.

triangular plate and has face-centered-cubic (fcc) gold features. Accordingly, the selected area electron diffraction (SAED) patterns of such nanoplates are indexed based on the fcc structure of gold.[12e] Figure 3.9 shows the SAED patterns of (a) spherical nanoparticles, (b) triangular nanoplates, and (c) hexagonal nanoplates. The elementary ring structure of the SAED pattern from the spherical nanoparticles is characteristic of polycrystalline gold, while the pattern 'b' in Figure 3.9 of nanoplates clearly indicates that the triangle is single crystalline. The hexagonal nature of the diffraction spots, infers that the triangles are highly (111) oriented with the top view is normal to the electron beam. Similar pattern is observed for hexagonal gold nanoplates indicating the identical crystal structure with that of triangles [Figure 3.9(c)]. XRD pattern also agrees well with the SAED pattern having overwhelmingly intense diffraction from (111) crystal planes

Ph. D. Thesis   *Chapter 3*   *University of Pune, May 2006*

----

located at $2\theta = 38.2$ degree, while diffraction from other planes such as (200), (220) and (311) of fcc gold respectively are insignificant [Figure 3.9(d)].[12h] This clearly indicates that (111) planes of gold nanoparticles are highly oriented parallel to the supporting substrate and is in good agreement with commonly observed similar lattice structures of silver, copper, and nickel.[59] The lattice constant calculated from this pattern is ~ 4.07 A^0, a value in agreement with that of the literature reports.[47b]
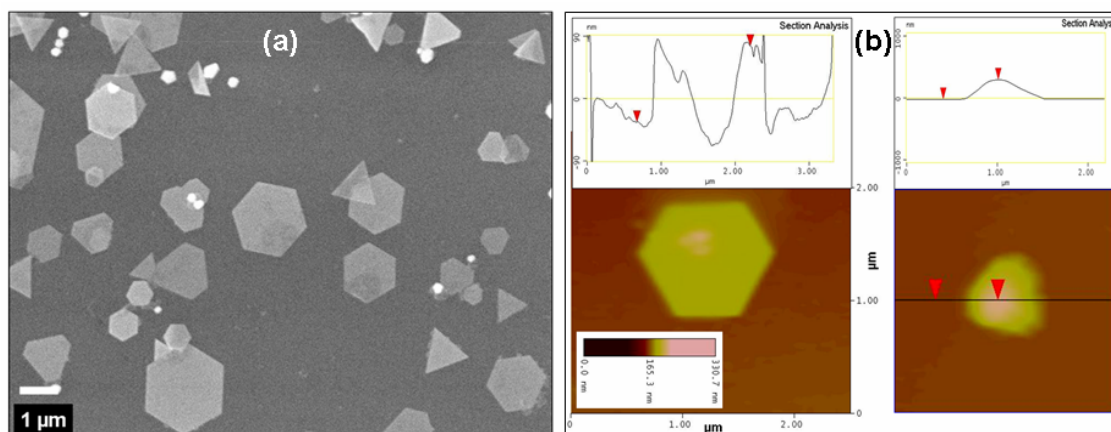
Figure 3.10: (a) SEM image of the various structures found in the final product in the reaction between 40 mL of aqueous BBR (0.1 mM) and 20 mL of aqueous $HAuCl_4$ (1 mM) solution in presence of 400 mg of PVP after 24 h. (b) AFM images of hexagonal and triangular nanoplates along with the respective height profile.

Figure 3.10(a) shows the SEM image of gold nanoplates prepared using BBR. The image shows a large amount of hexagonal and triangular nanoplates indicating the robustness of the synthesis to get a large quantity of nanoplates. The thickness of these plates was measured by atomic force microscopy (AFM). Accordingly, Figure 3.10(b) shows the AFM images of a hexagonal gold nanoplate along with the triangular counterpart. The thickness of a typical nanoplate is found to be ca. 108 nm from the height profile of the AFM image with a lateral dimension of 1.5 μm.

Figure 3.11(a) shows a typical broad, yet informative UV-visible spectrum exhibiting clear absorption corresponding to surface plasmon resonance of nanoplates with few distinct features. The absorption maximum at ca. 400 nm and ca. 650 nm correspond to the triangular gold nanoplates extending up to the NIR region of the electromagnetic

....

Physical and Materials Chemistry Division, National Chemical Laboratory   132

spectrum.[11a] Interestingly, a discernible absorption peak at 300 nm is also appeared due to the presence of UV active surface passivating agents. A plausible explanation of the broad spectrum is that it could possibly originate due to the presence of both triangularand hexagonal nanoplates with a wide distribution of particle (nanoplate) size. Figure 3.11(b) shows the evolution of UV-visible spectrum of nanoplate reaction mixture at different time intervals. The aqueous dispersion of these nanotriangles appears green upon irradiation by ultraviolet ray (365 nm, inset). FTIR spectrum [Figure 3.12(a)] confirms that a fraction of BBR molecules is present as surface passivating agent either in the un-reacted molecular state or as a mixture of reacted and un-reacted product, which probably undergoes charge transfer with gold nanocrystals upon UV-irradiation [Figure 3.12(a)], where appearance of well established stretching frequencies of different bonds at 933 (C-H deformation from tetra/penta-substituted benzene), 1111 (C-H deformation from substituted benzene ring), 1222 (C-N vibration), 1397 (CH3 deformation), 1510 (aromatic homocyclic C=C vibration), 2374 (charged amines, NH^+ stretching), 3124 (bonded NH, N-H stretching) cm^{-1} give conclusive evidence.
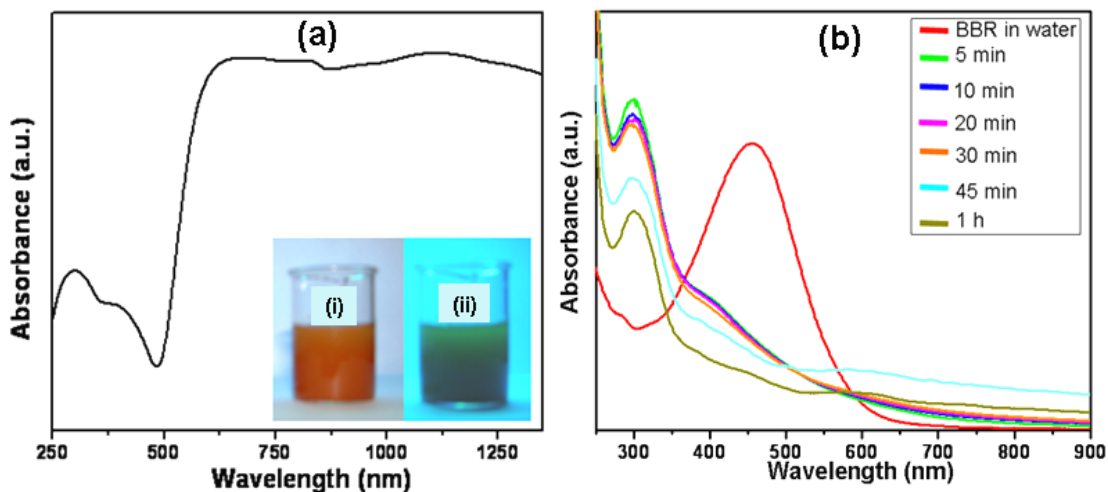
Figure 3.11: (a) UV-visible spectrum of the gold nanoplates synthesized by reacting 1 mM aqueous solution of $HAuCl_4$ with 0.1 mM aqueous solution of BBR in presence of 400 mg PVP. The inset shows photographs of the dispersion of gold nanoplates (i) in normal light and (ii) under UV-irradiation (365 nm). (b) Time dependent UV-visible spectra of the above reaction mixture along with the spectrum for pure BBR in water.

Qualitative elemental study was further carried out by X-ray photoelectron

spectroscopy. Accordingly, XP spectrum in Figure 3.12(b) confirms the presence of metallic gold with characteristic XP spectrum giving binding energy values at 83.9 eV
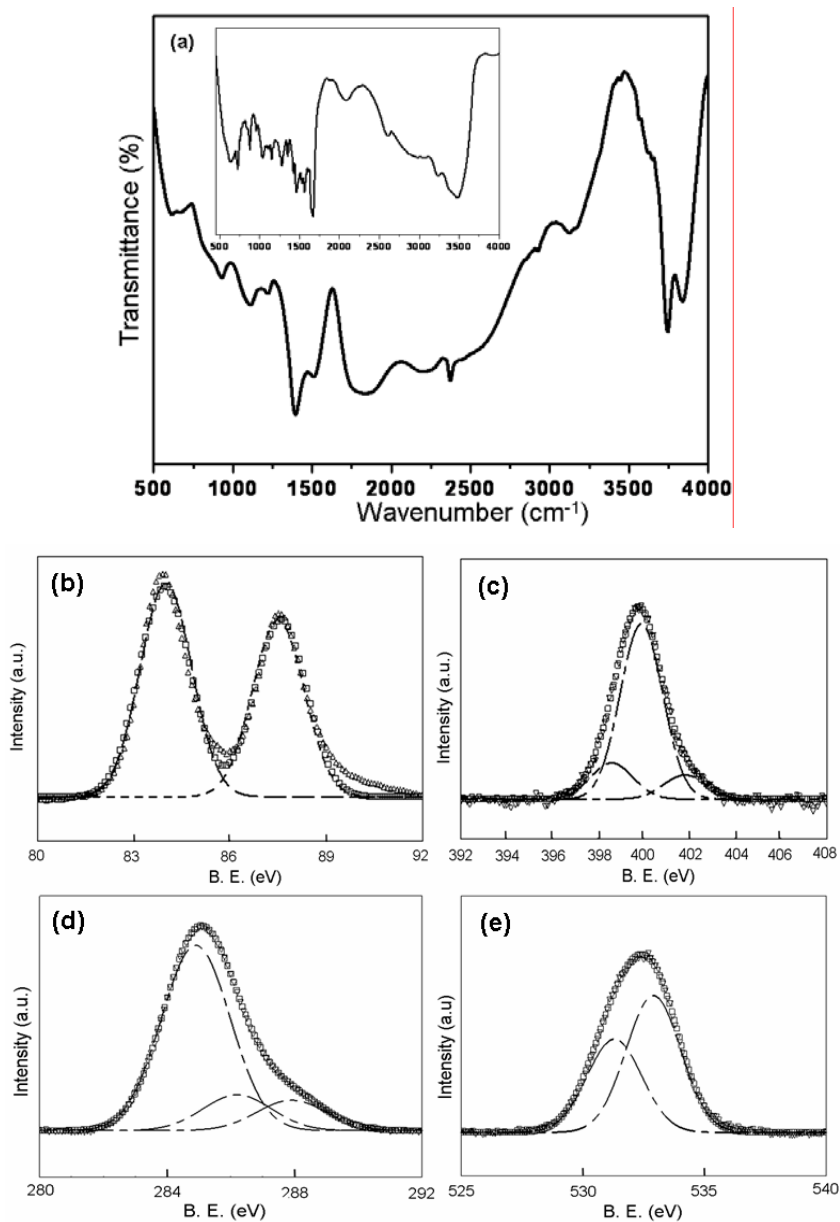
Figure 3.12: (a) FTIR spectrum of the product formed in the reaction of 40 mL aqueous BBR and 20 mL aqueous HAuCl₄. Inset shows the spectrum of pure BBR. Core level XP spectra of Au 4f, N 1s, C 1s, and O 1s respectively are also given (b-e). The triangles represent the experimental data; the squares represent Gaussian fits to the data. The dotted lines are the de-convoluted individual peaks. The XPS data were carbon corrected assuming the C 1s binding energy value at 285 eV.

(4f$_{7/2}$) and 87.5 eV (4f$_{5/2}$).[51d] Significantly, XP spectrum for N 1s region shows a triplet with a minor contribution from the gold amine complex giving a low intensity peak at 398.5 eV [Figure 3.12(c)]. The B. E. region 398-400 eV corresponds to the free amino group or bonded amine. Therefore, the peak at 399.7 eV could be attributed to the N 1s spectrum of bonded or free amine. A very low intensity peak at ca. 401.8 eV indicates the presence of N as charged species. This peak suggests the involvement of electrostatic interactions, particularly with nanoparticle surface and is in agreement with the earlier observation.[50a, 51a, 52, 53]
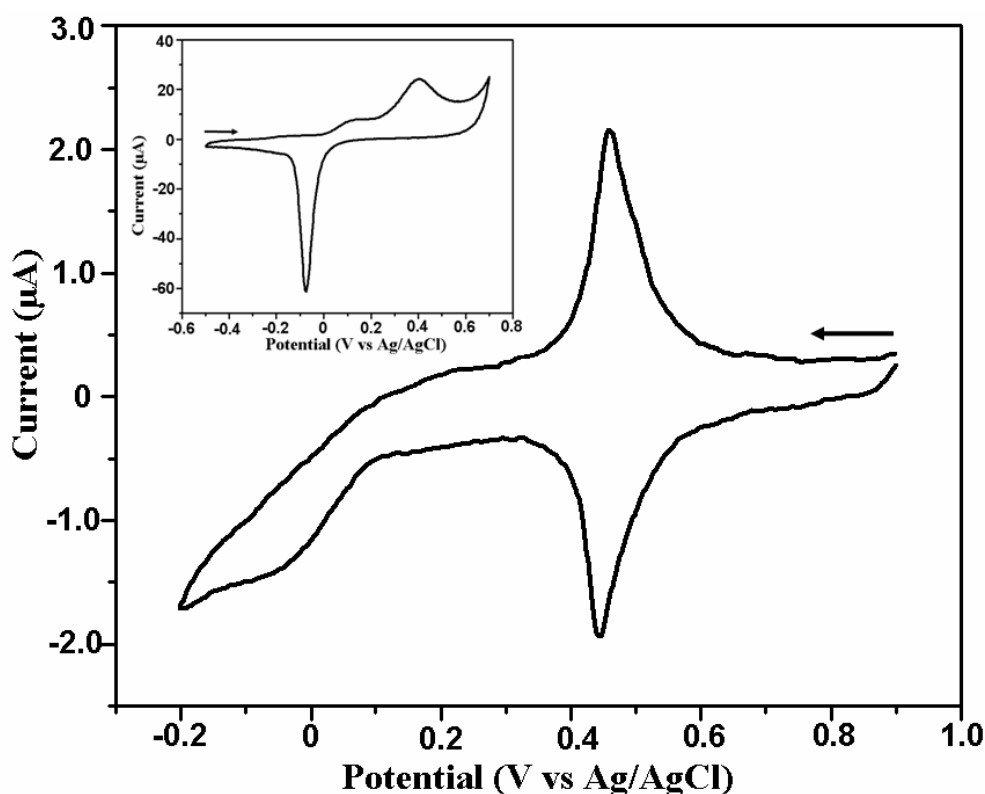
Figure 3.13: Cyclic voltammogram of Au nanoplates synthesized by BBY. The scan rate is 0.1 Vs^{-1}, whereas inset shows the cyclic voltammogram of pure BBY under identical scan rate. The potential was cycled between 0.9 V and -0.2 V in 0.1 M H$_2$SO$_4$. Au nanoparticles modified glassy carbon disk electrode (3 mm) was used as working electrode, while Pt flag as counter and Ag/AgCl as reference electrode.

Three peaks are observed in the C 1s region [Figure 3.12(d)] corresponding to the carbon atoms within the phenyl ring at 285 eV (major peak) and terminal carbons or

aliphatic carbons at ca. 286 eV (a minor peak), while the peak at ca. 288 eV corresponds to the >C=O group, indicating the presence of PVP on the surface. Oxygen 1s region shows two peaks at ca. 531 and 533.8 eV, and are presumed to be from the adsorbed oxygen or atmospheric oxygen species and from the pyrrolidone ring of PVP respectively [Figure 3.12(e)].[52]

These nanocrystals exhibit unprecedented redox properties as has been investigated by cyclic voltammetry with a sample coated glassy carbon electrode (3 mm) as working electrode in 0.1 M $HClO_4$ solution. Accordingly, Figure 3.13 is a typical cyclic voltammogram recorded at 0.1 Vs^{-1} in the potential window between -0.2 and 0.9 V
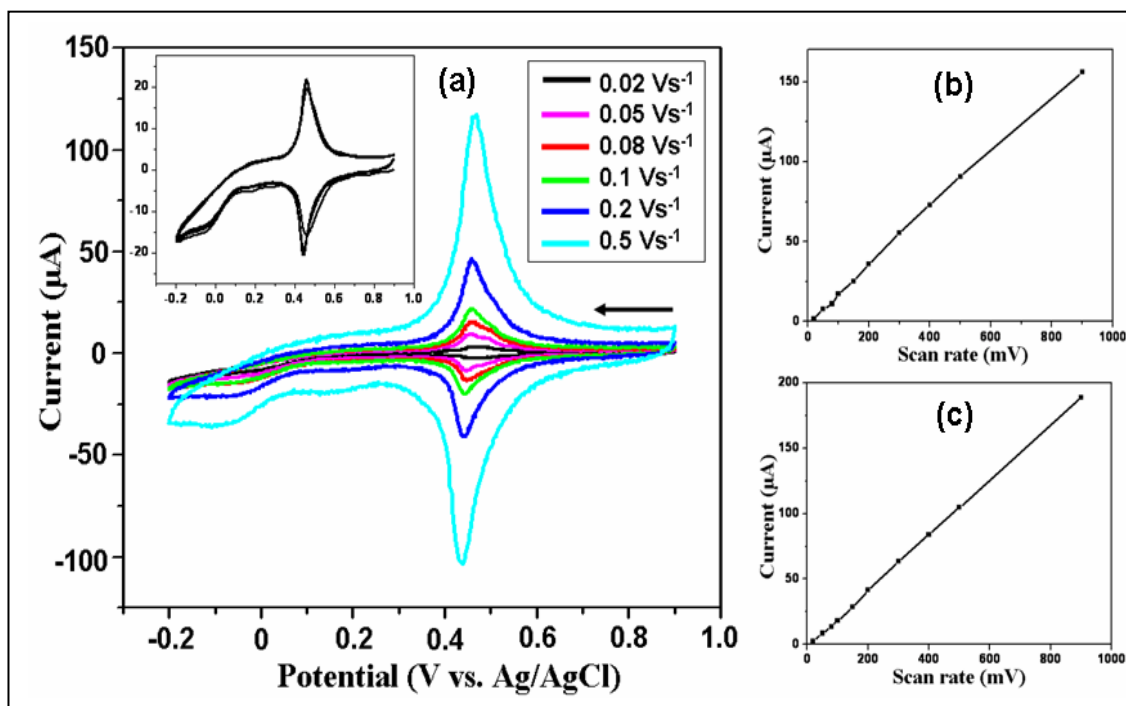
Figure 3.14: (a) Scan rate dependent cyclic voltammograms of Au nanoplates synthesized by BBY. The potential was cycled between -0.2 and 0.9 V in 0.1 M H_2SO_4 at different scan rates. Inset shows the cycle dependent cyclic voltammograms for first five cycles at a scan rate of 0.1 Vs^{-1}. Au nanoplate modified glassy carbon disk electrode was used as working electrode (3 mm), Pt flag as counter and Ag/AgCl electrode was used as reference electrode. b & c are the plots of variation of anodic and cathodic peak currents with scan rates respectively.

giving rise to a unique redox couple at 0.45 V. This redox couple arises from the redox activity of -N=N-bond attached to the nanoplates unambiguously establishing the nature

of a surface immobilized species.[60] In general, azo dyes exhibit several oxidation and reduction peaks leading to the formation of unstable amines or cleavage of the azo bonds.[61] More specifically, oxidation/reduction of azo group gives quasi-reversible redox peaks in the potential range 0.15 to 0.58 V, which can be correlated to the surface confined peak at 0.45 V. It is worth mentioning that the electrochemistry of bulk BBY/BBR (cyclic voltammetric response is identical for both the molecules) on gold electrode shows quasi-reversible redox behavior (see inset, Figure 3.13). The difference between the solution electrochemistry and surfaced immobilized electrochemistry of BBY/BBR could be interpreted due to the ability of electropolymerization in solution (as a result, precipitation occurs slowly), while for the latter case limited mobility of the surface confined species restrict it. The electropolymerization of o-phenylenediamine and the dependence of oxidation potential on the molecular structure of aryl amines have been demonstrated recently.[62]

Ideally, surface-confined redox species exclusively gives very symmetric waves without any peak separation between the anodic and cathodic peak positions. The full width at half-maximum (FWHM) is expected to be 0.096 V for an ideal, reversible, one-electron reaction of an adsorbed species.[63] In the present study, a peak separation of 0.01 V and FWHM of 0.09 V are observed at a scan rate of 0.1 Vs^{-1}, which is in agreement with the ideal surface-confined behavior. Figure 3.14(a) shows the cyclic voltammograms at different scan rates, which show that peak positions are invariant towards scan rate. However, when the FWHM values are analyzed for different scan rates, it is apparent that, for few cases, the values are lower than the expected 0.096 V. These observations point on the kinetic limitations or attractive interactions of the molecules on the surface of gold nanoparticles. A plot of the peak current vs. scan rate (Figure 3.14b and 3.14c) is found to be linear, as expected for a surface-confined species. The surface layers are stable, and the peak currents remain constant with repeated cycling in the potential range between –0.2 and 0.9 V (inset, Figure 3.14a).

Above experimental results clearly demonstrate the unique role of poly functional organic molecules in shape selective synthesis of metal nanoparticles. A series of organic molecules have been tested as summarized in Table 3.2. In few cases, surfactants, like PVP play a major role in deciding the yield, whereas the selection of solvents is also an important factor in few other cases. Surfactants play the role of

Table 3.2: Different shapes of nanoparticles obtained by various poly-functional molecules.

Molecules	Shape and size of the nanoparticles (gold)	Shape and size of the nanoparticles (silver)
4-ATP	Spherical, 3 nm	Nanowire, 60-80 diameter, 1-5 micrometer length
TDA	Spherical, controllable size	Spherical, controllable size
BBR	Triangular and hexagonal nanoplates, 80-120 nm thick, 1-2 micrometer breadth (70-80 yield)	Mixer of rod shaped and spherical nanoparticles (poor yield of rods)
BBY	Triangular and hexagonal nanoplates, 80-120 nm thick, 1-2 micrometer breadth (70-80 yield)	Mixer of rod shaped and spherical nanoparticles (poor yield of rods)
CD	Nanoparticles with arbitrary shapes (contains mixture of spherical, triangular, and other particles)	Spherical nanoparticles
MB	Nanoparticles with arbitrary shapes (contains mixture of spherical, triangular, and other particles)	-
FB	Non uniform ribbon like structures	Spherical nanoparticles

stabilizing and compartmentalizing agents as these shapes are also obtained in its absence although by sacrificing the selectivity of the final product. Importantly, BBR and BBY have several functional similarities and we did not observe any major differences toward the shape of gold nanoplates by these molecules. However, in case of BBY, relatively higher abundance of triangular plates (as compared to hexagons) has been achieved. The structural dependence of reducing agents on the shape selective growth of nanocrystals is either little known or has been ignored so far. One of the important advantages of the present study is the abundance of photo-responsive chromophoric groups on nanoparticle surfaces giving the important benefit of imparting and tailoring different optical functions to these types of hybrid materials especially for future applications.

3.5 Conclusions

We address specific issues related to the synthesis of spherical gold nanoparticles using 4-ATP, whereas gold nanoplates are exclusively formed by multifunctional dye

....

Physical and Materials Chemistry Division, National Chemical Laboratory   138

Ph. D. Thesis   *Chapter 3*   *University of Pune, May 2006*

----

molecules like BBR/BBY. A single step preparation of smaller sized (ca. 3 nm, approximate composition $Au_{923}ATP_{241}$) gold nanoparticles (Au NPs) followed by their self-assembly is demonstrated using 4-ATP as a reducing agent in DMF/water. The instantaneous UV-visible absorption spectrum shows a relatively sharp peak at 550 nm, which becomes a broad band after 1h of mixing due to the formation of aggregates. Transmission electron microscopic images reveal close packed assembly of gold nanoparticles induced by the bi-functionality of 4-ATP. Thermo-gravimetric analysis shows ca. 22 % organic molecules on the surface of Au NPs, while the molecular level analysis of the 'as prepared' gold nanoparticles by Fourier transform infra-red spectrum shows the presence of -SO stretching. X-ray photoelectron spectroscopic results also confirm the oxidation of –SH during the reduction of $AuCl_4^-$ ions. The cyclic voltammograms of the monolayer protected Au nanoparticles show quasi-reversible redox behavior, though the electrochemical features are different from those of self-assembled monolayer (SAM) of ATP on gold electrode. Similarly, highly crystalline hexagonal and triangular nanoplates of gold are synthesized in high yield by a new wet chemical method using multifunctional molecules, Bismarck brown R (BBR) and Bismarck brown Y (BBY). These nanoplates show unprecedented electrochemical properties exhibiting surface confinement behavior. The UV-visible spectrum shows certain distinct features with absorptions at 300, 400, and 650 nm extending up to the near-infrared region. Selected area electron diffraction patterns of these nanoparticles show highly oriented (111) crystal facets. X-ray diffraction analysis also confirms the predominant orientation in the (111) crystal planes with lattice constant ~ 4.07 A^0 of fcc gold. X-ray photoelectron (XP) and Fourier transform infrared (FTIR) spectroscopic analysis shows the presence of a fraction of reducing molecules as surface passivating agent either in the un-reacted molecular state or as a mixture of reacted and un-reacted product, which probably undergoes charge transfer with gold nanocrystals giving absorption at ~300 nm. These types of hybrid materials are expected to be useful for solving many challenges related to the applications of nanotechnology especially for optical and electronic devices.

....

Physical and Materials Chemistry Division, National Chemical Laboratory   139

3.6 References

1. (a). Templeton, A. C.; Wuelfing, W. P.; Murray, R. W. *Acc. Chem. Res.* **2000**, *33,* 27. (b). Kamat, P. V. *J. Phys. Chem. B* **2002**, *106*, 7729. (c) Cuenot, S.; Frétigny, C.; Demoustier-Champagne, S.; Nysten, B. *Phys. Rev. B* **2004**, *69*, 165410. (d) Xiao, S.; Hu, W.; Yang, J. *J. Phys. Chem. B* **2005**, *109*, 20339.

2. (a). Valden, M.; Lai, X.; Goodman, D. W. *Science* **1998**, *281*, 1647. (b). Minunn, M.; Mascini, M. *Anal. Lett.* **1993**, *26*, 1441. (c). Bruchez, M., Jr.; Moronne, M.; Gin, P.; Weiss, S.; Alivisatos, A. P. *Science* **1998**, *281*, 2013. (d). Grate, J. W.; Nelson, D. A.; Skaggs, R.; Synovec, R. E.; Gross, G. M. Metal Nanoparticles Protected with Monolayers: Applications for Chemical Vapor Sensing and Gas Chromatography. *In Encyclopaedia of NanoScience and Nanotechnology*; Marcel Dekker: New York, **2004**. (e). Zhang, J.; Malicka, J.; Gryczynski, I.; Lakowicz, J. R. *Anal. Biochem.* **2004**, *330*, 81. (f). Nie, S.; Emory, S. R. *Science* **1997**, *275*, 1102. (g). Kano, H.; Kawata, S. *Opt. Lett.* **1996**, *21*, 1848. (h). Maier, S. A.; Brongersma, M. L.; Kik, P. G.; Meltzer, S.; Requicha, A. A. G.; Atwater, H. A. *Adv. Mater.* **2001**, *13*, 1501. (i) Wertheim, G. K.; Dicenzo, S. B.; Youngquist, S. E. *Phys. Rev. Lett.* **1983**, *51*, 2310.

3. Brust, M.; Walker, M.; Bethell, D.; Schiffrin, D. J.; Whyman, R. J. *J. Chem. Soc., Chem. Commun.* **1994**, 801.

4. (a). Chaki, N. K.; Sudrik, S. G.; Sonawane, H. R.; Vijayamohanan, K. *Chem. Commun.* **2002**, 76. (b) Pastoriza-Santos, I.; Liz-Marzán, L. M. *Langmuir* **1999**, *15*, 948. (c) Stoeva, S.; Klabunde, K. J.; Sorensen, C. M.; Dragieva, I. *J. Am. Chem. Soc.* **2002**, *124*, 2305. (d) Rodríguez-Gattorno, G.; Díaz, D.; Rendón, L.; Hernández-Segura, G. O. *J. Phys. Chem. B* **2002**, *106*, 2482. (e) See for recent reviews Daniel, M-C.; Astruc, D. *Chemical Reviews* **2004**, *104*, 293. (f) Su, C-H.; Wu, P-L.; Yeh, C-S. *J. Phys. Chem. B* **2003**, *107*, 14240. (g) Ishii, T.; Otsuka, H.; Kataoka, K.; Nagasaki, Y. *Langmuir* **2004**, *20*, 561. (h) Kim, B.; Tripp, S. L.; Wei, A. *J. Am. Chem. Soc.* **2001**, *123,* 7955.

5. (a) Heath, J. R.; Brandt, L.; Leff, D. V. *Langmuir* **1996**, *12*, 4723. (b) Heath, J. R.; Knobler, C. M.; Leff, D. V. *J. Phys. Chem. B* **1997**, *101*, 189. (c) Gomez, S.; Philippot, K.; Collière, V.; Chaudret, B.; Senocq, F.; Lecante, P. *Chem. Commun.*

....

Physical and Materials Chemistry Division, National Chemical Laboratory   140

2000, 1945. (d) Bardaji, M.; Uznanski, P.; Amiens, C.; Chaudret, B.; Laguna, A. *Chem. Commun.* **2002**, 595. (e) Green. M.; O'Brien, P.; *Chem. Commun.* **2000**, 183. (f) Brust, M.; Fink, J.; Bethell, D.; Schiffrin, D. J.; Kiely, C. *J. Chem. Soc., Chem. Commun.* **1995**, 1655. (g) Chen, S. *Langmuir* **1999**, *15*, 7551. (h) Chen, S.; Murray, R. W. *Langmuir* **1999**, *15*, 682. (i) Han, L.; Luo, J.; Kariuki, N. N.; Maye, M. M.; Jones, V. W.; Zhong, C. J. *Chem. Mater.* **2003**, *15*, 29**.**

6.   Templeton, A. C.; Hostetler, M. J.; Kraft, C. T.; Murray, R. W. *J. Am. Chem. Soc.* **1998**, *120*, 1906.

7.   (a). Collier, C. P.; Vossmeyer, T.; Heath, J. R. *Annu. Rev. Phys. Chem.* **1998**, *49*, 371. (b). Pileni, M. P. *Supramolecular Science* **1998**, *5*, 321. (c) Redl, F. X.; Cho, K. –S.; Murray, C. B.; O'Brien, S. Nature **2003**, *423*, 968. (d) Brust, M.; Kiely, C. J.; Bethell, D.; Schiffrin, D. J. *J. Am. Chem. Soc.* **1998**, *120*, 12367.

8.   (a). Tucker, J. R. *J. Appl. Phys.* **1992**, *71*, 4399. (b) Korotkov, A. N.; Chen, R. H.; Likharev, K. *J. Appl. Phys.* **1995**, *78*, 2520. (c) Aslam, M.; Mulla, I. S.; Vijayamohanan, K. *Appl. Phys. Lett.* **2001**, *79*, 689.

9.   (a). Westcott, S. L.; Oldenburg, S. J.; Lee, T. R.; Halas, N. J. *Chem. Phys. Lett.* **1999**, *300.* 651. (b). Gole, A.; Sainkar, S. R.; Sastry, M. *Chem. Mater.* **2000**, *12*, 1234. (c). He, H. X.; Zhang, H.; Li, Q. G..; Zhu, T.; Li, S. F. Y.; Liu, Z. F. *Langmuir* **2000**, *16*, 3846. (d). Zhu, T.; Fu, X.; Mu, T.; Wang, J.; Liu, Z. *Langmuir* **1999**, *15*, 5197.

10.   Wang, T.; Zhang, D.; Xu, W.; Li, S.; Zhu, D. *Langmuir* **2002**, *18*, 8655.

11.   (a). Kim, F.; Connor, S.; Song, H.; Kuykendall, T.; Yang, P. *Angew. Chem. Int. Ed.* **2004**, *43*, 3673. (b) Sun, Y., Xia, Y. *Science* **2002**, *298* 2176. (c). Millstone, J. E.; Park, S.; Shuford, K. L.; Qin, L.; Schatz, G. C.; Mirkin, C. A. *J. Am. Chem. Soc.* **2005**, *127*, 5312.

12.   (a). Sau, T. P.; Murphy, C. J. *J. Am. Chem. Soc.* **2004**, *126*, 8648. (b) Milliron, D. J.; Hughes, S. M.; Cui, Y.; Manna, L.; Li, J.; Wang, L-W.; Alivisators, A. P. *Nature* **2004**, *430*, 190. (c). Hao, E.; Kelly, K. L.; Hupp, J. T.; Schatz, G. C. *J. Am. Chem. Soc.* **2002**, *124* 15182. (d) Chen, S.; Wang, Z. L.; Ballato, J.; Foulger, S. H.; Carroll, D. L. *J. Am. Chem. Soc.* **2003**, *125* 16186. (e). Jin, R.; Cao, Y. W.; Mirkin, C. A.; Kelly, K. L.; Schatz, G. C.; Zheng, J. G. *Science* **2001**, *294*, 1901. (f). Jin, R.;

....

Physical and Materials Chemistry Division, National Chemical Laboratory   141

Cao, C.; Hao, E.; Métraux, G. S.; Schatz, G. C.; Mirkin, C. A. *Nature* **2003**, *425*, 487. (g). Chen, S.; Carroll, D. L. *Nano Lett.* **2002**, 2, 1003. (h) Jiang, L-P.; Xu, S.; Zhu, J-M.; Zhang, J-R.; Zhu, J-J.; Chen, H-Y.; *Inorg. Chem.* **2004**, *43*, 5877. (i). Métraux, G. S. ; Mirkin, C. A. *Adv. Mater.* **2005**, *17*, 412.

13. (a). Todorov, T.; Nikolava, L.; Tomova, N. *Appl. Opt.* **1984**, *23*, 4309. (b). Eich, M. Wendorff, J. J. *Opt. Soc. Am. B* **1990**, *7*, 1428.

14. (a) Oliveira O. N. Jr.; Santos D. S. d. Jr.; Balgogh, D. T.; Zucolotto, V.; Mendonca, C. R. *Adv. Colloid Inter. Science.* **2005**, *116*, 179.

15. (a). Lakowicz, J. R. *Anal. Biochem.* **2001**, *298*, 1. (b) Dubertret, B.; Calame, M.; Libchaber, A. J. *Nat. Biotechnol.* **2001**, *19*, 365. (c). Thomas, K. G.; Kamat, P. V. *Acc. Chem. Res.* **2003**, *36*, 888.

16. (a) Drexhage, K. H. *Prog. Opt.* **1974**, *12*, 165. (b). Lakowicz, J. R.; Shen, Y.; D'auria, S.; Malicka, J.; Fang, J.; Gryczynski, Z.; Gryczynski, I. *Anal. Biochem.* **2002**, *301*, 261.

17. (a). M. Han, X. Gao, J. Z. Su, S. Nie, *Nature Biotechnol* **2001**, *19*, 631. (b). Lewis, L. N. *Chem. Rev.* **1993**, *93*, 2693. (c) Kamat, P. V. *J. Phys. Chem. B* **2002**, *13*, 1501. (d). Scultz, S.; Smith, D. R.; Mock, J. J.; Schultz, D. A. *Proc. Natl. Aca. Sci. USA.* **2000**, *97*, 996. (e). Silva, T. J.; Scultz, S.; Weller, D. *Appl. Phys. Lett.* **1994**, *65*, 658. (f). Thomas, K. G.; Kamat, P. V. *Acc. Chem. Res.* **2003**, *36*, 888.

18. (a). Huang, H-Y; Chen, W-F; Kuo, P-L *J. Phys. Chem.* **2005**, *109*, 24288. (b). Korgel, B. A.; Fullam, S.; Connolly, S.; Ftzmaurice, D. J. *Phys. Chem. B* **1998**, *102*, 8379.

19. Ohara, P. C. ; Leff, D. V.; Heath, J. R.; Gelbart, W. M. *Phys. Rev. lett.* **1995**, *75*, 3466.

20. (a). Hamaker, h. C. *Physica (Utrecht)* **1937**, *4*, 1058. (b). Korgel, B. A.; Fitzmaurice, D. *Phys. Rev. Lett.* **1998**, *80*, 3531.

21. (a). Whetten, R. L.; Shafigullin, M. M.; Khoury, J. T.; Schaaf, t. G.; Vezmar, I.; Alvarez, m. M.; Wilkinson, A. *Acc. Chem. Res.* **1999**, *32*, 397. (b) Heath, J. R.; Knobler, M. C.; Leff, D. V. *J. Phys. Chem. B* **1997**, *101*, 189. (c) Thomas, P. J.; Kulkarni, G. U.; Rao, C. N. R.; *J. Phys. Chem. B* **2000**, *104*, 8138.

22. (a). Hubbard, A. T. *Chem. Rev.* **1988**, *88*, 633. (b). Gui, J. Y.; Lu, F.; Stern, D. A.;

Hubbard, A. T. *J. Electroanal. Chem.* **1990**, *292*, 245. (c). Shannon, C.; Frank, D. G.; Hubbard, A. T. *Annu. Rev. Phys. Chem.* **1991**, *42*, 393.

23.   Futamata, M. *J. Phys. Chem.* **1995**, *99*, 11901.

24.   Sabatani, F.; Cohen-Boulakia, J.; Bruening, M.; Rubinstein, I. *Langmuir* **1993**, *9*, 2974.

25.   Kim, Y. –T.; McCarley, R. L.; Bard, A. J. *J. Phys. Chem.* **1992**, *96*, 7416.

26.   Zhong, C. –J.; Porter, M. D. *Anal. Chem.* **1995**, *67*, 709A.

27.   Sun, L.; Johnson, B.; Wade, T.; Crooks, R. M. *J. Phys. Chem.* **1990**, *94*, 8869.

28.   Bryant, M. A.; Crooks, R. M. *Langmuir* **1993**, *9*, 385.

29.   (a). Rubinstein, I.; Rishpon, J.; Sabatani, A.; Redondo, A.; Gottesfeld, S. *J. Am. Chem. Soc.* **1990**, *112*, 6135. (b). Sabatani, E.; Redondo, A.; Rishpon, J.; Rudge, A.; Rubinstein, I.; Gottesfeld, S. *J. Chem. Soc. Faraday Trans.* **1993**, *89*, 287. (c) Sabatani, E.; Gafni, Y.; Rubinstein, I. *J. Phys. Chem.* **1995**, *99*, 12305.

30.   Hayes, W. A.; Shannon, C. *Langmuir* **1996**, *12*, 3688.

31.   Lukkari, J.; Kleemola, K.; Meretoja, M.; Ollonqvist, T.; Kankare, J. *Langmuir* **1998**, *14*, 1705.

32.   Johsson, M.; Wayner, D. D. M.; Lusztyk, J. *J. Phys. Chem.* **1996**, *100*, 17539.

33.   Raj, C. R.; Kitamura, F.; Ohsaka, T. *Langmuir* **2001**, *17*, 7378.

34.   Roy, B. C.; Gupta, M. D.; Bhowmik, L.; Ray, J. K. *Bull. Mater. Sci.* **2001**, *24*, 389.

35.   Gao, P.; Gozstola, D.; Weaver, M. *J. Phys. Chem.* **1989**, *93*, 3753.

36.   Granot, E.; Patolski, Fernando,; Willner, I. *J. Phys. Chem. B* **2004**, *108*, 5875.

37.   Okamura, M.; Kondo, T.; Uosaki, K. *J. Phys. Chem. B* **2005**, *109*, 9897.

38.   Mie, G. Ann. Phys. **1908**, *25*, 377.

39.   Henglein, A. *J. Phys. Chem.* **1993**, *97*, 5457.

40.   (a) Brust, M.; Bethell, D.; Schiffrin, D. J.; Kiely, C. J. *Adv. Mater.* **1995**, *7*, 795. (b) Andres, R. P.; Bielefeld, J. D.; Henderson, J. I.; Janes, D. B.; Kolagunta, V. R.; Kubiak, C. P.; Mahoney, W. J.; Osifchin, R. G. *Science* **1996**, *273*, 1690. (c) Brust, M.; Bethell, D.; Kiely, C. J.; Schiffrin, D. J. *Langmuir* **1998**, *14*, 5425. (d) Chen, S. W., *J. Phys. Chem. B* **2000**, *104*, 663. (e) Hussain, I.; Wang, Z.; Cooper, A. I.;

....

Physical and Materials Chemistry Division, National Chemical Laboratory   143

Brust, M. Langmuir **2006**, *22*, 2938.

41. Fendler, J. H. in *Nanoparticles and Nanostructured films: Preparation, Characterization and Applications*, Wiley-VCH, Weinheim, **1998**.

42. Link, S.; El-Sayed, M. A. *J. Phys. Chem. B* **1999**, *103*, 8410.

43. (a). Su, K. –H.; Wei, Q. –H.; Zhang, X.; Mock, J. J.; Smith, D. R.; Schultz, S. *Nano. Lett.* **2003**, *3*, 1087. (b). Templeton, A. C.; Wuelfing, W. P.; Murray, R. W. *Acc. Chem. Res.* **2000**, *33*, 27. (c). Storhoff, J. J.; Mirkin, C. A. *Chem. Rev.* **1999**, *99*, 1849.

44. (a). Kreibig, U.; Vollmer, M. in *Optical Properties of Metal Clusters*, Springer: Berlin, **1995**. (b). Sarathy, K. V.; Kulkarni, G. U.; Rao, C. N. R. *Chem. Commun.* **1997**, 537. (c). Pal, A.; Ghosh, S. K.; Esumi, K.; Pal, T. *Langmuir* **2004**, *20*, 575.

45. Westcott, S. L.; Oldenburg, S. J.; Lee, T. R.; Halas, N. J. *Chem. Phys. Lett.* **1999**, *300*. 651.

46. Wang, Z. L. J. Phys. Chem. B **2000**, *104*, 1153.

47. (a). Nakamoto, M.; Yamamoto, M.; Fukusumi, M.; Chem. Commun. **2002**, 1622. (b). a = 4.078 A^{0}, *Joint Committee on Powder Diffraction Standards* File No.04-0784.

48. (a). Terril, R. H.; Postlethwaite, T. A.; Chen, C-h,; Poon, C-D.; Terzis, A.; Chen, A.; Hutchison, J. E.; Clark, M. R.; Wignall, G.; Londono, J. D.; Superfine, R.; Falvo, M.; Jonhnson Jr., C. S.; Samulski, E. T.; Murray, R. W. *J. Am. Chem. Soc.* **1995**, *117*, 12537. (b). Sandhyarani, N.; Resmi, M. R.; Unnikrishnan, R.; Vidyasagar, K.; Ma, S.; Antony, M. P.; Selvam, G. P.; Visalakshi, V.; Chandrakumar, N.; Pandian, K.; Tao, Y-T.; Pradeep, T. *Chem. Mater.* **2000**, *12*, 104.

49. Aiken III, J. D.; Finke, R. G. *J. Mol. Cata. A: Chem.* **1999**, *145*, 1.

50. (a). Johnson, S. R.; Evans, S. D.; Brydson, R. *Langmuir* **1998**, *14*, 6639. (b). The Aldrich Library of FTIR Spectra, 1st Ed.; Pouchert, C. J.; Aldrich Chemicals Co., Inc.: Milwaukee, WI **1985**. (c). Hayes, W. A.; Shannon, C. *Langmuir* **1996**, *12*, 3688. (d). Osawa, M.; Matsuda, N.; Yoshii, K.; Uchida, I. *J. Phys. Chem.* **1994**, *98*, 12702.

51. (a) NIST X-ray Photoelectron Spectroscopy Database (via internet:

http://srdata.nist.gov/xps. (b). Bensebaa, F.; Zhou, Y.; Deslandes, Y.; Kruus, E.; Ellis, T. S. *Surf. Sci.* **1998**, *405*, L472. (c). Luo, J.; Maye, M. M.; Han, L.; Kariuki, N. N.; Jones, V. W.; Lin, Y.; Engelhard, M. H.; Zhong, C-J. *Langmuir*, **2004**, *20*, 4254; Castner, D. G. *Langmuir* **1996**, *12*, 5083. (d). Bourg, M-C.; Badia, A.; Lennox, R. B. *J. Phys. Chem. B* **2000**, *104*, 6562.

52.   Hooper, A. E.; Werho, D.; Hopson, T.; Palmer, O. *Surf. Interface Anal.* **2001**, *31*, 809.

53.   (a). Leff, D. V.; Brandt, L.; Heath, J. R. *Langmuir* **1996**, *12*, 4723. (b). Kumar, A.; Mandal, S.; Selvakannan, P. R.; Pasricha, R.; Mandale, A. B.; Sastry, M. *Langmuir* **2003**, *19*, 6277.

54.   Büttner, M.; Kröger, H.; Gerhards, I.; Mathys, D.; Oelhafen, P. *Thin Solid Film* **2006**, *495*, 180.

55.   Katz, E.; Lion-Dagan, M.; Willner, I. *J. Electro. Anal. Chem.* **1996**, *408*, 107.

56.   Shankar, S. S.; Rai, A.; Ankamwar, B.; Singh, A.; Ahmad, A.; Sastry, M. *Nature Materials* **2004,** *3*, 482.

57.   Aslam, M. ; Fu, L. ; Su, M. ; Vijayamohanan, K. ; Dravid, V. P. *J. Mater. Chem.* **2004**, *14,* 1795. (d). Selvakannan, P. R.; Kumar, P. S.; More, A. S.; Shingte, R. D.; Wadgaonkar, P. P.; Sastry, M. *Adv. Mater.* **2004**, *16.* 966.

58.   (a). Malikova, N.; Pastoriza-Santos, I.; Schierhorn, M.; Kotov, N. A.; Liz-Marzán, L. M. Langmuir **2002**, *18*, 3694. (b). Sun, X. Dong, S. Wang, E. Angew. Chem. Int. Ed. **2004**, *43*, 6360.

59.   (a) Maillard, M.; Giorgio, S.; Pileni, M. P. *Adv. Mater.* **2002**, *14*, 1084. (b) Curtis, A. C.; Duff, D. G.; Edwards, P. P.; Jefferson, D. A.; Johnson, B. F. G.; Kirkland, A.; Wallace, A. S. *Angew. Chem. Int. Ed. Engl.* **1988**, *27*, 1530. (c). Bradley, J. S.; Tesche, B.; Busser, W.; Maase, M.; Teetz, M. T. *J. Am. Chem. Soc.* **2000**, *122*, 4631. (d). Zhou, Y.; Wang, C. Y.; Zhu, Y. R.; Chen, Z. Y. *Chem. Mater.* **1999**, *11*, 2310.

60.   Kashiwagi, Y.; Uchiyama, K.; Kurashima, F.; Anzai, J.; Osa, T. *Anal. Sciences* **1999**, *15*, 907.

61.   Zille, A.; Ramalho, P.; Tzanov, T.; Millward, R.; Aires, V.; Cardoso, M. H.; Ramalho, M. T.; Gübitz, G. M.; Cavaco-Paulo, A.; *Biotechnol. Prog.* **2004**, *20*,

....

Physical and Materials Chemistry Division, National Chemical Laboratory   145

Chapter 4

Bimetallic Assembly: Formation of Interlinked Gold and Silver Nanoparticles*

The present chapter describes bi-metallic assembly of silver and gold nanoparticles using 4-aminothiophenol as a cross linking unit. More precisely, interlinking of gold and
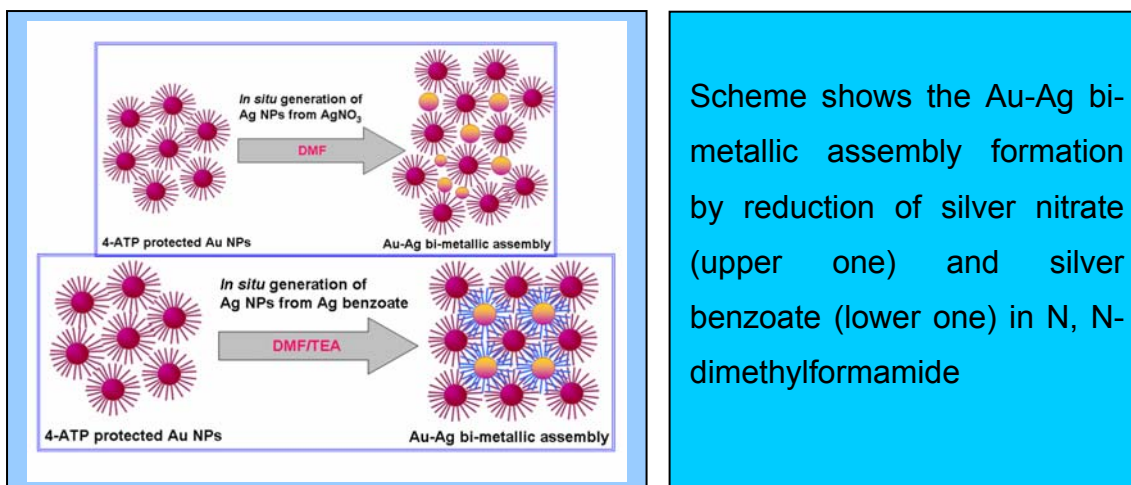
Scheme shows the Au-Ag bi-metallic assembly formation by reduction of silver nitrate (upper one) and silver benzoate (lower one) in N, N-dimethylformamide

silver nanoparticles has been demonstrated at controlled pH. A judicious control of pH at 7.8 enables synthesis of gold nanoparticles surface functionalized with amino group, which is then used for the interlinking of *in situ* generated silver nanoparticles. Such interlinked assemblies show surface plasmon absorption in the range 540-580 nm presumably due to the intercrystal surface plasmon coupling. Interestingly, silver nanoparticles synthesized from silver benzoate gives a highly ordered assembly as compared to that from silver nitrate. Benzoic acid produced in the reaction as byproduct links to silver nanoparticle surface, thus providing the necessary stability for the as synthesized assemblies.

4.1 Introduction

One of the major objectives of nanoscale materials research is to design methods for self-assembly formation without losing their individual characteristics by simple processing, thereby enabling the manipulation of their size and shape dependant properties, so that they can be understood as pure macromolecular substances with outstanding fundamental and potential technological consequences.[1] Several advanced techniques, such as electron beam lithography (EBL) have been previously employed to get ordered assemblies of metal nanoclusters with controllable geometry and dimensions and such methods allow the reliable production of large number of supperlattice particles of precisely controlled shape and particle-particle separations.[2] Therefore, many applications envisioned for nanotechnology require assembled nanometer scale elements of two or more metals or semimetals or semiconductors and their combinations (hetero-structures) to have hybrid properties. For example, a planar array of small metal islands separated from each other by tunnel barriers is of great interest for developing nanoscale electronic or digital circuits, which also has drawn tremendous interest for theoretical studies.[3]

The electronic conduction in such structures is said to be varied from metallic to the insulating limit by controlling the size and the strength of coupling. All such investigations have been inspired by the fact that optical and electronic properties of such assemblies and core-shell nanoparticles can be tuned with respect to interparticle separation and shell thickness.[4] Murray et al. have used an Arrhenius type activated tunneling model to describe the electron transport through such 3-D network of monolayer-protected gold nanoparticles as represented by the equation 4.1.[5]

$$\sigma_{EL}(\delta, T) = \sigma_0 (e^{-\beta\delta}) e^{-E_A/k_B T} \qquad 4.1$$

where, β is the electron tunneling coefficient in units of Å^{-1}, δ the average interparticle distance, E_A the activation energy, and $\sigma_0 e^{-\beta\delta}$ the conductivity at $k_{BT} \gg E_A$. The first exponential term describes the electron tunneling between the particles through organic linker molecules where the charge transport is governed by the nature of the molecule as conductivity of such molecules depends exponentially on the chain length. Methylene

....

Physical and Materials Chemistry Division, National Chemical Laboratory   148

(CH_2) groups are considered to be insulators, and therefore, Fermi level of the monolayer protected metal is located in the HOMO-LUMO gap of the molecule, which depends on the capping agents. Side orbitals provide a super-exchange pathway for the electrons to tunnel along the molecule, while the presence of aromatic rings can cause many interesting consequences.[5b]

Different models have been developed for the theoretical description of the activation energy of charge transport, which is indeed given by the second exponential term in equation 4.1. For example Abeles et al. developed a simple electrostatic model to describe the activation energy for the activated charge transport in granular metals.[6] In the low-field regime, $\sigma \approx \exp[-2(C/RT)^{0.5}]$, where $C = \delta\beta E_{A,GM}$ and $E_{A,GM}$ is given by

$$E_{A,GM} = \frac{e^2}{8\pi\varepsilon\varepsilon_0}\left(\frac{1}{r} - \frac{1}{r+\delta}\right) \qquad\qquad 4.2$$

where, r is the radius of the particle, δ the interparticle distance and ε the dielectric constant of the surrounding matrix. The free energy for activation (ΔG^*) of electron transfer can also be derived from the Marcus theory by the repolarization of the organic dielectric matrix.[5, 7, 8] Murray and co-workers compared experimentally obtained activation energies from films of noninterlinked Au NPs with both $E_{A,GM}$ and ΔG^* and have found that neither of the above models provides an adequate description of the experimentally observed activation energies. Later, Wessels and co-workers further extended the study to optical and electrical properties of 11-20 nm thick films of ~ 4 nm gold particles interlinked by several dithiols linker molecules with various chain lengths and functional moieties.[9] These films of assembled nanoparticles by alkyl dithiols undergo thermally activated charge transport with activation energies between 554 and 71 meV. In sharp contrast, similar studies carried out with aryl dithiols show relatively much lower activation energies (14 meV), because of the formation of a resonant state at the interface due to the overlap of molecular orbital and metal wave functions. However, electron tunneling decay constant is mainly governed by the nonconjugated parts of these molecules. Thus, these dithiol molecules can be viewed as serial connections of electrically insulating (nonconjugated) and conductive (conjugated) parts, allowing us to tune the conductivity from the insulating to the metallic limit by

manipulating the conjugated units, but without altering significantly the interparticle spacing.[9]

Similarly, changes in electron transport properties of such assemblies are also accompanied by changes in optical absorption characteristics due to interparticle coupling of surface plasmons having important implications for the development of optical devices and in techniques such as surface-enhanced Raman scattering.[10] For example, significant broadening and red shifting of the plasmon absorption band generally signifies assembly formation.[11] The absorption characteristics of nanoparticles in solution or deposited on substrates are determined by the local dielectric environment and size of the particles, the interparticle spacing, and the chemical nature of the interface.[12,13] If the particles are closely packed, the average polarization field from the surrounding particles additionally influences the plasmon resonance.[14]

In general, self-assembly of nanoclusters can be formed either by direct covalent attachment of different building blocks after functionalization or by some non-covalent (electrostatic, hydrophobic, hydrogen bonding etc.) interactions between functionalized nanoclusters.[15] For example, gold nanoparticle aggregation has been demonstrated using dithiols as linking units by virtue of the strong Au-S interaction.[16] Such organization of molecularly linked gold nanoclusters often leads to two dimensional superlattices.[17] The initiation of the aggregation process generally leads to distinct color changes from red to blue followed by quantitative precipitation of insoluble networked nanoparticles with the retention of individual character. Similarly, Murray and co-workers have used dissolved DNA and carboxylate-metal ion-carboxylate bridges to interlink monolayer protected metal nanoclusters.[18] Similar 3D assembly of gold nanoparticles have been achieved by several other poly-functional molecules.[19] Interestingly, such aggregation process can even be made reversible with changeable interparticle interactions by UV-photoactivation.[20] Some of these organizations are achieved by delicate procedures where several precautions are essential. For example, organization of clusters at the air/water interface using Langmuir Blodgett techniques requires extreme care.[21]

It is highly desirable to extend this type of assembly for two or more metal nanoparticles to synthesize hetero-assembly; so that interesting and new properties of such hybrid materials can be further explored. The study of bimetallic or trimetallic

nanoparticles is significant because of their interesting optical, magnetic, and catalytic properties.[22] For example, silver nanoparticles have been organized on Fe_3O_4 nanoparticle surface using electrochemical (galvanic) reduction of Ag^+ ions by Fe(II), which are fluorescent and also responsive to magnetic field.[23] Magnetic properties of such hetero-assemblies and alloys can be manipulated with respect to their mixing ratio.[22c, 24] Similarly, thin film assembly of binary metal nanoparticles via interparticle linkages of dicarboxylic acid mediators has been demonstrated recently.[25] This method is based on the combination of gold-sulfur and silver-carboxylate binding affinity via selective interparticle linkages at the silver sites for the assembly of Au-Ag nanoparticles. Despite of these various protocols for the assembly of nanoparticles, chemical control of such assembly formation appears to be difficult because it is not usually possible to adjust precisely the number and spatial orientation of chemically reactive linker groups on the surface of the particle. Therefore, an understanding of the binary or ternary hetero-assembly and the interparticle interactions is very important, since little is known about the assembly of binary or ternary metal nanoparticle systems. This is because lack of controllability over the interparticle linkages at the multi-component nanocrystal surfaces restricts their uniform assembly formation. Thus the development of simple and easy preparation techniques for chemically interlinked clusters is important which would help to overcome such limitations in organizing arrays of nanoparticles of two or more metals for the fabrication of more complex micro/nano-electronic devices.

In this context, present chapter reports a simple method for the formation of bi-metallic self-assembly by controlled inter-linking of Au and Ag nanoclusters using 4-ATP as molecular interconnects. 4-ATP was selected on the basis of its known pH dependent capping behavior, which could be used advantageously to anchor silver nanoclusters on Au.[26] The mode of linking depends on the source of silver as illustrated by using silver benzoate as a better source for getting close-packed assemblies compared to silver nitrate since benzoic acid formed during its reduction may direct the assembly into a well packed structure. Though we have not attempted to control the size and shape precisely, a judicious change of concentrations would enable to have the control over it too. 'As synthesized' hetero-assembly was characterized by UV-visible spectroscopy

and transmission electron microscopy. UV-visible spectrum of interconnected nanoparticles of gold and silver shows gradual changes during its formation and finally gives an absorption maximum at ca. 575 nm.

4.2 Experimental Section

4.2.1 Materials: Gold tetrachloro acid trihydride (HAuCl$_4$.3H$_2$O, 99.9 %), 4-aminothiophenol (4-ATP, 90%), tridecylamine (TDA, 98%), sodium borohydride (NaBH$_4$, 99%) and lithium perchlorate (LiClO$_4$, 99.9%) were purchased from Aldrich chemicals. Silver nitrate (AgNO$_3$, 99.9%), toluene (99.8%), and N, N-dimethyl formamide (DMF, 99.9%) were purchased from Merck. All these chemicals were used without further purification. Water used for these experiments was deionized with Milli-Q Reagent water system.

4.2.2 Procedure for the Preparation of Silver Benzoate: 1.2 M benzoic acid was mixed with 1M NaOH in water. Finally, solid silver benzoate was obtained by the dropwise addition of aqueous AgNO$_3$ (1M) into the as prepared sodium benzoate under vigorous stirring, followed by filtration, washing (with deionized water for several times) and drying under vacuum at 40 ^{0}C.

4.2.3 Synthesis of Nanoparticles

(a) Synthesis of Au NPs: Gold nanoparticles were prepared in a two-phase water/toluene system using modified Brust's method.[27] Briefly, equal volume (50 ml each) of ammoniacal aqueous solution of 0.5 mM HAuCl$_4$ (pH ca.7.8) and 1 mM ATP solution in toluene were taken, followed by reduction with freshly prepared 0.01 M aqueous NaBH$_4$ solution under continuous stirring for 30 min. 4-ATP capped Au NPs readily reached the interface due to the hydrophilic amine group, which were then separated out and washed thoroughly with water and toluene. After drying under nitrogen atmosphere [complete drying makes it difficult to re-disperse in DMF], Au NPs were re-dispersed in 40 ml DMF.

(b) Formation of Au-Ag Hetero-assembly, Set 1: 0.5 mM AgNO$_3$ was added to 40 ml of 4-ATP capped Au NP dispersion in DMF under continuous stirring. AgNO$_3$ was

....

Physical and Materials Chemistry Division, National Chemical Laboratory   152

Ph. D. Thesis   *Chapter 4*   *University of Pune, May 2006*

----

spontaneously reduced in DMF to form Ag NPs forming Au-Ag hetero-assembly.

Set 2: Similarly, 0.5 mM silver benzoate was added to 40 ml DMF containing Au NPs under vigorous stirring and was reduced instantaneously with 1 ml triethylamine (TEA).

4.2.4 Characterization Techniques

4.2.4.1 UV-visible Spectroscopy : All UV-visible (UV-vis) absorption measurements were recorded using UV-2101PC double beam spectrometer, Shimadzu with quartz cells of 1 cm path length. The spectra were background subtracted using the solvent used for nanoparticle dispersion.

4.2.4.2 TEM Analysis: The TEM micrographs were taken on a JEOL model 1200EX instrument operated at an accelerating voltage of 120 KV. The TEM samples were prepared by drop-casting the respective solutions on a carbon coated Cu grids (3 nm thick, deposited on a commercial copper grid) and air dried at room temperature.

4.2.4.3 XPS Analysis: XPS measurements were carried out on a VG MicroTech ESCA 3000 instrument at a pressure $>1 \times 10^{-9}$ Torr. The general scan inclusive of Au 4f, Ag 3d, C 1s, S 2p, and N 2p core-level spectra was recorded with un-monochromatized Mg $K\alpha$ radiation (photon energy = 1253.6 eV) at a pass energy of 50 eV and an electron takeoff angle (angle between electron emission direction and surface plane) of 60°. The overall resolution was ~1 eV for all the measurements. The core-level binding energies (BE) were aligned taking the adventitious carbon binding energy as 285 eV. The powdered samples of Au-ATP-Ag was separated from the precipitate and purified by successive washing with acetonitrile/water mixture and finally by dry acetonitrile. Similarly, initially prepared Au nanoparticles were washed thoroughly with water and toluene prior to the XPS analysis. These samples were then dried under vacuum.

4.3 Results and Discussion

UV-visible spectroscopy is a commonly used tool for monitoring the assembly formation, since such assemblies are associated with color changes due to the interaction of surface plasmons of neighboring nanoparticles.[28] Generally, absorption characteristics of assemblies are different to that of their individual component

....

Physical and Materials Chemistry Division, National Chemical Laboratory   153

nanoparticles. Therefore, it is highly desirable to study the individual UV-visible absorptions of component nanoparticles prior to their assembly. Accordingly, Figure 4.1 shows UV-visible spectra of (i) 4-ATP capped Au nanoparticles in N, N-dimethylformamide, (ii) similar sized Ag nanoparticles synthesized by the reduction of silver benzoate using triethylamine, and (iii) silver nanoparticles from *in situ* reduction of AgNO$_3$ by N, N-dimethylformamide.[29] The individual surface plasmon absorption of ATP capped gold, triethyl amine capped and bare silver at 532, 430, and 425 nm respectively indicate the formation of stable nanoparticles in N, N-dimethylformamide.[30] In comparison, spectrum 'iv' shows the surface plasmon band for tridecylamine capped silver nanoparticles, which gives a symmetric and sharp peak at 434 nm, confirming the feasibility of amine as a potential capping agent. Surface plasmon band of Au nanoparticles centered at 532 nm lies much higher in energy than the earlier report on 4-
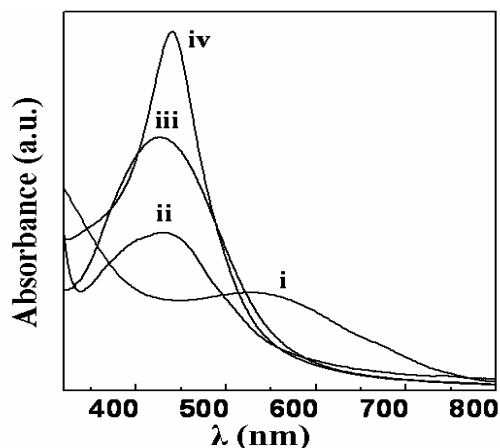
Figure 4.1: UV-visible spectra of different nanoparticle dispersions in N,N-dimethylformamide. (i) 4-ATP protected Au nanoparticles, (ii) Ag nanoparticles formed by reducing Ag-benzoate with triethylamine, (iii) Ag nanoparticles by spontaneous reduction of silver nitrate in DMF, and (iv) tridecylamine capped Ag nanoparticles.

ATP capped gold nanoparticles (650 nm in methanol).[31a] Our method of preparation presumably restricts the self-assembly formation during the synthesis and prevents any self-aggregation. The value at 650 nm arises mainly from the self-assembly of Au nanoparticles and the consequent coupling of the surface plasmon band. The appearance of surface plasmon peak at higher energies indirectly indicates the free availability of one of the functional groups (either amino or thiol) for further assembly

formation.

In sharp contrast, Figure 4.2(a) shows the evolution of surface plasmon band after the addition of $AgNO_3$ to the dispersion of 4-ATP capped Au NPs in DMF. A characteristic single plasmon peak at 558 nm is evident, which is significantly red-shifted from the original SPR peak of 4-ATP capped gold nanoparticles. The appearance of this peak at 558 nm suggests the generation of silver nanoparticles on the addition of silver nitrate followed by the interlinking with functionalized gold nanoparticles preferably by Ag-amine link. This peak is significantly a dampened one, which further diminishes in intensity with time due to aggregation process. The change in the color of the sample after the assembly formation is evident from the photographs given as inset in Figure 4.2(a). The stability of amine protected silver nanoparticles has been extensively investigated recently exhibiting effective protection of silver surface by amino group due
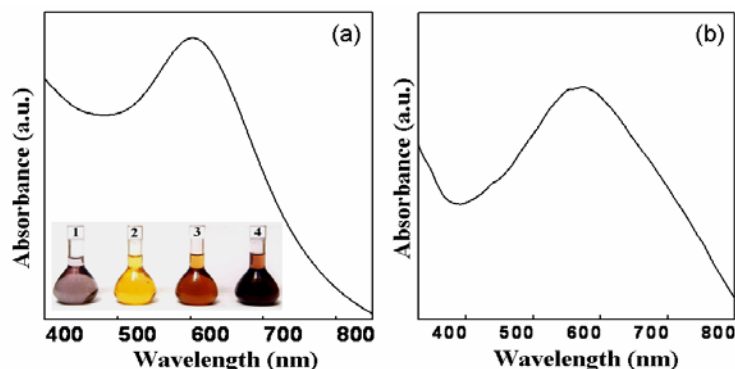
Figure 4.2: UV-visible spectra of Au-Ag bi-metallic assemblies in N, N-dimethylformamide. (a) spectrum for the aggregates formed on addition of $AgNO_3$ to a dispersion of 4-ATP capped gold nanoparticles in DMF; (b) spectrum for the bi-metallic assembly synthesized by reduction of Ag-benzoate on addition of triethylamine in the presence of Au nanoparticles; inset of 'a' shows the photographs of different samples (1) 4-ATP capped gold nanoparticles, (2) Ag nanoparticles, (3) physical mixture of Au and Ag nanoparticles, and (4) chemically interlinked Au-Ag nanoparticle assemblies (all dispersions are in DMF).

to which such nanoparticles are stable even after one year.[30b]

In order to understand the role of silver salts, we have investigated the assembly formation by replacing silver nitrate with silver benzoate. Silver nanoparticles are *in situ* synthesized by reducing silver benzoate with triethylamine in a solution of 4-ATP capped gold nanoparticles under identical experimental conditions. Interestingly, faster aggregation is observed as compared to that of the earlier case with a distinct color

change. The UV-visible spectrum of these interconnected nanoclusters shows a red shifted peak at 575 nm [Figure 4.2(b)]. This SPR absorption is further red-shifted compared to the earlier case. However, this band can also be assigned to the interparticle plasmon resonance band for the mixed metal aggregates, which is consistent with the data included in the earlier reports.[32] Effective assembly formation for the present organization process causes the relatively larger shifting. Thus the presence of UV-visible absorption maxima in the range 550-580 nm provides the vital proof for the assembly formation. Interestingly the optical property of this network structure is more or less similar to the gold encased silver nanoclusters where a red shifted single plasmon
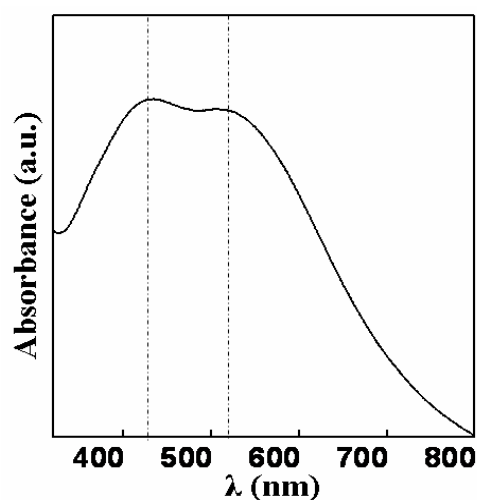
Figure 4.3: UV-visible spectrum of a physical mixture of 4-ATP protected Au nanoparticles and Ag nanoparticles in N, N-dimethylformamide.

peak has been observed.[33]

    To confirm that the above optical absorption characteristics are not simply from a physical mixture of individual gold and silver nanoparticles, UV-visible absorption for a mixture containing equal amount of pre-formed Au and Ag nanoparticles is investigated. Accordingly, Figure 4.3 shows a typical UV-visible spectrum for such a mixture with two shoulders, which can be de-convoluted into two peaks corresponding to the characteristic surface plasmon values at 432 nm for Ag and 530 nm for Au nanoparticles respectively. These peaks match well with their individual surface plasmon peaks (Figure 4.1) confirming our assignment for the interparticle coupling of the surface plasmon bands in the case of interlinked Au and Ag nanoparticles. Interestingly, the

appearance of plasmon peak at lower energy region precludes the possibility of alloy formation as absorption bands of alloys fall between the maxima of their constituent silver and gold surface plasmon absorption bands respectively and core-shell structures manifest themselves into two distinct bands depending on the thickness of the shell.[34]
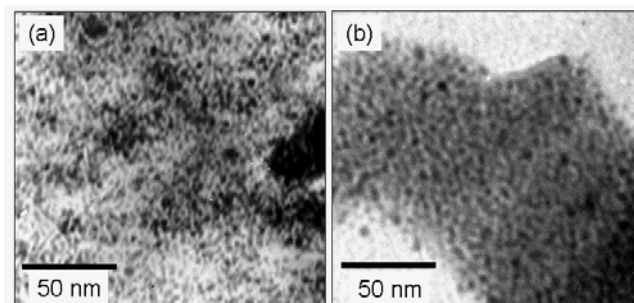
Figure 4.4 Transmission electron micrographs of interlinked Au and Ag nanoparticles. (a) Aggregates formed by the *in situ* reduction of $AgNO_3$ in solution containing 4-ATP protected gold nanoparticles. (b) Bi-metallic assembly formed from Ag-benzoate on reduction by triethylamine.

The formation of mixed metal assembly as suggested from the UV-visible spectra is further supported by the results of TEM studies. Accordingly, Figures 4.4(a) and 4.4(b) show a comparison of micrographs of mixed metal assemblies formed by the reduction of Ag^+ ions when $AgNO_3$ and Ag-benzoate are used as silver salts respectively. As seen in Figure 4.4(a), the *in situ* reduction of $AgNO_3$ by DMF shows crystalline hetero-assembly with individual clusters placed in random locations. In sharp contrast, TEM micrograph of sample from Ag-benzoate shows close-packed extended assembly [Figure 4.4(b)].

Thus a distinct difference in degree of assembly formation is observed as we go from silver nitrate to silver benzoate as source for silver nanoparticles. It is expected that benzoic acid formed as byproduct during the reduction process controls the assembly formation. Benzoic acid binds strongly to as synthesized silver nanoparticles due to the Ag^+-CO_2^- interaction and thereby controls the nucleation process.[35] This stabilization of silver nanoparticles controls the linking process ultimately leading to a close-packed crystalline bi-metallic assembly. This type of structural arrangement has a basic difference from the one reported by Schiffrin et al, where they have prepared non-

----

interactive superlattices of Au and Ag nanoclusters (no chemical linkage between Au and Ag) by evaporating the solvent from the mixture of thiol stabilized gold and silver nanoparticles.[36]
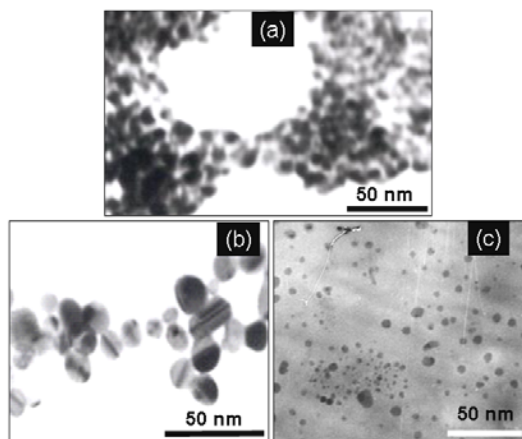
Figure 4.5: Transmission electron micrographs of different nanoparticles: (a) 4-ATP capped Au nanoparticles, (b) *in situ* prepared Ag nanoparticles in DMF, and (c) Ag nanoparticles synthesized using silver benzoate.

Figure 4.5 shows the TEM images of 4-ATP capped Au NPs (a), bare silver nanoparticles synthesized by *in situ* reduction of $AgNO_3$ in DMF (b), and benzoic acid protected silver nanoparticles by reducing silver benzoate with triethylamine. Figure 4.5(a) shows the smaller sized gold nanoparticles assembled together due to the presence of bi-functional 4-ATP, while silver nanoparticles synthesized from silver nitrate are not uniform in shape and size. The absence of stabilizers causes non-uniform growth of silver nanoparticles, because silver nanoparticles can grow in an uncontrolled manner as nucleation and growth continue without any interruption. In contrast, silver nanoparticles from silver benzoate are protected by benzoic acid concomitantly regulating the growth. Figure 4.5(c) shows the TEM image of benzoic acid protected silver nanoparticles with comparatively uniform shape and size compared to that obtained by the former route. Thus, *in situ* generated silver nanoparticles from $AgNO_3$ are highly poly-dispersed, while NPs from Ag-benzoate are comparatively uniform. This is schematically depicted in Scheme 4.1. Briefly, Scheme 4.1 a shows the formation of poly-dispersed Ag NPs from $AgNO_3$ due to the lack of stabilizers, while in 'b' the

formation of monodispersed Ag nanoparticles capped by benzoic acid is shown.

   Important information on the surface binding properties of 4-aminothiophenol is provided by the analysis of the X-ray photoelectron spectroscopy from a comparison of spectra recorded for both gold nanoparticles before and after bi-metallic assembly formation. Surface binding properties of 4-aminothiophenol is identical for both the assemblies, i.e., assemblies from silver nitrate and silver benzoate. Since, bi-metallic assembly from silver benzoate provides better ordering, XPS analysis is provided for the sample prepared from silver benzoate to see the role of benzoic acid. Figures 4.6.i(a) and 4.6.i(b) show a comparison of S 2p spectrum for 4-ATP capped gold nanoparticles
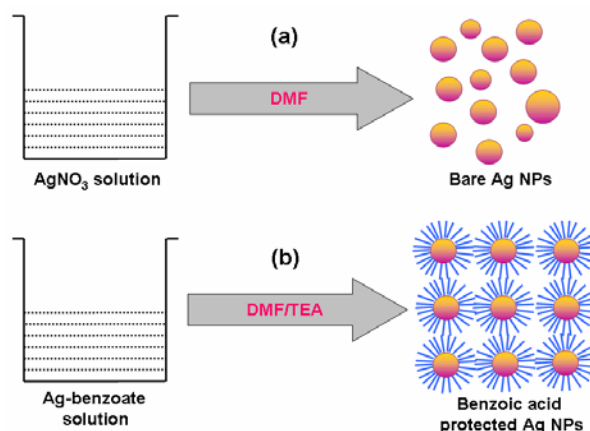
Scheme 4.1 (a) *In situ* reduction of $AgNO_3$ in DMF leading to poly-dispersed silver nanoparticles, while (b) reduction of Ag-benzoate by triethylamine (TEA) in DMF gives nearly monodispersed benzoic acid coated silver nanoparticles.

and Au-Ag assembly respectively. The exact assignments for the different peaks are quite difficult and available data is also ambiguous.[37] Though the major contribution is from the bound thiolate species, minor peaks are also seen in regions arising from the oxidized sulfur species.[38] For bound sulfur, S binding energies are obtained at 161.8 eV and at 163.2 eV from Au-ATP-Ag [Figure 4.6.i(b)]. Jonhson et al. have assigned these peaks as S $2p_{3/2}$ and S $2p_{1/2}$ respectively.[31] An important finding is that the ratio of the $2p_{3/2}$ and $2p_{1/2}$ peaks for the as synthesized Au-Ag nanoparticles is nearly 2 : 1 indicating thiolates adsorbed on Au surface.[39] However, we could get only an unresolved peak at 163.2 eV for Au-ATP. There are two other peaks at *ca*. 165.5 eV and at *ca*. 168.5 eV respectively, which are presumed to the formation of oxidized species. X-ray

Ph. D. Thesis   *Chapter 4*   *University of Pune, May 2006*
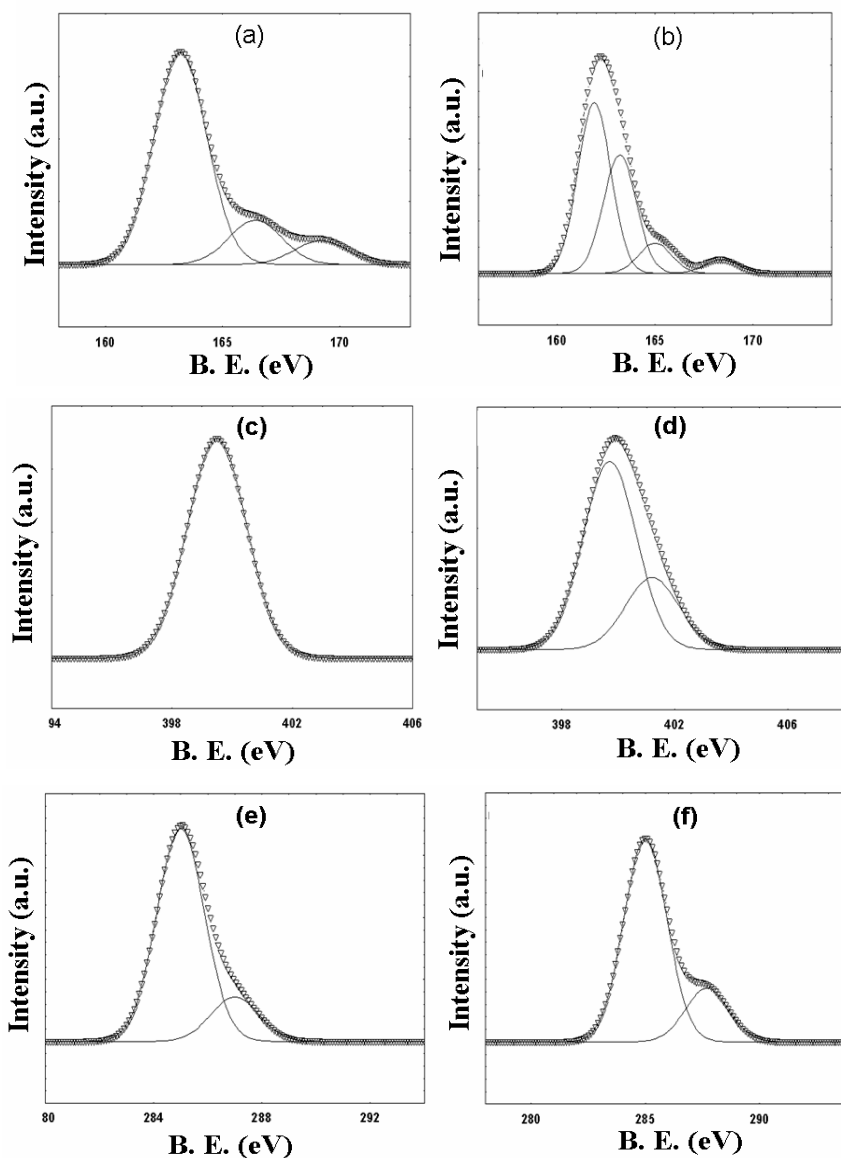
Figure 4.6 (i): Core level XP spectra of S 2p, N1s, and, C1s species present in Au-ATP and Au-ATP-Ag. The triangles represent the experimental data; the solid lines represent Gaussian fits to the data. a, c, e are for Au nanoparticles and b, d, f are for Au-Ag bi-metallic assembly.

photoelectron spectra also show a shift in the binding energies for nitrogen when Ag nanoparticle is attached to 4-ATP capped Au nanoparticles. For example, a single N 1s peak for Au nanoparticles is obtained at 399.5 eV, which is shown in Figure 4.6.i(c).[31] However, after bi-metallic assembly formation, this peak is resolved into two, thoughthe

most significant contribution to the spectrum still comes from the peak at 399.7 eV. A low intensity peak at 401.2 eV appears due to the interaction of N with silver [Figure 4.6.i(d)]. This peak suggests the presence of N as charged species, indicating the ionic interaction with silver.[31b] This gives a strong evidence for the attachment of silver nanoparticle on gold nanoparticle surface via the Ag-N linkage. The synthesis of gold nanoparticles at high pH leaves the amino group free on the surface, since it can attach to the gold surface only at low pH.[26] Moreover, Au-S (~1.6 eV) bond is comparatively stronger than the Au-N bond (~0.6 eV), leading to the monolayer formation predominantly through the Au-S linkage providing free availibilty of amino group to further link with *in situ* generated silver nanoparticles.[40]
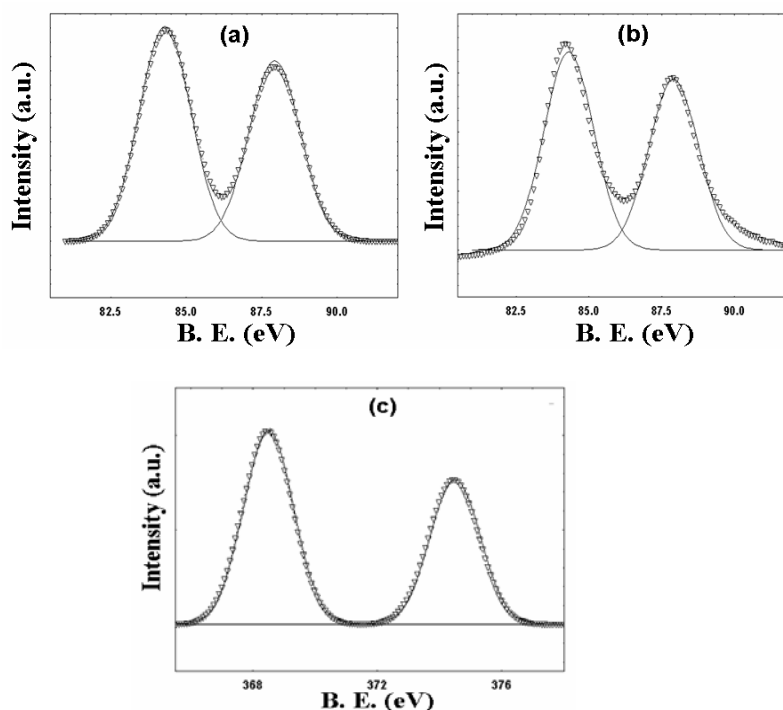
Figure 4.6 (ii): Core level XP spectra of Au 4f species present in Au nanoparticles (a) and Au-Ag bi-metallic assembly (b). (c) Ag 3d spectrum for Au-Ag bi-metallic assembly. The triangles represent the experimental data; the solid lines represent Gaussian fits to the data.

Figure 4.6.i(e) and 4.6.i(f) shows the C 1s region for samples Au-ATP and Au-ATP-Ag. A major peak is observed at 285 eV, which corresponds to the carbon atoms within the phenyl ring. There is a minor contribution from C-N carbon giving a peak at *ca.* 287

----

eV. Au 4f peaks show a slightly shifted value towards the higher binding energy. This shifting of binding energies compared to bulk gold implies a corresponding shift in the

Table 4.1: Binding Energy values for the atomic species present within Au-ATP and Au-ATP-Ag.

Species	Au-ATP	Au-ATP-Ag
	B. E (eV)	B. E. (eV)
N 1s	399.5	399.7, 401.2
C 1s	285.1, 287.4	285.1, 287.5
Au $4f_{7/2}$	84.3	84.3
$4f_{5/2}$	87.9	87.9
Ag $3d_{5/2}$	-	368.4
$3d_{3/2}$		374.4
S 2p	163.2	161.8, 163.2
Unbound/oxidized S 2p	165.9, 168.9	165.5, 168.5
O 1s		530, 533

Fermi level.[31] An elaborate explanation of the shifting of binding energies has been discussed in Chapter 3. Deconvoluted XP spectra in Figure 4.6.ii(a) and 4.6.ii(b) show the $4f_{7/2}$ peak at 84.3 eV and $4f_{5/2}$ peak at 87.9 eV respectively. Figure 4.6.ii(c) shows the XP spectra of Ag $3d_{5/2}$ and $3d_{3/2}$ for Au-ATP-Ag, indicating the presence of silver in its metallic state. However, it is worth mentioning that the binding energy shift between Ag(0) and Ag(I) state is too small to be used for differentiation between these two oxidation states.[37d, 41] Ag $3d_{5/2}$ and $3d_{3/2}$ bands occur at 368.4 and 374.4 eV, respectively, which correspond to Ag(0). These peak positions are again relatively higher in energies compared to the bulk metal (368 and 374 eV). This finding suggests that some of the surface atoms of the assembled nanoparticles carry partial positive charges. This is a result of the presence of partial Ag-CO_2^- bond on the nanoparticle surface leading to an increased positive charge on Ag.[25a] Oxygen 1s region shows two very weak peaks at ca. 533 and 530 eV, and are presumed to be from the oxygen of Ag-O-linkage and the adsorbed oxygen or atmospheric oxygen species respectively.[25b] A comparison of the XPS data is given in Table 4.1. From the table it is clear that benzoic

acid formed during the synthesis finally attaches to silver nanoparticle surface giving an ordered assembly. This is in excellent agreement with the UV-visible and TEM results suggesting the formation of more ordered assemblies from the reduction of silver benzoate.
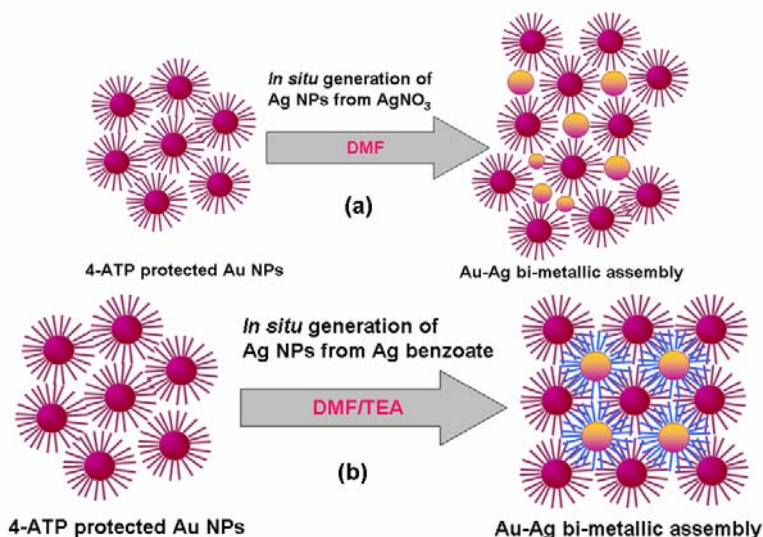
Scheme 4.2 Au-Ag hetero-assembly by *in situ* generation of Ag NPs from (a) Ag NO$_3$ and (b) Ag-benzoate

The above experimental results clearly suggests that at higher pH, the orientation of the 4-ATP is such that only thiol group is projected towards the interface (during synthesis of gold nanoparticles) and selectively chemisorbed on the gold nanoparticle surface. This orientation is the most favorable one at higher pH (as amines are weak base). This step is very crucial as 4-ATP shows pH dependent capping characteristic.[26] 4-ATP capped Au nanoparticles thus formed do not easily undergo cross-linking, however, they may undergo assembly formation due to hydrogen bonding in nonpolar solvents. To avoid further cross-linking, gold nanoparticles are dispersed in DMF. DMF is a better choice for two reasons: (a) the stability of Au nanoparticles is found to be higher in DMF compared to other solvents and (b) it acts as a reducing agent for silver nitrate.[29a] DMF also stabilizes Au nanoparticles possibly through dipolar interactions. This is in excellent agreement with the recent finding that polar solvents interact with surface of the gold nanoparticles through their nonbonding electrons.[29b] Therefore, the selection of solvent plays a very important role since solvents also stabilize these hybrid

assemblies.

Au-Ag hetero-assembly formation from both these methods is now clearly understood based on the above experimental results. The random assembly observed in the TEM image from $AgNO_3$ route is due to the formation of poly-dispersed particles which are mutually linked with 4-ATP capped Au NPs. There may also be some multilayers due to hydrogen bnding. However, for the Ag-benzoate route, silver nanoparticles are stabilized by benzoic acid to form uniformly sized particles which successively get linked with 4-ATP capped gold nanoparticles giving an ordered assembly. Both of these processes are schematically depicted in Scheme 4.2. illustrating the formation of random assembly during the *in situ* reduction of silver nitrate (a), while assembly from silver benzoate gives only ordered network structure in presence of 4-ATP protected gold nanoparticles.

In conclusion, the experimental results presented in this chapter clearly suggest Au-Ag bi-metallic assembly formation assisted by 4-aminothiophenol. The fact that at controlled pH gold nanoclusters can be functionalized with free amine group opens a new dimension to the hetero-metallic assembly formation through the controlled introduction of different metal nanoparticles. We have used silver nanoparticles as a case study to anchor on the gold surface via Ag-N linkage. UV-visible absorption studies confirm the Au-Ag bi-metallic assembly formation with an absorption maximum in the range 550-580 nm. TEM analysis further confirms the hetero-hetero-assembly formation, with more ordered assembly formation by the reduction of silver benzoate to that from silver nitrate. XPS studies suggest the existence of Au-S and Ag-N linkages, suggesting the bi-metallic assembly formation through the freely available amino group on the gold nanoparticle surface. The free availability of the amino group on the surface of gold nanoparticles is also important to anchor different multifunctional molecules such as bioactive macromolecules, redox moieties, and molecules of biomedical importance. Moreover, the formation of chemically linked superlattice structure is also possible with this technique by selectively anchoring pre-formed and well-defined monolayer protected nanoclusters. These hybrid nanostructures may be of increasing interest to diverse nanotechnology applications including the "bottoms-up" fabrication of nanoelectronic and photonic devices.

Ph. D. Thesis   *Chapter 4*   *University of Pune, May 2006*

4.4 References

1. Pileni, M. P. *Supramolecular Science* **1998**, *5*, 321.

2. (a) Maier, S. A.; Brongersma, M. L.; Kik, P. G.; Atwater, H. A. *Phys. Rev. B* **2002**, *65*, 193408. (b) Su, K. –H.; Wei, Q. –H.; Zang, X.; Mock, J. J.; Smith, D. R.; Schultz, S. Nano Lett. **2003**, *3*, 1087.

3. (a) Tucker, J. R., *J. Appl. Phys.* **1992**, 71, 4399. (b) Korotkov, A. N., Chen, R. H., Likharev, K., *J. Appl. Phys.* **1995**, *78*, 2520. (c) Maurer, S. M.; Patel, S. R.; Marcus, C. M.; Duruöz, C. I.; Harris, Jr. *Phys. Rev. Lett.* **1999**, *83*, 1403.

4. (a) Kottman, J. P.; Martin, O. J. F. *Opt. Lett.* **2001**, *26*, 1096. (b) Ung, T.; Liz-Marzan, L. M.; Mulvaney, P. *J. Phys. Chem. B* **2001**, *105*, 3441. (c) Collier, C. P.; Saykally, R. J.; Shiang, J. J.; Henrichs, S. E.; Heath, J. R. *Science* **1997**, *277*, 1978. (d) Henrichs, S.; Collier, C. P.; Saykally, R. J.; Shen, Y. R.; Heath, J. R. *J. Am. Chem. Soc.* **2000**, *122*, 4077.

5. (a) Welfing, W. P.; Murray, R. W. *J. Phys. Chem. B* **2002**, *106*, 3139. (b) Ratner, M. A.; Davis, B.; Kemp, M.; Mujica, V.; Roitberg, A.; Yaliraki, S. In *Molecular Electronics*; Avriam, A., Ratner, M. (Eds.), The New York Academy of Sciences: New York, 1998, 852, p 22.

6. Abeles, B.; Sheng, P.; Coutts, M. D.; Arie, Y. *Adv. Phys.* **1975**, *24*, 407.

7. Marcus, R. *Nobel Lectures "Electron Transfer Reactions in Chemistry: Theory and Experiment". Angewandte Chemie.* **1993**, *32(8)*, 1993.

8. (a) Wuelfing, W. P.; Green, S. J.; Pietron, J. J.; Cliffel, D. E.; Murray, R. W. *J. Am. Chem. Soc.* **2000**, *122*, 11465.

9. Wessels, J. M.; Nothofer, H-G., Ford, W. E.; Wrochem, F. v.; Scholz, F.; Vossmeyer, T.; Schroedter, A.; Weller, H.; Yasuda, A. *J. Am. Chem. Soc.* **2004**, *126*, 3349.

10. (a) Maier, S. A.; Kik, P. G.; Atwater, H. A. *Appl. Phys. Lett.* **2002**, *81*, 1714. (b) Ditlbacher, H. Krenn, J. R.; Lamprecht, B.; Leitner, A.; Aussenegg, F. R. *Opt. Lett.* **2000**, *25*, 563. (c) Xu, S.; Zhao, B.; Xu, W.; Fan, Y. *Colloids and Surfaces A: Eng. Aspects* **2005**, *257-258*, 313.

11. (a) Musick, M. D.; Keating, C. D.; Lyon, L. A.; Botsko, S. L.; Pena, D. J.; Holliway, D.; McEvoy, T. M.; Richardson, J. N.; Natan, M. J. *Chem. Mater.* **2000**, *12*, 2869. (b) Brust, M.; Kiely, C. J. *Colloids Surf. A* **2002**, *202*, 175. (c) Joseph, Y.; Besnard, I.;

....

Physical and Materials Chemistry Division, National Chemical Laboratory   165

Rosenberger, M.; Guse, B.; Nothofer, H. –G.; Wessels, J. M.; Wild, U.; Knop-Gericke, A.; Su, D.; Schlögl, R.; Yasuda, A.; Vossmeyer, T. *J. Phys. Chem.* **2003**, *107*, 7406.

12. (a) Underwood, S.; Mulvaney, P. *Langmuir* **1994**, *10*, 3427. (b) Mulvaney, P. *Langmuir* **1996**, *12*, 788. (c) Hövel, H.; Fritz, S.; Hilger, A. Ber. Bunsen-Ges. *Phys. Chem.* **1997**. *101*, 1593. (d) Persson, N. J. *Surf. Sci.* **1993**, *172*, 557.

13. Link, S.; Mohamed, M. B.; El-Sayed, M. A. *Int. Rev. Phys. Chem.* **2000**, *19*, 409.

14. Schmitt, J.; Mächtle, P.; Eck, D.; Möhwald, H.; Helm, C. A. *Langmuir* **1999**, *15*, 3526.

15. (a) Chen, S.; Kimura, K. *Chem. Lett.* **1999**, 233. (b) Westcott, S. L.; Oldenburg, S. J.; Lee, T. R.; Halas, N. J. *Chem. Phys. Lett.* **1999**, *300*, 651. (c) He, S. T.; Xie, S. S.; Yao, J. N.; Gao, H. J.; Pang, S. J. *Appl. Phys. Lett.* **2002**, *81*, 150. (d) Fullam, S.; Rensmo, H.; Rao, S. N.; Fitzmaurice, D. *Chem. Mater.* **2002**, *14*, 3643. (e) Han, L.; Luo, J.; Kariuki, N, N.; Maye, M. M.; Jones, V. W.; Zhong, C. *J. Am. Chem. Soc.* **2003**, *15*, 29.

16. (a) Anders, R. P.; Bielefeld, J. D.; Henderson, J. J.; Janes, D. B.; Kolagunta, V. R.; Kubiak, C. P.; Mahoney, W. J.; Oscifchin, R. G. *Science* **1996**, *273*, 1690. (b) Brust, M.; Bethell, D.; Schiffrin, D. J.; Kiely, C. J. *Adv. Mater.* **1995**, *7*, 795. (c) Brust, M.; Bethell, D.; Schiffrin, D. J. *Langmuir* **1998**, *14*, 5425.

17. Andres, R. P.; Bielefeld, J. D.; Henderson, J. I.; Janes, D. B.; Kolagunta, V. R.; Kubiak, C. P.; Mahoney, W. J.; Osifchin, R. G. *Science* **1996**, *273*, 1690.

18. (a) Wang, G.; Murray, R. W. *Nano Lett.* **2004**, *4*, 95. (b) Hicks, J. F.; Zamborini, F. P.; Osisek, A. J.; Murray, R. W. *J. Am. Chem. Soc.* **2001**, *123*, 7048.

19. (a) Maye, M. M.; Chun, S. C.; Han, L.; Rabinovich, D.; Zhong, C-J. *J. Am. Chem. Soc.* **2002**, *124*, 4958. (b) Kim, B.; Tripp, S. L.; Wei, A. *J. Am. Chem. Soc.* **2001**, *123*, 7955.

20. Pal, A.; Ghosh, S. K.; Esumi, K.; Pal, T. *Langmuir* **2004**, *20*, 575.

21. (a) Heath, J. R.; Knobler, C. M.; Leff, D. V. *J. Phys. Chem. B* **1997**, *101*, 189. (b) Murray, C. B.; Kagan, C. R.; Bawandi, M. G. *Science* **1995**, *270*, 1335.

22. (a) Stoyuk, A. L.; Shvalagin, V. V.; Kuchmii, S. Y. *J. Photochem. Photobiol. A: Chem.* **2005**, *173*, 185. (b). Rodriguez-Gonzalez, B.; Burrows, A.; Watanable, M.; Kiely, C. J.; Liz-Marzan, L. M. *J. Mater. Chem.* **2005**, *15*, 1759. (c) Sun, S. H.; Murray, C. B.; Weller, D.; Folks, L.; Moser, A. *Science* **2000**, *287*, 1989. (d) Chen, M.; Nikles, D. E.

....

Ph. D. Thesis   *Chapter 4*   *University of Pune, May 2006*

Nano Lett. **2002**, *2*, 211. (e) Roucoux, A.; Schulz, J.; Patin, H. *Chem. Rev.* **2002**, *102*, 3757. (f) Luo, J.; Maye, M. M.; Kariuki, N. N.; Wang, L.; Njoki, P.; Han, L.; Schadt, M.; Lin, Y.; Naslund, H. R.; Zhong, C. J. *Catal. Today* **2005**, *99*, 291. (g) Zhong, C. J.; Luo, J.; Maye, M. M.; Han, L.; Kariuki, N. N. *Nanostructured Gold and Alloy Electrocatalysts*. In *Nanotechnology in Catalysis*; Zhou, B.; Hermans, S.; Somorjai, G. A.; Eds.; Kluwer Academic/Plenum Publishers **2004**, Vol. 1., Chapter 11, pp 222. (h) Zhong, C. –J.; Maye, M. M. *Adv. Mater.* **2001**, *13*, 1507. (i) Pachón, L. D.; Thathagar, M. B.; Hartl, F.; Rothenberg, G. *Phys. Chem. Chem. Phys.* **2006**, *8*, 151.

23. Gu, H.; Yang, Z.; Gao, J.; Chang, C. K.; Xu, B. *J. Am. Chem. Soc.* **2005,** *127*, 34.

24. Sun, S. H.; Fullerton, E. E.; Weller, D.; Murray, C. B. *IEEE Trans. Magn.* **2001**, *37*, 1239.

25. (a) Kariuki, N. N.; Luo, J.; Hassan, S. A.; Lim, I. –Im, S.; Wang, L.; Zhong, C. J. *Chem. Mater.* **2006**, *18*, 123. (b) Gao, Y.; Jiang, P.; Liu, D. F.; Yuan, H. J.; Yan, X. Q.; Zhou, Z. P.; Wang, J. X.; Song, L.; Liu, L. F.; Zhou, W. Y.; Wang, G.; Wang, C. Y.; Xie, S. S.; Zhang, J. M.; Shen, D. Y. *J. Phys. Chem. B,* **2004**, *108*, 12877.

26. Zhu, T.; Fu, X.; Mu, T.; Wang, J.; Liu, Z. *Langmuir* **1999**, *15*, 5197.

27. Brust, M.; Walker, M.; Bethell, D.; Schiffrin, D. J.; Whyman, R. J. *Chem. Commun.* **1994**, 801.

28. (a) Srivastava, S.; Frankamp, B. L.; Rotello, V. M. *Chem. Mater.* **2005**, *17*, 487. (b) Chumanov, G.; Sokolov, K.; Cotton, T. M. *J. Phys. Chem.* **1996**, *100*, 5166. (c) Bouhelier, A.; Bachelot, R.; Im. J. S.; Wiederrecht, G. P.; Lerondel, G.; Kostcheev, S.; Royer, P. *J. Phys. Chem. B* **2005**, *109*, 3195. (d) Malynych, S.; Chumanov, G. *J. Am. Chem. Soc.* **2003**, *125*, 2896.

29. (a) Pastoriza-Santos, I.; Liz-Marza$^{/}$n, L. M. *Langmuir* **1999**, *15*, 948. (b) Thomas, K. G.; Zajicek, J.; Kamat, P. V. *Langmuir* **2002**, *18*, 3722.

30. (a) Chaki, N. K.; Sudrik, S. G.; Sonawane, H. R.; Vijayamohanan, K. *Chem. Commun.* **2002**, 76. (b) Nath, S.; Ghosh, S. K.; Praharaj, S.; Panigrahi, S.; Basu, S.; Pal, T. *New J. Chem.* **2005**, *29*, 1527. (c) N. K. Chaki, B. Kakade and K. Vijayamohanan, *Electrochem. Commun.* **2004,** *6*, 661.

31. (a) Johnson, S. R.; Evans, S. D.; Brydson, R. *Langmuir* **1998**, *14*, 6639. (b) Hooper, A. E.; Werho, D.; Hopson, T.; Palmer, O. *Surf. Interface Anal.* **2001,** *31*, 809. (c)

....

Physical and Materials Chemistry Division, National Chemical Laboratory   167

Büttner, M.; Kröger, H.; Gerhards, I.; Mathys, D.; Oelhafen, P. *Thin Solid Film* **2006**, *495*, 180.

32. (a) Fullam, S.; Rensmo, H.; Rao, S. N.; Fitzmaurice, D. *Chem. Mater.* **2002**, *14*, 3643. (b) Heath, J. R.; Knobler, C. M.; Leff, D. V. *J. Phys. Chem. B* **1997**, *101*, 189. (c) Hoevel, H.; Fritz, S.; Hilger, A.; Kreibig, U.; Vollmer, M. *Phys. Rev. B* **1993**, *48*, 18178. (d) Brust, M.; Bethell, D.; Kiely, C. J.; Schiffen, D. J. *Langmuir* **1998**, *14*, 5425. (e) Quinten, M.; Krebig, U. *Surf. Sci.* **1986**, *172*, 557. (f) Link, S.; El-Sayed, M. A. *J. Phys. Chem. B* **1999,** *103*, 4212.

33. Hutter, E.; Fendler, J. H. *Chem. Commun.* **2002**, 378.

34. (a) Mulvaney, P. *Langmuir* **1996**, *12*, 788. (b) Hodak, J. H.; Hanglein, A.; Hartland, G. V. *J. Phys. Chem. B* **2000**, *104*, 9954. (c) Hayat, M. A. *Collodal Gold. Academic Press, Inc. San Diego CA*, **1989,** 1**,** p. 23. (d) Mallik, K.; Mandal, M.; Pradhan, N.; Pal, T. *Nano Lett.* **2001**, *1*, 319.

35. Tao, Y. T.; Heitpas, G. D.; Allara, D. L. *J. Am. Chem. Soc.* **1996**, *118*, 67.

36. Kiely, C. J.; Fink, J.; Zheng, J. G.; Brust, M.; Bethell, D.; Schiffrin, D. J. *Adv. Mater.* **2000**, *12*, 640.

37. (a) Fenter, P.; Eberhardt, A.; Eisenberger, P. *Science* **1994**, *266*, 1216. (b) Zubragel, C.; Deuper, C.; Scheider, F.; Neumann, M.; Grunze, M.; Schertel, A.; Woll, C. *Chem. Phys. Lett.* **1995**, *238*, 308. (c) Kang, S. Y.; Kim, K. *Langmuir* **1998**, *14*, 226. (d) He, S.; J., Y.; Xie, S.; Pang, S.; Gao, H. *Chem. Phys. Lett.* **2001**, *343*, 28.

38. (a) Castner, D. G. *Langmuir* **1996**, *12*, 5083. (b) Mekhalif, Z.; Riga, J.; Pireaux, J. –J.; Delhalle, J. *Langmuir* **1997**, *13*, 2285.

39. Castner, D. G.; Hinds, K.; Grainger, D. W. *Langmuir* **1996**, *12*, 5083.

40. (a) Majumdar, C.; Briere, T. M.; Mizuseki, H.; kawazoe, Y. *J. Chem. Phys.* **2002**, *117*, 2819. (b) Ulman, A. Chem. Rev. **1996**, *96*, 1533. (c) Venkataraman, L.; Khare, J. E.; Tam, I. W.; Nuckolls, C.; Hybertsen, M. S.; Steigerwald, M. L. *Nano Lett.* **2006**, *6*, 458.

41. Bensebaa, F.; Ellis, T. H.; Kruus, E.; Voicu, R.; Zhou, Y. *Langmuir* **1998**, *14*, 6579.

Chapter 5

Hybrid Nanostructure Assembly: Controlled Organization of Gold Nanoparticles on Silver Nanowires[*]

The present chapter describes our attempts to form one-dimensional organization of gold nanoparticles on silver nanowire surfaces. More specifically, directional integration

The scheme shows the strategy adopted for the linear integration of gold nanoparticles on silver nanowires. Silver nanowires were initially functionalized with 3-aminobenzoic acid followed by the controlled attachment of gold nanoparticles.
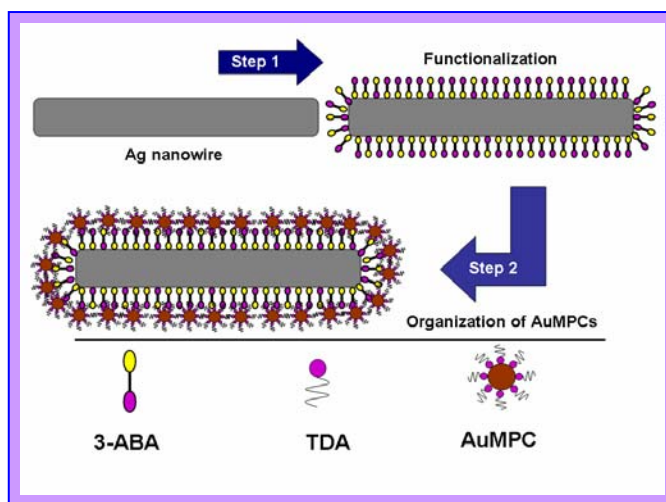
of tridecylamine protected gold (Au-TDA) nanoclusters (4-6 nm) on silver nanowires (Ag NWs, 60 nm) and their properties have been investigated using a variety of techniques including powder X-ray diffraction, Scanning and Transmission Electron Microscopy, X-ray Photoelectron Spectroscopy and four-probe electrical conductivity measurements to demonstrate significant changes in optical, and electrical properties. A new surface plasmon absorption peak is observed at 570 nm, while electrical measurement shows a transition from metallic to semiconductor behavior at 150 K.

5.1 Introduction

One dimensional nanostructures, such as nanowires, nanobelts, and nanoribbons constitute an ideal and interesting system to study the dependence of electrical, thermal, and mechanical properties on dimensionality and size confinement.[1] Consequently, these structures have generated tremendous research interest in recent times due to their unique applications in mesoscopic physics including the fabrication of nanoscale electronic, optoelectronic, electrochemical, and electromechanical devices as both interconnects and functional units.[2] For example, silver nanoparticles and nanowires (Ag NWs) have attracted considerable interest because bulk silver exhibits highest electrical and thermal conductivities and it is very important to see the size and aspect ratio dependence in contrast to the bulk analogues. Interestingly, the elastic modulus of smaller diameter (30 nm) silver nanowires is found to be higher than that of the larger ones (250 nm) as has been investigated by resonant contact atomic force microscopy (AFM) recently.[3] Similarly, they also have large scattering cross sections at specific wavelengths and show local electrical field enhancement due to resonant excitation of plasmons leading to a large enhancements of the local electromagnetic field at the nanoparticle surface with a positive effect on Raman scattering.[4]

Metallic nanostructure possess geometry-dependent localized plasmon resonances, which fascinates many researchers to synthesize and study rapidly expanding array of metallic nanoparticle geometries, such as nanorods, nanorings, nanocubes, and nanoshells.[5] For example, high aspect ratio nanostructures (nanorods, nanobelts, and nanowires) provide unique ability to control different properties by tuning their diameter and length. More specifically, the tunability of surface plasmon resonance (SPR) absorption is limited in case of spherical nanoparticles since its frequency is independent of the size as long as r « λ (where r is the radius and λ is the wavelength at SPR absorption), while the resonance frequency is very sensitive to the shape of the nanoparticles, covering whole visible and near-infrared range. Therefore, quasi-one-dimensional structures like nanowires are promising systems for optical and other studies as their properties can be easily tuned by varying the aspect ratio (R).[6] For example, the variation of the longitudinal plasmon resonance of gold nanorods from 2.4 to 0.6 eV has been demonstrated by increasing R from 1 (sphere) to 13 (nanorod).[6b] Another important way of tuning their properties is by formation of hetero-structured

assembly as has been recently demonstrated by thickness-controlled synthesis of silver coated coaxial gold nanorods with exceptional optical properties.[7]

This type of hetero-assembly provides a unique control over electrical and thermal carriers by modulating the connecting spacer molecule or doping level with consequent enhancement of their functionalities.[8] For instance, modulation of the composition or doping level enables the passivation of interfaces of various semiconductor heterostructures, which interestingly, generates devices with multiple functions.[9] Hierarchical structures with controllable interfaces by the formation of core–shell heterostructures in nanoscale building blocks have been increasingly exploited by many researchers for the assembly of several multifunctional electronic, sensor, and photonic devices with enhanced efficiency.[10] It is expected that more potential applications of these materials can be fully realized only by creating nanowires with controllable structural complexity, such as coaxial heterostructured nanowires and their superlattice assembly, radial heterostructured nanowires, and branched nanowires.[1c, 11] For example, Halas and co-workers have recently designed and fabricated a new hybrid nanorods that combines the intense local fields of nanorods and nanoshells in a single structure, with highly tunable plasmon resonances leading to the understanding of its plasmon resonances.[12a] This new resonance absorption arises from a hybridization of the primitive plasmons of a solid spheroid and an ellipsoidal cavity inside a continuous metal. Thomas et al. have demonstrated the longitudinal organization of gold nanorods by hydrogen bonding, which shows interesting optical properties.[12b] Consequently, considerable research effort is being expended world wide for creating such heterostructures, however, mainly for the semiconductor nanowires.[13] For example, randomly formed interfaces as kinks between metallic and semiconducting parts of CNTs and several other doping (pn) junctions have been more recently identified and investigated extensively.[11g, 14] Although different strategies have been adopted to organize metallic or semiconductor nanoparticles on carbon nanotubes for the pursuit of their applications with tailored properties, there is no such report available on the organization of nanoclusters on general nanowires, and Ag NWs in particular.[9e, 11c,d, 15] More significantly, these type of hetero nanostructures form a new class of hybrid materials with tunable electronic and optical properties similar to nanoparticle decorated

....

Physical and Materials Chemistry Division, National Chemical Laboratory   171

carbon nanotubes and silicone nanowires, except that the nature and length of the organic interconnecting molecule plays a critical role in deciding their properties.[16]

In this chapter, we report directional organization of tridecyl amine (TDA) protected gold nanoparticles (Au-TDA NPs) on Ag NWs using ligand exchange forming heteronanowires (for convenience, 'Au-Ag heteronanowires'). The strategy adopted for these nanostructures is the manipulation of the ligand exchange reactions with the introduction of bi-functional molecules as organic linkers, followed by the controlled introduction of preformed Au-TDA NPs, which can alternatively act as heterojunctions.[17] More significantly, each of the gold q-dots attached on the Ag nanowires can be further used for creating branched structures in pursuit of their applications in molecular electronics. Additional surface exchange reactions by appropriate linker molecules with controlled chain length can facilitate the creation of higher order hierarchical nanostructures.

5.2 Experimental Section

5.2.1 Materials: Hydrogen tetrachloroaurate(III) trihydrate (HAuCl$_4$.3H$_2$O, 99.9 %), lithium perchlorate (LiClO$_4$, 95 %), c (TDA), 3-aminobenzoic acid (3-ABA, 90%), hexachloroplatinic acid (H$_2$PtCl$_6$, 99.9%) and poly(N-vinyl pyrrolidone) (PVP, MW 55,000) were purchased from Aldrich Chemicals. All other reagent grade chemicals such as silver nitrate (AgNO$_3$, 99.9 %), dichloromethane (DCM, CH$_2$Cl$_2$), acetone [(CH$_3$)$_2$CO], and ethylene glycol (CH$_2$OHCH$_2$OH) were purchased from Merck, India and were used without further purification. Water used for these experiments was de-ionized with Milli-Q Reagent system (18 MΩ cm).

5.2.2 Synthesis of Au-TDA NPs, AgNWs and Au-Ag Heteronanowires: Au-TDA nanoparticles (4-6 nm) were synthesized by the modified Brust's synthesis procedure. Briefly, tridecylamine solution in toluene was mixed with aqueous auric chloride solution (1 mM, 50 mL each) in 250 mL round bottom flask under vigorous stirring for 30 min in a ice bath (273 K). Then, freshly prepared aqueous solution of NaBH$_4$ (0.1 M, 5 mL) was added to it dropwise so that the solution turned wine red immediately. Stirring was continued for another 1 h. The organic phase containing gold nanoparticles was separated from the aqueous phase with a separating funnel and procedure was

....

Physical and Materials Chemistry Division, National Chemical Laboratory   172

repeated for several times (10) to get a large amount of gold nanoparticles, which was then purified by size selective precipitation method on addition of excess ethanol. [18]

Similarly, Ag NWs were synthesized by the polyol method with a minor modification and the resultant product was washed several times to get pure AgNWs.[1d] Purified Ag NWs (*ca.* 0.03 g) were re-dispersed in 20 mL ethylene glycol and stirred in presence of 3-ABA (0.05 g) overnight at 80 ^{0}C followed by the repeated washing (with excess acetone, 7 times) and centrifugation at 3000 rpm. These Ag NWs were then mixed with the 'as synthesized' Au-TDA nanoclusters (*ca.* 0.01 g) in 30 mL dichloromethane and stirred for 24 h and again purified by washing with dichloromethane (Au-Ag heteronanowires readily settled in dichloromethane, while un-reacted Au-TDA nanoclusters were highly dispersible thus facilitating easy separation). This purification process was repeated several times until the dichloromethane fraction contained no gold nanoparticles beyond the detectable level in UV-visible spectrum. A large quantity of the sample was prepared by repeating the above procedure several times.

5.2.3 Characterization Techniques

Most of the characterization techniques used in the present chapter are similar to that described in chapter 2 and therefore, only new techniques used to characterize these hybrid materials are discussed in the present section.

5.2.3.1 STM/STS Measurements: One of the most widely used test samples for STM is highly oriented pyrolytic graphite (HOPG), which was used after cleaving off surface layers of graphite using good quality tape to create a fresh, atomically flat surface, with distinct cleavage steps. Later, they were cleaned with acetone and ultrasonically agitated in methanol bath to remove impurities and adhered particles, if any. The samples for STM analysis were prepared by putting a drop of nanoparticle solution on HOPG substrate and subsequently keeping it for 5 minutes for drying. STM studies were carried out immediately after the deposition, using tips made from 0.25 mm diameter polycrystalline Pt - Ir wire by mechanically cutting them at a specific angle.

A home-built STM based on fine mechanical-screw-lever arrangement assembly with a compact, four-quadrant, three-dimensional scanner was used for this investigation. Details of the system and the general procedure for imaging with the help of SPIP

....

Physical and Materials Chemistry Division, National Chemical Laboratory　　　　　　173

software are discussed elsewhere.[19] The STM imaging was carried out in air with optimum values of tunnel current (I = 0.5 nA) and bias voltage (V = 0.59 V) in constant current mode. I-V characteristics were always repeated several times and finally the signal was averaged over tens of runs.

5.2.3.2 AFM Measurements: The samples for AFM analysis were prepared by putting a drop of nanoparticle solution on HOPG substrate and keeping it for 5 minutes for drying. Non contact atomic force microscopy (NcAFM) experiment was carried out immediately (within 10 minutes) after the deposition using Si cantilevers (NSC12/W2C/5, Ultra sharp cantilevers by Micromasch) with a force constant of 0.30 N/m.

5.3 Results and Discussion

Transmission electron microscopy is a very useful technique to compare the morphology of nanowires before and after their surface functionalization especially by this ligand exchange. Accordingly, a typical low magnification TEM image of such a heterostructure is shown in Figure 5.1(a), which clearly depicts the extensive organization of gold nanoparticles on silver nanowire surface. This organization arises primarily due to the covalently attached monolayer of 3-ABA, presumably acting as a linker moiety between Au-TDA nanoparticles and Ag NWs. It is interesting to note that the reactivity of nanowires is relatively high at both the termini as higher abundance of gold nanoparticles can be seen at the ends as compared to that on the lateral side walls (see inset). This is in complete agreement with the earlier observation that PVP binds to the {100} face more strongly than to the {111} surface.[20] It appears that during washing, the PVP layer does not get completely removed from the side walls due to the strong interaction with the {100} surface, while both the ends are relatively PVP free. However, high magnification image of a part of the nanowire in Figure 5.1(b) shows a strong lateral organization of gold nanoparticles with a concomitant increase of the diameter of the nanowire, suggesting the formation of a new monolayer. An approximate increase of diameter by 8-10 nm is observed in the inset of Figure 5.1(b), which could be normally expected from 4-6 nm sized Au-TDA nanoparticles. Interestingly, only a single layer of Au-TDA NPs gets organized on the surface of Ag NWs suggesting the effectiveness of functionalization and the absence of excess 3-ABA after the purification process. It is particularly significant to note that silver nanowires withstand the stress generated during

the reaction at high temperature as the 1D morphology is mostly intact since no chopping or breaking is seen in these images. For comparison, TEM image of pure Ag NWs (diameter ca. 60 nm) is also given in Figure 5.1(c), where the image clearly shows the surface smoothness [sharp edges compared to the jagged edge of hetero nanowires in Figure 5.1(b)] and absence of any nanoparticles on its surface.
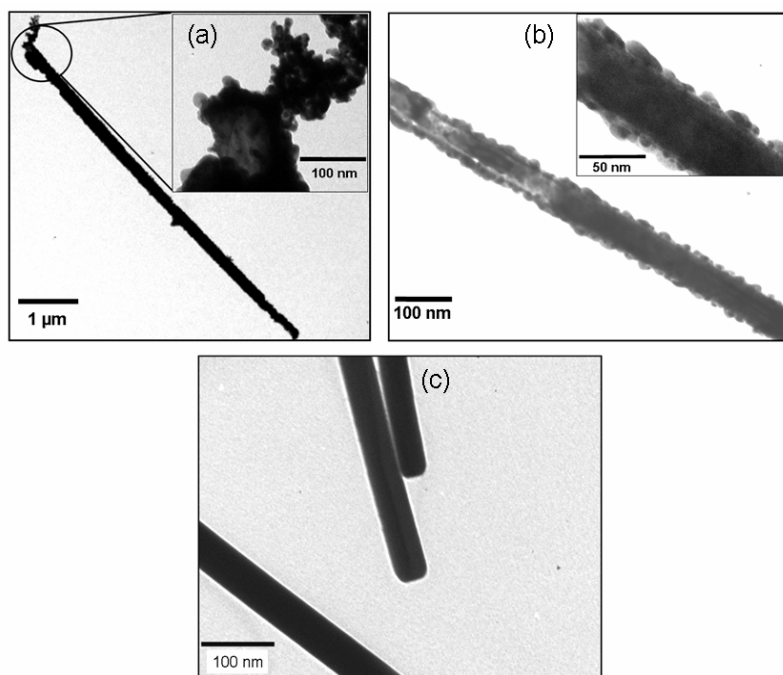
Figure 5.1 TEM images of as synthesized Au-Ag heteronanowires and pure Ag nanowires; (a) a typical low magnification TEM image of a Au-Ag hetero-nanowire along with the enlarged image (inset) of the tip, (b) high magnification TEM image of a part of the Au-Ag hetero-nanowire, while inset shows TEM image of the section of the hetero-nanowire to show the organization of Au nanoclusters, and (c) TEM image of pure Ag nanowires. Silver nanowires are synthesized by the polyol method followed by surface functionalization with 3-aminobenzoic acid.

Further, these Au-Ag heteronanowires were deposited on a highly oriented pyrolytic graphite (HOPG) substrate using drop coating (solution was made in acetone) technique and subsequently dried for 5 minutes for Non-contact AFM imaging. Accordingly, Figure 5.2(a) shows the NcAFM image of Au-TDA nanoclusters aligned along Ag NWs. A linear array of nanoparticles is evident from the AFM image. The line profile [shown in Figure 5.2(b)] along the Au-Ag heteronanowires gives an estimated diameter of around 80 nm. Further, for the same sample, STM/STS studies were carried out using Pt-Ir tip with

....

Physical and Materials Chemistry Division, National Chemical Laboratory   175

JSPM-5200 and accordingly, Figure 5.3(a) shows the constant current STM image of Au-Ag heteronanowires. Four linear arrays of nanoclusters aligned parallel to each other are clearly seen. Figure 5.3(b) shows the line profile across the length of nanowire including these four linear arrays which gives an approximate diameter of 70 nm. However, the diameter of the Au-Ag heteronanowires estimated from NcAFM is larger than that obtained from TEM/STM suggesting the dominance of tip convolution effects. The size of Au-TDA nanoclusters estimated from STM is around 5 nm which is comparable to the TEM data. The difference in numerical values of width of heteronanowires obtained from TEM and STM can be attributed to distribution in the width of nanowires, perhaps due to the aggregation of nanoclusters on particular portions or due to tip induced aggregations.
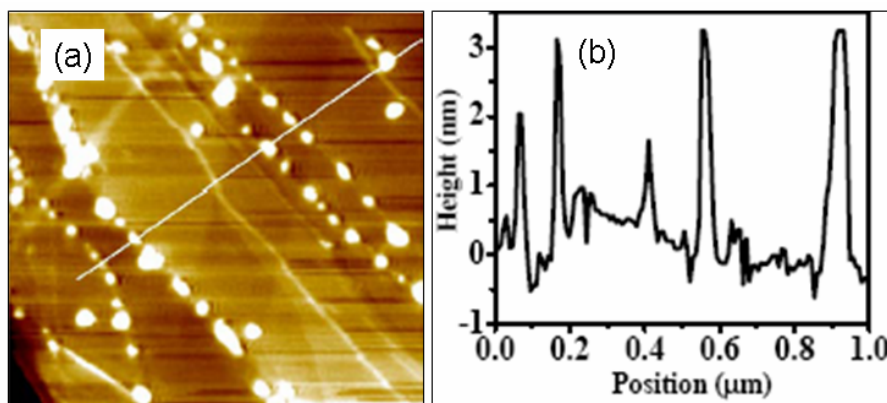
Figure 5.2 (a) Non-contact AFM image of gold nanoparticle decorated silver nanowires. Scan area: 1000 x 1000 nm. (b) Line profile of nanoparticles and nanowires marked by a line in (a).

Scanning electron microscopy images in Figures 5.4(a) and 5.4(b) reveal the change in morphology of Ag NWs after the surface modification. Importantly, SEM image of as synthesized Ag NWs clearly show the uniform distribution of silver nanowires with length ranging from 1 to several μm. Similarly, the SEM image of Au-Ag heteronanowires indicates that the structural integrity of nanowires is largely intact during the modification [Figure 5.4(b)]. The only difference observed is the aggregated structures after the modification due to the presence of bi-functional linker molecules on the surface, which obviously enhances the branching capability. Thus, the observation of a certain extent of

....

Physical and Materials Chemistry Division, National Chemical Laboratory   176
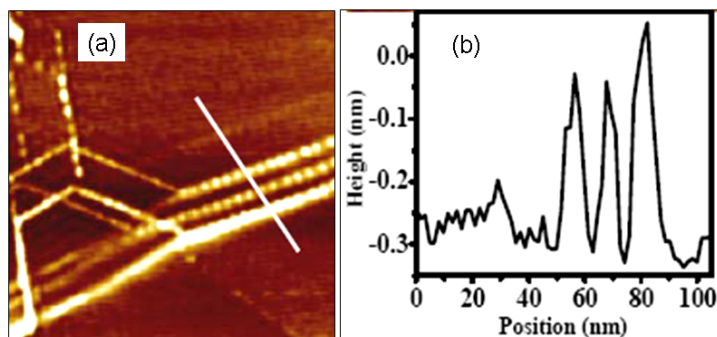
Figure 5.3 (a) Constant current STM image of gold nanoparticle decorated Ag nanowires, scan area: 192 x 192 nm, I = 0.50 nA, V = 0.59 V (b) Line profile across the nanowire marked by a line in (a).

assembly formation among nanowires is justified. The elemental analysis of Au-Ag heteronanowires by EDAX during the SEM measurements provides important information of the organization process. Within the nanowire regions, strong signals from silver and carbon can be seen along with a significant gold signal originating from the Au-TDA NPs, while signals from the Al substrates of sample holder are also found [Figure 5.4(c)]. This substantiates the presence of gold nanoparticles on the surface of silver nanowires.
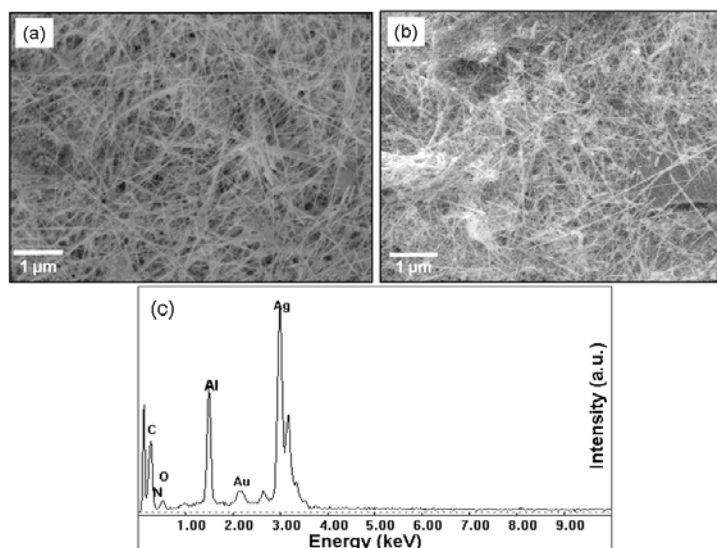
Figure 5.4 SEM images of (a) pure Ag nanowires, (b) Au-Ag heteronanowires and (c) EDAX spectrum of Au-Ag heteronanowires. Samples were prepared by drop casting respective solutions (in acetonitrile) on aluminum sample holders.

....

Physical and Materials Chemistry Division, National Chemical Laboratory   177

The strong evidence for the presence of different elemental species and their interaction with gold and silver has been further achieved from the results of X-ray photoemission studies. Figure 5.5 shows the XP spectra of different species present within the Au-Ag heteronanowires. First, the XP spectrum of gold shows peaks at 83.7 ($4f_{7/2}$) and 87.4 ($4f_{5/2}$) eV respectively, with a peak to peak separation of 3.7 eV confirming the presence of Au (0) in these nanostructures [Figure 5.5(a)]. Interestingly, no shift in B. E. values compared to that of bulk gold is observed, contrary to an earlier
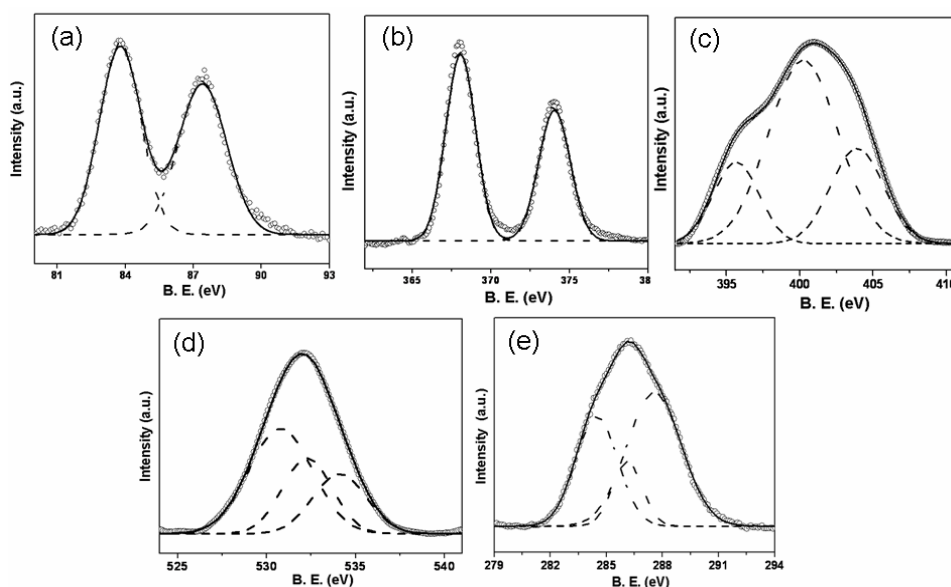
Figure 5.5 Core level XP spectra of (a) Au 4f, (b) Ag 3d, (c) N 1s, (d) O 2p, and (e) C 1s species present in Au-Ag heteronanowires. The circles represent the experimental data while the solid lines represent Gaussian fits to the data.

report of a size dependent positive shift in the 4f core-level for gold nanoparticles. [21] Themaximum shift of 0.41 eV has been reported for smallest particle (~ 1nm) without any significant line width broadening, suggesting that these changes can affect the whole particle and not only the particle surface, where the actual Au-S or Au-N bond is localized. One possible reason for the discrepancy is that the particle size of present study is comparatively larger than that of the reported particle size, where positive shift in binding energy has been observed. Similarly, XP spectrum of Ag shows peaks at 368.1 and 374 eV corresponding to $3d_{5/2}$ and $3d_{3/2}$ respectively confirming the presence of metallic silver [Figure 5.5(b)]. Interestingly, XP spectrum for N 1s region shows peaks corresponding to charged amino and neutral amino groups, as has been reported for

----

other similar gold-amine interactions.[22] The peaks at ca. 396.2 and 399.9 eV are ascribed to pyridinic N and neutral amino group respectively, while the peaks at ca. 402.7 eV could be assigned to the charged amino species [Figure 5.5(c)]. Similarly, O1s gives peaks corresponding to binding energies of >C=O and >C−O− species at ca. 532.4 and 530 eV respectively [Figure 5.5(d)], while C 1s region shows three peaks at 284.3, 286.7, and 287.7 eV [Figure 5.5(e)].[23] One of the major conclusions drawn from the XPS studies is the electrostatic interactions of amino group with nanoparticles indirectly suggesting that the carboxyl group is linked by covalent interactions to the Ag surface.

XRD is used to investigate the crystal structure of the Au-Ag heteronanowires, although, the precise identification of structural differences is quite difficult due to the identical crystal structures (face centered cubic with similar lattice constants, Au: 4.0786 A⁰, Ag: 4.0862 A⁰ respectively) of both gold and silver. Nevertheless, the elucidation of crystal growth and its structure is qualitatively derived from the X-ray diffraction data. Accordingly, Figure 5.6 shows a comparison of X-ray diffraction patterns of pure Au-TDA nanoparticles (a), Ag NWs (b), and Au-Ag heteronanowires (c) for all these samples drop-casted on glass slides. The high intensity (111) peak of pure Ag NWs clearly suggests the existence of 1D structure as is the case for similar other structures, while
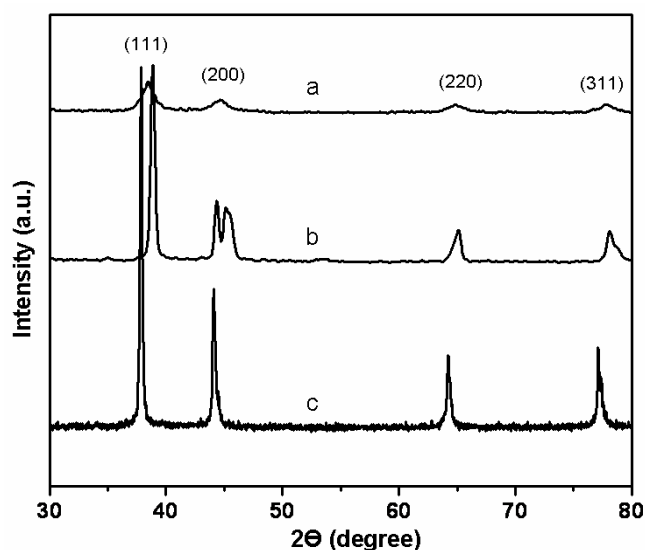
Figure 5.6 XRD patterns of (a) pure tridecylamine protected Au nanoparticles, (b) pure Ag nanowires, and (c) Au-Ag heteronanowires. Corresponding crystal planes are also indicated. Samples were drop casted from respective solutions in acetone on glass slides for XRD measurements.

....

Physical and Materials Chemistry Division, National Chemical Laboratory   179

intensities of all other peaks are insignificant. More significantly, the splitting of the (200) peak suggests the deformation of the five-twined structures (commonly observed for Ag NWs). This is in clear agreement with X-ray diffraction pattern reported for the Ag NWs earlier.[23] In contrast, XRD of Au-Ag heteronanowires shows certain distinct differences from that of pure silver nanowires. For example, Figure 5.6(b) shows the X-ray diffraction for Au-Ag heteronanowires. One of the major differences is the increase of diffraction intensities for (200), (220) and (311) crystal planes along with a minor shift (towards the lower value) of 2θ values for the (111) peak. The splitting of the (200) peak disappears, perhaps due to the high coverage by Au-TDA NPs on Ag NWs which is in excellent agreement with the conclusion drawn from TEM analysis. The change in the crystal patterns and existence of a minor shift (0.8 degree) together suggests the presence of polycrystalline Au-TDA NPs on the surface of Ag NWs.
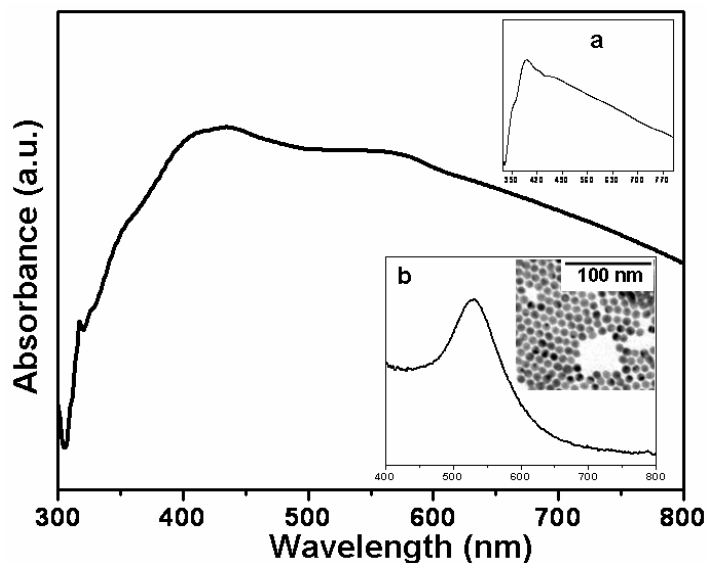
Figure 5.8 UV-visible spectrum of Au-Ag heteronanowires from a dispersion in acetonitrile; inset a represents the spectrum for pure Ag nanowires, while inset b is for Au-TDA nanoclusters in the same solvent. TEM image of Au-TDA nanoclusters is also given along with spectrum in inset b.

The UV-visible absorption spectrum of Au-Ag heteronanowires is given in Figure 5.8, which shows many interesting surface plasmon features distinctly different from that of pure Ag NWs. As a result, an additional absorption shoulder appears at *ca.* 570 nm apart from the well known characteristic longitudinal and transverse absorptions at 380-

430 nm for silver nanowires. For comparison, inset 'a' of Figure 5.8 shows the absorption spectrum for pure Ag NWs with characteristic peaks at 352, 390, and 424 nm. The absorption at 390 nm is a typical optical signature of Ag NWs. The surface plasmon absorption corresponding to the longitudinal band of Ag NWs is not observed as aspect ratio exceeds 5, while the characteristic bulk silver absorption occurs as a shoulder at 350 nm and these results are in complete agreement with the optical properties of silver nanowires reported earlier.[24] Interestingly, the characteristic absorption peak of Ag NWs is red shifted to *ca.* 430 nm and more significantly, a new shoulder appears at *ca.* 570 nm for Au-Ag heteronanowires. The intercrystal resonance absorption of cross-linked Au NPs also shows absorption maxima in this region. However, this is a rare possibility as special care has been taken to remove excess of 3-ABA and hence formation of aggregates can be neglected since both TEM and SEM images also do not show such aggregates, while parent Au-TDA NP solution shows
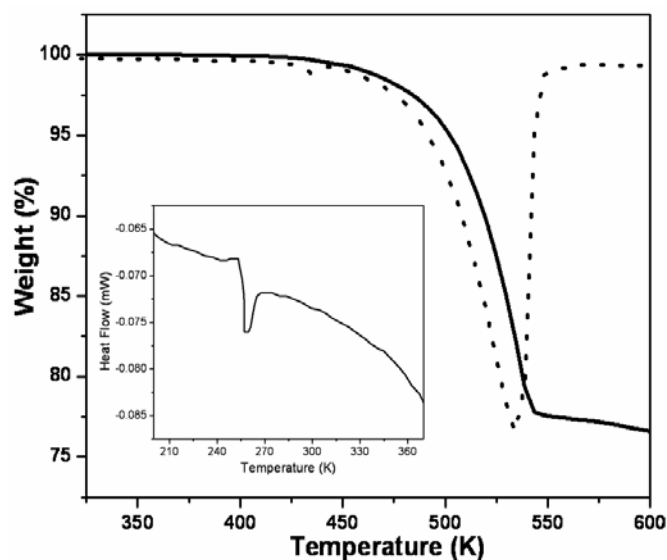
Figure 5.9 Thermogravimetric   data for Au-Ag heteronanowires in nitrogen environment along with the derivative plot (dotted line); the inset shows differential scanning calorimetry profile for Au-Ag hetero-nanowires in the temperature range 200 to 370 K under constant N_2 flow at a heating rate of 10 K/min.

surface plasmon absorption peak only at *ca.* 520 nm. For the ease of comparison, the UV-visible spectrum of Au-TDA NPs in the same solvent is also given as inset 'b' in Figure 5.8 along with its TEM image. The red shifted optical signature of silver nanowires after the modification clearly suggests the formation of hetero-structures.

Therefore, the peak at 570 nm can be assigned to the intercrystal oscillations of Ag NWs with Au-TDA NPs. Recently, Keating and co-workers have studied the optical properties of linear Au and Ag nanoparticle chains with controllable aspect ratio and found a similar red shifted surface plasmon absorption at 600 nm corresponding to the intercrystal coupling between gold and silver.[25] Interestingly, the UV- visible spectrum of present Au-Ag heteronanowires does not show any absorption in this region. The minor difference observed is apparently originated from the structural differences with that of the Au and Ag chains and the Au-Ag heteronanowires. Additionally, this approach of obtaining Au-Ag heteronanowires is conceptually different from the nanometer sized linear chain structures of Ag and Au synthesized by templated alternate electro-deposition in the pores of alumina membrane.[25] Thermal analysis of Au-Ag heteronanowires shows the initial onset of a minor mass loss at 435 K signifying the loss of tridecylamine monolayer of the Au-TDA NPs. The degradation process completes with the major and final mass loss at 535 K as shown in Figure 5.9. This mass loss accounts for the degradation of 3-ABA layer on the silver nanowires. More significantly, the total mass loss is nearly 20% as calculated from this thermal profile compared to only a marginal (2%) mass loss for pure silver nanowires in this temperature range. The weight loss due to PVP layer of pure silver nanowires has been observed at *ca*. 873 K.[23]   DSC studies (inset of Figure 5.9) show an endothermic peak at around 255 K during heating and interestingly this peak is reversible on repeated cycling although a minor shift in peak position occurs. The corresponding enthalpy value calculated from the area under the peak is very small (0.03 J/g) compared to that normally observed for the phase transition of pure alkyl chains, since only a minor fraction of hydrocarbon chains is involved in the present structural changes.[26]   Also, alkyl thiol protected nanoparticles undergo phase transitions due to melting/crystallization of alkyl chains at relatively higher temperatures, in general, implying that the observed transition is due to the ordering of nanoparticles on the nanowire surface with a direct relationship with the electrical conductivity of Au-Ag heteronanowires.

The variation of electrical conductivity (4-probe) of Au-Ag heteronanowires with temperature is represented in Figure 5.10. Accordingly, Figure 5.10(a) shows an interesting variation of dc conductivity with temperature for Au-Ag heteronanowires, where these hybrid structures exhibit a clear transition of electron transport behavior at

----

150 K. Initially, conductivity decreases with increasing temperature up to 150 K, followed by a sudden increase. In the temperature range of 150-280 K, Au-Ag heteronanowires exhibit electrical behavior similar to that of a pure semiconductor. However, after transition point at 150 K, conductivity increases with a decrease in temperature
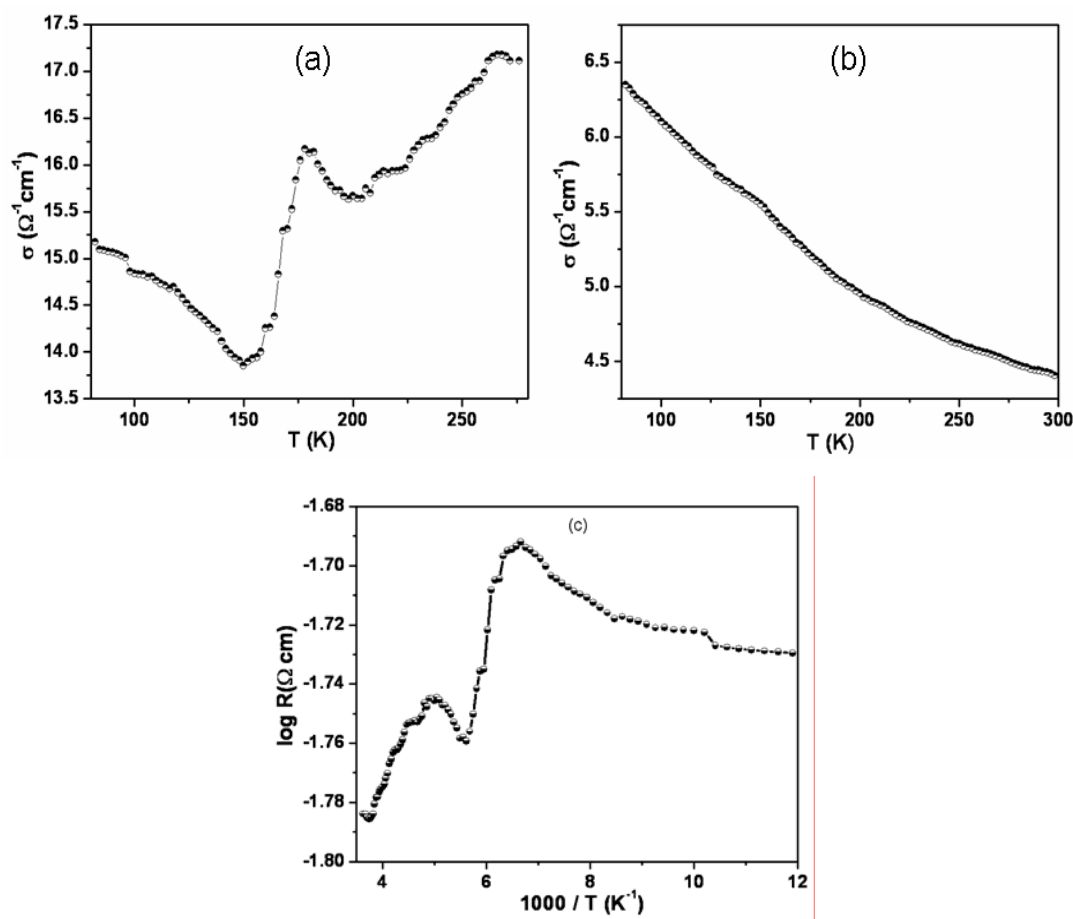
Figure 5.10 Variation of conductivity vs. temperature for (a) Au-Ag heteronanowires and for (b) pure silver nanowires; these measurements were carried out by keeping the probe distance constant at 3 mm and contact was provided by standard silver paint. (c) Logarithm of resistance vs. 1000/T plot for Au-Ag heteronanowires.

exhibiting the PTC (positive temperature coefficient) behavior of a pure metal. The reason for the appearance of a minor transition point at around 200 K is presently not clear although we believe that the organic interlinking molecules with aromatic rings are responsible for this. The variation of logarithm of resistance with temperature is also shown in Figure 5.10(c). Interestingly, a direct correlation of the onset of this transition in electrical conductivity with phase changes revealed by the DSC results is observed,

....

----

despite with a distinct temperature variation. A sudden increase in conductance and phase changes in the DSC could be ascribed to a favorable orientation of capping organic molecules. A plausible explanation considers the ordering of disordered Au-TDA nanoclusters (at transition points) by re-organization of organic molecules, which
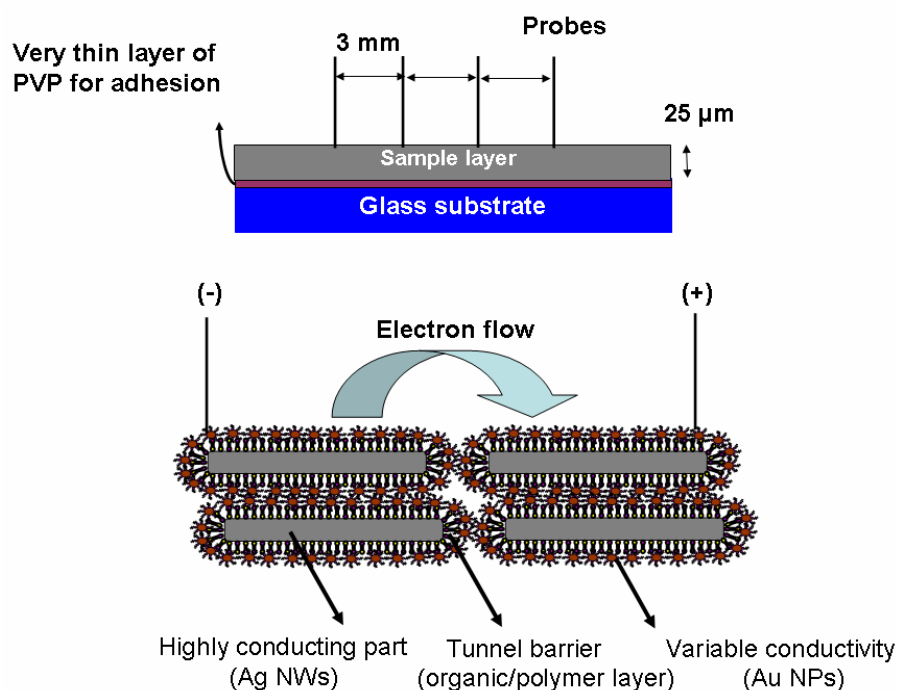
Scheme 5.1: Schematic representation of the 4-probe conductivity measurement and associated electron transfer processes involving highly conducting part, tunnel barriers, and variable conductivity regions.

facilitates the electron transfer at low temperature leading to a sudden increase in conductivity. In sharp contrast, similar measurements carried out for silver nanowires (surface modification with 3-ABA) exhibit pure metallic behavior [Figure 5.10(b)], indicating the involvement of complex electron transfer dynamics from nanoparticles to nanowires. More intricate mechanism of electronic transport has to be invoked to explain such changes as these Au-Ag heteronanowires consist of highly conducting part (Ag NWs), tunnel barriers (organic/polymer layer) and variable conducting zone (Au NPs) as indicated in Scheme 5.1.

It is instructive to compare present result with the electrical conductivity of a single silver nanowire along the longitudinal axis measured at room temperature using the

....

Physical and Materials Chemistry Division, National Chemical Laboratory   184

four-probe method ($\sim$ 0.8 x 10^5 Scm^{-1})[24a] although, the present experimental data represent an ensemble of nanowires with much lower conductivity values. Therefore, a study of electron tunneling transport across the decorated nanowires is important in the context of understanding overall electron transport properties of these heterostructures. Accordingly, tunneling spectroscopy (I-V) measurements were carried out in STM after locating the Au-TDA nanoclusters aligned on Ag NWs and also on a bare Ag NW by positioning the tip above a nanoparticle and a nanowire respectively. Figure 5.11 shows the comparison of I-V measurements on bare Ag NW, isolated Au-TDA nanocluster and Au-Ag heteronanowires along with the line profile along the aligned Au MPCs on silver nanowire [Figure 5.3(a)]. Comparative I-V behavior shows that electron transport across the bare Ag NW is entirely different to that of Au-Ag heteronanowires. A linear I-V curve for the bare Ag NW suggests metallic behavior, although a high tunnel resistance (0.15 GΩ) indicates the presence of an insulating layer on the surface, while Au-Ag
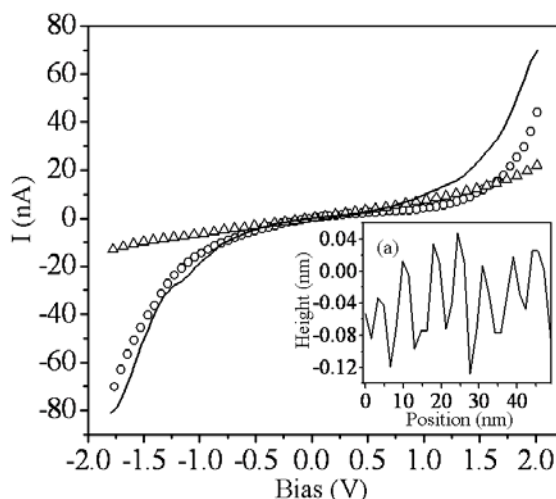
Figure 5.11: I-V characteristics taken on bare AgNW (marked by 'Δ') and Au-Ag hetronanowire (marked by dark solid line). Inset (a) shows the line profile along the aligned AuMPCs on silver nanowire in Figure 5.3a.

heteronanowire gives a tunnel resistance of 0.013-0.015 GΩ. Thus, an approximate order of magnitude variation of tunnel resistance is indicative of a change in electron transport mechanism due to the integration of Au-TDA nanoclusters. Also, the I-V behavior for Au-Ag heteronanowires is very similar to that of Au-TDA nanoclusters indicating that the tunneling electron transport across Au-Ag heteronanowires is mostly

governed by the features of Au-TDA nanoclusters, like the size of the Au core, length of TDA chains, distance between Ag wire edges to the Au cluster edge etc. The non-linear I-V for Au-Ag heteronanowire with large current suppression region near zero bias suggests more complex mechanism for carrier transport in these hybrid materials. Along the length of the nanowires electron transport will be ballistic or diffusive depending on whether the mean free path is considerably larger than or smaller than diameter.
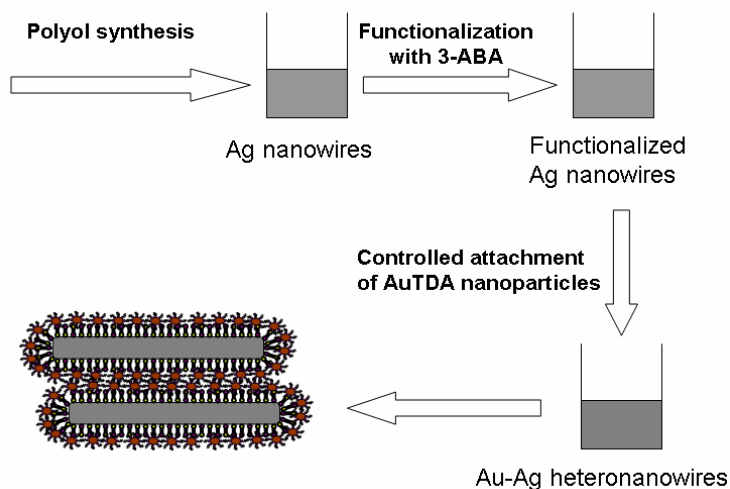
Scheme 5.2 Different steps speculated during the formation of Au-Ag hetero-assembly. Silver nanowires were initially surface functionalized with 3-aminobenzoic acid, and was subsequently treated with tridecyl amine protected gold nanoparticles to form Au-Ag heteronanowires.

Across the nanowires it will be governed by double barrier tunnel junction (DBTJ) formed between AgNWs by the presence of Au-TDA nanoclusters. The carrier transport in such DBTJ will depend on size of nanoclusters, HOMO-LUMO gap of capping agent and the spacing between nanowires and nanoclusters. Earlier, the fabrication of hyperbranched nanowires and electrodes with controllable gap between Au and Ag nanowires has been demonstrated using lithographic techniques.[4f, 6a] However, the present work is considerably different to above organization processes as the interconnecting organic molecule offers unique opportunity to modulate the barrier properties. The gold nanocluster size as well as the cluster to silver nanowire spacing can be tuned to suit the applications although this ideal situation may be different from the actual directed assembly due to the possibility of orientational changes induced by the electrical field.

On the basis of experimental results, we speculate a mechanism of formation of these heteronanowires in several steps. Scheme 5.2 shows the sequences involved in the Au-Ag heteronanowire formation by different chemical steps. Briefly, as synthesized silver nanowires are surface functionalized with 3-aminobenzoic acid to form surface functionalized silver nanowires. In the succeeding steps, tridecylamine protected gold nanoparticles are introduced to form heteronanowires, which are linked to nanowire surface by covalent bonding through organic layer.

5.4 Conclusions

In conclusion, the effective organization of gold nanoparticles on silver nanowire surfaces is demonstrated using various techniques such as TEM, SEM, XRD, XPS, and UV-visible spectroscopy. These hybrid materials exhibit exceptional optical and electrical properties as illustrated by a characteristic surface plasmon absorption peak (570 nm) and a remarkable conductivity change with temperature at 150 and 180 K respectively. Although, this hybrid material displays an exciting combination of semiconductor and metallic behavior from resistivity measurements and phase changes from differential scanning calorimetric results, several other factors such as reorganization of capping molecules, possibility of tunneling pathways, orientation dependent interdigitation of hydrocarbon chains, and variable cluster–cluster spacing and variations in silver nanowire surface coverage will need to be further investigated before their applications as electronic or photonic components. If the outcome of such studies are successful, this type of heteronanowires would be important components in molecular electronics, where each nanoparticle acts as branching point attached through organic linker molecules.

....

Physical and Materials Chemistry Division, National Chemical Laboratory   187

Ph. D. Thesis   *Chapter 5*   *University of Pune, May 2006*

5.5 References

1. (a) Ciraci, S.; Buldum, A.; Batra, I. P. *J. Phys.: Condens Matter.* **2001**, *13*, R537. (b) Wang, Z. L. *Annu. Rev. Phys. Chem.* **2004**, *55*, 159. (c) Law, M.; Goldberger, J.; Yang, P. *Annu. Rev. Mater. Res.* **2004**, *34*, 83. (d) Sun, Y.; Xia, Y. *Adv. Mater.* **2002**, *14*, 833.

2. (a) Husain, A.; Hone, J.; Postma, H. W. Ch.; Huang, X. M. H.; Drake, T.; Barbic, M.; Scherer, A.; Roukes, M. L. *Appl. Phys. Lett.* **2003**, *83*, 1240. (b) Mc Alpine, M. C.; Friedman, R. S.; Jin, S.; Lin, K. –h.; Wang, W. U.; Lieber, C. M. *Nano Lett.* **2003,** *3*, 1531. (c) Kovtyukhova, N. I.; Mallouk, T. E. *Chemistry - A European Journal* **2002**, *8*, 4354. (d) Friedman, R. S.; McAlpine, M. C.; Ricketts, D. S.; Ham, D.; Lieber, C. M. *Nature* **2005**, *434*, 1085. (e) Patolsky, F.; Lieber, C. M. *Materials Today* **2005**, *8*, 20. (f) Huang, Y.; Duan, X.; Wei, Q.; Lieber, C. M. *Science* **2001**, *291*, 630.

3. Cuenot, S.; Frétigny, C.; Demoustier-Champagne, S.; Nysten, B. *Phys. Rev. B* **2004**, *69*, 165410.

4. (a) Nie, S.; Emory, S. R. *Science* **1997**, *275*, 1102. (b) Xu, H. X.; Bjerneld, E. J.; Kall, M.; Borjesson, L. *Phys. Rev. Lett.* **1999**, *83*, 4357. (c) Jackson, J. B.; Halas, N. J. *Proce. Natl. Acad. Sci. U.S.A.* **2004**, *101*, 17930. (d) Lu, Y.; Liu, G. L.; Lee, L. P. *Nano. Lett.* **2005**, *5*, 5. (e) Scultz, S.; Smith, D. R.; Mock, J. J.; Schultz, D. A. *Proc. Natl. Aca. Sci. USA.* **2000**, *97*, 996. (f) Silva, T. J.; Scultz, S.; Weller, D. *Appl. Phys. Lett.* **1994**, *65*, 658.

5. (a) Link, S.; El-Sayed, M. A. *J. Phys. Chem. B* **1999**, *103*, 8410. (b) Murphy, C. J.; Sau, T. K.; Gole, A.; Orendorff, C. J. *MRS Bull.* **2005**, *30*, 349. (c) Aizpurua, J.; Hanarp, P.; Sutherland, D. S.; Kall, M.; Bryant, G. W.; de Abajo, F. J. G. *Phys. Rev. Lett.* **2003**, *90*, 057401. (d) Sun, Y. G.; Xia, Y. *Science* **2002**, *298*, 2176. (e) Oldenburg, S. J.; Averitt, R. D.; Westcott, S. L.; Halas, N. J. *Chem. Phys. Lett.* **1998**, *288*, 243.

6. (a) Link, S.; El-Sayed, M. A. *Annu. Rev. Phys. Chem.* **2003**, *54*, 331. (b) Liu, M. Z.; Guyot-Sionnest, P. J. Phys. Chem. B **2004**, *108*, 5882.

7. Ah, C. S.; Hong, S. D.; Jang, D-J. *J. Phys. Chem. B* **2001**, *105*, 7871.

....

Physical and Materials Chemistry Division, National Chemical Laboratory   188

----

8.   (a) Mukdadi, O. M.; Datta, S. K.; Dunn, M. L. *J. Appl. Phys.* **2005**, *97*, 074313. (b) Agraït, N.; Untiedt, C.; Rubio-Bollinger, G.; Vieira, S. *Chem. Phys.* **2002**, *281*, 231.

9.   (a) Whang, D.; Jin, S.; Wu, Y.; Lieber, C. M. *Nano Lett.* **2003**, *3*, 1255. (b) Huang, X.; Li, J.; Zhang, Y.; Mascarenhas, A. *J. Am. Chem. Soc.* **2003**, *125*, 7049. (c) Tanaka, M.; Shimizu, H.; Miyamura, M. *J. Cryst. Growth* **2001**, *227*, 839. (d) Hornyak, G.; Kröll, M.; Pugin, R.; Sawitowski, T.; Schmid, G.; Bovin, J.-O.; Karsson, G.; Hopfe, S. *Chemistry - A European Journal* **1997**, *3*, 1951. (e) Odom, T. W.; Huang, J-L.; Cheung, C. L.; Lieber, C. M. *Science* **2000**, *290*, 1549.

10.   (a) Lieber, C. M. *The incredible shrinking circuit. Sci. Am.* **2001**, *285*, 58. (b) Cui, Y.; Lieber, C. M. *Science* **2001**, *291*, 851. (c) Duan, X.; Huang, Y.; Cui, Y.; Wang, J.; Lieber, C. M. *Nature* **2001**, *409*, 66. (d) Cui, Y. ; Wei, Q. ; Park, H. ; Lieber, C. M. *Science* **2001**, *293*, 1289. (e) Huang, Y. ; Duan, X. ; Cui, Y. ; Lauhon, L. J. ; Kim, K-H. ; Lieber, C. M. *Science* **2001**, *294*, 1313. (f) Nirmal, M. ; Brus, L. *Acc. Chem. Res.* **1999**, *32*, 407. (g) Bruchez, M.; Moronne, M. Jr. ; Gin, P. ; Weiss, S. ; Alivisatos, A. P. *Science* **1998**, *281*, 2013. (h) Chan, W. C. W. ; Nie, S. *Science* **1998**, *281*, 2016. (i) Klimov, V. I. ; Mikhailovsky, A. A. ; Xu, S. ; Malko, A. ; Hollingsworth, J. A. ; Leatherdale, C. A. ; Eisler, H.-J. ; Bawendi, M. G. *Science* **2000**, *290*, 314.

11.   (a) Gudiksen, M. S.; Lauhon, L. J.; Wang, J.; Smith, D. C.; Lieber, C. M. *Nature* **2002**, *415*, 617. (b) Solanki, R.; Huo, J.; Freeouf, J. L.; Miner, B. *Appl. Phys. Lett.* **2002**, *81*, 3864. (c) Hu, J. T.; Min, O.; Yang, P.; Lieber, C. M. *Nature* **1999**, *399*, 48. (d) Zhang, Y.; Ichihashi, T.; Landree, E.; Nihey, F.; Iijima, S. *Science* **1999**, *285*, 1719. (e) Wu, Y. ; Fan, R. ; Yang, P. *Nano Lett.* **2002**, *2*, 83. (f) Bjork, M. T. ; Ohlsson, B. J. ; Sass, T. ; Persson, A. I. ; Thelander, C. ; Magnusson, M. H. ; Deppert, K.; Wallenberg, L. R. ; Samuelson, L. *Nano Lett.* **2002**, *2*, 87. (g) Lauhon, L. J.; Gudiksen, M. S.; Wang, D.; Lieber, C. M. *Nature* **2002**, *420*, 57. (h) Dick, K. A.; Deppert, K.; Larsson, M. W.; Martensson, T.; Seifert, W.; Wallenberg, L. R.; Samuelson, L. *Nature Mater.* **2004**, *3*, 380. (i) Wang, D.; Qian, F.; Yang, C.; Zhong, Z. H.; Lieber, C. M. *Nano Lett.* **2004**, *4*, 871. (j) Manna, L. ; Milliron, D. J. ; Meisel, A. ; Scher, E. C. ; Alivisatos, A. P. *Nature Mater.* **2003**, *2*, 382.

....

Physical and Materials Chemistry Division, National Chemical Laboratory   189

12.   (a) Wang, H.; Brandl, D. W.; Nordlander, P.; Halas, N. J. *Nano. Lett.* **2006**, 6, 827. (b) Thomas, K. G.; Barazzouk, S.; Ipe, B. I.; Joseph, S. T. S.; Kamat, P. V. *J. Phys. Chem. B.* **2004,** *108,* 13066.

13.   Park, W. I. ; Yi, G.-C. ; Kim, M. ; Pennycook, S. J. *Adv. Mater.* **2003,** *15*, 526.

14.   (a) A special issue on carbon nanotubes: *Acc. Chem. Res.* **2002**, *35*, 997-1113. (b) Sui, Y. C.; González-León, J. A.; Bermúdez, A.; Saniger, J. M. *Carbon* **2001**, *39*, 1709. (c) Yao, Z.; Postma, H. W. Ch.; Balents, L.; Dekker, C. *Nature* **1999**, *402*, 273. (d) Yu, H.; Li, J.; Loomis, R. A.; Wang, L.-W.; Buhro, W. E. *Nature Mater.* **2003**, *2*, 517. (e) Derycke, V.; Martel, R.; Appenzeller, J.; Avouris, Ph. *Nano Lett.* **2001**, *1*, 453. (f) Haraguchi, K.; Katsuyama, T.; Hiruma, K.; Ogawa, K. *Appl. Phys. Lett.* **1992**, *60*, 745.

15.   (a) Jiang, K.; Eitan, A.; Schadler, L. S.; Ajayan, P. M.; Siegel, R. W.; Grobert, N.; Mayne, M.; Reyes-Reyes, M.; Terrones, H.; Terrones, M. *Nano Lett.* **2003**, *3,* 275. (b) Banerjee, S.; Wong, S. S. *Nano Lett.* **2002,** *2,* 195. (c) Fullam, S.; Cottell, D.; Rensmo, H.; Fitzmaurice, D. *Adv. Mater.* **2000**, *12*, 1430. (d) Kuo, C. T.; Lin, C. H.; Lo, A. Y. *Diamond Relat. Mater.* **2003,** *12,* 799.

16.   Sun, X. H.; Teo, B. K. *J. Cluster Science* **2004**, *15*,199.

17.   (a) Hosteteler, M. J.; Templeton, A. C.; Murray, R. W. *Langmuir* **1999**, *15*, 3782. (b) Kovtyukhova, N. I.; Martin, B. R.; Mbindyo, J. K. N.; Smith, P. A.; Razavi, B.; Mayer, T. S.; Mallouk, T. E. *J. Phys. Chem. B* **2001**, *105*, 8762.

18.   Chaki, N. K.; Kakade, B.; Vijayamohanan, K. *Electrochem. Commun.* **2004,** *6*, 661.

19.   (a) Kaiser, W. J.; Jaklevic, R. C. *Surf. Sci.* **1987**, *181*, 55. (b) Binning, G.; Smith, D.P.E. *Rev. Sci. Instrum.* **1986**, *57*, 1688. (c) Dharmadhikari, C.V. *Final Consolidated Report on the project entitled, "Development of Scanning Tunneling Microscope for Surface Studies", BRNS, Department of Atomic Energy, Govt. of India*, 1996. (d) SPIP stands for Scanning Probe Image Processor, which is software for Scanning Probe Microscopy and other Microscopy Techniques developed by Image Metrology, Denmark.

20.   Sun, Y.; Mayers, B.; Herricks, H.; Xia, Y. *Nano Lett.* **2003**, *3*, 955.

21.   Büttner, M.; Kröger, H.; Gerhards, I.; Mathys, D.; Oelhafen, P. *Thin Solid Film* **2006**, *495*, 180.

....

Physical and Materials Chemistry Division, National Chemical Laboratory   190

----

22. Hooper, A. E.; Werho, D.; Hopson, T.; Palmer, O. *Surf. Interface Anal.* **2001,** *31***,** 809.

23. Gao, Y.; Jiang, P.; Liu, D. F.; Yuan, H. J.; Yan, X. Q.; Zhou, Z. P.; Wang, J. X.; Song, L.; Liu, L. F.; Zhou, W. Y.; Wang, G.; Wang, C. Y.; Xie, S. S.; Zhang, J. M.; Shen, D. Y. *J. Phys. Chem. B* **2004**, *108*, 12877.

24. (a) Sun, Y.; Gates, B.; Mayers, T.; Xia, Y. *Nano. Lett.* **2002**, *2*, 165. (b) Sun, Y.; Yin, Y.; Mayers, B. T.; Herricks, T.; Xia, Y. *Chem. Mater.* **2002**, *14*, 4736. (c) Wang, Z.; Liu, J.; Chen, X.; Wan, J.; Qian, Y. *Chem. Eur. J.* **2005**, *11*, 160.

25. Sioss, J. A.; Keating, C. D. *Nano. Lett.* **2005**, *5*, 1779.

26. Badia, A.; Cuccia, L.; Demers, L.; Morin, F.; Lennox, R. B. *J. Am. Chem. Soc.* **1997**, *119*, 2682.

....

Physical and Materials Chemistry Division, National Chemical Laboratory   191

Chapter 6

Conclusions and Future Prospects

This chapter provides a summary of the major outcomes of the present study, illustrating several important merits and challenges faced during the synthesis and characterization of different nanomaterials of monolayer protected silver and gold. A brief discussion on the applications of these nanowires is given along with the future prospects of these materials in a broad perspective of the societal impact of nanotechnology. Few of the limitations of these nanostructured materials are also discussed in the end along with their environmental concerns.

6.1 Introduction

High aspect ratio nanostructured materials, more precisely anisotropic nanomaterials have generated tremendous research interest both for fundamental and practical point of view.[1] For example, metal nanowires are important components of electronic circuits, which are envisioned as conductors, rectifiers, switches, and photoconductors of future generation devices.[2] Accordingly, several methods have been developed for the synthesis of high aspect ratio nanostructured materials.[3] However, certain factors such as incomplete knowledge on actual growth controlling steps, lack of a more generalized method of synthesis, and control over yield or scale up issues motivate researchers to develop newer and newer methods of synthesis. We have successfully developed new strategies for the synthesis of several such nanostructures including nanowires and triangular nanoplates.

The thesis starts with a brief introduction to the world of high aspect ratio nanomaterials, with special emphasis on gold and silver. Subsequently, an elaborate discussion on the significance of such nanostructures and their theoretical relevance has been given. This chapter also discusses some of the most recent developments for producing high aspect ratio nanomaterials of gold and silver followed by a brief summary of the size and shape dependant properties of such nanomaterials and their possible applications.

Solvent properties and organic reducing agents are two important parameters, which also control the anisotropic growth. Interestingly, silver nanowire can be synthesized using 4-aminothiophenol (4-ATP), a unique reducing and shape directing agent in aqueous-acetonitrile. It has been established that $AgNO_3$ and 4-ATP concentration along with the solvent mixing ratio control the growth of silver nanowires. Modulations of such parameters leads to the formation of spherical silver nanoparticles to the high aspect ratio (R = 1-100) silver nanowires. Surprisingly, reduction of auric chloride by 4-ATP in aqueous N,N-dimethylformamide leads only to spherical gold nanoparticles, which subsequently forms spherical aggregates establishing the versatile role of polyfunctional organic molecules in achieving shape selectivity. For example, gold nanoplates are exclusively formed by other multifunctional dye molecules like BBR/BBY.

The electrochemical study on well-defined silver nanowires and nanoparticles demonstrates that electron transfer features, as revealed by the half wave potential ($E_{1/2}$)

....

Physical and Materials Chemistry Division, National Chemical Laboratory   193

and ΔE_p, are dependent on the shape and size of silver nanoparticles. Significantly, the $E_{1/2}$ values of silver nanowires and larger sized nanoparticles are relatively higher than that of the smaller sized DDT capped Ag NPs (2-7 nm). This is in agreement with the reported observation that for smaller sized nanoparticles, E^0 ($\approx E_{1/2}$ for ideal reversible system) should shift negatively to that of larger counterparts. More interestingly, *in situ* generated smaller sized silver nanoparticles act as electrocatalysts in Wolff rearrangement of α-diazoketones which occurs through a ECCE or ECE coupled reaction pathway.

Similarly, cyclic voltammograms of the 4-ATP protected Au nanoparticles show quasi-reversible redox behavior, different from those of self-assembled monolayer (SAM) of ATP on gold electrode. Surprisingly, BBR/BBY protected gold nanoplates show unprecedented electrochemical properties exhibiting surface confinement features. X-ray photoelectron (XP) and Fourier transform infrared (FTIR) spectroscopic analysis show the presence of a fraction of BBR/BBY as surface passivating agent either in the un-reacted molecular state or as a mixture of reacted and un-reacted product, which probably undergoes charge transfer with gold nanoplates. X-ray diffraction analysis confirms the predominant orientation of gold nanoplates in the (111) crystal planes with a lattice constant ~ 4.07 A^0 of fcc gold.

Further, 4-ATP also acts as a linker molecule for Au-Ag bi-metallic assembly formation. The fact that at controlled pH, synthesis of 4-ATP capped gold nanoclusters functionalizes with free amino group is applied for the hetero-metallic assembly formation. UV-visible absorption studies confirm the Au-Ag bi-metallic assembly formation with an absorption maximum in the range 550-580 nm. Interestingly, effective organization of gold nanoparticles on silver nanowires exhibits exceptional optical and electrical properties as illustrated by a characteristic surface plasmon absorption peak (570 nm) and a remarkable conductivity change with temperature at 150 and 180 K respectively. Although, this hybrid material displays an exciting combination of semiconductor and metallic behavior from resistivity measurements and phase changes from differential scanning calorimetric results, several other factors such as reorganization of capping molecules, possibility of tunneling pathways, orientation dependent interdigitation of hydrocarbon chains, and variable cluster–cluster spacing

and variations in silver nanowire surface coverage will need to be further investigated before their applications as electronic or photonic components.

Several difficulties were also associated with the synthesis and processing of high aspect ratio nanostructures of silver and gold. Few of such difficulties are:

- Silver nanoparticles and nanowires are easy to synthesize, but difficult to handle due to the possibility of oxide formation. We could not purify 4-ATP capped silver nanowires from excess surface layers. Although, we presented a comparison of electrochemical properties of similar sized silver nanoparticles and silver nanowires, it may not be the ideal case as we could not synthesis nanoparticles beyond the size range of 40 nm;

- Although we have synthesized gold nanoplates with comparatively good yield, they are actually a mixture of hexagonal and triangular shaped plates with little impurities of spherical particles. We could not achieve 100 % selectivity. The fate of poly-functional organic molecules, BBR and BBY is also not clearly understood and need further study;

- We have demonstrated the usefulness of 4-ATP towards the synthesis and assembly formation of different nanomaterials. However, it is not clear which end of 4-ATP actually links selectively with gold and silver and how to control this.

- The organization of gold nanoparticles on silver nanowires opens up several new opportunities, but the percentage of actual coverage is still not known.

Despite such inherent limitations, we have presented several new findings which could be of use for future applications. In particular, catalysis by nanoparticles is an active area of research and the shape dependence on catalytic activity is recently demonstrated.[4] This is because different crystal facets of such nanomaterials have different catalytic activity, therefore, most of their properties also depend on their crystal facets. Wolff rearrangement of α-diazoketones using silver nanoparticles provides an efficient preparative electrochemical route to realize Wolff-rearranged products in excellent yields at room temperature. Apart from catalytic activity, such nanomaterials will find place in optics, plasmonics, molecular electronics, and bio-medical diagnosis. Further extension of present study, especially the organization of magnetic nanoparticles on silver nanowires could generate new properties and application possibilities. Several such promises and fundamental interest on nanomaterials will lure researchers in

coming days for finding out more general synthetic route and newer and newer properties to be useful for commercial exploitation. A promising brighter future is envisioned for nanotechnology as coming days will solve several such difficulties associated with the applications of nanomaterials.

6.2 Opportunities, Risks, and Future of Nanotechnology

Convergence of different technologies, such as nanotechnology, biotechnology could generate new materials which behave differently beyond the common perception of present generation of materials. However, nanomaterials exist all around us – nature also produces them. The supporters of nanotechnology believe that it is because today's knowledge and scientific tools enable scientists to begin to discover what has been previously impossible: building new products and compounds atom by atom. This is the reason behind the common belief that nanotechnology is the next "transformative technology", like the Internet or electricity.[5] Some of the nanotechnology products have already been developed and commercialized and few others are still concepts which require further rigorous research. Consequently, this outcome of nanotechnology is likely to cause many innovative solutions for generating improved water purification systems, nonpolluting and inexhaustible energy systems, smart and non-invasive health care systems, and information and communication technologies.[6] For example, there are a number of filter systems based on nanotechnology, which are capable of filtering bacteria and even viruses out of water.[7] Several such products could save millions of human lives in the developing countries potentially having drinking water scarcities. Similarly, bio-nanotechnology can have breakthroughs in health sector by developing effective drugs and detection tools for several diseases like AIDS, TB, Cancer, etc.[7d]

However, above outcomes of nanotechnology may posses potential danger to mankind as little is known about how nanometer sized materials interact with living cells, and therefore, existing regulations, guidelines, norms, and ways of thinking may be irrelevant to nanotechnology. The smaller a particle is the larger is the surface area, causing enhanced reactivity (and perhaps toxicity too) and their accumulation in living organisms can cause many serious concerns. A report from "Swiss Re" about nanotechnology states: "Human contact with nanoparticles takes various forms: they are inhaled with air, swallowed, and may possibly enter the body via the skin. How do these

particles behave on or in the organism?"[8] Surprisingly, information on the effects, if any, of nanoparticles on ecosystems, animals, plants, and microorganisms is still inadequate.[9] Apart from aforementioned environmental issues, nanotechnology may also create socioeconomic and ethical problems.[10] This is because nanotechnology could be a major problem for poorer countries if it makes their labor, commodities, and other exports less necessary in the global market. Similarly, nanotechnology monitoring devices raise ethical problems because of their small size, could be ubiquitous and invisible and thereby interfering the right to privacy issues by such common surveillance systems.

Despite the commonly perceived apprehensions on the use of nanotechnology, several such drawbacks can be easily circumvented by responsible and equally distributed benefits of nanotechnology.[11] Therefore, opponents and believers have to decide how to use benefits of nanotechnology advantageously to overcome the threat perceptions arising from it.

6.3 References

1.   (a) Hao, E.; Schatz, G. C.; Hupp, J. T. *J. Fluoresc.* **2004**, *14*, 331. (b) Chen, C.; Wang, L.; Jiang, G.; Yu, H. *Rev. Adv. Mater. Sci.* **2006**, *11*, 1. (b) Eustis, S.; El-Sayed, M. A. *Chem. Soc. Rev.* **2006**, *35*, 209. (c) El-Sayed, M. A. *Acc. Chem. Res.* **2001**, *34*, 257. (d) Link, S.; El-Sayed, M. A. *J. Phys. Chem. B* **1999**, *103*, 8410.

2.   Kovtyukova, N. I.; Mallouk, T. E. *Chem. Eur. J.* **2002**, *8*, 4354.

3.   (a) Rao, C. N. R.; Cheetham, A. K. *J. Mater. Chem.* **2001**, *11*, 2887. (b) Pérez-Juste, J.; Pastoriza-Santos, I.; Liz-Marzán, L. M.; Mulvaney, P. *Coord. Chem. Rev.* **2005**, *249*, 1870. (c) Murphy, C. J.; Sau, T. K.; Gole, A. M.; Orendorff, C. J.; Gao, J.; Gou, L.; Hunyadi, S. E.; Li, T. *J. Phys. Chem. B* **2005**, *109*, 13857. (d) Wiley, B.; Sun, Y.; Mayers, B.; Xia, Y. *Chem. Eur. J.* **2005**, *11*, 454.

4.   Narayanan, R.; El-Sayed, M. A. *J. Phys. Chem. B* **2005**, *109*, 12663.

5.   (a) *Nanoscience and Nanotechnologies: Opportunities and Uncertainties* The Royal Society and the Royal Academy of Engineering. 2004. http://www.nanotech.org.uk/finalreport.htm. (b) *Industrial Application of Nanomaterials: Chances and Risks.* Luther, W. (Ed). Düsseldorf, Germany. **2004**.

6.   *Benefits of Molecular Manufacturing,* Centre for Responsible Nanotechnology at http://www.crnano.org/benefits.htm.

7.   (a) http://www.argonide.com (b) http://www.seldontechnologies.com/products/ (c) http://www.physorg.com/preview803.html. (d) '*Nanotechnology Takes Aim at cancer*' *Science* (News) **2005**, *310*, 1132.

8.   *Nanotechnology: Small Matter, Many Unknowns.* Swiss Re **2004**. Zurich, Switzerland.

9.   (a) Lam. C. W. *Toxicological Sciences* 2004, 77, 126. (b) Oberdörster, E. *Environmental Health Perspectives* **2004**, 112, No. 10.

10.   Forgel, R. W. *The Escape from Hunger and Premature Death 1700-2100: Europe, America, and the Third world.* Cambridge University Press, Cambridge, UK, **2004**.

11.   (a) www.nanoandthepoor.org. (b) www.merid.org. (C) World Business Council for Sustainable Development (WBCSD). "Doing Business with the Poor: a Field   Guide."   Geneva,   Switzerland.   **2004**   at http://www.wbcsd.org/web/publications/sl-field-guide.pdf. (d) '*Nanotechnology Grows Up*' Science (news), **2004**, *304*, 1732

List of Publications

1. '*Tuning the aspect ratio of silver nanostructure: the effect of solvent mole fraction and 4-aminothiophenol concentration*' **Sharma**, **J.**; Chaki N. K.; Mahima, S.; Gonnade, R. G.; Mulla, I. S. and Vijayamohanan, K. *J. Mater. Chem.* **2004**, *14,* 970.

2. '*Controlled interlinking of Au and Ag nanoclusters using 4-aminothiophenol as molecular interconnects*' **Sharma, J.**; Chaki, N. K.; Mandale, A. B.; Pasricha, R. and Vijayamohanan, K. *J. Colloid interface sci.* **2004**, *272*, 145.

3. '*Size dependent redox behaviour of monolayer protected silver nanoparticles (2-7 nm) in aqueous medium*' Chaki, N. K ; **Sharma, J.**; Mandale, A. B.; Mulla, I. S.; Pasrricha, R. and Vijayamohanan, K. *Phys. Chem. Chem. Phys.* **2004**, *6*, 1304.

4. '*Effect of chain length and the nature of the monolayer on the electrical behavior of hydrophobically organized gold clusters*' Chaki, N. K.; Aslam, M.; Gopakumar, G.; **Sharma**, **J.** and Vijayamohanan K. *J. Phys. Chem. B* **2003**, *107*, 13567.

5. 'Device applications of self-assembled monolayers and monolayer-protected nanoclusters' Aslam, M.; Chaki, N. K.; **Sharma**, **J.** and Vijayamohanan, K. *Current Applied Phys.* **2003**, *3,* 115 (Review).

6. '*Application of self-assembled monolayers in materials chemistry*', Chaki, N. K.; Aslam, M.; **Sharma, J.** and Vijayamohanan*, K. Proc. Indian Acad. Sci. (Chem. Sci.)* **2001**, *113 (5/6)*, 1 (Review).

7. '*Solvent-assisted one-pot synthesis and self-assembly of 4-aminothiophenol-capped gold nanoparticles*' **Sharma, J.**; Mahima, S.; Kakade, B. A.; Pasricha, R.; Mandale, A. B. and Vijayamohanan, K. *J. Phys. Chem. B* **2004**, *108*, 13280.

8. '*Highly resolved quantized double-layer charging of relatively larger dodecanethiol-passivated gold quantum dots*', by Chaki, N. K.; Kakade, B. A.; **Sharma, J.**; Mahima, S. and Vijayamohanan, K. *J. Appl. Phys.* **2004**, *96*, 5032.

9. '*Organic dye molecules as reducing agent for the synthesis of electroactive gold nanoplates*' **Sharma, J.** and Vijayamohanan, K. *Journal of Colloid and Interface Science* (**in press,** doi:10.1016/j.jcis.2005.12.048).

10. '*Directed organization of gold nanoclusters on silver nanowires: a step forward in heterostructure assembly'* **Sharma, J.**, et al. *App. Phys. Lett.* **2006**, *88*, 193103.

11. '*Wolff rearrangement of α-diazoketones using in situ generated silver nanoclusters as electron mediators*' S. Sudrik, **Sharma, J.**; Chavan, V. B.; Chaki, N. K.; Sonawane, H. R. and Vijayamohanan, K. P. *Organic Letters*, **2006**, *8*, 1089.

12. '*Preparation and characterization of novel hetero-structures by the directed assembly of spherical gold nanoparticles on silver nanowires'* **Sharma, J.** and Vijayamohanan, K. P. *J. Phys. Chem. B.* (**submitted)**.

13. '*Electron transfer behavior of monolayer protected nanoclusters and nanowires of silver and gold*' **Sharma J**. et al. *Journal of Nanoscience and Nanotechnology* (**in press**).

14. '*Role of polyfunctional organic molecules in synthesis and assembly of metal nanoparticles*' **Sharma J**. et al. (**submitted to *Journal of Nanoscience and Nanotechnology***).

15. '*Electrochemical Organization of Monolayer Protected Gold Nanoclusters on Single-Walled Carbon Nanotubes: Significantly Enhanced Double Layer Capacitance*' Mahima, S.; Chaki, N. K.; **Sharma, J.**; Kakade, B. A.; Pasricha, R.; Rao, A. M.; Vijayamohanan, K. *Journal of Nanoscience and Nanotechnology* (**in press**).

Erratum